

## University of Southampton Research Repository ePrints Soton

Copyright © and Moral Rights for this thesis are retained by the author and/or other copyright owners. A copy can be downloaded for personal non-commercial research or study, without prior permission or charge. This thesis cannot be reproduced or quoted extensively from without first obtaining permission in writing from the copyright holder/s. The content must not be changed in any way or sold commercially in any format or medium without the formal permission of the copyright holders.

When referring to this work, full bibliographic details including the author, title, awarding institution and date of the thesis must be given e.g.

AUTHOR (year of submission) "Full thesis title", University of Southampton, name of the University School or Department, PhD Thesis, pagination

**UNIVERSITY OF SOUTHAMPTON**

FACULTY OF ENGINEERING, SCIENCE & MATHEMATICS

School of Chemistry

**Preparation, Characterisation and Structural  
Assessment of Salts and Co-Crystals of Organic  
Compounds**

by

Samantha Callear

Thesis for the degree of Doctor of Philosophy

January 2008

UNIVERSITY OF SOUTHAMPTON  
ABSTRACT  
FACULTY OF ENGINEERING, SCIENCE, & MATHEMATICS  
SCHOOL OF CHEMISTRY  
Doctor of Philosophy  
PREPARATION, CHARACTERISATION AND STRUCTURAL ASSESSMENT OF  
SALTS AND CO-CRYSTALS OF ORGANIC COMPOUNDS  
By Samantha Callear

In this thesis the factors influencing the formation of a binary compound and the proton transfer within the binary compound have been investigated. The formation of a binary compound, or heteromeric system, over a homomeric system requires the heteromeric system to be more energetically favourable than the homomeric system. In some circumstances, however, no solid crystallises at all. Proton transfer within the binary compound can lead to the formation of a salt, whereas a binary compound containing neutral components is called a co-crystal. The 'rule of three' which predicts that proton transfer requires a difference of at least three units between the  $pK_a$  of the acid and the  $pK_a$  of the conjugate acid has also been investigated. In particular the relevance of this rule to diprotic acids and bases, and amide groups has been examined. The expression of starting material properties in the binary compounds was also explored.

To achieve this an array of diacids and bases have been chosen that consist of  $\alpha,\omega$ -alkanedicarboxylic acids,  $\alpha,\omega$ -alkenedicarboxylic acids and tartaric acids with a selection of aliphatic amines, nitrogen-containing heterocycles and imidazole derivatives. The nitrogen-containing heterocycles include some amide functionalities. These compounds have been systematically crystallised together using a liquid-handling robot in a high-throughput manner commonly used in the pharmaceutical industry.

The novel structures of 42 salts, 11 co-crystals and 6 mixed co-crystal/salt systems have been prepared and characterised using single crystal X-ray diffraction. Together with the binary compounds already present on the CSD, this has provided the opportunity to assess the impact of various factors on the crystal structures and properties of a total of 61 salts, 11 co-crystals and 8 mixed salt/co-crystal systems. Across the series of  $\alpha,\omega$ -alkanedicarboxylic acids it has been found that members with an even number of carbons in their alkyl chain (even diacids) form binary compounds more often than those with an odd number of carbons (odd diacids). The diacids with four carbons in their alkyl chains are most likely to form binary compounds. The melting point alternation seen in the  $\alpha,\omega$ -alkanedicarboxylic acids is also expressed in the binary products. This is particularly prominent with the 2-imidazolidinone-alkanedicarboxylic acid co-crystals, where the supramolecular structure formed by the even diacids is different to that formed by the odd diacids. This has been attributed to the different orientation of the carboxyl groups in the odd diacids.

Although the 'rule of three' has been found to be applicable to the first ionisation of the diacids, it does not account for the ubiquitous formation of diprotonated bases where the  $pK_a$  difference is often less than 2 units. Indeed the stoichiometry of the binary compounds was found to often be unpredictable and difficult to rationalise simply. The deprotonation of the diacids appeared to be determined by the optimal hydrogen bonding motifs rather than the  $pK_a$ . There were also found to be similarities in supramolecular structures within the groups of compounds which could be used to predict the structures of other similar compounds.

## LIST OF CONTENTS

<b>Figure List</b>	vi
<b>Table List</b>	xiii
<b>Authors Declaration</b>	xiv
<b>Acknowledgements</b>	xv
<b>Abbreviations</b>	xvi
 <b>CHAPTER 1 – The Organic Solid State</b>	
<b>1.1 INTRODUCTION</b>	1
<b>1.2 INTERMOLECULAR INTERACTIONS</b>	1
1.2.1 <i>Van der Waals Interactions and Close Packing</i>	2
1.2.2 <i>Hydrogen Bonding</i>	2
1.2.3 <i>Other Anisotropic Interactions</i>	5
<b>1.3 CRYSTALLISATION</b>	5
1.3.1 <i>The Role of Temperature and Solvent</i>	6
1.3.2 <i>Crystallisation Techniques</i>	6
1.3.3 <i>Crystallisation and Polymorphism</i>	7
<b>1.4 MULTI-COMPONENT SYSTEMS</b>	9
<b>References</b>	11
 <b>CHAPTER 2 – Pharmaceutical Solid Forms: Salts and Co-Crystals</b>	
<b>2.1 INTRODUCTION</b>	13
<b>2.2 DRUG PROPERTIES</b>	13
2.2.1 <i>Polymorphism</i>	14
2.2.2 <i>Selection of Drug Candidates</i>	14
<b>2.3 SALT AND CO-CRYSTAL FORMATION</b>	15
2.3.1 <i>Selection of Salt and Co-Crystal Formers</i>	16
2.3.2 <i>Crystallisation of Salts and Co-Crystals</i>	17
2.3.3 <i>pH-Solubility Profiles</i>	18
<b>2.4 SALT VERSUS CO-CRYSTAL FORMATION</b>	19
2.4.1 <i>pK<sub>a</sub></i>	19
2.4.2 <i>Proton Transfer</i>	20
2.4.3 <i>Effect of Solvent on pK<sub>a</sub></i>	20
<b>2.5 AIMS OF RESEARCH</b>	20
<b>2.6 STARTING MATERIALS</b>	22
2.6.1 <i>Acids</i>	23
2.6.2 <i>Bases</i>	26
2.6.3 <i>Binary Compounds of Chosen Acid-Base Combinations Already Present on CSD</i>	28
2.6.4 <i>Possible Hydrogen Bond Synthons</i>	28
<b>References</b>	31
 <b>CHAPTER 3 – Analytical Techniques</b>	
<b>3.1 INTRODUCTION</b>	34
<b>3.2 CRYSTALLOGRAPHY</b>	34
3.2.1 <i>Solid Form – Crystal Structure</i>	34
3.2.2 <i>Crystal Systems</i>	35
3.2.3 <i>Lattice Types</i>	35
3.2.4 <i>Bravais Lattices</i>	36
3.2.5 <i>Symmetry</i>	36
3.2.6 <i>X-rays</i>	37
3.2.7 <i>The Laue Equations</i>	37



3.2.8	<i>Bragg's Law</i>	38
3.2.9	<i>Scattering Factors</i>	39
3.2.10	<i>The Phase Problem</i>	39
3.2.11	<i>Direct Methods</i>	40
3.2.12	<i>Refinements</i>	40
3.2.13	<i>Fourier Methods and Least-Squares Analysis</i>	41
3.2.14	<i>R-factor</i>	41
3.2.15	<i>Powder X-ray Diffraction (PXRD)</i>	41
<b>3.3</b>	<b>THERMAL STUDIES OF ORGANIC SOLIDS</b>	42
3.3.1	<i>Differential Scanning Calorimetry</i>	42
3.3.2	<i>Hot-Stage Microscopy</i>	43
<b>References</b>		44
<b>Chapter 4 – Experimental</b>		
<b>4.1</b>	<b>INTRODUCTION</b>	45
<b>4.2</b>	<b>CRYSTALLISATION METHODS</b>	45
4.2.1	<i>Method 1</i>	45
4.2.2	<i>Method 2</i>	45
4.2.3	<i>Method 3</i>	46
<b>4.3</b>	<b>INITIAL PRODUCT ASSESSMENT</b>	46
<b>4.4</b>	<b>SXRD INSTRUMENTATION AND DATA COLLECTION</b>	46
4.4.1	<i>Crystal Selection and Mounting</i>	46
4.4.2	<i>The Diffractometer</i>	47
4.4.3	<i>Data Collection.</i>	47
4.4.4	<i>Twin Collections</i>	48
4.4.5	<i>Synchrotron Collections.</i>	49
<b>4.5</b>	<b>PXRD INSTRUMENTATION AND DATA COLLECTION</b>	49
<b>4.6</b>	<b>THERMAL ANALYSIS METHODS</b>	49
<b>4.7</b>	<b>STRUCTURAL ANALYSIS</b>	49
<b>References</b>		50
<b>Chapter 5 – Results and Discussion – Aliphatic Amines</b>		
<b>5.1</b>	<b>INTRODUCTION</b>	51
<b>5.2</b>	<b>1,1,3,3-TETRAMETHYLBUTYLAMINE</b>	52
5.2.1	<i>Oxalic Acid and 1,1,3,3-Tetramethylbutylamine</i>	52
5.2.2	<i>Malonic Acid and 1,1,3,3-Tetramethylbutylamine</i>	55
5.2.3	<i>Succinic Acid and 1,1,3,3-Tetramethylbutylamine</i>	56
5.2.4	<i>Glutaric Acid and 1,1,3,3-Tetramethylbutylamine</i>	57
5.2.5	<i>Adipic Acid and 1,1,3,3-Tetramethylbutylamine</i>	59
5.2.6	<i>Pimelic Acid and 1,1,3,3-Tetramethylbutylamine</i>	61
5.2.7	<i>DL-Tartaric Acid and 1,1,3,3-Tetramethylbutylamine</i>	62
5.2.8	<i>Maleic Acid and 1,1,3,3-Tetramethylbutylamine</i>	65
5.2.9	<i>Fumaric Acid and 1,1,3,3-Tetramethylbutylamine</i>	66
5.2.10	<i>Discussion of 1,1,3,3-Tetramethylbutylamine Structures</i>	67
<b>5.3</b>	<b>1,2-DIAMINOETHANE</b>	70
5.3.1	<i>Oxalic Acid and 1,2-Diaminoethane (PEPMOM).</i>	70
5.3.2	<i>Malonic Acid and 1,2-Diaminoethane (WOBXIU)</i>	71
5.3.3	<i>Succinic Acid and 1,2-Diaminoethane (PINNIJ)</i>	72
5.3.4	<i>Glutaric Acid and 1,2-Diaminoethane</i>	73
5.3.5	<i>Adipic Acid and 1,2-Diaminoethane (ZZZGYW)</i>	74
5.3.6	<i>D-Tartaric Acid and 1,2-Diaminoethane (EDATAR10)</i>	74
5.3.7	<i>DL-Tartaric Acid and 1,2-Diaminoethane</i>	75
5.3.8	<i>Maleic Acid and 1,2-Diaminoethane (ROHKUU).</i>	75
5.3.9	<i>Fumaric Acid and 1,2-Diaminoethane</i>	77
5.3.10	<i>Discussion of 1,2-Diaminoethane Structures</i>	78
<b>5.4</b>	<b>2-AMINOETHANOL</b>	80
5.4.1	<i>Oxalic Acid and 2-Aminoethanol (QAMRIF)</i>	80
5.4.2	<i>Succinic Acid and 2-Aminoethanol</i>	81

5.4.3	<i>Suberic Acid and 2-Aminoethanol</i>	82
5.4.4	<i>L-Tartaric Acid and 2-Aminoethanol (XAGDAK)</i>	85
5.4.5	<i>Fumaric Acid and 2-Aminoethanol</i>	86
5.4.6	<i>Discussion of 2-Aminoethanol Structures</i>	88
<b>5.5</b>	<b>TETRAMETHYLETHYLENEDIAMINE</b>	90
5.5.1	<i>Oxalic Acid and Tetramethylethylenediamine</i>	90
5.5.2	<i>Malonic Acid and Tetramethylethylenediamine</i>	92
5.5.3	<i>Succinic Acid and Tetramethylethylenediamine (ISUTEV)</i>	92
5.5.4	<i>Glutaric Acid and Tetramethylethylenediamine</i>	94
5.5.5	<i>DL-Tartaric Acid and Tetramethylethylenediamine</i>	95
5.5.6	<i>Maleic Acid and Tetramethylethylenediamine</i>	97
5.5.7	<i>Fumaric Acid and Tetramethylethylenediamine (QAFVEZ)</i>	98
5.5.8	<i>Discussion of Tetramethylethylenediamine Structures</i>	99
<b>5.6</b>	<b>DISCUSSION OF ALIPHATIC AMINES</b>	100
<b>References</b>		102

## Chapter 6 –Results and Discussion – Nitrogen-Containing Heterocycles

<b>6.1</b>	<b>INTRODUCTION</b>	103
<b>6.2</b>	<b>2-PYRROLIDINONE</b>	104
6.2.1	<i>Succinic Acid and 2-Pyrrolidinone</i>	104
6.2.2	<i>Fumaric Acid and 2-Pyrrolidinone</i>	105
6.2.3	<i>Discussion of 2-Pyrrolidinone Structures</i>	107
<b>6.3</b>	<b>2-IMIDAZOLIDINONE</b>	108
6.3.1	<i>Oxalic Acid and 2-Imidazolidinone</i>	108
6.3.2	<i>Malonic Acid and 2-Imidazolidinone</i>	109
6.3.3	<i>Succinic Acid and 2-Imidazolidinone</i>	110
6.3.4	<i>Glutaric Acid and 2-Imidazolidinone</i>	112
6.3.5	<i>Adipic Acid and 2-Imidazolidinone</i>	113
6.3.6	<i>Pimelic Acid and 2-Imidazolidinone</i>	114
6.3.7	<i>L-Tartaric Acid and 2-Imidazolidinone</i>	115
6.3.8	<i>DL-Tartaric Acid and 2-Imidazolidinone</i>	116
6.3.9	<i>Maleic Acid and 2-Imidazolidinone</i>	118
6.3.10	<i>Discussion of 2-Imidazolidinone Structures</i>	119
<b>6.4</b>	<b>1,3-DIMETHYLIMIDAZOLIDINONE</b>	123
<b>6.5</b>	<b>MORPHOLINE</b>	123
6.5.1	<i>Oxalic Acid and Morpholine</i>	123
6.5.2	<i>Succinic Acid and Morpholine</i>	125
6.5.3	<i>Adipic Acid and Morpholine</i>	127
6.5.4	<i>DL-Tartaric Acid and Morpholine</i>	128
6.5.5	<i>Maleic Acid and Morpholine</i>	130
6.5.6	<i>Fumaric Acid and Morpholine</i>	130
6.5.7	<i>Discussion of Morpholine Structures</i>	131
<b>6.6</b>	<b>DISCUSSION OF NITROGEN-CONTAINING HETEROCYCLES</b>	133
<b>References</b>		135

## Chapter 7 – Aromatic Amines

<b>7.1</b>	<b>INTRODUCTION</b>	136
<b>7.2</b>	<b>IMIDAZOLE</b>	137
7.2.1	<i>Oxalic Acid and Imidazole (MEQPAZ)</i>	137
7.2.2	<i>Malonic Acid and Imidazole</i>	139
7.2.3	<i>Succinic Acid and Imidazole (MEQPON)</i>	140
7.2.4	<i>Adipic Acid and Imidazole (MEQQEE)</i>	141
7.2.5	<i>Suberic Acid and Imidazole</i>	143
7.2.6	<i>L-Tartaric Acid and Imidazole (HAZHEV)</i>	145
7.2.7	<i>DL-Tartaric Acid and Imidazole</i>	146
7.2.8	<i>Maleic Acid and Imidazole (IMZMAL10)</i>	148
7.2.9	<i>Fumaric Acid and Imidazole (MEQPED)</i>	149
7.2.10	<i>Discussion of Imidazole Structures</i>	150

<b>7.3</b>	<b>1-METHYLIMIDAZOLE</b>	152
7.3.1	<i>Oxalic Acid and 1-Methylimidazole</i>	152
7.3.2	<i>Succinic Acid and 1-Methylimidazole</i>	153
7.3.3	<i>Glutaric Acid and 1-Methylimidazole</i>	155
7.3.4	<i>D-Tartaric Acid and 1-Methylimidazole (ZAMXIU)</i>	157
7.3.5	<i>DL-Tartaric Acid and 1-Methylimidazole</i>	159
7.3.6	<i>Maleic Acid and 1-Methylimidazole</i>	160
7.3.7	<i>Discussion of 1-Methylimidazole Structures</i>	160
<b>7.4</b>	<b>2-METHYLIMIDAZOLE</b>	162
7.4.1	<i>Oxalic Acid and 2-Methylimidazole</i>	162
7.4.2	<i>Malonic Acid and 2-Methylimidazole</i>	164
7.4.3	<i>Succinic Acid and 2-Methylimidazole</i>	166
7.4.4	<i>Glutaric Acid and 2-Methylimidazole</i>	167
7.4.5	<i>Adipic Acid and 2-Methylimidazole</i>	169
7.4.6	<i>Suberic Acid and 2-Methylimidazole</i>	170
7.4.7	<i>D-Tartaric Acid and 2-Methylimidazole (ZELRIR)</i>	171
7.4.8	<i>DL-Tartaric Acid and 2-Methylimidazole</i>	172
7.4.9	<i>Fumaric Acid and 2-Methylimidazole</i>	174
7.4.10	<i>Discussion of 2-Methylimidazole Structures</i>	175
<b>7.5</b>	<b>4-METHYLIMIDAZOLE</b>	177
7.5.1	<i>Oxalic Acid and 4-Methylimidazole</i>	177
7.5.2	<i>Succinic Acid and 4-Methylimidazole</i>	178
7.5.3	<i>Glutaric Acid and 4-Methylimidazole</i>	180
7.5.4	<i>Suberic Acid and 4-Methylimidazole</i>	182
7.5.5	<i>L-Tartaric Acid and 4-Methylimidazole</i>	183
7.5.6	<i>DL-Tartaric Acid and 4-Methylimidazole</i>	185
7.5.7	<i>Maleic Acid and 4-Methylimidazole</i>	186
7.5.8	<i>Discussion of 4-Methylimidazole Structures</i>	188
<b>7.6</b>	<b>1,2-DIMETHYLIMIDAZOLE.</b>	189
7.6.1	<i>Succinic Acid and 1,2-Dimethylimidazole</i>	189
7.6.2	<i>Glutaric Acid and 1,2-Dimethylimidazole</i>	190
7.6.3	<i>L-Tartaric Acid and 1,2-Dimethylimidazole</i>	192
7.6.4	<i>DL-Tartaric Acid and 1,2-Dimethylimidazole</i>	193
7.6.5	<i>Fumaric Acid and 1,2-Dimethylimidazole</i>	195
7.6.6	<i>Discussion of 1,2-Dimethylimidazole Structures</i>	197
<b>7.7</b>	<b>DISCUSSION OF IMIDAZOLE-DERIVATIVES</b>	198
7.7.1	<i>Density and Melting Points</i>	200
7.7.2	<i>Deprotonation and Stoichiometry Trends</i>	200
7.7.3	<i>Bond Distances</i>	201
7.7.4	<i>Hydrogen Bonding</i>	201
7.7.5	<i>Other Intermolecular Interactions</i>	202
7.7.6	<i>Fingerprint Plots (Appendix, Tables A10)</i>	203
<b>References</b>		205
 <b>Chapter 8 – Discussion With Respect to the Diacids</b>		
<b>8.1</b>	<b>INTRODUCTION</b>	206
<b>8.2</b>	<b>TRENDS IN DEPROTONATION AND STOICHIOMETRY</b>	206
<b>8.3</b>	<b>HYDROGEN BONDING</b>	208
8.3.1	<i>Anion/Acid Hydrogen Bonding</i>	208
8.3.2	<i>Acid-Base Hydrogen Bonding</i>	210
8.3.3	<i>Intramolecular Hydrogen Bonding</i>	211
<b>8.4</b>	<b>ANION/ACID CONFORMATION AND BOND DISTANCES</b>	212
8.4.1	<i>Carbon-Carbon Bond Lengths</i>	212
8.4.2	<i>Carbon Backbone Conformation</i>	212
8.4.3	<i>Angle Between Carboxyl(ate) Planes</i>	213
<b>8.5</b>	<b>CRYSTALLOGRAPHIC PATTERNS</b>	214
<b>References</b>		215

---

**Chapter 9 – Conclusions and Further Work**

<b>9.1</b>	<b>CONCLUSIONS</b>	.	.	.	.	.	.	.	.	216
<b>9.2</b>	<b>FURTHER WORK</b>	.	.	.	.	.	.	.	.	219
<b>References</b>	.	.	.	.	.	.	.	.	.	221
<b>Appendix</b>	.	.	.	.	.	.	.	.	.	222

## LIST OF FIGURES

1.2.2.1	Geometrical terms of a hydrogen bond.	3
1.2.2.2	C-O and C=O bond distances: for strong hydrogen bonds the difference between c and d is greater than that for normal hydrogen bonds. Theoretically, for a carboxylate group that is not hydrogen bonded c=d, however hydrogen bonds and other interactions act to lengthen the C-O bonds.	4
2.6.1.1	Graph to show the salt formers found in the top 100 drugs by US prescriptions.	24
2.6.1.2	Graph to show the alternation in melting point with the carbon chain length in the simple diacid series.	25
2.6.1.3	ScA chain structure.	25
2.6.1.4	GlA chain structure.	26
2.6.4.1	a) <i>Syn-syn</i> and b) <i>anti-anti</i> hydrogen bonded dimers.	29
2.6.4.2	Schematic representation of a cation acting as a bridge between two anion chains.	29
2.6.4.3	a) Catemeric and b) non-catemeric hydrogen bonded chain.	30
2.6.4.4	Various acid and amide hetero- and homosynthons.	30
3.2.1.1	The unit cell.	35
3.2.4.1	The Bravais Lattices.	36
3.2.9.1	Deriving Bragg's Law using trigonometry.	38
4.4.1.1	The goniometer head.	46
4.4.2.1	The diffractometer.	47
5.2.1.1	Ortep diagram for the asymmetric unit of OxA and TMBA.	53
5.2.1.2	Schematic diagram of the hydrogen bond synthon (hydrogen bonds shown as dotted lines) involving the anions and cations (B).	53
5.2.1.3	Hydrogen bond distances (error +/-0.009 Å) for the synthon involving molecules 5 and 8 which is further linked to molecule 4.	53
5.2.1.4	Hydrogen bond distances (error +/-0.008 Å) for the synthon involving molecules 3 and 4 which is further linked to molecule 8.	54
5.2.1.5	Hydrogen bond distances (error +/-0.008 Å) for the synthon involving molecules 1 and 2 which is further linked to molecule 6.	54
5.2.1.6	Hydrogen bond distances (error +/-0.009 Å) for the synthon involving molecules 7 and 6 which is further linked to molecule 2.	54
5.2.1.7	The top sheet contains molecules 1, 2, 6 and 7, the bottom sheet contains molecules 3, 4, 5 and 8 – the sheets are related by rotation, however, the exact positions of the molecules are not identical in each sheet; viewed down the <i>a</i> -axis.	55
5.2.3.1	Ortep diagram for the asymmetric unit of ScA and TMBA.	56
5.2.3.2	Tape structure with anion chain from which cations are subtended; error in A-B hydrogen bond distances are +/-0.004 Å, and +/-0.019 Å for hydrogen bonds involving water.	56
5.2.3.3	Stacking of sheets viewed side-on, each tape viewed end-on.	57
5.2.4.1	Ortep diagram for the asymmetric unit of GlA and TMBA.	57
5.2.4.2	Tape structure with hydrogen bond distances marked (error +/-0.002 Å).	58
5.2.4.3	Sheet structure with tapes viewed end-on, viewed down the <i>c</i> -axis.	58
5.2.4.4	Adjacent sheets viewed side-on, shown in dark blue and light blue, with bridging acid molecule.	59
5.2.5.1	Ortep diagram for the asymmetric unit of AdA and TMBA.	59
5.2.5.2	Tape structure hydrogen bond distances marked (error +/-0.003 Å).	60
5.2.5.3	Edge of sheet, with each tape viewed end-on, viewed down the <i>b</i> -axis.	60
5.2.5.4	Adjacent sheets viewed side-on, shown in dark blue and light blue, with bridging acid molecule.	61
5.2.6.1	Ortep diagram for the asymmetric unit of PmA and TMBA.	61
5.2.6.2	Tape structure, hydrogen bond distances marked (error +/-0.005 Å).	62
5.2.6.3	3-D network with each tape viewed end-on, viewed down the <i>c</i> -axis.	62
5.2.7.1	Ortep diagram for the asymmetric unit of DLTA and TMBA.	63

5.2.7.2	Edge of the sheet, viewed down the <i>a</i> -axis; the water molecules are omitted for clarity (hydrogen bond distance error +/-0.005 Å).	63
5.2.7.3	a) Space-filling water molecules within the sheet; b) Possible short contacts between the water molecules	64
5.2.7.4	Stacking of sheets viewed down the <i>a</i> -axis, water molecules omitted for clarity.	64
5.2.8.1	Ortep diagram for the asymmetric unit of MeA and TMBA.	65
5.2.8.2	Tape structure, hydrogen bond distances marked (error +/-0.003 Å).	65
5.2.8.3	Arrangement of tapes, viewed down the <i>a</i> -axis.	66
5.2.9.1	Ortep diagram for the asymmetric unit of FmA and TMBA.	66
5.2.9.2	Tape structure, hydrogen bond distances marked (error +/-0.012 Å).	67
5.2.9.3	Arrangement of sheets, each sheet viewed side-on.	67
5.2.10.1	Overlay of the two TMBA molecules from the ScA-TMBA structure to show the two conformations of the cation.	70
5.3.1.1	Anion chains linked by hydrogen bonding across the cations (hydrogen bond distance error +/-0.003 Å).	71
5.3.1.2	The 3-D network, viewed down the <i>b</i> -axis (hydrogen bond distance error +/-0.003 Å).	71
5.3.2.1	3-D network with N-H...O hydrogen bond distance marked, viewed down the <i>a</i> -axis (hydrogen bond distance error +/-0.020 Å).	72
5.3.3.1	3-D structure, viewed down the <i>a</i> -axis.	73
5.3.4.1	Ortep diagram for the asymmetric unit of GlA and DAE.	73
5.3.4.2	3-D network, hydrogen bond distances (error +/-0.003 Å) from one carboxylate group are shown in blue, those from the other are shown in purple; viewed down the <i>c</i> -axis.	74
5.3.6.1	Hydrogen bonded dianion sheet.	75
5.3.6.2	3-D network, hydrogen bond distances from one of the ammonium groups is shown in blue, those from the other are shown in purple; viewed down the <i>b</i> -axis.	75
5.3.7.1	3-D network made up of layers of anions with cations and water molecules linking the layers, viewed down the <i>a</i> -axis.	76
5.3.8.1	3-D network viewed down the <i>a</i> -axis, hydrogen bond distances marked (error +/-0.002 Å).	77
5.3.9.1	Ortep diagram for the asymmetric unit of FmA and DAE.	77
5.3.9.2	Hydrogen bonded 3-D network of alternate anions and cations (hydrogen bond distance error +/-0.002 Å), viewed down the <i>a</i> -axis.	78
5.4.1.1	Bilayer structure viewed side-on, down the <i>b</i> -axis (hydrogen bond distance error +/-0.003 Å).	81
5.4.2.1	Ortep diagram for the asymmetric unit of ScA and AEI.	81
5.4.2.2	'Bilayer' type chain structure, viewed down the <i>a</i> -axis (hydrogen bond distance error +/-0.003 Å).	82
5.4.2.3	3-D network with acid-anion chains linked by hydrogen bonding across the cations, viewed down the <i>c</i> -axis.	82
5.4.3.1	Ortep diagram for the asymmetric unit of ScA and AEI.	83
5.4.3.2	Chain structure involving monoanion 1.	83
5.4.3.3	Chain structure involving acid molecule 3 and dianion 5.	84
5.4.3.4	Chain structure involving monoanion 7.	84
5.4.3.5	Chain structure involving acid molecule 9 and dianion 10.	84
5.4.3.6	3-D network comprising of pairs of chains linked by the cations, viewed down the <i>a</i> -axis.	85
5.4.4.1	Hydrogen bonded anion chain with subtended cations and water molecules, viewed down the <i>a</i> -axis.	85
5.4.4.2	3-D network, viewed down the <i>b</i> -axis.	86
5.4.5.1	Ortep diagram for the asymmetric unit of FmA and AEI.	87
5.4.5.2	Acid-anion chain structure with cations subtended.	87
5.4.5.3	Arrangement of acid-anion chains, linked by hydrogen bonds from the cations.	88
5.5.1.1	Ortep diagram for the asymmetric unit of OxA and TEMED.	90
5.5.1.2	Chain structure, viewed down the <i>b</i> -axis (hydrogen bond distance error +/-0.018 Å).	91

5.5.1.3	Sheet viewed from above; the central chain is coloured red (the anions are viewed end-on) and the adjacent chains are blue; the linking water molecules are shown in light blue.	91
5.5.1.4	Stacking of sheets.	91
5.5.2.1	Hydrogen bonded tertiary unit.	92
5.5.2.2	Arrangement of tertiary units to form sheets; N-H...O hydrogen bonds shown in light blue, C-H...O hydrogen bonds shown in dark blue.	92
5.5.3.1	Sheet structure with anion-acid chains linked by cations.	93
5.5.3.2	Interlinking of cations of adjacent sheets, alternate sheets are coloured red and blue.	93
5.5.4.1	Ortep diagram for the asymmetric unit of GlA and TEMED.	94
5.5.4.2	Tape structure with cations linking anionic chains, hydrogen bond distances marked (hydrogen bond distance error +/-0.008 Å).	94
5.5.4.3	Tapes viewed end-on, C-H...O hydrogen bonds link tapes to form a 3-D network.	95
5.5.5.1	Ortep diagram for the asymmetric unit of DLTA and TEMED.	95
5.5.5.2	Anionic tape structure with hydrogen bonded cations.	96
5.5.5.3	Linking of tapes to form a sheet (edge of sheet is viewed here).	96
5.5.5.4	The 3-D structure with the sheets viewed side-on; the adjacent layers are coloured blue and red, the connecting water molecules are light blue.	96
5.5.6.1	Ortep diagram for the asymmetric unit of MeA and TEMED.	97
5.5.6.2	Hydrogen bonded triplet (hydrogen bond distance error +/-0.004 Å).	97
5.5.6.3	3-D network – units linked by C-H...O hydrogen bonds.	98
5.5.7.1	Hydrogen bonded chains of anions and acid molecules linked by hydrogen bonding across the cations to form a sheet.	98
6.2.1.1	Ortep diagram for the asymmetric unit of ScA and Pyr.	104
6.2.1.2	Hydrogen bonded chains are arranged into flat ‘sheets.’	105
6.2.1.3	Chain viewed end-on.	105
6.2.2.1	Ortep diagram for the asymmetric unit of FmA and Pyr.	106
6.2.2.2	Arrangement of chains into stacks that are at a different orientation to each other and non-parallel.	106
6.2.2.3	Hydrogen bonded chain viewed end-on.	106
6.3.1.1	Ortep diagram for the asymmetric unit of OxA and Idn.	108
6.3.1.2	Hydrogen bonded sheet structure made up of acid-base triplets (error +/-0.008 Å).	108
6.3.1.3	Stacking of sheets – bottom sheet is coloured blue, top sheet is red.	109
6.3.2.1	Stacking of sheets – bottom sheet is coloured blue, top sheet is red.	109
6.3.2.2	Arrangement of chains to form a non-hydrogen bonded ‘sheet’ (error +/-0.007 Å).	110
6.3.2.3	Stacking of ‘sheets.’	110
6.3.3.1	Ortep diagram for the asymmetric unit of ScA and Idn.	111
6.3.3.2	Hydrogen bonded sheet structure (error +/-0.002 Å).	111
6.3.3.3	Stacking of sheets; one sheet coloured blue, adjacent coloured red.	111
6.3.4.1	Ortep diagram for the asymmetric unit of GlA and Idn.	112
6.3.4.2	Hydrogen bonded chain of alternate acid and base molecules (error +/-0.003 Å).	112
6.3.4.3	V-shaped pairs of chains form stacks.	112
6.3.5.1	Ortep diagram for the asymmetric unit of AdA and Idn.	113
6.3.5.2	Sheet structure, hydrogen bond distances marked (error +/-0.004 Å).	113
6.3.5.3	Sheet viewed side-on.	113
6.3.5.4	Stacking of sheets, one coloured red, adjacent coloured blue.	114
6.3.6.1	Ortep diagram for the asymmetric unit of PmA and Idn.	114
6.3.6.2	Hydrogen bonded chain of alternate acid and base molecules (error +/-0.003 Å).	114
6.3.6.3	Stacking of chains so as acid and base molecules are adjacent.	115
6.3.7.1	Ortep diagram for the asymmetric unit of LTA and Idn.	115
6.3.7.2	Acid tape structure, hydrogen bond distances marked (error +/-0.002 Å).	116
6.3.7.3	Base molecules subtended from the acid tape.	116
6.3.7.4	Hydrogen bonded 3D network consisting of acid tapes linked by base molecules.	116
6.3.8.1	Ortep diagram for the asymmetric unit of DLTA and Idn.	117
6.3.8.2	Acid chains linked by hydrogen bonding across the base molecules, hydrogen bond distances marked (error +/-0.002 Å).	117

6.3.8.3	3-D network – acid molecules in chains are positioned directly over each other; viewed down the <i>a</i> -axis.	118
6.3.9.1	Ortep diagram for the asymmetric unit of MeA and Idn.	118
6.3.9.2	'Sheet' arrangement of hydrogen bonded chains with hydrogen bond distances marked on one chain (error +/-0.006 Å).	119
6.3.9.3	Stacking of sheets, bottom sheet is coloured red, the top is coloured blue.	119
6.3.10.1	Graph showing the melting point and packing indexes for the diacid-Idn co-crystals.	121
6.3.10.2	Graph showing the melting points of the Idn co-crystals and the free diacids.	122
6.5.1.1	Ortep diagram for the asymmetric unit of OxA and Mo.	124
6.5.1.2	Tape structure viewed down the <i>b</i> -axis with the four hydrogen bond distances marked (error +/-0.002 Å).	124
6.5.1.3	The sheet layout, viewed down <i>a</i> -axis.	124
6.5.1.4	Offset stacking of sheets, sheets viewed side-on down the <i>b</i> -axis.	125
6.5.2.1	Ortep diagram for the asymmetric unit of ScA and Mo.	125
6.5.2.2	Hydrogen bond unit of anions and cations, hydrogen bond distances marked (error +/-0.002 Å).	126
6.5.2.3	Bilayer arrangement, sheet viewed side-on down the <i>b</i> -axis; C-H...O hydrogen bond distances marked (dark blue); N-H...O hydrogen bonds (light blue).	126
6.5.3.1	Ortep diagram for the asymmetric unit of AdA and Mo.	127
6.5.3.2	The hydrogen bonded tape structure (error +/-0.006 Å), viewed down the <i>c</i> -axis.	127
6.5.3.3	The arrangement of tapes viewed down <i>a</i> -axis; C-H...O hydrogen bonds marked.	128
6.5.4.1	Ortep diagram for the asymmetric unit of DLTA and Mo.	128
6.5.4.2	Sandwich structure.	129
6.5.4.3	3-D network, pairs of chains viewed end-on.	129
6.5.5.1	Ortep diagram of the product from crystallisation of MeA and Mo in methanol.	130
6.5.6.1	Ortep diagram for the asymmetric unit of FmA and Mo.	130
6.5.6.2	Bilayer arrangement, sheet viewed side-on down the <i>b</i> -axis; N-H...O and C-H...O hydrogen bond distances marked (light blue and dark blue respectively; error +/-0.002 Å).	131
6.6.1	Graph to show distance and angle between donor and acceptor of base-base, acid-base, base-acid and acid-acid hydrogen bonds in Pyr and Idn structures.	134
7.2.1.1	The hydrogen bonded sheets of OxA-Im, viewed down the <i>c</i> -axis.	138
7.2.1.2	Stacking of the sheets with each sheet coloured alternately red and blue for clarity.	138
7.2.1.3	Undulation of the sheets with cations slightly protruding above and below the plane of the anions.	138
7.2.2.1	Ribbon structure, hydrogen bond distances N-H...O = 1.710 and 1.706 Å.	140
7.2.2.2	Stepped sheets viewed from the side (ribbons are viewed end-on and extend into the plane of the page); one sheet is coloured red and the other blue to show their interpenetration.	140
7.2.3.1	Sheet structure with cations linking chains of anions.	141
7.2.3.2	Stacking of sheets – the central sheet is coloured red and the sheets above and below are blue.	141
7.2.4.1	Sheet structure of AdA-Im with hydrogen bond distances marked, viewed down the <i>c</i> -axis.	142
7.2.4.2	Arrangement of sheets into pairs, viewed down the <i>a</i> -axis.	142
7.2.4.3	Arrangement of sheets, viewed down the <i>b</i> -axis.	142
7.2.5.1	Ortep diagram for the asymmetric unit of SbA and Im.	143
7.2.5.2	The hydrogen bonded sheets of SbA-Im consisting of anion chains linked by cations.	143
7.2.5.3	Arrangement of the sheets leads to the anion chains being stacked but with the molecules slightly offset along their length, viewed down the <i>a</i> -axis.	144
7.2.5.4	Second type of chain present in the structure (hydrogen bond distance error +/-0.002 Å).	144
7.2.5.5	The arrangement of the stepped SbA chain and the anion-cation sheets.	144
7.2.6.1	The 2-D anion network that creates a sheet with cations subtended; strong hydrogen bonds occur between the chains of anions running from left to right across the page; viewed down the <i>c</i> -axis.	145



7.2.6.2	3-D network created as sheets are linked via hydrogen bonding across the cations, hydrogen bond distances shown; viewed down the <i>a</i> -axis.	146
7.2.7.1	Ortep diagram for the asymmetric unit of DLTA and Im.	146
7.2.7.2	Hydrogen bonded anion network (O-H...O error +/-0.007 Å, N-H...O error +/-0.016 Å); the N-H...O hydrogen bond distances for the <i>b</i> position of the cation are 2.00(2), 2.15(2) and 2.31(2) Å.	147
7.2.7.3	Different directions of the chains of adjacent sheets.	147
7.2.8.1	MeA-Im quadruplet, hydrogen bond distances marked.	148
7.2.8.2	Tilted arrangement of the acid molecules in the quadruplet.	148
7.2.8.3	Arrangement of quadruplets, viewed down the <i>a</i> -axis.	149
7.2.9.1	Hydrogen bonded sheet of FmA-Im.	149
7.2.9.2	Sheets viewed side-on, C-H...O hydrogen bonds shown in dark blue, viewed down <i>a</i> -axis.	150
7.2.10.1	Schematic representations of the sheet structures of the diacid-Im products.	151
7.2.10.2	Graph to show the variation in melting point and density with carbon chain length of the Im products.	152
7.3.1.1	Ortep diagram for the asymmetric unit of OxA and 1MI.	153
7.3.1.2	N-H...O (light blue) and C-H...O (dark blue) hydrogen bonds between anions and cations.	153
7.3.2.1	Ortep diagram for the asymmetric unit of ScA and 1MI.	154
7.3.2.2	Sheets of anions and cations, held together by hydrogen bonds: N-H...O (light blue), C-H...O (dark blue).	154
7.3.2.3	Arrangement of adjacent sheets; the red sheet cations poke downwards filling the voids of the blue sheet below, and vice versa.	155
7.3.3.1	Ortep diagram for asymmetric unit of GlA and 1MI.	156
7.3.3.2	Sheet held together by hydrogen bonds; N-H...O light blue, C-H...O dark blue, O-H...O orange.	156
7.3.3.3	Arrangement of sheets; bottom sheet coloured blue, top sheet coloured red.	157
7.3.4.1	Hydrogen bonded anion lattice.	158
7.3.4.2	Anion lattice with cations subtended from one of the hydroxyl groups.	158
7.3.4.3	Zigzag formation of the anion backbone of the sheet.	158
7.3.5.1	Ortep diagram for the asymmetric unit of DLTA and 1MI.	159
7.3.5.2	Lattice arrangement of anion molecules, viewed down the <i>b</i> -axis (hydrogen bond distance error +/-0.002 Å).	159
7.3.5.3	Anion network with cations subtended from this, viewed down the <i>a</i> -axis.	160
7.3.6.1	Reaction of MeA and 1MI to form this zwitterion.	160
7.3.7.1	Schematic representations of the Sheet structures in the 1MI binary compounds.	161
7.4.1.1	Ortep diagram for the asymmetric unit of OxA and 2MI.	163
7.4.1.2	Hydrogen bonding of the dianions and cations (error +/-0.004 Å), viewed down the <i>b</i> -axis.	163
7.4.1.3	Stacking of sheets into pairs.	164
7.4.1.4	a) Arrangement of stacked sheets, viewed down the <i>b</i> -axis; b) sheets viewed side-on, down the <i>a</i> -axis.	164
7.4.2.1	Ortep diagram for the asymmetric unit of MnA and 2MI.	165
7.4.2.2	Hydrogen bonded chain of anions and cations, hydrogen bond distances marked (error +/-0.005 Å).	165
7.4.2.3	Orientation of chains in adjacent stacks – one stack is coloured red and the other is coloured blue, viewed down the <i>a</i> -axis.	165
7.4.3.1	Ortep diagram for the asymmetric unit of ScA and 2MI.	166
7.4.3.2	Sheet structure with the hydrogen bond distances marked (error +/-0.002 Å), viewed down the <i>b</i> -axis.	166
7.4.3.3	Stacking of the sheets – one layer is coloured blue and the adjacent layer is coloured red.	167
7.4.4.1	Ortep diagram for the asymmetric unit of GlA and 2MI.	167
7.4.4.2	Arrangement of molecules to form sheets (hydrogen bond distance error +/-0.004 Å).	168
7.4.4.3	Undulation of sheets, viewed side-on.	168
7.4.4.4	Arrangement of sheets.	168

7.4.5.1	Ortep diagram for the asymmetric unit of AdA and 2MI.	169
7.4.5.2	Hydrogen bonded sheet of anions, cations and water molecules, distances marked (error +/-0.003 Å).	169
7.4.5.3	Stacking of sheets, one coloured blue and adjacent coloured red.	170
7.4.6.1	Ortep diagram for the asymmetric unit of SbA and 2MI.	170
7.4.6.2	The hydrogen bonded sheet, O-H...O hydrogen bonds shown in orange, N-H...O shown in light blue (distances marked, error +/-0.003 Å), C-H...O shown in dark blue.	171
7.4.6.3	Step formation of the sheets, viewed down the <i>b</i> -axis.	171
7.4.7.1	Hydrogen bonded sheet structure.	172
7.4.7.2	Sheet viewed side-on to see the arrangement of the 3-D network; the middle sheet is coloured blue.	172
7.4.8.1	Ortep diagram for the asymmetric unit of DLTA and 2MI.	173
7.4.8.2	2-D lattice of hydrogen bonded anions (error +/-0.003 Å).	173
7.4.8.3	3-D network with sheet viewed side-on; the linking of the sheets by hydrogen bonding across the base molecules can be seen, viewed down the <i>a</i> -axis.	173
7.4.9.1	Ortep diagram for the asymmetric unit of FmA and 2MI.	174
7.4.9.2	Sheet structure, O-H...O hydrogen bonds shown in orange, N-H...O in light blue, C-H...O in dark blue (hydrogen bond distance error +/-0.004 Å).	174
7.4.9.3	Stacking of sheets; one sheet is coloured red, the adjacent is coloured blue.	175
7.4.10.1	Graph to show the variation in melting point and density with carbon chain length of the 2MI binary compounds.	176
7.4.10.2	Schematic representation of the sheet structures found in some of the 2MI binary compounds.	176
7.5.1.1	Ortep diagram for the asymmetric unit of OxA and 4MI.	177
7.5.1.2	Hydrogen bonded arrangement where one anion is hydrogen bonded to the surrounding four cations and two water molecules (hydrogen bond distance error +/-0.002 Å).	178
7.5.1.3	Arrangement of sheets linked by hydrogen bonding across water molecules.	178
7.5.2.1	Ortep diagram for the asymmetric unit of ScA and 4MI.	179
7.5.2.2	Hydrogen bonded chain structure, hydrogen bond distances marked (error +/-0.002 Å), C-H...O hydrogen bond examples shown in dark blue.	179
7.5.2.3	3-D network, one chain is highlighted; it can be seen that each of the cations are shared between two chains.	180
7.5.3.1	Ortep diagram for the asymmetric unit of GlA and 4MI.	180
7.5.3.2	Sheet arrangement containing both types of hydrogen bonded anion chain bridged by cations, hydrogen bond distances marked (error +/-0.005 Å).	181
7.5.3.3	Stacking of the sheets so as the different types of chains are next to each other – the central sheet is coloured red and the sheets above and below are coloured blue.	181
7.5.4.1	Ortep diagram for the asymmetric unit of SbA and 4MI.	182
7.5.4.2	Hydrogen bonded sheet viewed down the <i>b</i> -axis, hydrogen bond distances marked (error +/-0.004 Å).	182
7.5.4.3	Stacking of the sheets so as the methyl groups on the cations fill the voids in the adjacent pair of sheets.	183
7.5.5.1	Ortep diagram for the asymmetric unit of LTA and 4MI.	183
7.5.5.2	Anion lattice, hydrogen bond distances marked (error +/-0.003 Å).	184
7.5.5.3	Anion lattice with hydrogen bonded cations subtended.	184
7.5.5.4	Anion and cation hydrogen bonded lattice.	185
7.5.6.1	Ortep diagram for the asymmetric unit of DLTA and 4MI.	185
7.5.6.2	Tape structure with subtended water molecules, N-H...O and O-H...O hydrogen bond distances marked (error +/-0.004 Å).	186
7.5.6.3	3-D network made up of anion-cation ladders linked by water molecules.	186
7.5.7.1	Ortep diagram for the asymmetric unit of MeA and 4MI.	187
7.5.7.2	Hydrogen bonded sheet; N-H...O light blue, C-H...O dark blue, O-H...O orange.	187
7.5.7.3	Stacking of units - units form sheets, one is coloured red, the adjacent is coloured blue.	187
7.6.1.1	Ortep diagram for the asymmetric unit of ScA and DMI.	189

7.6.1.2	Chain structure with the anion backbone and subtended cations (hydrogen bond distance error $\pm 0.003$ Å).	190
7.6.1.3	Arrangement of the chains into pairs which are linked by C-H...O hydrogen bonds.	190
7.6.2.1	Ortep diagram for the asymmetric unit of GIA and DMI.	191
7.6.2.2	The hydrogen bonded chain of anions and cations (error $\pm 0.006$ Å).	191
7.6.2.3	Arrangement of the chains into stacks and the orientation of adjacent stacks, viewed down the <i>b</i> -axis.	192
7.6.3.1	Ortep diagram for the asymmetric unit of LTA and DMI.	192
7.6.3.2	Hydrogen bonded lattice of anions (error $\pm 0.003$ Å), viewed down the <i>c</i> -axis.	193
7.6.3.3	Two adjacent sheets (coloured red and blue) viewed side-on with cations subtended either side of the anion core, viewed down the <i>a</i> -axis.	193
7.6.4.1	Ortep diagram for the asymmetric unit of DLTA and DMI.	194
7.6.4.2	Anion lattice, hydrogen bond distances marked (error $\pm 0.006$ Å).	194
7.6.4.3	Sheet structure with cations subtended.	195
7.6.4.4	Arrangement of sheets viewed end-on (down the <i>a</i> -axis); each sheet is coloured differently, the interdigitating cations of adjacent tapes stack on top of each other.	195
7.6.5.1	Ortep diagram for the asymmetric unit of FmA and DMI.	196
7.6.5.2	Sheet structure of hydrogen bonded anions and cations, O-H...O orange, N-H...O light blue, C-H...O dark blue.	196
7.6.5.3	Stacking of 'sheets', one is coloured red, the adjacent are coloured blue.	197
7.7	Tree diagram showing the relationships between the schematic sheet structures in the Im derivative binary compounds.	199
7.7.1	Graph to show the variation in melting point with the Im derivative, 1 = Im, 2 = 1MI, 3=2MI, 4=4MI, 5=DMI. The points are not actually related and the fact that they are joined is purely for clarity when viewing the trends for each diacid.	200
8.3.2.1	Hydrogen bonding arrangements for an OxA dianion and neutral molecule. Diagrams for <i>a</i> and <i>b</i> are purely skeletal – hydrogens and charges are not included, nor are double bonds.	210
8.4.3.1	Variation of the angle between planes of COO(H) groups with the number of carbons in the diacid chain.	213

## LIST OF TABLES

<b>2.6.1</b>	Chosen diacids together with some properties ( $pK_a$ values from ACD/I-Lab: literature $pK_a$ values were used where possible, the remainder were calculated); crystal structures are available on the CSD (refcodes given).	<b>23</b>
<b>2.6.2</b>	Chosen bases and some properties ( $pK_a$ values from ACD/I-Lab: literature $pK_a$ values were used where possible, the remainder were calculated); the cif files for Idn and 2MI are available on the Appendix CD, the others are available on the CSD (refcodes given).	<b>27</b>
<b>3.2.2</b>	Crystal systems with their cell parameters and constraints	<b>35</b>
<b>5.1</b>	Observations of the well-plate products for the acid-base combinations containing aliphatic amines and their appropriate method of analysis.	<b>51</b>
<b>5.2.10</b>	Various structural and physical parameters of the diacid-TMBA structures (Note: 'Me' in formula column indicates methylation of one of the carboxyl groups).	<b>68</b>
<b>5.3.10</b>	Various structural and physical parameters of the diacid-DAE structures.	<b>78</b>
<b>5.4.6</b>	Various structural and physical parameters of the diacid-AEI structures.	<b>88</b>
<b>5.5.8</b>	Various structural and physical parameters of the diacid-TEMED structures.	<b>99</b>
<b>6.1</b>	Observations of the well-plate products for the acid-base combinations involving nitrogen-containing heterocycles and their appropriate method of analysis.	<b>103</b>
<b>6.2.3</b>	Various structural properties of the ScA-Pyr and FmA-Pyr co-crystals.	<b>107</b>
<b>6.3.10</b>	Table of the crystal structure descriptions and properties for the simple diacid co-crystals.	<b>120</b>
<b>6.5.7</b>	Some of the structure properties for each of the salt structures and the possible binary product with SbA.	<b>132</b>
<b>7.1</b>	Observations of the well-plate products for the acid-base combinations containing Im derivative bases and their appropriate method of analysis.	<b>136</b>

## DECLARATION OF AUTHORSHIP

I, Samantha Callear, declare that the thesis entitled:

**Preparation, Characterisation and Structural Assessment of Salts and Co-Crystals of Organic Compounds**

and the work presented in it are my own and have been generated by me as the result of my own original research. I confirm that:

- this work was done wholly while in candidature for a research degree at this University;
- where I have consulted the published work of other this is always clearly attributed;
- where I have quoted from the work of others, the published source is always given. With the exception of such quotations this thesis is entirely my own work;
- I have acknowledged all main sources of help;
- where the thesis is based on work done by myself jointly with others, I have made clear exactly what was done by others and what I have contributed myself;
- none of this work has been published before submission.

**Signed:** .....

**Date:** .....

## ACKNOWLEDGEMENTS

I would first of all like to thank my supervisor Mike Hursthouse for giving me the opportunity to undertake an enjoyable and exciting piece of research. His support and guidance throughout have been invaluable. I extend my gratitude to everyone at the NCS, for their informative discussions, insights and running my trickier samples at Daresbury. I would particularly like to thank Pete Horton, who was always available to help me solve the more difficult structures. I would also like to thank the X-ray crystallography group, members both past and present, for their support and ‘informative’ chats!

---

## ABBREVIATIONS

OxA	Oxalic Acid
MnA	Malonic Acid
ScA	Succinic Acid
GlA	Glutaric Acid
AdA	Adipic Acid
PmA	Pimelic Acid
SbA	Suberic Acid
TAs	Tartaric Acids
LTA	L-Tartaric Acid ((R,R)-(+)-tartaric acid)
DTA	D-Tartaric Acid ((S,S)-(-)-tartaric acid)
DLTA	DL-Tartaric Acid ((S,S/R,R)-(+/-)-tartaric acid)
MeA	Maleic Acid
FmA	Fumaric Acid
TMBA	1,1,3,3-Tetramethylbutylamine
DAE	1,2-Diaminoethane
AEI	2-Aminoethanol
TEMED	Tetramethylethylenediamine
Pyr	2-Pyrrolidinone
Idn	2-Imidazolidinone
DMIdn	1,3-Dimethylimidazolidinone
Mo	Morpholine
Im	Imidazole
1MI	1-Methylimidazole
2MI	2-Methylimidazole
4MI	4-Methylimidazole
DMI	1,2-Dimethylimidazole
API	Active pharmaceutical ingredient

## CHAPTER 1

### The Organic Solid State

#### 1.1 INTRODUCTION

Organic crystals consist of molecules held together in a periodic arrangement by a variety of interactions. Some interactions are short-range and directional (e.g. hydrogen bonds), others are longer range and formally non-directional (e.g. van der Waals), but all are involved in molecular recognition and complexation. The physical, and sometimes chemical, properties of the actual solid forms are derived from the often complex interplay between the various interactions present. This thesis is concerned with a study of the interactions in solid forms of a particular class of compounds, in which two chemically different components are present. Before discussing these, however, it is relevant to consider the nature of the interactions that can be present in solid forms, so that the interplay between the different types can be better assessed. It is also pertinent to consider the influence of different forces on the selection of procedures for the preparation of solid forms.

#### 1.2 INTERMOLECULAR INTERACTIONS

Intermolecular and interionic interactions are responsible for the cohesion of crystal structures and solid-state properties. The potential energy of a crystal can be attributed to various kinds of interactions including ion-ion, ion-dipole, dipole-dipole, hydrogen bonding,  $\pi$ - $\pi$  interactions and van der Waals. By balancing the attractive forces that bring the molecules from infinite separation to mutual contact and the repulsive forces that are minimised by the molecular packing, an equilibrium structure is produced. In Desiraju's highly regarded book, 'The Crystal as a Supramolecular Entity,'<sup>1</sup> he separates intermolecular interactions into two types:

- Isotropic – medium range forces which define molecular shape, size and close packing.
- Anisotropic – including ionic forces, directional hydrogen bonds (strong and weak) and other weak forces involving halogens.



However, as is often the case with attempts to rigidly compartmentalise features or events, the borderlines are actually very soft due to the complexity of the situation. For example, ionic interactions can also be considered isotropic interactions when spherical ions are considered.

### 1.2.1 *Van der Waals Interactions and Close Packing*

These are isotropic dispersive and repulsive forces; dispersive forces are attractive in nature and result from the interaction between fluctuating multipoles in adjacent molecules. Repulsive forces define molecular shape and balance the dispersive forces at short range. Kitaigorodskii's close packing principle<sup>2,3</sup> follows from the atom-atom potential method<sup>3,4</sup> that is a trade off between the repulsive and dispersive forces and includes a contribution from electrostatic forces. Thus the molecules in crystals tend to fill space as tightly as possible with the 'bumps' of one molecule fitting into the 'hollows' of adjacent molecules. Brock and Dunitz<sup>5</sup> note that this idea that the complementarity of molecular surfaces governs crystal stability dates back to 1940. Kitaigorodskii's principle assumes that molecules in a crystal tend towards equilibrium positions as the potential energy of a system is minimised i.e. the number of intermolecular contacts is maximised. The close packing principle generally holds well for hydrocarbons, however, structures with strong hydrogen bonds may have more open arrangements due to the strongly directional nature of the interactions.

### 1.2.2 *Hydrogen bonding*

References to the concept of hydrogen bonding date back to the early 1900's, however the definition of a hydrogen bond is still debated due to the complexity of the phenomenon.<sup>6</sup> A traditional starting point is provided by Pauling who defines a hydrogen bond as the largely ionic interaction formed between two electronegative atoms where the hydrogen atom is attracted to both of the atoms thus acting as a bond between them.<sup>7</sup> This definition therefore includes N-H...O, O-H...O and F-H...F hydrogen bonds where the donors and acceptors are activated. In the last 50 years evidence has been found for further examples of hydrogen bonding such as C-H...O and O-H... $\pi$  which are now universally accepted, however they would not be included in Pauling's definition. Accordingly, Pimental and McClellan further developed a definition: 'a hydrogen bond is said to exist when (1) there is evidence of a bond and (2) there is evidence that this bond sterically involves a hydrogen atom already bonded to another atom.'<sup>8</sup> In a monograph by Desiraju and Steiner it is noted that the deshielding of a hydrogen atom, that occurs due to its single electron being involved in a covalent bond, is irrespective of the nature of the donor atom.<sup>9</sup> This further supports Pimental and McClellan's phenomenological definition that includes weak hydrogen bonds which may otherwise be excluded on energetic grounds. Considering the chemical

connotations of the word bond, it has also been suggested that the term hydrogen bridge may be more suitable for the phenomenon than 'hydrogen bond.'<sup>10</sup> Although there are functional, geometrical, energetic and spectroscopic versions of the definition, the geometrical definition will be used here as this is the most relevant to how the hydrogen bonding interactions will be studied. The hydrogen bond  $X-H\cdots A$  consists of a donor  $X$  and an acceptor  $A$  and is described in terms of  $d$ ,  $D$ ,  $\theta$  and  $r$  (Figure 1.2.2.1). For a typical hydrogen bond,  $X\cdots A$  distances are shorter than the sum of the van der Waals radii (i.e. for  $O\cdots O$ ,  $D < 3.10 \text{ \AA}$  and for  $N\cdots O$ ,  $D < 3.25 \text{ \AA}$ ;  $\theta > 90-120^\circ$ ).

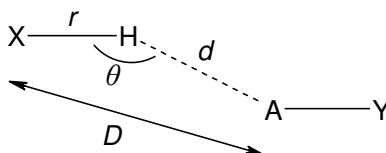


**Figure 1.2.2.1** Geometrical terms of a hydrogen bond

Hydrogen bonding is the most reliable anisotropic interaction in supramolecular recognition and crystal engineering. It is particularly important due to its prevalence and combination of strength and directionality. The strength of a hydrogen bond contributes cohesion and stability to a solid and the directionality of the bond allows topological control and selectivity. This latter property is particularly useful as it gives reproducibility to the interactions and subsequent crystal structure, thus opening up the field of crystal structure prediction. Being of intermediate energy, hydrogen bonds can also be easily broken and formed. A hydrogen bond is complex as it involves at least three atoms; bifurcated and trifurcated hydrogen bonds consist of one donor and hydrogen atom, and two or three acceptor atoms respectively. It is also composite in nature as its main constituents are electrostatic, covalency, dispersion-repulsion and polarisation. It is widely agreed that the interaction is predominantly electrostatic in nature with an  $r^{-1}$  to  $r^{-3}$  ( $r$  = radius) energy-distance dependence so that dipole-dipole interactions are included.

Strong hydrogen bonds, or hard hydrogen bonds, involve a highly electronegative hydrogen bond donor which removes electron density from the hydrogen atom leaving it with a significant positive charge. The resulting coulombic interaction with an electronegative acceptor atom generally has a bond energy of  $20-40 \text{ kJ mol}^{-1}$ , e.g.  $O-H\cdots O$  and  $N-H\cdots O$  interactions. Typically  $D\cdots A$  is significantly less than the sum of the van der Waals radii ( $D(O\cdots O) < 2.80 \text{ \AA}$  and  $D(N\cdots O) < 2.95 \text{ \AA}$ ), however, the distances are further influenced by their environment and these values are merely guides. The geometry of the interaction is also important as the more linear the interaction, the stronger it is. Other characteristics of a strong hydrogen bond include:

- symmetric charge distribution,
- significant lengthening of the covalent O-H bond resulting in the proton being located near the centre of  $X\cdots A$ ,
- significant shortening of the  $O\cdots O$  distance,

- lengthening of the C-O bond distance of the acceptor on an anion compared to the C-O bond distance of the moiety not participating in the near linear interaction (see Figure 1.3.2.2).

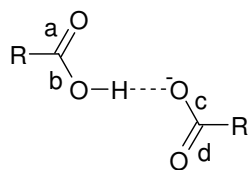


**Figure 1.2.2.2** C-O and C=O bond distances: for strong hydrogen bonds the difference between c and d is greater than that for normal hydrogen bonds. Theoretically, for a carboxylate group that is not hydrogen bonded  $c=d$ , however hydrogen bonds and other interactions act to lengthen the C-O bonds.

Some very strong hydrogen bonds involve a single-minimum potential energy well or a double well with a small barrier and are therefore referred to as symmetric or low-barrier hydrogen bonds.<sup>11</sup> Such interactions usually involve charged species between which a proton is shared. The position of the hydrogen between the donor and acceptor is therefore indicative of the presence of a very strong hydrogen bond. Crystallographic data from SXR D can give an indication of the presence of a strong hydrogen bond through the disorder of a hydrogen atom across the donor and the acceptor, however, the precise location of the hydrogen atom cannot be accurately determined. This requires neutron diffraction data for which the large neutron scattering power of the hydrogen atom nuclei means that it can be located with the same accuracy as many heavier atoms.

Weak hydrogen bonds, or soft hydrogen bonds, have a bond energy of  $2\text{--}20\text{ kJ mol}^{-1}$ , e.g.  $\text{C-H}\cdots\text{O}$  and  $\text{O-H}\cdots\pi$  interactions. Typical  $\text{H}\cdots\text{O}$  distances are between  $2.20\text{--}3.00\text{ \AA}$ .  $\text{C-H}\cdots\text{O}$  is primarily an electrostatic interaction therefore strength decreases over distance more slowly than in a van der Waals interaction and hence distances longer than or equal to the van der Waals limit are viable. Weak hydrogen bonds are thought to have orientating effects prior to nucleation and crystallisation.  $\text{C-H}\cdots\text{O}$  and  $\text{O-H}\cdots\pi$  hydrogen bonds have hardly any covalent character and are only marginally electrostatic.  $\text{C-H}\cdots\pi$  interactions are rarer than  $\text{O-H}\cdots\pi$  because carbon is not as electronegative as oxygen and carbon is also not commonly situated in a sterically unhindered position. However, a sufficiently electron rich carbon atom such as one involved in a  $\pi$ -system can form a hydrogen bond like interaction. There was some debate as to whether  $\text{C-H}\cdots\pi$  interactions are actually hydrogen bonds, however, and evidence has been found that they have residual electrostatic character in spite of being mainly dispersive-repulsive in nature.<sup>12</sup>

The general rules for the packing of hydrogen bonded molecules in crystals were developed by Etter<sup>13-15</sup> who expanded on Donohue's rule that all available acidic hydrogen atoms participate in hydrogen bonds in the solid state.<sup>16</sup> The main rules that are not specific to certain systems are:

- all good proton donors and acceptors are used in hydrogen bonding
- six-membered ring intramolecular hydrogen bonds form in preference to intermolecular hydrogen bonds

- the best proton donors and acceptors remaining after intramolecular hydrogen bond formation will form intermolecular hydrogen bonds.

### 1.2.3 Other Anisotropic Interactions

Halogens such as Cl, Br and I form short non-bonded interactions; there is some debate as to the origin of the interaction: Nyburg<sup>17</sup> and Price<sup>18</sup> hold that they are the result of the elliptically shaped atoms (anisotropy) whereas Desiraju<sup>19</sup> and others<sup>20, 21</sup> maintain there are special attractive forces between halogen atoms in crystals. The clear distinctions between symmetrical (Cl-Cl) and unsymmetrical (Cl-Br) interactions indicate that atomic polarisation is a factor.

$\pi$ - $\pi$  interactions occur between aromatic sections of molecules due to their polarisable  $\pi$ -electron density that enhances the stabilising dispersion interactions between the aromatic molecules. There is also an electrostatic component of the intermolecular stabilisation that provides directionality thus making the interaction anisotropic. A multipole is introduced by the small polarisation of the C-H bonds in an aromatic hydrocarbon; the hydrogen atoms are slightly positive relative to the slightly negative  $\pi$ -bonded core. Favourable orientation of the relatively positive and negative sections of the molecule commonly results in offset face-to-face and edge-to-face motifs. It should be noted that a  $\pi$ -stack is only said to occur when there are more than two molecules involved.

## 1.3 CRYSTALLISATION

In the purification of an organic compound and production of a solid form by crystallisation, the process involves successive growth from a nucleation centre to form a crystal. The final form of the crystal is determined by the manner of crystal growth which is directed by the conditions of the crystallisation system.<sup>22</sup>

Crystal growth from a supersaturated solution is a common method used in both research and industry. The term 'supersaturation' describes a solution that is at a higher concentration than the saturation value. 'Saturation' is defined as the state of a system where the solid is in equilibrium with the solution therefore the solution will neither dissolve crystals nor let them grow. The concentration of a solution at saturation represents the solubility for a particular crystal phase at a given temperature and pressure.

Supersaturation is required for crystal growth;<sup>23</sup> it can be achieved by a number of methods such as evaporation of solvent, cooling the solution from a known initial supersaturation, addition of a poor solvent, chemical reaction between two or more soluble species or variation of pH. The first

process in crystal growth is the assembly of ordered molecules into viable nuclei – nucleation. A critical number of ordered molecules per assembly is required to prevent dissolution and hence form a viable nucleus. This is due to the surface area of a spherical body increasing with radius squared whereas volume increases with radius cubed; therefore as the radius of the assembly increases the surface forces (solvent-solute interactions) acting to pull it apart become less significant than the internal bonds acting to hold it together.

Supersaturation is a driving force for crystallisation as it boosts the nucleation process. Nucleation is more energetically demanding than crystal growth; it is a complex process that is influenced by a number of factors and is therefore difficult to control. Secondary nucleation involves further crystallisation after initial crystals are formed. It is affected by agitation, temperature and concentration gradients, friable (breakable) crystal form or habit, and crystal irregularities caused by impurities. Nucleation events determine the number of particles and the crystal form resulting from a crystallisation procedure.<sup>24</sup>

### *1.3.1 The Role of Temperature and Solvent*

If crystallisation conditions induce thermodynamic control then the nature of the solvent is irrelevant with respect to the form of the polymorph produced, provided the solubility is adequate to allow the prescribed concentrations to be reached.<sup>25</sup> Under kinetic control, however, the type of solvent can influence crystal growth through solvent-solute interactions at a molecular level. Whether the role played by solvent-solute interactions is enhancing or inhibitory in crystal growth is still under examination. One theory is that the solvent can facilitate favourable interactions on specific growing faces which lead to reduced interfacial tension and improved speed of crystal growth.<sup>26</sup> Conversely, it has also been proposed that if the solvent and solute molecules are strongly bonded at a specific face the rate limiting step of growth at that face will be the removal of the solvent. This additional energy barrier results in the bonded face growing slowly or not at all.<sup>27</sup> Studies into the effect of additives on crystal morphology and growth support this theory.<sup>28</sup>

The temperature of a system affects a number of elements of crystal growth from diffusion of molecules from the bulk to the crystal surface, to the solubility.

### *1.3.2 Crystallisation Techniques*

There are a number of techniques that are used for the purification of substances that include both solution and solid phase methods:

- Slow evaporation – this is perhaps the most widely used method for growing single crystals. A solution of the compound is left to evaporate slowly by covering with a perforated lid; evaporation of the solvent takes the mixture to supersaturation, where crystals start to form. Continued evaporation provides a continual source of solute molecule to add to the growing faces. Crystal quality is better when the evaporation occurs slowly due to the laws of thermodynamics; the levels of entropy induced defects are lower the slower the crystal grows. Solvent selection is important as different solvents can result in different products. This technique is also applicable for high-throughput screening as most of the work can be performed by a robot and a well-plate can be used as the crystallisation vessel.

- Crystallisation by cooling – this technique is effective as usually solubility decreases with temperature. The compound is heated in a solvent to dissolve it and then the system is allowed to cool, preferably slowly, thus forming crystals.

- Mixed solvents – this involves two solvents, one of which the compound is readily soluble in (the ‘good’ solvent) and another in which it is mostly insoluble (the ‘poor’ solvent). The compounds are first dissolved in the ‘good’ solvent then the ‘poor’ solvent is added dropwise with a pipette causing the solute to crystallise out.

- Layered solvents – this technique is based on the fact that solvents of substantially different densities mix remarkably slowly when they are not stirred. The compound is dissolved in the ‘good’ solvent and then a top layer of the ‘poor’ solvent is added slowly. The layered solvents are left for several days for the layers to mix, during which the slow diffusion across the solvent boundary results in crystals.

- Seeding – a seed crystal of the same or a similar material is added to a supersaturated solution in order to induce the growth of single crystals of a certain form as the solution evaporates.

- Slurry – a small amount of solvent is added to a compound (so that the compound does not dissolve completely) and the mixture is stirred, often at elevated temperatures, for at least twenty-four hours.

- From melts – this method is only successful if the compounds are sufficiently thermally stable and do not decompose on, or near, melting. It is also important to carefully control the cooling rate to ensure good crystal growth. This method is commonly used to grow crystals of high temperature solids but has recently become popular for the synthesis of low temperature molten salts.

- Sublimation – if a compound is sufficiently volatile at accessible vacuum pressures it can be crystallised. This technique is often used in the purification of crude mixtures.

### 1.3.3 Crystallisation and Polymorphism

Solid pure compounds may occur with several distinct and isolable crystal structures known as polymorphs rather than in one unique crystal structure.<sup>29</sup> A polymorph is generally defined as ‘a

solid crystalline phase of a given compound resulting from the possibility of at least two crystalline arrangements of the molecules of that compound in the solid state.<sup>30</sup> The first observation of polymorphism was published by Wöhler and Liebig<sup>31</sup> in 1832 on the changing morphology of benzamide crystals and since then the property has been widely investigated. There are two types of polymorphs: monotropes where the transition from the metastable polymorph to the more stable polymorph is irreversible, and enantiotropes where the reversible transition between the polymorphs can be achieved by heating or cooling.

In the liquid or gaseous phases a polymorphic compound will display the same properties, yet in the solid state different polymorphs may exhibit different physicochemical properties such as melting, solubility, dissolution rate, stability, etc. As the link between molecular conformation and physicochemical properties can be seen clearly in polymorphic compounds, the effect of different structural patterns and molecular packing on the properties of different polymorphs of a compound can be explored.

At a specific temperature and pressure only one polymorph of a given compound is thermodynamically stable and all other polymorphs are metastable to varying degrees. The nuclei of different polymorphs have unique structural and interfacial properties; their free energies of activation differ and hence the nucleation rates of different polymorphs of the same compound generally differ. Consequently conditions may favour the nucleation of a metastable polymorph over that of a more stable (less soluble) polymorph, thus crystallisation of the former will be favoured. The observation that an unstable form is frequently obtained first then subsequently transforms into a stable form can be explained by Ostwald's rule of stages.<sup>32</sup> This is a manifestation of the interplay between the thermodynamic and kinetic factors operating in a system; it can be stated, 'in all processes, it is not the most stable state with the lowest amount of free energy that is initially formed, but the least stable state lying nearest in free energy to the original state.'<sup>33</sup>

Concomitant polymorphs arise when kinetic factors prevent achievement of equilibrium in a given crystallisation where different crystal structures co-exist.<sup>34</sup> This results in a mixture of crystal forms being produced. Polymorph selection can be achieved, for example, by the use of solvents or additives which inhibit the growth of a stable polymorph over that of the metastable form of a system.

During the investigation of polymorphism through the use of solution crystallisation, it was also found that the solvent itself could become a component of the crystalline form obtained. Such products were often called pseudopolymorphs but this term has recently lost its usage in favour of more specific names, solvates and hydrates.<sup>35-38</sup> In these multi-component systems the solvent can either be an integral part of the hydrogen bonded framework or it can occupy a cavity in the crystal in which case a sub-descriptor, clathrate, is used.

## 1.4 MULTI-COMPONENT SYSTEMS

As alluded to earlier, solid forms include not only pure single compounds but also mixed systems comprising a focus molecule plus some other component or components. The intermolecular interactions in these mixed systems can be varied and there is currently much debate over the nomenclature for crystals containing more than one component. In general, the naming is linked closely to the nature of the identities and interactions between the components. Historically, a *salt* is the ionic product formed from the neutralisation reaction of an acid and a base. Thus the integral feature of this type of multicomponent crystal is the transfer of a proton from the acid to the base. When there is no such transfer and the components are instead present in the crystal as neutral entities, the product is generally defined as a *co-crystal*. Indeed, salts and co-crystals are considered to be the two extremes of a continuum of multi-component structures.<sup>39-41</sup> This will be discussed further in the next chapter.

Desiraju objects to the use of the term co-crystal, saying that co-crystal suggests a crystal together with a crystal, i.e. a composite crystal, and that a multicomponent crystal should be referred to as a molecular crystal.<sup>42</sup> Dunitz counters this in his article on the subject: the term co-crystal ‘encompasses molecular compounds, molecular complexes, hydrates, solvates, inclusion compounds, channel compounds, clathrates and possibly other types of multicomponent crystals.’<sup>43</sup> This idea that hydrates and solvates are a subset of the term co-crystals is echoed by Stahly, who notes that a classification ‘based on structure is superior to one based on frequency of observance or the nature of one of the components.’<sup>39</sup> Aakeröy suggests that a possible characteristic of a co-crystal is having components that are solids at ambient temperature<sup>44</sup> thus excluding hydrates and solvates. This causes problems for systems where two compounds are co-crystallised together that are either both liquid at ambient temperature or solid and gas at ambient temperature, as noted by Bond.<sup>45</sup> Further to this Stahly also writes that the ‘nomenclature [should] be based on unambiguous properties of the multicomponent crystals themselves, not on some unrelated property of one of the components.’<sup>39</sup> The separation of co-crystals from solvates and hydrates is also contested by Bernstein who suggests that co-crystals should be named as such not according to the phase of the components at ambient temperature but according to the intent or ‘element of design.’<sup>46</sup> It has even been proposed that the situation should be further complicated with the subset of ‘pharmaceutical co-crystal’ where all components are solid at ambient temperature and one component is an active pharmaceutical ingredient (API).<sup>47</sup> In his review of the term, Bond recommends that co-crystal should be used merely as a synonym for ‘multi-component molecular crystal.’<sup>45</sup> However, the dispute is not only limited to the definition and instead extends to whether the word should be spelt co-crystal or cocrystal.<sup>39, 43</sup>



In light of this debate a multicomponent crystal where there is no hydrogen transfer between the components will be called a *co-crystal* in this study. Multicomponent crystals that also contain water molecules will be named as *salt hydrates* or *co-crystal hydrates* accordingly. Systems in which there is proton transfer between some of the components while other components remain neutral will be classified as *mixed systems*.

## References

1. G. R. Desiraju, *The Crystal as a Supramolecular Entity, Perspectives in Supramolecular Chemistry, Vol. 2*, Wiley: Chichester, 1995.
2. A. I. Kitaigorodskii, *Organic Chemical Crystallography*, Consultants Bureau: New York, 1961.
3. A. I. Kitaigorodskii, *Molecular Crystals and Molecules*, Academic Press: New York, 1973.
4. A. J. Pertsin, A. I. Kitaigorodskii, *The Atom-Atom Potential Method*, Springer-Verlag: Berlin, 1987.
5. C. P. Brock, J. D. Dunitz, *Chem. Mater.*, 1994, **6**, 1118-1127.
6. G. R. Desiraju, Hydrogen Bonding, in *Encyclopaedia of Supramolecular Chemistry*; J. L. Atwood, J. W. Steed (Eds), Marcel Dekker: New York, 2004, 658-665.
7. L. Pauling, *The Nature of the Chemical Bond*, Cornell University Press: Ithaca, 1939.
8. G. C. Pimental, A. L. McClellan, *The Hydrogen Bond*, W.H. Freeman: San Francisco, 1960.
9. G. R. Desiraju, T. Steiner, *The Weak Hydrogen Bond in Structural Chemistry and Biology*, Oxford University Press: New York, 1999.
10. G. R. Desiraju, *Acc. Chem. Res.*, 2003, **35**, 565-573.
11. C. B. Aakeröy, Strong Hydrogen Bonds, in *Encyclopaedia of Supramolecular Chemistry*; J. L. Atwood, J. W. Steed (Eds), Marcel Dekker: New York, 2004, 1379-1386.
12. M. Nishio, *CrystEngComm*, 2004, **6**, 130-158.
13. M. C. Etter, *J. Am. Chem. Soc.*, 1982, **104**, 1095-1096.
14. M. C. Etter, *J. Phys. Chem.*, 1991, **95**, 4601-4610.
15. M. C. Etter, *Acc. Chem. Res.*, 1990, **23**, 120-126.
16. J. Donohue, *J. Phys. Chem.*, 1952, **56**, 502-510.
17. S. C. Nyburg, W. Wong-Ng., *Proc. R. Soc. London, Ser A.*, 1979, **367**, 29-45.
18. S. L. Price, A. J. Stone, J. Lucas, R. S. Rowland, A. Thornley, *J. Am. Chem. Soc.*, 1994, **116**, 4910-4918.
19. G. R. Desiraju, R. Parthasarathy, *J. Am. Chem. Soc.*, 1989, **111**, 8725-8726.
20. V. R. Pedireddi, D. S. Reddy, B. S. Gould, D. C. Craig, A. D. Rae, *J. Chem. Soc. Perkin Trans. 2*, 1994, 2353-2360.
21. D. E. Williams, L.-Y. Hsu, *Acta Crystallogr., Sect. A*, 1985, **41**, 296-301.
22. G. R. Desiraju, *Crystal Engineering: The Design of Organic Solids*, Elsevier: Amsterdam, 1989.
23. H. E. Buckley, *Crystal Growth*, John Wiley & Sons, Inc.: New York, 1951.
24. R. J. Davey, K. Allen, N. Blagden, W. I. Cross, H. F. Lieberman, M. J. Quayle, S. Righini, L. Seton, G. J. T. Tiddy, *CrystEngComm*, 2002, **4**, 257-264.
25. T. Threlfall, *Org. Pro. Res Dev.*, 2000, **4**, 384-390.
26. P. Bennema, G. Gilmer, *Crystal Growth: An Introduction*, P. Hartman (Ed.), North-Holland Publishing Co.: Amsterdam, 1973.
27. S. Rohani, S. Horne, K. Murthy, *Org. Process Res. Dev.*, 2005, **9**, 858-872.

28. M. Lahav, L. Leiserowitz, *Chem. Eng. Sci.*, 2001, **56**, 2245-2253.
29. J. D. Dunitz, A. Gavezzotti, *Angew. Chem. Int. Ed.*, 2005, **44**, 1766-1787.
30. W. C. McCrone, in *Physics and Chemistry of the Organic Solid State*, Vol. 2; D. Fox, M. M. Labes, A. Weissberger (Eds.), Interscience: New York, 1965, 725-767.
31. F. Wöhler, J. Liebig, *Ann. Pharm.*, 1832, 249-282.
32. Z. Ostwald, *Z. Phys. Chem.*, 1897, **22**, 289.
33. D. J. W. Grant, Theory and Origin of Polymorphism, in *Polymorphism in Pharmaceutical Solids*; H. G. Brittain, (Ed.), Drugs and the Pharmaceutical Solids, Marcel Dekker Inc: New York, 1999, 1-34.
34. J. Bernstein, R. J. Davey, J.-O. Henck, *Angew. Chem. Int. Ed.*, 1999, **38**, 3440-3461.
35. K. R. Seddon, *Cryst. Growth Des.*, 2004, **4**, 1087.
36. J. Bernstein, *Cryst. Growth Des.*, 2005, **5**, 1661-1662.
37. G. R. Desiraju, *Cryst. Growth Des.*, 2004, **4**, 1089-1090.
38. A. Nangia, *Cryst. Growth Des.*, 2006, **6**, 2-4.
39. G. P. Stahly, *Cryst. Growth Des.*, 2007, **7**, 1007-1026.
40. S. L. Childs, G. P. Stahly, A. Park, *Molecular Pharmaceutics*, 2007, **4**, 323-338.
41. C. B. Aakeröy, M. E. Fasulo, J. Desper, *Molecular Pharmaceutics*, 2007, **4**, 317-322.
42. G. R. Desiraju, *CrystEngComm*, 2003, **5**, 466-467.
43. J. D. Dunitz, *CrystEngComm*, 2003, **5**, 506.
44. C. B. Aakeröy, D. J. Salmon, *CrystEngComm*, 2005, **7**, 439-448.
45. A. D. Bond, *CrystEngComm*, 2007, **9**, 833-834.
46. J. Bernstein, *Chem. Commun.*, 2005, **40**, 5007-5012.
47. O. Almarsson, M. J. Zaworotko, *Chem. Commun.*, 2004, 1889-1896.

## CHAPTER 2

### Pharmaceutical Solid Forms: Salts and Co-Crystals

#### 2.1 INTRODUCTION

Following the success of high-throughput screening, combinatorial chemistry, robotics and miniaturisation there is an abundance of novel drug candidate molecules. However, the process of selecting the optimal lead compound for development still requires much time and expenditure.<sup>1</sup>

Active pharmaceutical ingredients (APIs) are often solid, existing as polymorphs, solvates, hydrates, or in amorphous forms. Most drugs are developed in their crystalline form due to advantages in their mechanical properties such as milling, tablet compressing, and solubility, etc. Ideally a drug should be:

- chemically stable
- non-toxic
- non-hygroscopic
- present no processing problems
- exhibit good bioavailability
- dissolve appropriately from solid dosage forms (i.e. quickly unless it is formed with the intent to delay dissolution)

#### 2.2 DRUG PROPERTIES

Traditionally, the properties of organic materials have been considered in terms of the molecular structure; in the last 3 decades the possibilities for designing and utilising solid state properties have begun to be realised. The arrangement of molecules in a crystal structure is dependent upon the nature of the molecules and the way they interact with each other.<sup>2</sup> The crystalline structure determines the physical properties of a drug and also has a profound effect on the physicochemical properties such as:

- density
- water uptake

- 
- |                         |                               |
|-------------------------|-------------------------------|
| - optical properties    | - chemical stability          |
| - physical stability    | - cleavage                    |
| - hardness              | - thermo-analytical behaviour |
| - solubility            | - solid state reactivity      |
| - electrical properties |                               |

For example, the fraction of a drug absorbed is a function of solubility and an absorption rate constant that reflects the intrinsic permeability of the intestinal wall to the drug. The absorption rate constant is a function of the lipophilicity, molecular weight, number of hydrogen bonding groups and number of charges on the drug molecule.<sup>3</sup> The changes in bulk properties resulting from differences in crystal structures are known as structure-property relations.<sup>4</sup> The practical significance of altering these properties differs from case to case. Other drug crystal properties may vary even when the crystal structure is fixed, such as:

- |                  |                          |
|------------------|--------------------------|
| - filtration     | - mixing                 |
| - yield          | - tableting              |
| - milling        | - drying                 |
| - lyophilisation | - suspension formulation |
| - washing        | - flowability            |
| - dissolution    |                          |

These properties are important in pharmaceutical operations and are largely controlled by crystal habit and size distribution.<sup>5</sup>

### 2.2.1 Polymorphism

In the case of pharmaceuticals, any change from the desired physicochemical properties is unwanted as ultimately it leads to patient risk. The possibility of producing undesirable polymorphs is a potential danger during both drug manufacture and storage. Polymorphism not only presents challenges in reproducible preparation and retention of a specific solid form with desired properties, but also in the protection of intellectual property via patent litigation. Screening for and characterization of polymorphs are considered important activities within research to gain insight in to the role of structure in determining the properties of compounds and are also imperative in drug development where the crystal form can have a large impact on drug properties and performance.<sup>6</sup>

### 2.2.2 Selection of Drug Candidates

Historically, the parent drug selected from in vitro and in vivo screens for pharmacological activity was not necessarily the optimal form and instead was most likely to be the compound which proved easiest for the synthetic chemist to prepare and isolate in pure crystalline form. This lead compound

was then often found to exhibit less than ideal physicochemical properties. In fact, in the last 20 years the solubility of new drug molecules has decreased sharply as the introduction of combinatorial chemistry and high-throughput screening has identified numerous new chemical entities. This is further exacerbated by the quest for more potent and highly specific molecules resulting in larger, more lipophilic and less water soluble leads being selected. According to a study by Serajuddin ‘approximately one third of new compounds synthesised by medicinal chemistry laboratories have an aqueous solubility less than 10 µg/mL.’<sup>7</sup> Nowadays, a pharmaceutical profile for each lead is constructed to assess the suitability of drug candidates; an ensemble of “drug-like” properties is measured to ascertain the developability of the drug candidate.

In a review by Panchagnula *et al.*<sup>8</sup> a few empirical rules for the selection of drug candidates are outlined. These include the basic requirements for good pharmacokinetic parameters in a drug: optimum water solubility, lipophilicity and chemical stability as these affect bioavailability. Many high-throughput screening methods have centred on these properties as poor bioavailability makes drug development difficult.<sup>9</sup> For a compound to be absorbed easily into the body it needs to have high solubility and moderate lipophilicity (moderate intrinsic permeability).<sup>10</sup> It is thought that the major influences on these two factors are the molecular weight of the compound, the number of hydrogen bond donors and acceptors available, and the fraction of hydrophilic versus hydrophobic molecular surface area.<sup>11</sup>

### 2.3 SALT AND CO-CRYSTAL FORMATION

It is well documented that the properties of a drug can be altered by using various salt formers,<sup>12-14</sup> and recently there has also been work involving the use of drugs in neutral solid forms known as co-crystals.<sup>15, 16</sup>

Salt and co-crystal formation is usually achieved by combination of an API with a salt or co-crystal former. Through the selection of an appropriate salt or co-crystal former the physicochemical, formulation, biopharmaceutical, and therapeutic properties of a drug can be altered without modifying its basic chemical structure. It is a relatively simple chemical manipulation; an estimated half of all the drug molecules used in medicinal therapy are administered as salts.<sup>12</sup>

Salt formation for the improvement of solubility dates back to the 1950’s when Nelson<sup>17, 18</sup> demonstrated that dissolution rates of salt forms of several weakly acidic compounds were much higher than those of their respective free acid forms. Since then interest has grown and recently salt formation has become the ‘most commonly applied technique [for] increasing solubility and dissolution rate in drug product development.’<sup>7</sup> Salt formation is also commonly employed for improving mechanical properties which affect the solid form processing properties.<sup>13</sup>

Conversely co-crystal formation is a less widespread technique in the pharmaceutical industry in spite of the use of co-crystals to alter the properties of pharmacologically active compounds dating back to 1946.<sup>19</sup> More recently, research into co-crystals has increased where they have been found to improve solubility, crystallinity and stability e.g. itraconazole<sup>20</sup> and carbamazepine.<sup>21</sup>

Although salt and co-crystal formation can improve a desired property, a range of other properties will also be affected. An increase in melting point by maximising or encouraging crystal symmetry (and hence an increase crystallinity) improves stability for easier formulation processing and storage, but will generally lead to reduced solubility in all solvents. Furthermore, a new form of a drug can not only enhance desired physicochemical properties but is also considered as new intellectual property – a valuable asset for a pharmaceutical business.

It would be of great benefit to both chemists and formulators to be able to predict the effects that a particular salt or co-crystal form would impart on a drug. Selecting the appropriate form is largely an empirical process, based on consideration of the cost of raw materials, yield, ease of preparation and purification. Although selection still remains a difficult decision, various attempts have been made to predict salt and, to a lesser extent, co-crystal performance.

### 2.3.1 Selection of Salt and Co-crystal Formers

In order to successfully synthesise a salt or a co-crystal, there are a number of generally agreed requirements for the selection of an appropriate former. In the pharmaceutical industry, initial synthesis of a salt or co-crystal involves performing a screen from which potential candidates can be selected. Following these criteria for selecting the salt and co-crystal formers for the screen generally make the process cheaper and more efficient:<sup>22</sup>

- |                             |  |
|-----------------------------|--|
| - low cost                  | - previously reported crystal structure      |
| - widely available          | - pK <sub>a</sub> value and number of values |
| - low melting point         | - a distribution of charge and               |
| - MW<300                    | stereochemistry across the range of          |
| - analytical data available | potential formers                            |
| - crystalline               |  |

For a binary compound to form, it is also widely regarded that molecules with complimentary functional groups should be used in order to form hydrogen bonds between the two components that are more energetically favourable than those in a homomeric system. Therefore the number and arrangement of hydrogen bond donors and acceptors is important. Indeed, an understanding of the supramolecular chemistry of the functional groups of a given molecule and their hierarchy will

be particularly beneficial when designing effective and versatile synthetic supramolecular strategies.<sup>23, 24</sup>

Aakeröy and co-workers suggest choosing a former that is polymorphic as the compound has shown it can adopt alternative packing patterns as well as display synthon flexibility.<sup>25</sup> The ability to participate in a number of intermolecular interactions allows the successful formation of multiple hydrogen bond synthon on a variety of molecules. He also notes that the flexibility of a molecule can influence the product. A more flexible salt or co-crystal former may enhance the solubility which in turn aids solution based co-crystal formation. However, if the aim is to maintain high symmetry (and hence crystallinity) then a more structurally rigid salt or co-crystal former may be employed, provided any solubility issues during crystallisation are overcome. In the pharmaceutical industry the improvement of physical properties through salt and co-crystal formation are more valuable than being able to predict the supramolecular structure.

### 2.3.2 *Crystallisation of Salts and Co-crystals*

Whilst recrystallisation is commonly used as a method of separation and purification of mixtures of dissolved substances due to the inherent structural selfishness of molecules,<sup>26</sup> crystallisation of a heteromeric solution may result in the homomeric components forming separately, or the components may form a heteromeric solid. For a heteromeric, or multicomponent, solid to form it must be more energetically favourable than the crystallisation of the parent compounds separately.

Solution crystallisation, in particular slow evaporation, is commonly used for the synthesis of salts and co-crystals in industry and research.<sup>27</sup> This is because the technique is simple to perform and can even be mostly performed by robotics thus allowing the screening of a large number of salt and co-crystal forms.<sup>28</sup> It is important that both of the components are soluble in the chosen solvent, however, this is not as demanding as in other solution crystallisation techniques such as mixed and layered solvents, where ideally the components should have similar solubilities otherwise the components will crystallise out separately.

Grinding and solvent-drop grinding are two techniques that have recently become more popular in both salt and co-crystal synthesis.<sup>29, 30</sup> The ability to manipulate the product by using different solvents, and even reverse the formation of a binary compound, makes the technique adept for research in spite of it sometimes being labour intensive and time consuming.

Although the role of the solvent in nucleation of crystals remains poorly understood, the choice of solvent in solution crystallisations and solvent drop grinding can be critical in obtaining a particular binary compound. Therefore the design of screening protocols should take into account the effect



of solvents on solution speciation. Ideally a solvent should be selected which gives the crystallising species a solubility of between 5 and 200 mg mL<sup>-1</sup> at room temperature. The choice of solvent depends on its:<sup>31</sup>

- solvation power
- boiling point
- safety
- toxicity
- cost
- ability to participate in hydrogen bonds as an acceptor or donor
- viscosity
- the slope of the solubility curve versus temperature

It should also be considered whether the solvent will react with the compound of interest and its environmental impact. Time is also a key variable in crystallisation, especially when waxy solids form on solvent evaporation. If oils form, crystallisation may be induced by scratching the sides of the crystallisation vessel to provide nucleation sites.

### 2.3.3 *pH-solubility profiles*

It has been proposed by Serajuddin that ‘the aqueous solubility of an acidic or basic drug as a function of pH dictates whether the compound will form suitable salts or not and, if salts are formed, what some of their physicochemical properties might be.’<sup>7</sup> Some examples of these profiles are discussed in a study by Anderson and Flora.<sup>32</sup>

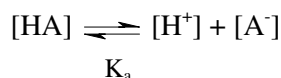
pH-solubility profiles can give an indication of whether a salt form is feasible, the solubility of the salt form and its potential conversion to its free form on formulation or storage. Although these profiles are potentially useful there are a number of pitfalls, mainly concerning the difficulties encountered when determining the solubility of a given salt. It is vital to establish the nature of the solid phase at equilibrium to ensure the solubility of the salt is being measured and not the solubility of the free acid or base. Problems are also encountered during measurement of the solubility as typically the pivotal factor in experiments is the detection of remaining solid after the sample has been left to equilibrate. The assumption that this indicates equilibrium with respect to the salt solid phase is not necessarily correct as the solid phase present is the free acid or base. It is vital excess solid is identified by thermal analysis and PXRD. In some cases a ‘gel’ may form due to complete conversion of the salts to the free form at all the solid-to-solvent ratios.<sup>33</sup> The formation of supersaturated solutions will also give inconsistencies in the solubility behaviour, possibly due to kinetic effects where the nucleation of one phase occurs more readily than that of the other. More importantly, however, these profiles require the prior synthesis of the salt. Their information would indeed be of much use when assessing the suitability of an already synthesised pharmaceutical salt, but the time taken to construct the profiles does not predispose them to high-throughput screening.

## 2.4 SALT VERSUS CO-CRYSTAL FORMATION

As mentioned in Chapter 1, salts and co-crystals can be considered as opposite ends of a continuum. Transfer of a proton is thought to largely depend on the  $pK_a$  values of the components.

### 2.4.1 $pK_a$

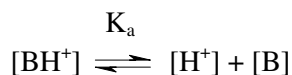
From the Brønsted-Lowry definition of an acid and a base, an acid is a substance that can donate a proton and a base is a substance that can accept a proton. Therefore in aqueous solution, the dissociation of a monoprotic acid HA can be described by the following equilibrium



In this reaction  $K_a$  is the equilibrium constant of the ionisation of HA, i.e. the ionisation constant

$$K_a = \frac{[H^+][A^-]}{[HA]}$$

Similarly for a monobasic compound, the dissociation equilibrium can be expressed



where

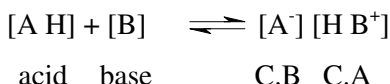
$$K_a = \frac{[H^+][B]}{[BH^+]}$$

Here  $K_a$  is the dissociation constant of  $[BH^+]$ .

Acid strength is given by the acid dissociation constant  $K_a$ . Strong acids, e.g. HCl, completely dissociate in water and hence have a large  $K_a$ , whereas weak acids, e.g.  $CH_3COOH$ , have a small  $K_a$  as they only partially dissociate in water. For convenience, acidity is measured using a log scale:

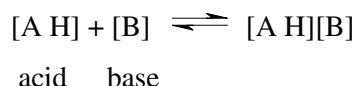
$$-\log K_a = pK_a$$

During salt formation an acid loses a proton to form its conjugate base (C.B), and a base accepts a proton to form its conjugate acid (C.A)



By considering the conjugate acid as the corresponding acid of the free base, the  $pK_a$  values may be compared. Hence the  $pK_a$  difference is the  $pK_a$  of the conjugate acid minus the  $pK_a$  of the acid. The  $pK_a$  values compared in each case are those of the most ionisable group in the molecule, i.e. the  $pK_a$  of the most acidic proton.

When the formal ‘acid-base pair’ crystallise together in a form in which there is no proton transfer, the product may be termed a co-crystal



#### 2.4.2 Proton Transfer

Some of the first work published regarding the occurrence of proton transfer between components was published by Johnson and Rumon.<sup>34</sup> They found that a  $\text{pK}_a$  difference of more than 3.8 units between the conjugate acid and the acid resulted in stable salt formation. This is the basis of what has become to be known as the ‘rule of three.’<sup>35</sup> Further studies have shown that there is a transition area where a  $\text{pK}_a$  difference of 2-3 may result in a salt or co-crystal formation. A  $\text{pK}_a$  difference greater than 3 results in a salt, and less than 2 results in a co-crystal.<sup>36</sup> Further work since this has shown that  $\text{pK}_a$  data alone is not sufficient to predict whether a proton is transferred from one component to another in a crystalline solid. Instead the crystalline environment together with the competition between different intermolecular forces and  $\text{pK}_a$  determine the position of a binary compound on the continuum.<sup>37-39</sup>

Various attempts have also been made to correlate  $\text{pK}_a$  difference with hydrogen bond distances however, most authors report disappointing results.<sup>40</sup> Aakerøy echoes that in spite of this, and their inability to translate into free-energies of complexation, they are ‘clearly valuable indicators when applied to members of the same functional group class in a systematic manner.’<sup>24</sup>

#### 2.4.3 Effect of Solvent on $\text{pK}_a$

When calculating the  $\text{pK}_a$  difference between two compounds, the values used are often those in water even though another solvent is then used for the crystallisation. It would be expected that the  $\text{pK}_a$  values in the crystallisation solvent represent the speciation and hence acidity strength of the system and should therefore be more applicable. For example, the  $\text{pK}_a$  values of carboxylic acids in methanol are shifted 4-5 units above their values in water. This makes quite a difference when crystallising the acids with weak bases as the  $\text{pK}_a$  difference will be altered dramatically.

### 2.5 AIMS OF RESEARCH

The main objective of this project is to investigate the formation of solid forms of organic compounds of pharmaceutical relevance with a view to understanding the factors controlling the

formation of salts and co-crystals using simple organic molecules with weakly interacting functional groups.

A systematic study will be carried out with a selection of simple acids and bases that have a range of structures and some that are part of a series (see the next Section for a full description of the starting materials). A fuller appreciation of the factors that determine success or failure in salt and co-crystal formation would provide further information for salt and co-crystal screening protocols. The study will therefore use small amounts of the chosen compounds and be performed in a high-throughput manner to mimic the conditions of a salt or co-crystal screen. The crystallisation products will be assessed as to whether a binary compound forms or the compounds prefer to crystallise out separately, or form an oil. When salts and co-crystals form, the patterns in proton transfer between the components will be examined according to the  $pK_a$  differences and the crystal structure. In particular, systems will be used where there are more than one acidic or basic group to investigate how the competition, cooperation and balance between the different intermolecular forces influence proton transfer.

The relationship between the properties and crystal structure of the starting materials, and those of the binary products will also be explored; melting temperature is a vital property for an API as it generally reflects the stability and solubility of the compound. Any correlation between the melting temperatures of the starting materials and their products, which have previously been found to correlate,<sup>41</sup> will be studied. As will the relationship between the melting point across a series of binary compounds and their crystal structures and intermolecular interactions. By understanding any observed trends in melting point or crystal structure in a series, such properties may be predicted in the future with similar compounds. Knowledge gained from hydrogen bond networks provides insights in understanding and predicting the proton transfer and hydrogen bonding networks of multi-component APIs involving structurally similar molecular species.

To achieve the objectives outlined, this work can be split into three main topics:

- crystallisation
- product analysis
- compilation of data and inspection

The study will be performed systematically in that the same crystallisation method will be used for most of the acid-base combinations, and all under the same conditions. This will allow the products to be compared directly and the merits of the crystallisation technique chosen to be assessed. Methanol and water will be used as solvents with methanol being the first choice and, if the compounds are not sufficiently soluble in methanol, water as the second choice. Methanol and water have been chosen as they are both small, polar solvents and compounds often behave similarly in them.

## 2.6 STARTING MATERIALS

When studying the properties of compounds with the purpose of gaining insight into the behaviour of pharmaceuticals, it is important to study “drug-like” molecules. These are molecules which have the same functional groups as would be found on a pharmaceutical compound such as carboxylic acids, amides and amines.

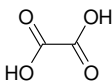
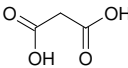
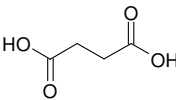
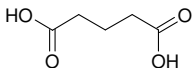
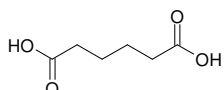
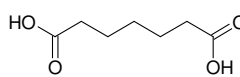
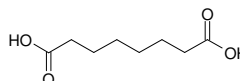
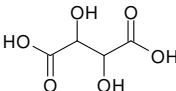
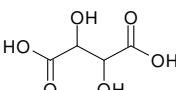
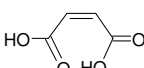
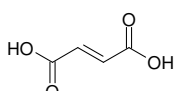
As most drugs are basic, the bases were selected to be the example APIs with the acids as the salt/co-crystal formers. Selection of both of the acids and bases was based on the criteria outlined in Section 2.3.1; the compounds chosen are readily available, cheap, small and simple for ease of comparison of the interactions in the structures. The crystal structures for the starting materials can be obtained from the Cambridge Structural Database (CSD)<sup>42</sup> where available.

### 2.6.1 Acids

The acids chosen are listed in Table 2.6.1 together with some of their properties;  $\alpha,\omega$ -alkanedicarboxylic acids (diacids) were chosen in order to assess the ionisation patterns when there are two ionisable groups available.

The series provides a range of  $pK_a$  values for the first and second ionisation thus allowing the ionisation patterns over a range of  $pK_a$  differences to be evaluated. The addition of a carbon atom to each diacid also increases the hydrophobicity and flexibility of the compound enabling the effects of these properties on the formation of binary compounds and their crystal structures to be noted. The inclusion of the hydroxy diacids and the alkene diacids further extends the spectrum of compounds assessed and allows further interactions to occur between the molecules. The importance of these interactions will be highlighted by the different crystal structures that form.

In the tartaric acids (TAs) only one of the optical isomers will be investigated as theoretically both D and L will form the same crystal structure with an appropriate base. Indeed, all the D-tartaric acid (DTA) binary compounds on the CSD are isostructural with their L counterparts (LTA). It has been noted by Farrell and co-workers<sup>43</sup> that there have been few systematic studies designed to explore the structural effects of using chiral versus racemic TAs. In fact, searches of the CSD show that there are substantially fewer binary compounds containing DL-tartaric acid (DLTA) than a single enantiomer. This may be because TA has been used to resolve fairly complex amines and the crystal structure data was simply being used to establish the chirality of the amine. The involvement of both DLTA and LTA in this work will allow further investigation into the structures each of the compounds form.

	Diacid	Abbreviation	Molecular Structure	MW	Melting point /°C	polymorphs	pK <sub>a</sub> 1	pK <sub>a</sub> 2
Simple diacids	Oxalic Acid	OxA		90.03	189	2: OXALAC	1.23	4.19
	Malonic Acid	MnA		104.06	132-135	2: MALNAC	2.83	5.69
	Succinic Acid	ScA		118.09	184-186	2: SUCACB	4.20	5.61
	Glutaric Acid	GlA		132.11	95-98	2: GLURAC	4.31	5.41
	Adipic Acid	AdA		146.16	151-154	2: ADIPAC	4.43	5.41
	Pimelic Acid	PmA		160.17	103-105	2: PIMELA	4.48	5.42
	Suberic Acid	SbA		174.19	140-144	SUBRAC	4.52	5.40
Hydroxy diacids	L-Tartaric Acid	LTA		150.09	170-172	D=TARTAC	2.98	4.34
	DL-Tartaric Acid	DLTA		150.09	210-212	ZZZDUI	2.98	4.34
Alkene diacids	Maleic Acid	MeA		116.07	137-140	2: MALIAC	1.83	6.07
	Fumaric Acid	FmA		116.07	298-300	2: FUMAAC	3.03	4.44

**Table 2.6.1** Chosen diacids together with some properties (pK<sub>a</sub> values from ACD/I-Lab:<sup>44</sup> literature pK<sub>a</sub> values were used where possible, the remainder were calculated); crystal structures are available on the CSD (refcodes given).

As pharmaceutical salt/co-crystal formers it is also important that the compounds are non-toxic; most of the acids selected are generally recognised as safe (GRAS) by the Food and Drug Administration (FDA).<sup>45</sup> In fact, more than a third of the top 100 drugs by US prescriptions are salts; the types of salts are shown in Figure 2.6.1.1, focussing on the diacid salts.

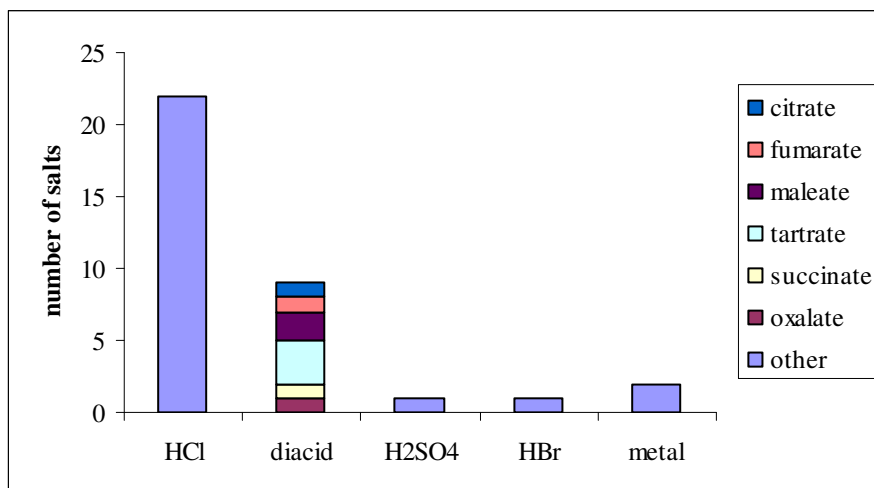


**Figure 2.6.1.1** Graph to show the salt formers found in the top 100 drugs by US prescriptions.<sup>46</sup>

Each of the diacids, except for SbA and the TAs, has been found to be polymorphic with at least two crystal structures present on the CSD. It has been suggested by Aakeröy and co-workers<sup>47</sup> that polymorphic compounds make good co-crystallising agents due to increased synthon flexibility. The authors note that compounds that can form different hydrogen bond interactions in the same polymorph are able to accommodate other molecules into a lattice more readily than other compounds which only engage in one type of primary interactions. This is nearly irrelevant with the diacids chosen as the carboxyl groups are always involved in the same interaction, except for OxA. It will be interesting to investigate if the polymorphic compounds form more binary compounds in this study.

Mostly, the polymorphs of each of the diacids are quite similar, consisting of the same chain structure but with a slightly different arrangement of the chains. The MeA polymorphs form the same sheet structure, but with different sheet arrangements. For AdA, the polymorphs are temperature dependant, however, again, the difference between the structures is the arrangement of the chains. OxA is an exception to this; the two polymorphs have similar lattice energies, however, the  $\beta$ -form consists of hydrogen bonded chains, whereas in the  $\alpha$ -form each molecule is hydrogen bonded to four different OxA molecules to form a sheet. It is unknown as to which form is more stable at room temperature as OxA decomposes on heating before the expected transition point. The only compound that has a significant conformational difference between its polymorphs is PmA, where torsion in the carbon chain makes each of the hydrogen bonded chains different. Some of the cells recorded on the CSD do not have atomic co-ordinates, making it impossible to compare the structures.

The simple diacids are an interesting series as the melting point alternates with even and odd carbon chain length (Figure 2.6.1.2), a trend that is also seen in the *n*-alkanes,<sup>48</sup>  $\alpha,\omega$ -alkanedithiols,<sup>49</sup>  $\alpha,\omega$ -alkanediols<sup>50</sup> and  $\alpha,\omega$ -alkanediamines.<sup>50</sup> Other solid state properties such as

solubility and sublimation enthalpy also display pronounced alternation, however the liquid state properties do not show any alternating trend. Work with regards to melting point alternation in the diacids was first published in 1877 by Baeyer<sup>51</sup> and since then comprehensive crystallographic work has been carried out on the series in a number of attempts to relate the diacid crystal structure to the melting point alternation, culminating in a paper by Thalladi and co-workers.<sup>52</sup> They note that unlike the aforementioned compounds, the densities of the odd members of the diacids (odd-diacids) with five carbons or more are relatively higher than those of the even-diacids. This indicated to the authors that the reason for the melting point alternation is a factor other than close-packing.

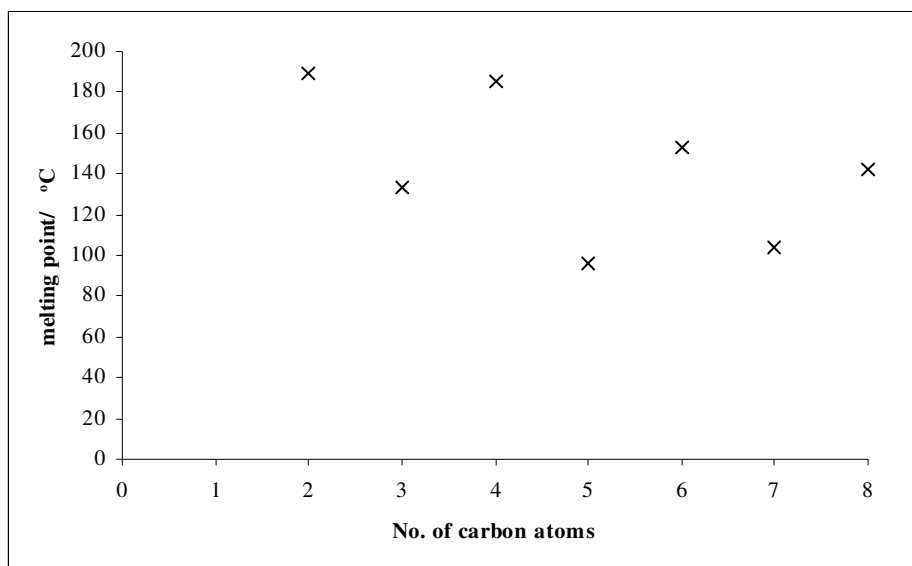


**Figure 2.6.1.2** Graph to show the alternation in melting point with the carbon chain length in the simple diacid series.

Thalladi and co-workers attribute the melting point behaviour to ‘geometry-allowed or geometry-forbidden attainment of an offset packing with a non-twist molecular conformation.’ Although the diacids all form similar structures with head-to-tail hydrogen bonding of the carboxyl groups to form infinite chains that are stacked into columns, there are also important differences between the even- and odd-diacids. The even diacids have offset chains within the stacks, thereby reducing the repulsion between the carboxyl dimers of the adjacent chains. The molecules also adopt an energetically favourable, non-twisted, all *trans* conformation with the carboxyl groups in the molecular plane (Figure 2.6.1.3).

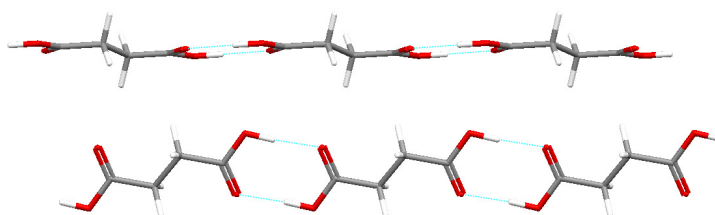


**Figure 2.6.1.3** ScA chain structure.



In both of the odd-diacid polymorphs, the carboxyl groups turn out of the molecular plane leading to energetically unfavourable twisted molecular conformations. The chains also cannot attain the off-set packing seen in the even-diacids due to packing restrictions; the repulsion between the carboxyl groups further destabilises the structures therefore reducing the melting points (Figure 2.6.1.4). It would be interesting to investigate if this property is also expressed across a series of binary compounds.

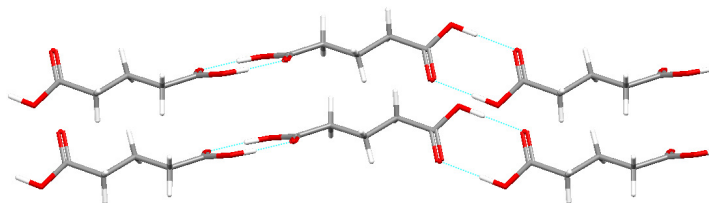


**Figure 2.6.1.4** GlA chain structure.

From CSD searches (Appendix, Table A1) it was found that each of the diacids can exist in binary compounds as neutral entities, mono-deprotonated anions (monoanions) and di-deprotonated anions (dianions), however some forms are more prevalent than others. In fact, the diacids with chains of five carbons or less all have more monosalts than disalts. MnA is most commonly present as a monoanion with an intramolecular hydrogen bond. Similarly, MeA was found to only exist as a dianion in two structures (out of over 150 structures) with an intramolecularly hydrogen bonded monoanion being most common. OxA and TA also have a large number of binary compounds present on the CSD which follow the deprotonation trend with nearly twice as many mono-deprotonated OxA structures and more than three times as many mono-deprotonated TA structures than di-deprotonated structures. Diacids with more than five carbons are less prevalent on the CSD therefore trends in their deprotonation are less clear, however, AdA is present most often as a dianion whereas PmA and SbA monoanions and dianions are equally common.

## 2.6.2 Bases

A range of structures were selected which can broadly be split into three groups: aliphatic amines, nitrogen-containing heterocycles and aromatic amines. All of the compounds chosen are detailed along with some of their properties in Table 2.6.2.

Some of the aliphatic amines have two ionisable groups to further study the ionisation patterns in compounds with more than one ionisable group. The aromatic amines are a series of substituted imidazoles to investigate how the position of the functional groups affects the formation of binary compounds and their structure. Some of the nitrogen-containing heterocycles contain amide functional groups in order to study the interaction of this functionality with the diacids. So far, none of the bases have been found to be polymorphic.

	Base	Abbreviation	Molecular Structure	MW	Melting point/ °C	Polymorphs	pK <sub>a</sub> 1	pK <sub>a</sub> 2
Aliphatic amines	1,1,3,3-Tetramethylbutylamine	TMBA		129.2	-67	-	11.76	-
	1,2-Diaminoethane	DAE		60.1	8.5	ETDIAM	10.88	7.66
	2-Aminoethanol	AEI		61.08	10-11	JAKKEL	10.12	-
	Tetramethyl-ethylenediamine	TEMED		116.2	-55	-	9.01	5.93
N-containing heterocycles	2-Pyrrolidinone	Pyr		85.1	23-25	NILYAI	16.30	-
	2-Imidazolidinone	Idn		95.1	58	06skc0074	17.97	14.39
	1,3-Dimethyl-imidazolidinone	DMIdn		114.2	8.2	-	7.97	-
	Morpholine	Mo		87.12	-7--5	ITIZUG	9.11	-
Aromatic amines	Imidazole	Im		68.08	88-91	IMAZOL	7.21	-
	1-Methylimidazole	1MI		82.1	-60	-	7.27	-
	2-Methylimidazole	2MI		82.1	142-143	06skc0003	8.09	-
	4-Methylimidazole	4MI		82.1	44-47	-	7.72	-
	1,2-Dimethyl-imidazole	DMI		96.13	37-39	-	7.97	-

**Table 2.6.2** Chosen bases and some properties (pK<sub>a</sub> values from ACD/I-Lab;<sup>44</sup> literature pK<sub>a</sub> values were used where possible, the remainder were calculated); the cif files for Idn and 2MI are available on the Appendix CD, the others are available on the CSD (refcodes given).

Some structurally similar compounds were chosen in order to assess the affect of changing one functional group on the formation and structure of the binary compounds. Some of the bases are also similar in structure to the diacids while others are not in order to investigate the importance of complimentary acid and base structures in the formation of binary compounds

The  $pK_a$  difference between the acid and the conjugate acid are shown in Appendix, Table A2 in water and Table A3 in methanol. It can be seen that while the  $pK_a$  differences in water generally predict the formation of a mono-deprotonated salt, the values in methanol predict predominantly co-crystal formation. As co-crystal formation does not concur with the crystal structures of the acid-base combinations already present on the CSD, the  $pK_a$  values in water will be used herein, however the importance of this will be discussed later.

The crystal structures of pure 2MI and Idn have been obtained during the study and data for which is included in the Appendix (Table A20). The crystal structures for the other bases that are solid at room temperature are available on the CSD.

### 2.6.3 *Binary Compounds of Chosen Acid-Base Combinations Already Present on CSD*

The CSD provides a vital source of information regarding compounds that have been synthesised and their structures determined. Searches were performed on this database to find any binary compounds containing both an acid and a base from the aforementioned starting materials. The important features of these structures will be discussed in the results sections for ease of comparison of the structures across the series; the CSD reference code is given for each of the structures obtained from the literature.

Further searches of the CSD (version 5.28 updates until Aug 2007) used in this work include only structurally unique entries of organic compounds only (no metals) and were performed using ConQuest 1.10.<sup>53</sup>

Since writing this thesis, further work regarding imidazolium-dicarboxylate salts has come to light. Pogorzelec and co-workers have recently published papers<sup>54, 55</sup> regarding the crystal structures of the acid-base combinations MnA-Im, ScA-Im, GlA-Im, AdA-Im (monohydrate salt) and SbA-Im. The data for these crystal structures, however, is not yet available on the CSD except for MnA-Im. The two MnA-Im salts will be discussed in the results section.

### 2.6.4 *Possible Hydrogen Bond Synthons*

Possible hydrogen bonding synthons are best found by assessing the pure forms and binary compounds of the parent compounds that are present on the CSD. From this information, the formation of binary compounds and their synthons can be predicted.<sup>56</sup>

The possession of two carboxylic groups by the diacids also allows the formation of monoanion chain structures via head-to-tail hydrogen bonding in the binary compounds. This type of hydrogen bonding can be in the *syn* or *anti* conformation:

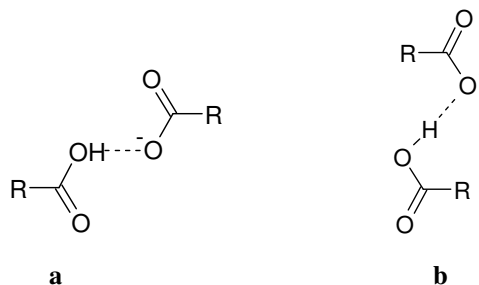


**Figure 2.6.4.1** a) *Syn-syn* and b) *anti-anti* hydrogen bonded dimers.

Repetition of each synthon results in slightly different chains; the *syn-syn* conformation is strongest and thus often preferred by the best hydrogen bond donor and acceptor (when different groups are present). In each of the above synthons, there are two further oxygen atoms that are available for the cation to form hydrogen bonds with, thus extending the structure. Di-deprotonation of the diacids would prevent this chain structure from occurring. This could be due to the formation of a binary compound with a dibase which gains both of the acidic protons, or caused by a change in stoichiometry of the binary compound compared to that of the crystallisation whereby two mono-base molecules are protonated by one diacid molecule. It will be investigated whether deprotonation directs the supramolecular structure that is formed, or whether the possible hydrogen bond synthons, and hence crystal structure that can be formed, directs the deprotonation.

If the monoanions form chains, the cations may act to link the chains if there are two hydrogen bond donors present on the cation, or there is one donor which can form a bifurcated hydrogen bond (i.e. has two hydrogens to donate). This is drawn schematically in Figure 2.6.4.2. This type of hydrogen bond arrangement can occur for the Im derivatives and some of the aliphatic amines such as DAE.

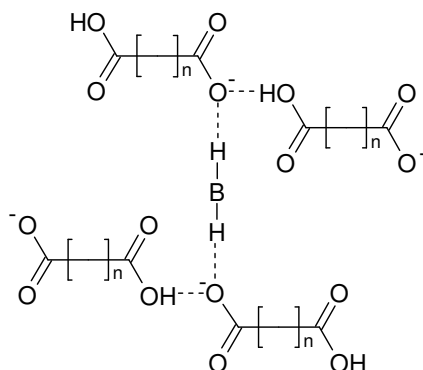


**Figure 2.6.4.2** Schematic representation of a cation acting as a bridge between two anion chains.

Monoanions and dianions can both form catemeric chain structures with the cations where only the carboxylate of the anion forms part of the chain; for this the cation needs to have two hydrogen

bond donor sites, or one hydrogen bond donor and one acceptor site. Other chains can form where the whole of the dianion is involved in the chain and the dianions and cations (again with two hydrogen bond donor sites) are alternately hydrogen bonded together (Figure 2.6.4.3). As with the anion chains previously mentioned, further hydrogen bonding from the available oxygen atoms can extend the structure into a 3-D lattice.

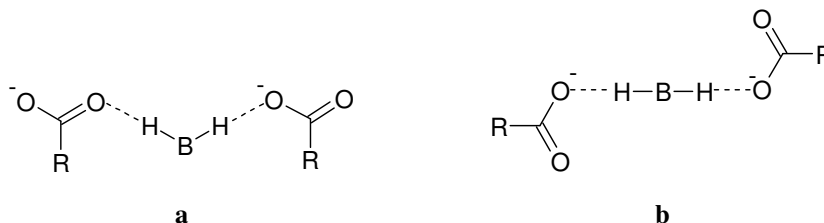


**Figure 2.6.4.3** a) Catemeric and b) non-catemeric hydrogen bonded chain.

As mentioned earlier in Chapter 1, the formation of hydrogen bond synthons generally follows Etter's rules. For example, the acid-amide synthon is favoured over acid-acid and amide-amide thus making this synthon useful for the synthesis of heteromeric systems (co-crystals) over homomeric systems (purification) (Figure 2.6.4.4). The competition between these hydrogen bonding motifs and the subsequent supramolecular structures that form within a series of compounds will be investigated.

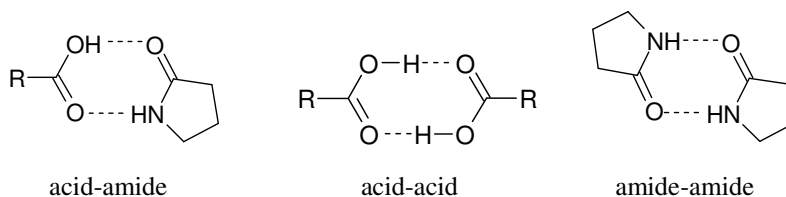


**Figure 2.6.4.4** Various acid and amide hetero- and homosynthons.

## References

1. R. A. Lipper, *Mod. Drug Disc.*, 1999, **2**, 55-60.
2. L. F. Huang, W. Q. Tong, *Adv. Drug Deliver. Rev.*, 2004, **56**, 321-334.
3. W. Curatolo, *Pharmaceutical Science & Technology Today*, 1998, **1**, 387-393.
4. J. Bernstein, *J. Phys. D: Appl. Phys.*, 1993, **26**, B66-B76.
5. S. R. Byrn, R. R. Pfeiffer, J. G. Stowell, *Solid-State Chemistry of Drugs*, 2nd Ed.; SSCI Inc: West Lafayette, IN, USA, 1999.
6. D. J. W. Grant, *Polymorphism in Pharmaceutical Solids*, Vol. 95, H. Brittain, M. Dekker, Marcel Dekker: New York, 1999.
7. A. T. M. Serajuddin, *Adv. Drug Deliver. Rev.*, 2007, **59**, 603-616.
8. R. Panchagnula, N. S. Thomas, *Int. J. Pharm.*, 2000, **201**, 131-150.
9. C. A. Lipinski, F. Lombardo, B. W. Dominy, P. J. Feeney, *Adv. Drug Deliver. Rev.*, 1997, **23**, 3-25.
10. L. Pan, Q. Ho, K. Tsutsui, L. Takahashi, *J. Pharm. Sci.*, 2001, **90**, 521-529.
11. A. T. Florence, D. Atwood, *Physicochemical Principles of Pharmacy*, 4th Ed., Pharmaceutical Press: London, 2006.
12. Anon, *Handbook of Pharmaceutical Salts: Properties, Selection and Use.*, P. H. Stahl, C. G. Wermuth, Verlag Helvetica Chimica Acta/Wiley-VCH: Zurich, 2002.
13. R. J. Bastin, M. J. Bowker, B. J. Slater, *Org. Process Res. Dev.*, 2000, **4**, 427-435.
14. L. D. Bighley, S. M. Berge, D. C. Monkhouse, Salt Forms of Drugs and Absorption, in *Encyclopedia of Pharmaceutical Technology*; J. Swarbrick, J. C. Boylan, Marcel Dekker, Inc.: New York, 1996, 453-499.
15. O. Almarsson, M. J. Zaworotko, *Chemical Communications*, 2004, 1889-1896.
16. S. L. Morissette, O. Almarsson, M. L. Peterson, J. F. Remenar, M. J. Read, A. V. Lemmo, S. Ellis, M. J. Cima, C. R. Gardner, *Adv. Drug Deliver. Rev.*, 2004, **56**, 275-300.
17. E. Nelson, *J. Am. Pharm. Assoc. (Sci. Ed.)*, 1958, **47**, 446-449.
18. E. Nelson, *J. Am. Pharm. Assoc. (Sci. Ed.)*, 1958, **47**, 297-299.
19. J. C. Krantz Jr., J. M. Holbert, H. K. Iwamoto, C. J. Carr, *J. Am. Pharm. Assoc.*, 1947, **36**, 248-250.
20. J. F. Remenar, S. L. Morissette, M. L. Peterson, B. Moulton, J. M. MacPhee, H. R. Guzman, O. Almarsson, *J. Am. Chem. Soc.*, 2003, **125**, 8456-8457.
21. S. G. Fleischman, S. S. Kuduva, J. A. McMahon, B. Moulton, R. D. B. Walsh, N. Rodríguez-Hornedo, M. J. Zaworotko, *Cryst. Growth Des.*, 2003, **3**, 909-919.
22. S. N. Black, E. A. Collier, R. J. Davey, R. J. Roberts, *J. Pharm. Sci.*, 2007, **96**, 1053-1068.
23. P. Vishweshwar, J. A. McMahon, J. A. Bis, M. J. Zaworotko, *J. Pharm. Sci.*, 2006, **95**, 499-516.
24. C. B. Aakeroy, J. Desper, B. M. T. Scott, *Chem. Commun.*, 2006, 1445-1447.

25. C. B. Aakeröy, A. M. Beatty, B. A. Helfrich, M. Nieuwenhuyzen, *Cryst. Growth Des.*, 2003, **3**, 159-165.
26. J. D. Dunitz, in *Perspectives in Supramolecular Chemistry: The Crystal as a Supramolecular Entity*; G. R. Desiraju, Wiley: Amsterdam, 1995,
27. B. Y. Shekunov, P. York, *J. Cryst. Growth*, 2000, **211**, 122-136.
28. S. L. Morissette, O. Almarsson, M. L. Peterson, J. F. Remenar, M. J. Read, A. V. Lemmo, S. Ellis, M. J. Cima, C. R. Gardner, *Adv. Drug Deliver. Rev.*, 2004, **56**, 275-300.
29. A. V. Trask, D. A. Haynes, W. D. S. Motherwell, W. Jones, *Chem. Commun.*, 2006, 51-53.
30. A. V. Trask, J. van de Streek, W. D. S. Motherwell, W. Jones, *Cryst. Growth Des.*, 2005, **5**, 2233-2241.
31. S. Rohani, S. Horne, K. Murthy, *Org. Process Res. Dev.*, 2005, **9**, 858-872.
32. B. D. Anderson, K. P. Flora, Preparation of Water-Soluble Compounds through Salt Formation, in *The Practice of Medicinal Chemistry*; P. H. Stahl, C. G. Wermuth (Eds.), Academic Press: London, 1996, 739-754.
33. M. Pudipeddi, A. T. M. Serajuddin, D. J. W. Grant, P. H. Stahl, Solubility and Dissolution of Weak Acids, Bases and Salts, in *Handbook of Pharmaceutical Salts: Properties, Selection and Use*; P. H. Stahl, C. G. Wermuth (Eds.), Verlag Helvetica Chimica Acta/Wiley-VCH: Zurich, 2002, 19-39.
34. S. L. Johnson, K. A. Rumon, *J. Phys. Chem.*, 1965, **69**, 74-86.
35. M. J. Bowker, A Procedure for Salt Selection and Optimization., in *Handbook of Pharmaceutical Salts: Properties, Selection and Use.*; P. H. Stahl, C. G. Wermuth (Eds.), Verlag Helvetica Chimica Acta/Wiley-VCH: Zurich, 2002, 161-190.
36. W. Q. Tong, G. Whitesall, *Pharma. Rev. Tech.*, 1998, **3**, 215-223.
37. G. P. Stahly, *Cryst. Growth Des.*, 2007, **7**, 1007-1026.
38. T. Steiner, I. Majerz, C. C. Wilson, *Angew. Chem. Int. Ed.*, 2001, **40**, 2651-2654.
39. Z. J. Li, Y. Abramov, J. Bordner, J. Leonard, A. Medek, A. V. Trask, *J. Am. Chem. Soc.*, 2006, **128**, 8199-8210.
40. F. H. Herbststein, Hydrogen bonded Molecular Complexes and Compounds, in *Crystalline Molecular Complexes and Compounds*; Oxford University Press: Oxford, 2005, 908-911.
41. P. L. Gould, *Int. J. Pharm.*, 1986, **33**, 201-217.
42. F. H. Allen, *Acta Crystallogr. Sect. B*, 2002, **58**, 380-388.
43. D. M. M. Farrell, G. Ferguson, A. J. Lough, C. Glidewell, *Acta Crystallogr., Sect. B*, 2002, **B58**, 272-288.
44. *ACD/I-Labs Web Service (ACD/pKa 8.03)*, Advanced Chemistry Development Inc.,
45. <http://vm.cfsan.fda.gov/~dms/eafus.html>, FDA/CFSAN/OPA: Inventory of GRAS Notices: Summary of all GRAS Notices, 2007,
46. <http://www.rxlist.com/script/main/hp.asp>, WebMD: RxList: The internet Drug Index, 2007, San Clemente.

- 
47. C. B. Aakeroy, A. M. Beatty, B. A. Helfrich, M. Nieuwenhuyzen, *Cryst. Growth Des.*, 2003, **3**, 159-165.
  48. R. Boese, H. C. Weiss, D. Bläser, *Angew. Chem. Int. Ed.*, 1999, **38**, 988-992.
  49. V. R. Thalladi, R. Boese, H. C. Weiss, *J. Am. Chem. Soc.*, 2000, **122**, 1186-1190.
  50. V. R. Thalladi, R. Boese, H. C. Weiss, *Angew. Chem. Int. Ed.*, 2000, **39**, 918-922.
  51. A. Baeyer, *Ber. Chem. Ges.*, 1877, **10**, 1286.
  52. V. R. Thalladi, M. Nüsse, R. Boese, *J. Am. Chem. Soc.*, 2000, **38**, 9227-9236.
  53. CCDC, ConQuest Version 1.0, CCDC, 2007.
  54. K. Pogorzelec, C. Pawlacyzk, A. Pietraszko, E. Markiewicz, *J. Power Sources*, 2007, **173**, 800-805.
  55. K. Pogorzelec, J. Garbarczyk, C. Pawlacyzk, E. Markiewicz, *Mat. Sci. -Poland*, 2006, **24**, 245-252.
  56. I. D. H. Oswald, W. D. S. Motherwell, S. Parsons, E. Pidcock, C. R. Pulham, *Crystallogr. Rev.*, 2004, **10**, 57-66.



## CHAPTER 3

### Analytical Techniques

#### 3.1 INTRODUCTION

In this chapter, a brief summary of the analytical techniques used during this study is given.

#### 3.2 CRYSTALLOGRAPHY

X-ray crystallography is the study of crystals and their structure by means of the diffraction of X-rays by the regularly spaced atoms of crystalline materials.<sup>1</sup> When an X-ray beam is directed at a crystalline sample, the atomic structure of the lattice causes the X-rays to be scattered in a defined manner creating a diffraction pattern. The electron density in the crystal may be deduced from this diffraction pattern, enabling an accurate molecular structure to be determined.

To understand this concept further and accurately determine crystal structures it is useful to have a general knowledge of crystal structures and their interaction with X-rays.

##### 3.2.1 *Solid Form – Crystal Structure*

Crystalline solid materials are highly ordered structures; the molecules are arranged in a precisely regular array that is repeated by translation in three dimensions. Therefore crystal structures consist of structural units that are stacked side by side in all directions, thereby forming a lattice in which the molecules in the repeated structural units are thought of as points. The lattice is considered to be infinitely large. The lattice points connect to form unit cells - a unit cell is the smallest group of atoms which has the overall symmetry of a crystal structure. The entire lattice can be built up by repetition of the unit cell in three dimensions. Figure 3.2.1.1 depicts a unit cell; it is a parallelepiped defined by sides of length  $a$ ,  $b$  and  $c$ , and three angles  $\alpha$ ,  $\beta$ ,  $\gamma$ . The number of

molecules in the unit cell is given as  $Z$ ; the number of molecules in the asymmetric unit is given as  $Z'$ .

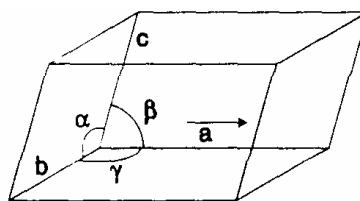


**Figure 3.2.1.1** The unit cell.

### 3.2.2 Crystal Systems

Due to restrictions imposed by reflection and rotation symmetry on the unit cell parameters, there are only seven types of crystal systems possible. These are shown in Table 3.2.2.

Crystal System	Restrictions of unit cell	Essential Symmetry
Triclinic	None	None – but can have a centre of inversion
Monoclinic	$\alpha = \gamma = 90^\circ$	One 2-fold rotation and/or mirror (perpendicular)
Orthorhombic	$\alpha = \beta = \gamma = 90^\circ$	Three 2-fold rotations and/or mirrors (mutually orthogonal)
Tetragonal	$a = b; \alpha = \beta = \gamma = 90^\circ$	One 4-fold rotation $C_4$
Trigonal	$a = b \neq c; \alpha = \beta = 90^\circ; \gamma = 120^\circ$	One 3-fold rotation $C_3$
Hexagonal	$a = b; \alpha = \beta = 90^\circ; \gamma = 120^\circ$	One 6-fold rotation $C_6$
Cubic	$a = b = c; \alpha = \beta = \gamma = 90^\circ$	Four three-fold rotation axes

**Table 3.2.2** Crystal systems with their cell parameters and constraints.

### 3.2.3 Lattice Types

Within these seven crystal systems there are two possible lattice types: primitive and non-primitive. A primitive lattice ( $P$ ) only has lattice points at the corners of the unit cell, whereas a non-primitive lattice also has points on the faces or within the unit cell as well as on the corners. Non-primitive lattices may be side-centred ( $A$ ,  $B$  or  $C$ ), face-centred ( $F$ ) with a lattice point at the centre of each face, body-centred ( $I$ ) with a lattice point at the centre of the unit cell, or in the special case of trigonal rhombohedral, doubly-centred at  $(\frac{1}{3}, \frac{1}{3}, \frac{2}{3})$  and  $(\frac{2}{3}, \frac{2}{3}, \frac{1}{3})$ .

### 3.2.4 Bravais Lattices

When the above crystal systems and lattice types are combined, only 14 crystal lattices are possible. These lattices are called Bravais lattices as they were defined by Bravais and Frankenheimer in the 19<sup>th</sup> century. Figure 3.2.4.1 depicts these lattices – they correspond to the seven unit cell shapes of the seven different crystal systems. Each lattice has a centre of inversion and all the points in the lattice are equivalent by inversion.

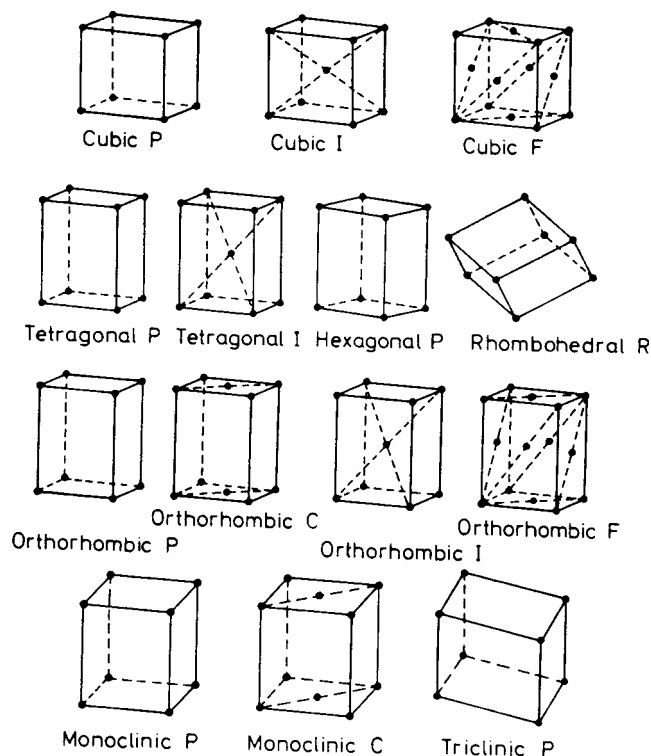


**Figure 3.2.4.1** The Bravais Lattices.<sup>2</sup>

### 3.2.5 Space Groups

In a single molecule the various combinations of symmetry operations are called point groups as all the symmetry elements refer to one point.<sup>3</sup> For a crystal, however, the symmetry elements are arranged in space in accordance with the lattice translational symmetry, therefore these sets of symmetry operations are called space groups.<sup>4</sup> There are 230 possible space groups; each space group represents a combination of point and space symmetry elements that is compatible with the geometrical requirements of 3-D lattices. The complete crystal structure can be obtained from the asymmetric unit and its appropriate space group symmetry operations.

Each space group is denoted by a symbol comprising of an upper case letter showing the Bravais lattice type followed by lower case numbers and letters to represent the combination of symmetry elements present. Rotation and screw axes are symbolised by numbers, and mirror and glide planes

by letters. For example,  $P2_1/c$  is the most common space group consisting of a primitive unit cell with a screw axis parallel to the  $b$ -axis and a glide plane perpendicular to  $b$  with translation along  $c$ .

The International Tables for Crystallography list all 230 space groups and their associated systematic absent reflections.<sup>5</sup>

### 3.2.6 X-rays

X-rays were discovered by German physicist Willhelm Conrad Roöntgen in 1895; they are a form of electromagnetic radiation of wavelength  $\sim 1\text{\AA}$  found between ultra violet and gamma rays in the electromagnetic spectrum. In 1912 Max von Laue recognised the ability of X-rays to be diffracted by crystalline solids. This is possible due to the wavelength of X-rays being of the same order of magnitude as the interatomic distances in crystals.

X-rays are produced by bombarding a molybdenum or copper target with a beam of accelerated electrons. The absorption of the high-energy electrons in the metal target results in a release of radiation over a continuous range of wavelengths called the Bremsstrahlung. On impact with the metal target the energetic electrons also expels some of the inner 1s electrons of the metal causing an electron from an outer 2p or 3p orbital to drop down to fill the gap. The excess energy is released as an X-ray photon. The desired X-ray radiation can be selected from the range of wavelengths by passing the radiation through a monochromator such as a graphite crystal.<sup>4</sup>

### 3.2.7 The Laue Equations

Through his analysis of diffraction patterns, Max von Laue devised three equations required to describe the diffraction of X-rays by crystals. These equations represent the three conditions needed for the diffracted X-rays to interfere constructively. Each equation corresponds to the diffraction condition for rows of atoms in one particular direction:

$$a (\cos \alpha_o - \cos \alpha) = h\lambda \quad (\text{Equation 1})$$

$$b (\cos \beta_o - \cos \beta) = k\lambda \quad (\text{Equation 2})$$

$$c (\cos \gamma_o - \cos \gamma) = l\lambda \quad (\text{Equation 3})$$

$\alpha_o$ ,  $\beta_o$  and  $\gamma_o$  are the angles between the incident X-ray beam and the unit cell axes  $a$ ,  $b$  and  $c$ . The corresponding angles for the diffracted beam are  $\alpha$ ,  $\beta$  and  $\gamma$ . For a diffracted beam to occur, values of the six angles must be picked so the  $h$ ,  $k$  and  $l$  parameters are integers.<sup>6</sup>

Although these equations provide a correct mathematical description of diffraction by crystals, an easier, alternative interpretation of diffraction based on Bragg's Law is more commonly used.

### 3.2.8 Bragg's Law

Following Max von Laue's work, in 1913 Bragg and his son showed that crystals could be regarded as being built up of parallel layers or planes passing through lattice points. Each plane acts as a semi-transparent mirror whereby some of the X-rays are transmitted through the plane and some are reflected.

The X-ray beams are always parallel and in phase up to a point at which the top beam strikes the top layer at atom z (Figure 3.2.9.1) and is scattered with an angle of reflection equal to the incident angle. The second beam then strikes the next layer at atom B, where it is also scattered with the same equal angle of incidence and reflection. This reflection by the adjacent planes gives rise to interference effects; for constructive interference to occur the first and the second beam must be in phase.

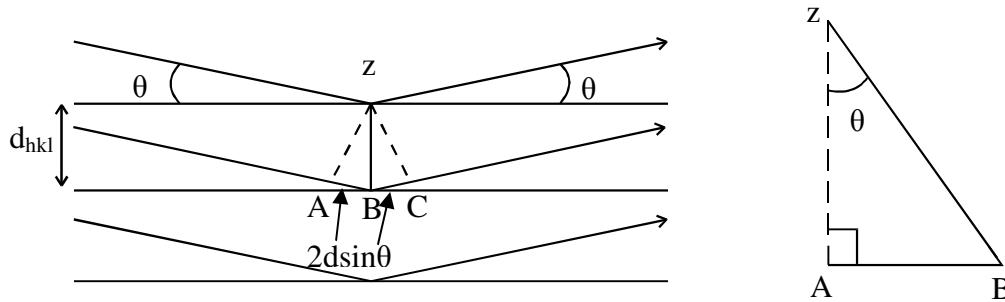


**Figure 3.2.9.1** Deriving Bragg's Law using trigonometry.

This requires the path difference between the two beams to be an integer value of the wavelength for constructive interference to occur. For rays reflected by two adjacent planes:

$$\text{path difference} = 2d_{hkl} \sin\theta = n\lambda \quad (\text{Equation 4})$$

$\theta$  = 'Bragg' angle

$n$  = integer

$d_{hkl}$  = interplanar spacing

$\lambda$  = wavelength of radiation

The interplanar spacing subscripts  $hkl$  are the indices used to define the orientation of the plane with respect to its three unit cell edges. Each  $d_{hkl}$  spacing and scattering angle is a function of the unit cell geometry and is calculated for each diffracted beam.<sup>7</sup> The Bragg equation also demonstrates mathematically the inverse relationship between the diffraction pattern and the unit cell parameters of the crystal lattice:

$$\sin\theta = \left(\frac{\lambda}{2}\right) \times \left(\frac{1}{d_{hkl}}\right) \quad (\text{Equation 5})$$

### 3.2.9 Structure Factors

The diffraction of incident X-rays by an atom is due to the electrons associated with the atom. The amount of scatter produced by the electrons depends on the scattering angle of the X-rays, the atomic number of the atom (and hence the number of electrons present), and the level of absorption of X-rays by the atom. When  $2\theta = 0$ , all the electrons in an atom scatter in phase and the scattering power is equal to the atomic number of the atom. For scattering angles greater than  $0^\circ$ , the scattered X-rays interfere with each other, hence the scattering amplitude,  $f$ , for an atom decreases with increasing  $\theta$ . The scattering power of the atom is also inversely proportional to the vibration of the atom which varies according to temperature.<sup>8</sup>

As it is the entire crystal that causes diffraction, the atomic scatterings from all of the atoms must be taken into account. The scattering of a group of atoms in a structure is known as the structure factor,  $F_{hkl}$ . It is a complex number with amplitude and a phase; for a reflection  $h, k, l$  it is defined by:

$$F_{hkl} = \sum_{j=1}^{atoms} f_j \exp(2\pi i [hx_j + ky_j + lz_j]) \quad (\text{Equation 6})$$

This extends over all atoms  $j$ , with  $x, y$  and  $z$  as their fractional co-ordinates.

Electron density has to be computed in order to determine a crystal structure from diffraction data. The structure factor can be considered as the sum of waves scattered from the electron density within the unit cell, and the electron density is the number of electrons per unit volume. By applying a Fourier transformation to Equation 6 the electron density can be expressed

$$\text{in terms of } \rho(xyz) = \frac{1}{V} \sum_h \sum_k \sum_l F(hkl) \exp(-2\pi i [hx + ky + lz]) \quad (\text{Equation 7})$$

This gives the electron density  $\rho(xyz)$  at any point  $x, y, z$ , from which the structure can be determined;  $V$  is the unit cell volume. Using Equation 7 the image of reciprocal space given by the diffraction pattern can be transformed into the real space of electron density.

### 3.2.10 The Phase Problem

To perform the Fourier transformation the complex structure factors  $F(hkl)$  are required, but only their magnitude,  $|F(hkl)|$ , is known and not their phase (direction). This is known as the phase problem. The phase angle can be isolated from the electron density to give the equation in the following form,

$$\rho(xyz) = \frac{1}{V} \sum_h \sum_k \sum_l |F(hkl)| \exp[-2\pi i (hx + ky + lz) - \phi(hkl)] \quad (\text{Equation 8})$$

By separating the structure factor into the experimentally observed values of  $|F(hkl)|$  and derived values of the phase part  $\phi(hkl)$  a trial electron density map can be created by a computer. If this map appears to be a reasonable structure then it may be refined.

### 3.2.11 Direct Methods

‘Direct methods’ is a term applied to methods that use phase relationships based on the observed intensities in the diffraction pattern to obtain approximate reflection phases.<sup>9</sup> This involves calculating the probability that the reflections have particular phase values by analysing the intensities and trigonometric relationships between the amplitudes of the reflections. A variety of different possible phases are then tried to assess how well they satisfy the probability relationships.

This process can be accomplished using a computer program; the whole structure can be drawn from the first electron density map produced by direct methods, providing the data is good enough. Once all the non-hydrogen atoms have been recognised the trial structure must be refined.

The direct methods technique is generally used when the compound contains atoms of approximately equal atomic number e.g. C, N, O. For compounds where a heavier atom is involved in the structure, e.g. organometallic compounds, a technique called the Patterson method is most widely used. In this project the direct methods approach was the only procedure used.

### 3.2.12 Refinements

The refinement process improves upon the initial solution obtained through the structural determination process by mathematically varying atomic parameters to give the best possible agreement between observed  $|F(hkl)|$  values and those calculated for the proposed structure.

There are a number of features that must be considered during refinement, one of which is the thermal vibration of the atom. Each atom is considered to have three positional co-ordinates  $x$ ,  $y$ ,  $z$  and a displacement parameter  $U$ . Therefore the vibration of the atom may be interpreted as having an isotropic mean-square amplitude. If another displacement factor per atom is introduced, allowing each atom to vibrate by different amounts in different directions, the model structure often fits the data better. This is known as anisotropic vibration where the atoms are considered as ellipsoids as opposed to spheres. It is usually applied to the model as a final improvement.

### 3.2.13 Fourier Methods and Least-Squares Analysis

Fourier methods and least-squares analysis are the two most common refinement techniques used. The least-squares analysis tries to find the best fit for a set of atomic positions by minimising the sum of the squares of the deviations between observed and calculated structure factor parameters. This statistical process is important as each observed value has an unknown measurement of error; eventually by repeating the calculation a number of times the model may be improved sufficiently that the changes in the parameters are insignificant.

Using Fourier methods either electron density or difference electron density maps may be calculated. A peak on a difference map indicates too much scattering in the trial structure whereas a trough represents too little scattering. The model is refined so ideally the map is zero everywhere, however in practice experimental uncertainties and errors in the intensity data make this unattainable.

In this project the multidimensional least-squares analysis will be used to refine the data.

### 3.2.14 R-factor

The residual factor (R-factor) is a measure of the difference between the calculated diffraction pattern and the observed one, i.e. between the sets  $|F_c|$  (calculated value) and  $|F_o|$  (observed value). The R-factor can therefore be defined as:

$$R = \frac{\sum ||F_o| - |F_c||}{\sum |F_c|} \quad (\text{Equation 9})$$

Typically good quality data can give an initial model structure of less than 0.5 depending on the fraction of electron density found. During refinement the R-factor decreases to generally reach a minimum of 0.02 - 0.07. R is not a measurement of accuracy, but is a useful guide to judge the agreement between the model and the experimental data.

Once refinement is complete, the unit cell geometry and space group are known, the accurate molecular structure (bond lengths and angles) can be calculated using the atomic positions within the unit cell.

### 3.2.15 Powder X-ray Diffraction (PXRD)

Experimentally the PXRD method is simpler than SXRD as it does not require large single crystals; it yields a pattern of peaks, the positions of which correspond to periodic spacings of atoms in the



solid state. However, it only gives data about relatively few  $hkl$  planes of a substance that are the most strongly diffracting. Different lattice constants will, in general, give rise to different peak positions and hence the technique provides a method for distinguishing solid phases that have a different internal structure.

A complete powder pattern can be indexed to obtain the unit cell parameters; this requires sufficient sample that has a small and uniform particle size. Problems arise when the micro-crystals are of a plate or needle morphology which tend to lie preferentially in one orientation. This causes an increase in the intensity of certain diffraction peaks compared to others and thus makes determining the unit cell more difficult. Grinding is not a viable method for reducing the effects of preferred orientation as, as mentioned in Section 2.3.2, grinding can induce a phase change or the formation of a binary compound. Problems also arise when there are two types of crystal, with different structures, present in the sample. In this situation obtaining the unit cell parameters is particularly difficult as the two structures each contribute to the powder pattern.

Structure determination from PXRD data is also possible using programs such as DASH<sup>10</sup> or Topas<sup>11</sup> which uses a simulated annealing algorithm. Due to the nature of powder X-ray diffraction data, the 3-D diffraction pattern obtained from a SXRD experiment is reduced to a 1-D pattern of intensity versus  $2\theta$ . This can result in the overlap of reflections with different Miller indices, creating difficulties in obtaining the unit cell parameters and determining the intensity of each reflection. Thus the more complicated the structure, the more problematic the structure determination from PXRD data. As particle size positively correlates with peak width, a sample should ideally have small particle size to reduce the problem of peak overlap. The chances of successful indexing and structure solution are also improved by packing the sample in a capillary to prevent preferred orientation of the micro-crystals.

### 3.3 THERMAL STUDIES OF ORGANIC SOLIDS

#### 3.3.1 *Differential Scanning Calorimetry*

Differential scanning calorimetry (DSC) is a useful technique as almost every phase transition is accompanied by an exchange of heat. It involves measuring the amount of energy absorbed or released by a sample under heating, cooling or isothermal conditions in a controlled atmosphere. This energy is related to the difference in heat flow between a sample and reference cell.<sup>12</sup> This method can obtain a range of thermodynamic data including melting point, enthalpy change of a transition, heat capacity and heat of fusion.

### 3.3.2 *Hot-Stage Microscopy*

Hot-stage microscopy (HSM) is one of the oldest and simplest methods for studying phase transitions in crystals. It involves varying the temperature of a substance while viewing it under a microscope thus providing information regarding the melting/recrystallisation behaviour as well as solid-state transformations. Combining HSM with DSC further expands the utility of both of the methods as the origin of an event on a DSC trace can be confirmed by HSM and vice versa.

---

**References**

1. *Oxford Dictionary of English, 2nd Ed.*, C. Soanes, A. Stevenson (Eds), Oxford University Press: Oxford, 2003.
2. P. W. Atkins, *Physical Chemistry, 6th Ed.*, Oxford University Press: Oxford, 1995.
3. D. F. Shriver, P. W. Atkins, *Inorganic Chemistry, 3rd Ed.*, Oxford University Press: Oxford, 2001.
4. W. Clegg, *Crystal Structure Determination*, Oxford University Press: Oxford, 1998.
5. *International Tables for Crystallography*, Kynoch Press: Birmingham, 1952.
6. A. R. West, *Solid State Chemistry and its Application*, John Wiley and Sons Ltd.: New York, 1984.
7. D. E. Sands, *Introduction to Crystallography*, Dover Publications Inc.: New York, 1993.
8. J. P. Glusker, K. N. Trueblood, *Crystal Structure Analysis A Primer, 2nd Ed.*, Oxford University Press: New York, 1985.
9. *Accurate Molecular Structures*, A. Domenicano, I. Hargittai (Eds), Oxford University Press: New York, 1992.
10. W. I. F. David, K. Shankland, N. Shankland, *Chem. Commun.*, 1998, 931-932.
11. A. A. Coelho, *J. Appl. Cryst.*, 2000, **32**, 1169-1179.
12. M. E. E. Brown, *Volume 1, Principles and Practice.*, P. K. Gallagher, 2; Elsevier Science B. V.: Amsterdam, 1998.

## CHAPTER 4

### Experimental

#### 4.1 INTRODUCTION

In this chapter, a full description of the methods used during this study is given.

#### 4.2 CRYSTALLISATION METHODS

##### 4.2.1 *Method 1*

Crystals were grown on a small-scale in a well-plate using a liquid handling robot. Solutions of each acid and base were prepared at a 0.1M concentration, 100µl of each acid and each base solution were then combined in equimolar quantities in the appropriate well using the liquid handling robot. The well-plate was then left undisturbed for the solvent to evaporate leaving crystals. After the solvent had evaporated the well-plate was placed in the fridge to try to induce crystallisation of any oils.

##### 4.2.2 *Method 2*

The TA combinations were prepared using a slightly different method; 1M solutions of each TA were prepared in water and two equivalents of each base were added (the base dissolves in the acidic solution). The well-plates were then left undisturbed for the solvent to evaporate leaving crystals.

##### 4.2.3 *Method 3*

1mmol of the base was dissolved in an ethanol-water mixture (approximately 2ml ethanol plus 1 drop of water). 1mmol of acid was then added and the mixture was warmed to dissolve the acid. The solution was then left to cool slowly.

### 4.3 INITIAL PRODUCT ASSESSMENT

The products were first assessed using optical microscopy to determine their crystallinity; a crystalline sample is seen to extinguish when rotated under polarised light. It is a quick technique to ascertain whether the bulk sample contains both liquid and solid phases, and also the morphologies of the crystals, if present. From this initial assessment of the product the best course of action for a more thorough analysis was decided.

### 4.4 SXRD INSTRUMENTATION AND DATA COLLECTION

#### 4.4.1 Crystal Selection and Mounting

Using an optical microscope a suitable single crystal was selected so as all unit cells were identical and aligned in the same orientation to give a clear diffraction pattern. The crystal should not be cracked or twinned and must be of the correct size so as the X-ray beam bathes the whole crystal in X-rays otherwise systematic errors would be produced in the diffraction pattern. The crystal was mounted onto a glass fibre using silicon grease. The glass fibre was secured onto a brass pin and the pip was subsequently mounted in a goniometer head (see Figure 4.4.1.1). This held the pip firmly in the X-ray beam and allowed adjustments to be made to ensure the crystal was positioned accurately on each rotation axis, as the crystal was rotated in the diffraction experiment.

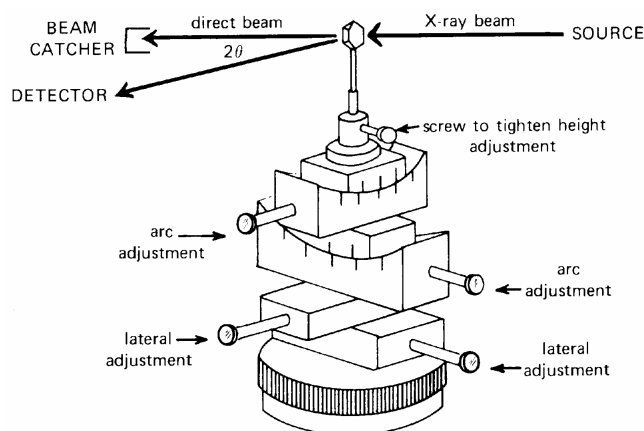
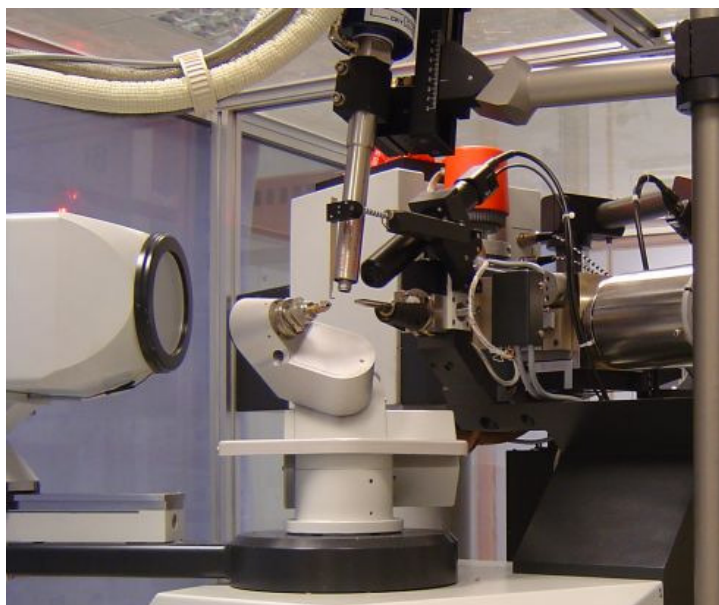


Figure 4.4.1.1 The goniometer head.<sup>1</sup>

#### 4.4.2 The Diffractometer

The diffraction data was collected using a Bruker Nonius Kappa CCD diffractometer mounted at the window of a Nonius FR591 rotating anode X-ray generator (Figure 4.4.2.1).



**Figure 4.4.2.1** The diffractometer<sup>2</sup>

Electrons are accelerated towards a molybdenum anode and X-rays are produced when they hit the molybdenum target. The anode constantly rotates allowing the heat to be dissipated across the entire source and thus is able to generate more intense X-rays than a conventional sealed-tube generator. The beam of X-rays is passed through a graphite crystal monochromator which reflects only the  $K\alpha$  radiation (wavelength =  $0.71073\text{\AA}$ ) onto the crystal. An Oxford Cryosystems Cryostat cooler uses liquid nitrogen to cool the crystal to 120K to stop the decomposition of the crystals and reduce molecular motion.

The CCD detector is an area detector, able to record a number of diffracted beams simultaneously as it records over a large area. This reduces collection time dramatically (days to hours). It consists of a phosphor faceplate which produces an image of visible light when hit by X-rays, this image is then transmitted to a CCD chip by fibre optic cables. The phosphor faceplate is positioned behind a beryllium window that is transparent to X-rays, but protects the faceplate from the outside environment. The CCD chip is cooled and then read by the computer to produce a digital image.

#### 4.4.3 Data Collection

The crystal was first scanned for a few minutes to obtain a trial diffraction: this gave a good indication of the quality of the crystal and hence the subsequent diffraction data. If the diffraction was good then a set of ten frames was collected. Each frame lasted ten seconds and they were collected a degree apart from each other. This data was indexed to obtain the parameters and

orientation of the unit cell. A collection strategy that ensures all the relevant data was collected was calculated using this information.

The graphical user interface, Collect,<sup>3</sup> contains the programs needed for data collection, and is used to obtain a full data set. The software package Denzo<sup>4</sup> was used to index and collect the data. The data collection took one to two hours for a good quality crystal but lasted longer when the reflections were weak or the crystal was very small. Once complete, the reflection intensities were obtained by integrating the frames, and then scaled using Scalepack;<sup>4</sup> the absorption corrections were performed using the SADABS<sup>5</sup> program; SADABS compares the intensities from equivalent reflections measured at different crystal orientations to calculate the necessary absorption corrections.

The structures were mainly solved using the direct methods technique in SHELXS<sup>6</sup> though some were solved using SIR.<sup>7</sup> Once the positions of all the non-hydrogen atoms were revealed, they were developed via difference electron density synthesis. The structures were refined on  $F_o^2$  by full-matrix least squares analysis (SHELXL97)<sup>6</sup> using all the unique data. The C-H hydrogens were fixed using idealised C-H distances according to their environment. The positions of the remaining hydrogens were found by looking at the residual electron density peaks. Once the hydrogen positions were found, the transferable hydrogens were put in the opposite positions and left to refine, to check the hydrogens returned to their original positions. Their positions were also confirmed using the C-O and C=O bond distances of the carboxyl(ate) groups. The position of the transferable hydrogen determines whether a salt or co-crystal had formed, so it was important to ensure this hydrogen was in the correct position. The refined structures were viewed using PLATON<sup>8</sup> and ORTEP<sup>9</sup> within the WinGX<sup>10</sup> suite of programs.

Confusion can occur when calculating  $Z$  for binary compounds. In this thesis a ‘molecule’ is defined as an acid-base unit  $[A]_x[B]_y$  where  $x$  and  $y$  are integers of the lowest denomination. Therefore  $Z'$  gives the number of whole ‘molecules’ in the asymmetric unit, and  $Z$  gives the number of whole ‘molecules’ in the unit cell. Therefore if half an acid molecule and a whole base molecule is present in the asymmetric unit,  $Z' = 0.5$  and, if in  $P-1$ ,  $Z = 1$ .

#### 4.4.4 Twin collections

The same basic procedure for the data collection was employed but also included face indexing (within the Collect software). The twin matrices were determined in Dirax;<sup>11, 12</sup> once found they were placed in the EVAL<sup>13</sup> program and the data was integrated to produce the hklf5 file. The structures were then solved as described above.

#### 4.4.5 *Synchrotron Collections*

Due to the poor quality and small size of some of the crystals, some samples were sent to Station 9.8<sup>14</sup> at Daresbury synchrotron to be analysed. The X-ray beams produced at a synchrotron are of a higher intensity to those produced using a rotating anode thus enabling the analysis of weakly diffracting samples.<sup>15</sup> Data here was collected using APEX2,<sup>16</sup> data reduction and cell refinement was performed using SAINT.<sup>17</sup> Absorption corrections were made using SADABS.<sup>18</sup>

### 4.5 PXRD INSTRUMENTATION AND DATA COLLECTION

Low angle ( $\theta = 5\text{-}15^\circ$ ) PXRD analysis using a Bruker C2 diffractometer (which combines a D8 generator and goniometer with a Hi-Star multiwire detector) was employed to ascertain if any of the powder products consisted of the starting materials having crystallised out separately. A small amount of each sample was mounted on a slide using grease and the diffraction pattern was recorded over 5 min using the GADDS software.<sup>19</sup> The data was integrated and the resulting pattern was compared with those generated from the starting material cif files.

### 4.6 THERMAL ANALYSIS METHODS

In an ideal situation DSC is a very informative and revealing technique; a DSC trace was obtained for each bulk product and in some cases the melting point could be confidently matched with the crystal structure. The technique suffers, however, if the sample is not uniform and contains a number of components thus making the trace is difficult to interpret without further investigation. In this work, if the DSC showed a well-behaved system with a clear single phase then the melting point was used. If the DSC showed a number of events then HSM was used by taking a single crystal from the sample that has the same unit cell parameters as the structure obtained by SXR. D.

### 4.7 STRUCTURAL ANALYSIS

Following crystal structure determination, the molecular assembly was viewed using Mercury<sup>20</sup> where the supramolecular structure and hydrogen bonding motifs were identified. Bond lengths were measured, in particular the C-O, C=O bond distances, as well as the bond angles and torsion angles of the molecules. The C-O bond distances vary significantly with the number and type of hydrogen-bonding donors bonded to the oxygen atom. In the absence of hydrogen bonding and other electronic perturbations, the bond lengths in a carboxylate group should be equal because of resonance. The packing index of each structure was calculated using PLATON.<sup>8</sup>



## References

1. A. R. West, *Solid State Chemistry and its Application*, John Wiley and Sons Ltd.: New York, 1984.
2. <http://www.xray.chem.soton.ac.uk>, M. Light, 2006, University of Southampton.
3. R. Hooft, B. V. Nonius, Collect: Data Collection Software, R. Hooft, B. V. Nonius, 1998.
4. Z. Otwinowski, W. Minor, *Macromol. Crystallogr., Part A*, 1997, **276**, 307-326.
5. G. M. Sheldrick, SADABS, Version 2.10, Bruker AXS Inc., Madison, Wisconsin, USA, 2003.
6. SHELXS [includes SHELX97 and SHELXL97], Programs for Crystal Structure Analysis (Release 97-2), G. M. Sheldrick, Institut für Anorganische Chemie der Universität, 1998.
7. A. Altomare, G. Cascarano, C. Giacovazzo, A. Guagliardi, *J. Appl. Crystallogr.*, 1993, **26**, 343-350.
8. PLATON, A Multipurpose Crystallographic Tool, A. L. Spek, Utrecht University, 1998.
9. C. K. Johnson, ORTEP, C. K. Johnson, Report ORNL-3794, Oak Ridge National Laboratory, Tennessee, USA, 1965.
10. L. J. Farrugia, WinGX – A Windows Program for Crystal Structure Analysis, L. J. Farrugia, University of Glasgow, 1998.
11. A. J. M. Duisenberg, *J. Appl. Crystallogr.*, 1992, **25**, 92-96.
12. A. J. M. Duisenberg, R. W. W. Hooft, A. M. M. Schreurs, J. Kroon, *J. Appl. Cryst.*, 2000, **33**, 893-898.
13. A. J. M. Duisenberg, L. M. J. Kroon-Batenburg, A. M. M. Schreurs, *J. Appl. Crystallogr.*, 2003, **36**, 220-229.
14. R. J. Cernik, W. Clegg, C. R. A. Catlow, G. Bushnell-Wye, J. V. Flaherty, G. N. Greaves, M. Hamichi, I. Burrows, D. J. Taylor, S. J. Teat, *J. Synchrotron Radiation*, 1997, **4**, 279-286.
15. W. Clegg, *J. Chem. Soc. Dalton Trans.*, 2000, 3223-3232.
16. APEX2, Bruker AXS Inc., Madison, USA, 2004.
17. SAINT, Madison, USA, Bruker AXS Inc., 2004.
18. SADABS, Bruker AXS Inc., Madison, USA, 2004.
19. GADDS: General Area Detector Diffraction system V4.1.13, Bruker, 2002.
20. Mercury 1.5 - A Crystal Structure Visualisation Program, The Cambridge Crystallographic Data Centre, 2006.

## CHAPTER 5

### Results and Discussion – Aliphatic Amines

#### 5.1 INTRODUCTION

In this chapter the products from the various crystallisation procedures of the acid-base combinations containing the aliphatic amines are described and discussed. The well-plate observations and the type of characterisation performed for the products of this chapter are summarised in Table 5.1.

	1,1,3,3-Tetramethyl- butylamine (TMBA)	1,2-Diaminoethane (DAE)	2-Aminoethanol (AEI)	Tetramethyl- ethylenediamine (TEMED)
OxA	Micro crystals Synchrotron	PEPMOM	QAMRIF	Blocks SXR
MnA	Oil*	WOBXIU	Oil	QAFVID
ScA	Oil*	PINNIJ	Plates SXR	ISUTEV
GlA	Micro crystals Synchrotron	Plates SXR	Oil	Blocks SXR
AdA	Plates SXR	ZZZGYW	Powder	Oil
PmA	Blocks SXR	Powder	Oil	Oil
SbA	Micro crystals Synchrotron	Powder	Blocks SXR	Oil
LTA	Blocks SXR	DTA = EDATAR10	XAGDAK	Oil
DLTA	Plates SXR	ENHTAR	Oil	Laths SXR
MeA	Micro crystals Synchrotron	ROHKUU	Amorphous	Laths SXR
FmA	Plates SXR	Blocks SXR	Plates SXR	QAFVEZ

**Table 5.1** Observations of the well-plate products for the acid-base combinations containing aliphatic amines and their appropriate method of analysis.

Where a CSD reference code is given in Table 5.1, the crystallographic data for the compound was obtained from the CSD. Any further information about the compound was gathered from the literature. Unless stated it should be assumed that the crystallisation procedure used was Method 1, or Method 2 for the TAs. Further crystallisation experiments (Method 3) were performed for the acid-base combinations that contained TMBA and produced oils (marked \*); these resulted in poor small crystals that were analysed by SXRD. Powder products were analysed on a small scale by PXRD to ascertain if the product was either of the starting materials.

In the following sections the outcomes of each of the SXRD studies will be discussed along with the thermal analysis results. Unless stated, the transferable hydrogen atom positions were found in the electron density difference map, and their correct assignment was confirmed not only by the difference between the C-O and C=O bond lengths, but also by moving the hydrogen atom to the other possible position and seeing where it refined to. All other hydrogen positions were added at calculated positions and refined using a riding model. The Ortep<sup>1</sup> diagrams for each of the structures display the molecules present in the asymmetric unit, the numbering scheme and 50% probability displacement ellipsoids; hydrogen atoms are shown as spheres.

The cell dimensions for each of the products are listed in Appendix, Table A4. For reference, the types of binary compounds formed and their melting points are displayed in Appendix, Tables A3 and A5 respectively. The crystal structure data is available on the Appendix CD.

## 5.2 1,1,3,3-TETRAMETHYLBUTYLAMINE

### 5.2.1 Oxalic Acid and 1,1,3,3-Tetramethylbutylamine

This crystal structure was obtained from synchrotron data due to the very small size of the crystals. It was found that the components crystallised in a 1:1 ratio in the triclinic space group *P*-1, with *Z* = 8. The small size and poor quality of the crystals resulted in weak data from which it was difficult to place one of the transferable hydrogens. The hydrogens were found and fixed on three of the base molecule nitrogens, but on the fourth only two electron density peaks were seen. No electron density peaks were found around the carboxyl group of the acid molecule with which the base molecule would hydrogen bond. From the C-O, C=O bond distances (1.248(9) and 1.222(9) Å) and the hydrogen bonding motifs present in the structure it was deduced that the hydrogen was on the base molecule and hence it was fixed there, resulting in a salt. The other carboxyl group on each of the diacids was found to have reacted with the methanol and become methylated.

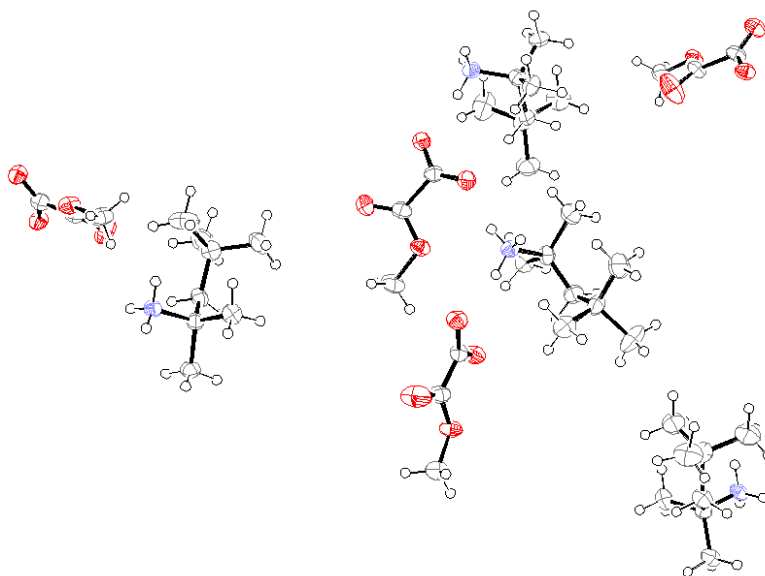


**Figure 5.2.1.1** Ortep diagram for the asymmetric unit of OxA and TMBA.

Each anion is involved in a similar hydrogen bond synthon that links two anions and two cations via bifurcated hydrogen bonds to form a unit. As there are four anions and four cations in the asymmetric unit, there are four variations of this synthon (each shown in Figures 5.2.1.3 to 5.2.1.6) that is schematically given in Figure 5.2.1.2; some have further hydrogen bonding within the unit due to the orientation of the ions (e.g. Figure 5.2.1.2 O51B and O51A are also hydrogen bonded to N85 and N45 respectively) but they all follow the same basic form. It should be noted that the units lie across a centre of inversion.

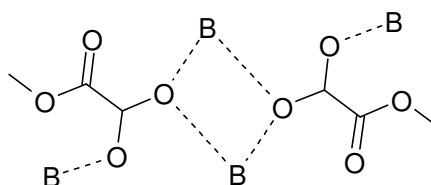


**Figure 5.2.1.2** Schematic diagram of the hydrogen bond synthon (hydrogen bonds shown as dotted lines) involving the anions and cations (B).

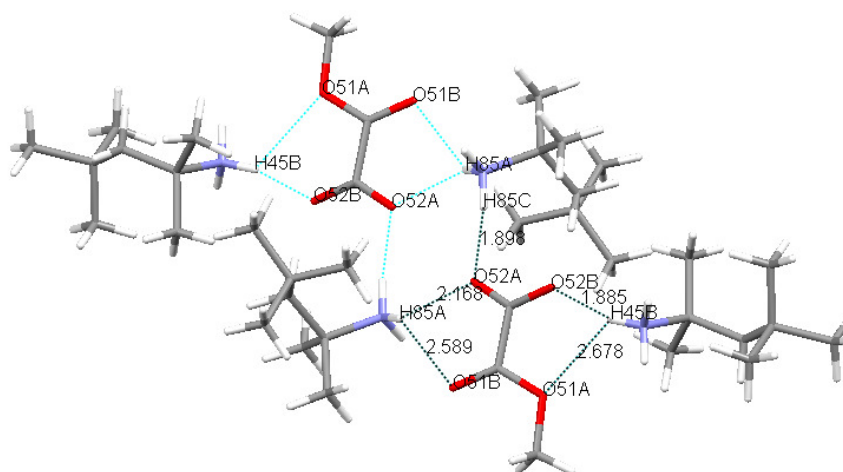


**Figure 5.2.1.3** Hydrogen bond distances (error  $\pm 0.009$  Å) for the synthon involving molecules 5 and 8 which is further linked to molecule 4.

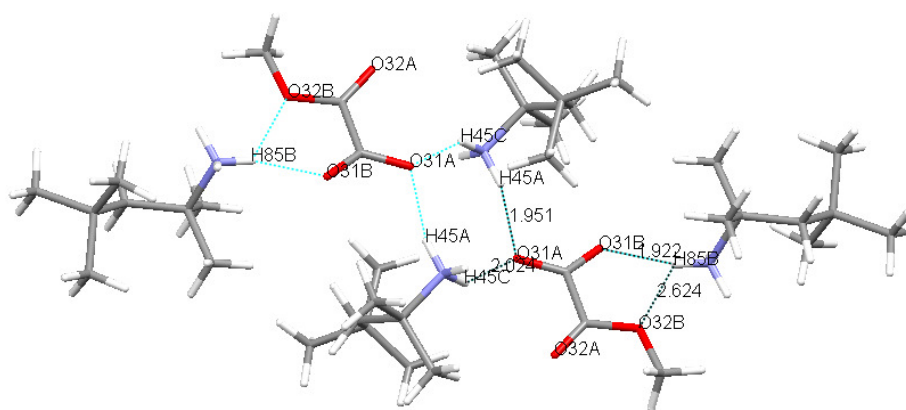


**Figure 5.2.1.4** Hydrogen bond distances (error  $\pm 0.008$  Å) for the synthon involving molecules 3 and 4 which is further linked to molecule 8.

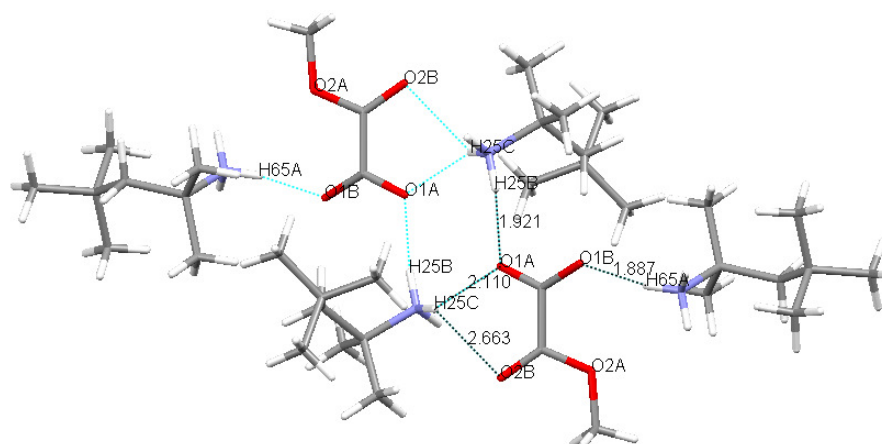


**Figure 5.2.1.5** Hydrogen bond distances (error  $\pm 0.008$  Å) for the synthon involving molecules 1 and 2 which is further linked to molecule 6.

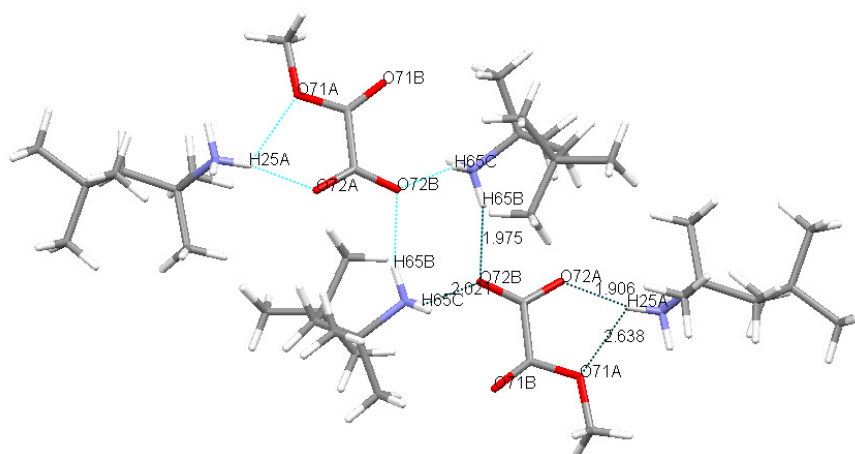


**Figure 5.2.1.6** Hydrogen bond distances (error  $\pm 0.009$  Å) for the synthon involving molecules 7 and 6 which is further linked to molecule 2.

Further hydrogen bonding between the ions links adjacent units to form 2-D sheets. Each sheet contains only two moieties of each anion and cation; one sheet contains molecules 1, 2, 6 and 7 and the other contains molecules 3, 4, 5 and 8. Each of the sheets is parallel to the *ab*-plane and has the

same approximate arrangement of molecules, however the exact positions of the atoms are slightly different (and hence the hydrogen bond distances are also slightly different). There are also weak C-H...O hydrogen bonds from the methyl groups of the cations and anions in the same layer (range = 2.523-2.711 Å).

The sheets are arranged as shown in Figure 5.2.1.7. In this pair of sheets, the layer below is nearly the same arrangement but with the molecules rotated through 90° around an imaginary axis that is perpendicular to the plane of the sheet and then flipped through 180° around the *a*-axis. Pairs of sheets with this relationship between them are then stacked on top of each other.

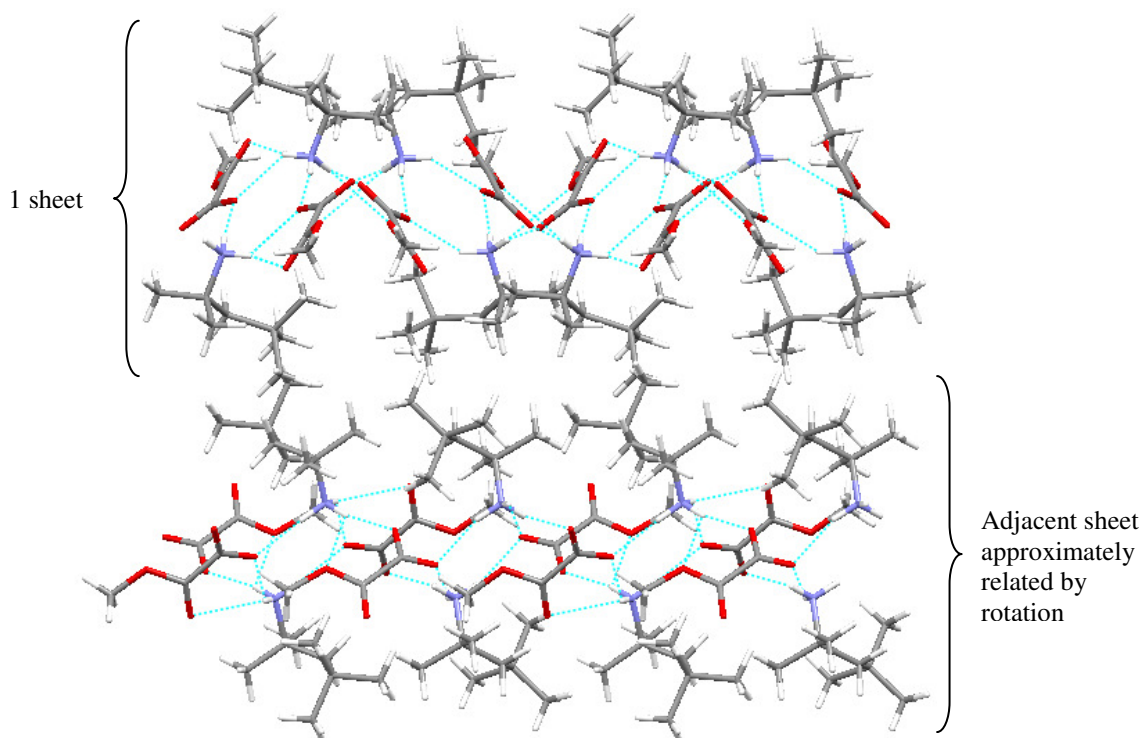


**Figure 5.2.1.7** The top sheet contains molecules 1, 2, 6 and 7, the bottom sheet contains molecules 3, 4, 5 and 8 – the sheets are related by rotation, however, the exact positions of the molecules are not identical in each sheet; viewed down the *a*-axis.

### 5.2.2 Malonic Acid and 1,1,3,3-Tetramethylbutylamine

Initially, these two compounds formed an oil when combined using Method 1. Using Method 3, however, the combination crystallised to form crystals which appear to have an incommensurate structure, the possible unit cell dimensions for which are in Appendix, Table A5. An incommensurate structure is a non-periodic structure that has competing structural forces, hence the unit cell is not repeated in the usual lattice fashion. It may be, for example, rotated by a certain degree but instead of this occurring after one unit cell, the new rotation is implemented after three-quarters of the unit cell. The data was processed using EVAL,<sup>2</sup> however, it was not possible to solve the structure to anything meaningful.

### 5.2.3 Succinic Acid and 1,1,3,3-Tetramethylbutylamine

Initially these two compounds formed an oil when combined using Method 1, however, using Method 3, plate crystals formed. These were found to contain the components in a 1:1 ratio, with water also present, in the monoclinic space group  $P2_1/c$ , with  $Z = 8$ . Each of the acids is mono-deprotonated thus creating a salt hemihydrate. After refinement of the structure, the R-factor remained quite high (10.85%) and the ellipsoids for some of the methyl groups on molecule 4 (TMBA) are slightly larger than the others (Figure 5.2.3.1). This is probably due to these groups being slightly disordered; as the methyl groups at this end of the cation are not adjacent to a hydrogen bond donor it leaves them able to rotate more freely, which can lead to disorder if there are sufficient voids in the structure.

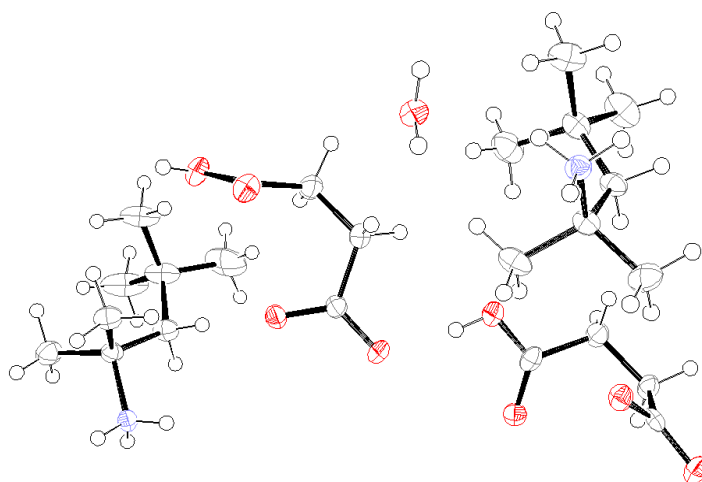


**Figure 5.2.3.1** Ortep diagram for the asymmetric unit of ScA and TMBA.

This structure consists of chains of monoanions hydrogen bonded head-to-tail in the *syn-anti* conformation. The monoanions are not flat and instead adopt the *gauche* conformation with a torsion angle of  $-59.0(5)^\circ$  for one monoanion and  $64.8(5)^\circ$  for the other. The cations are then subtended from this chain.

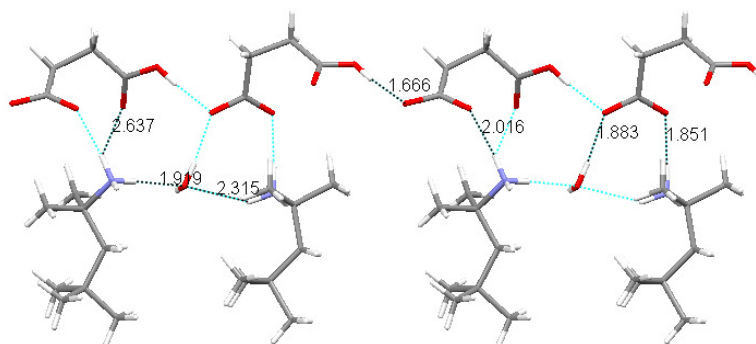


**Figure 5.2.3.2** Tape structure with anion chain from which cations are subtended; error in A-B hydrogen bond distances are  $\pm 0.004$  Å, and  $\pm 0.019$  Å for hydrogen bonds involving water.

The adjacent chains are linked together by further hydrogen bonding between the anions and cations and also across the water molecules which are positioned between the cations in the tapes,

thus creating a sheet. The hydrogen bonding groups are in the centre of the sheet with the hydrophobic groups towards the outside of the sheet. The sheets are arranged so as the anions are above and below the cations and vice versa. As the hydrocarbon chain of the anion is not as bulky as the methyl groups of the cation, this arrangement allows the sheets to pack more closely together.

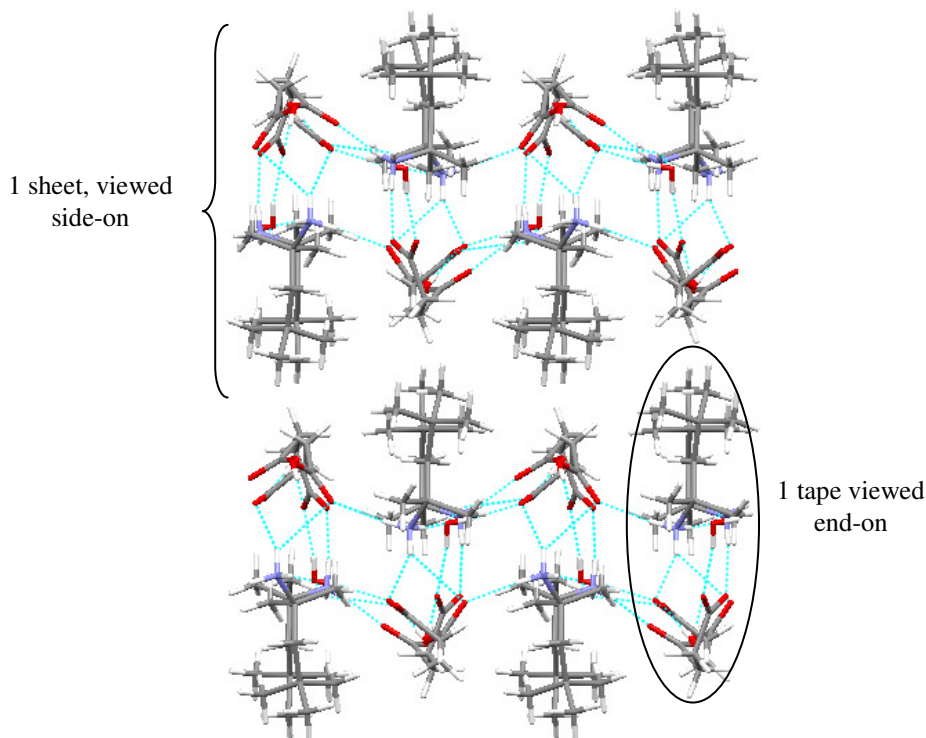


**Figure 5.2.3.3** Stacking of sheets viewed side-on, each tape viewed end-on.

#### 5.2.4 Glutaric Acid and 1,1,3,3-Tetramethylbutylamine

The data for this crystal structure was obtained from synchrotron data due to the very small size of the crystals. It was found that the components crystallised in a 3:4 acid:base ratio in the monoclinic space group  $C2$ , with  $Z = 2$ . One of the acid molecules is doubly deprotonated, with the hydrogens having been transferred to the base molecules. The remaining half of an acid molecule present in the asymmetric unit lies across a 2-fold rotation axis; it has retained its acidic hydrogen creating a mixed system.

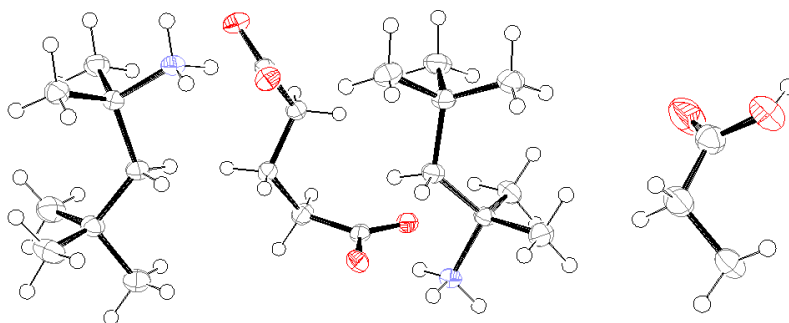


**Figure 5.2.4.1** Ortep diagram for the asymmetric unit of GIA and TMBA.



The dianion and cations are hydrogen bonded together alternately to form a tape. Each of the ions is hydrogen bonded to the adjacent three ions of the opposite charge; one of the donors on the anion is monofurcated and the other is bifurcated.

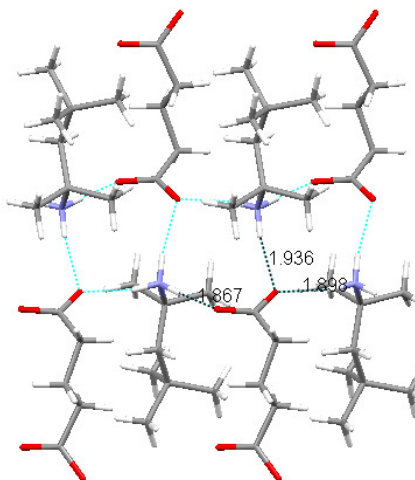


**Figure 5.2.4.2** Tape structure with hydrogen bond distances marked (error  $\pm 0.002$  Å).

The dianion adopts a *gauche* conformation (torsion angle  $72.5(3)^\circ$ ) which can be seen in Figure 5.2.4.3. As there are two carboxylate groups on the dianion and each is involved in hydrogen bonding in the tape unit shown above, the dianions link the tapes to create a 2-D sheet.

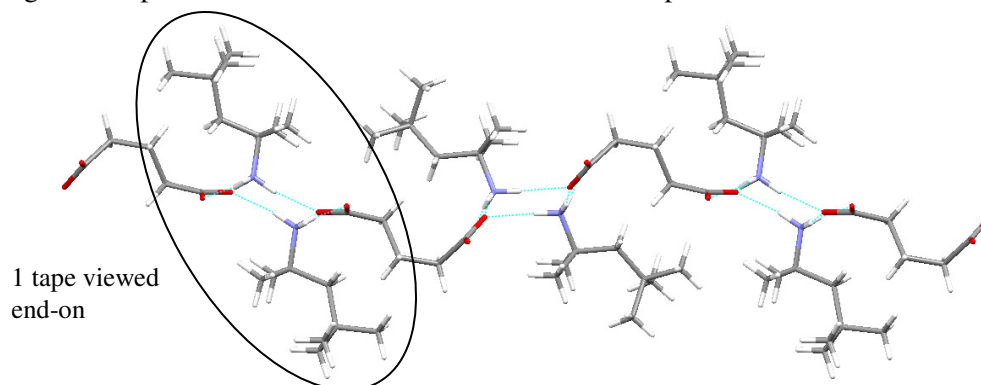


**Figure 5.2.4.3** Sheet structure with tapes viewed end-on, viewed down the *c*-axis.

The sheets are bridged together by O-H...O hydrogen bonding, in the *syn-anti* conformation, from the acid molecule that retained its protons to the dianion carboxylate groups in the sheets ( $1.862(2)$  Å) (Figure 5.2.4.4). This linking acid molecule has a twisted conformation with each half having a torsion angle of  $-55.5(2)^\circ$ .

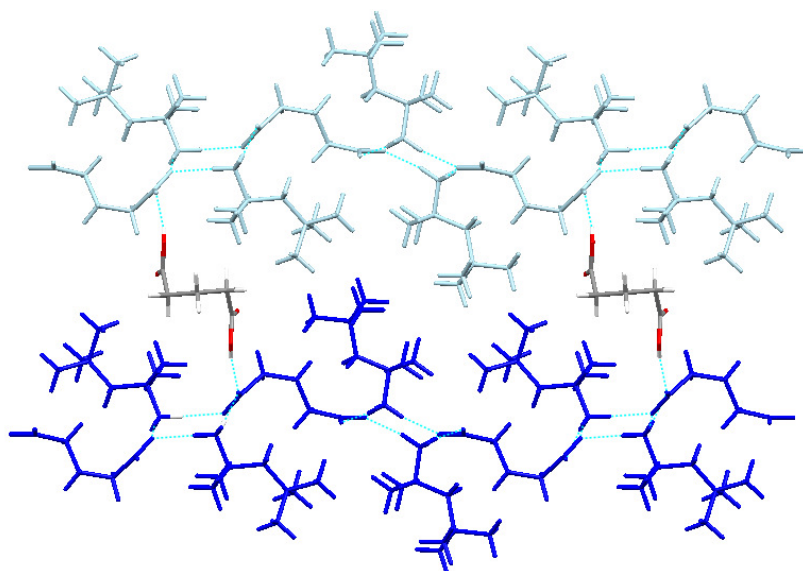


**Figure 5.2.4.4** Adjacent sheets viewed side-on, shown in dark blue and light blue, with bridging acid molecule.

#### 5.2.5 Adipic Acid and 1,1,3,3-Tetramethylbutylamine

These compounds crystallised in a 1:1 ratio in the monoclinic space group  $P2_1/c$ , with  $Z = 4$ . The asymmetric unit comprises of two distinct halves of an acid molecule both of which lie across inversion centres. One half has lost its proton to form half a dianion while the other has retained its proton, thus creating a mixed system.

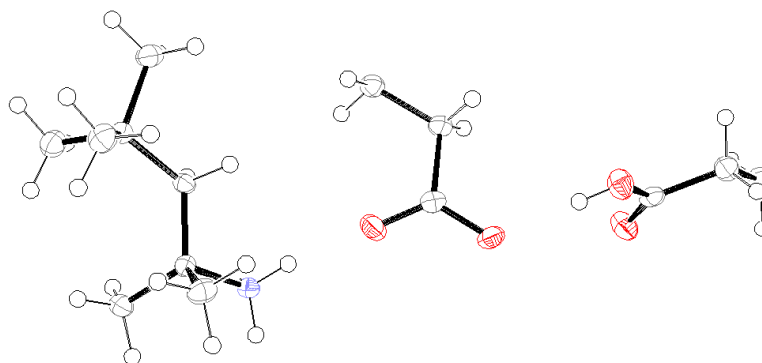


**Figure 5.2.5.1** Ortep diagram for the asymmetric unit of AdA and TMBA.

The structure consists of the cations and dianions hydrogen bonded together alternately to form a tape similar to that seen in GIA-TMBA. In this structure, however, the molecules are positioned slightly differently resulting in a bifurcated hydrogen bond from the cation to both of the oxygens on one end of the dianion.

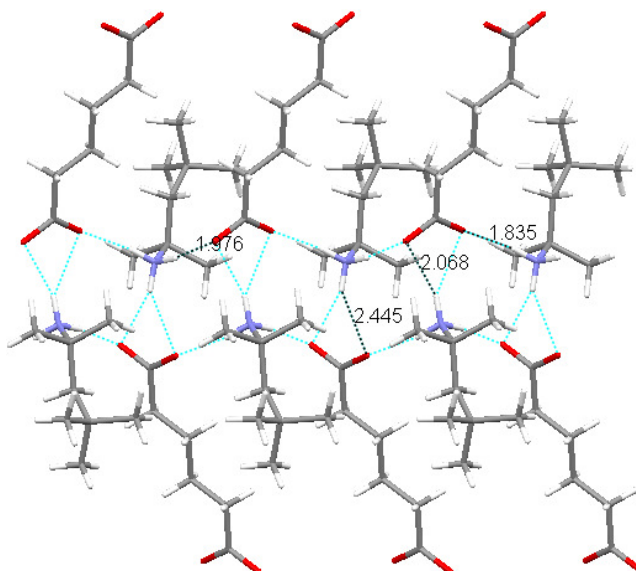


**Figure 5.2.5.2** Tape structure hydrogen bond distances marked (error  $\pm 0.003$  Å).

In this structure the dianion adopts a flat *anti* conformation with very little torsion ( $-176.0(3)^\circ$ ). As seen previously, both ends of the dianion are involved in hydrogen bonding in the manner shown above. This creates a sheet where each unit is connected by the dianion molecule (Figure 5.2.5.3).

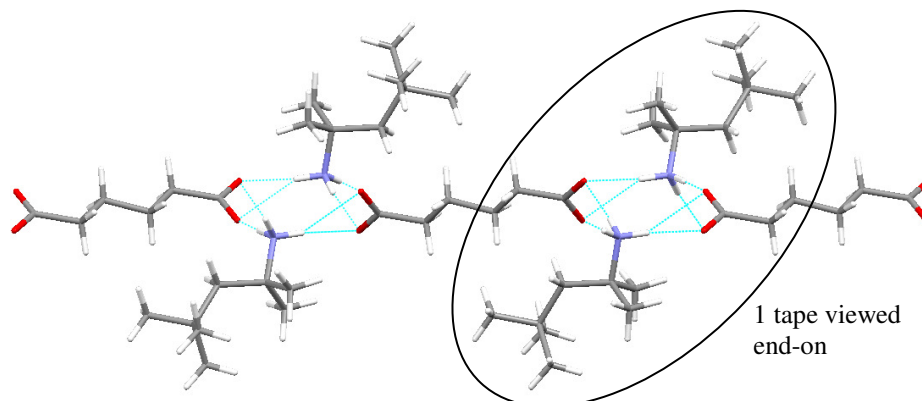


**Figure 5.2.5.3** Edge of sheet, with each tape viewed end-on, viewed down the *b*-axis.

As with the GIA-TMBA structure, the protonated acid molecule acts to bridge the adjacent sheets by forming a hydrogen bond with the dianion in the *syn-anti* conformation ( $1.814$  Å) to create a 3-D network (Figure 5.2.5.4). The acid molecules adopt the *anti* conformation (torsion angle  $178.1(3)^\circ$ ) and are positioned in the gaps in the sheets between the cations. As the two ends of the dianion are equivalent, each is hydrogen bonded to a bridging acid molecule.

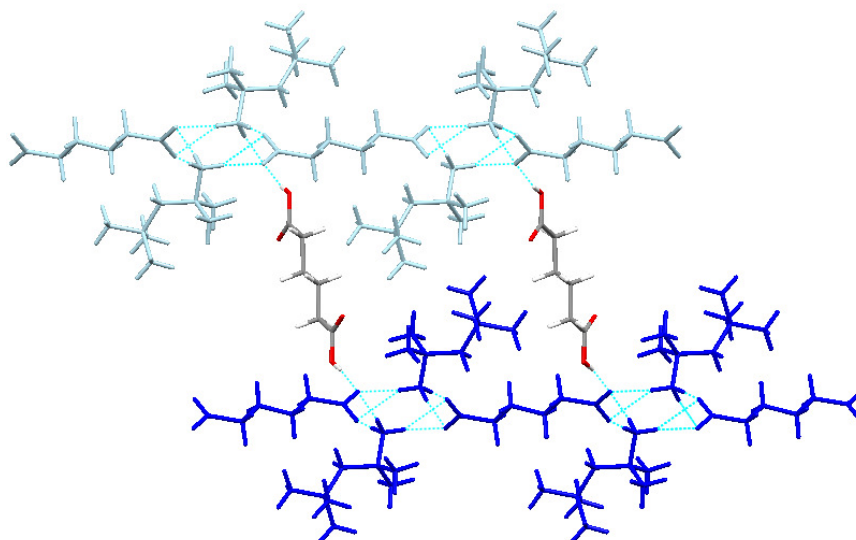


**Figure 5.2.5.4** Adjacent sheets viewed side-on, shown in dark blue and light blue, with bridging acid molecule.

#### 5.2.6 *Pimelic Acid and 1,1,3,3-Tetramethylbutylamine*

This combination crystallised in a 1:1 ratio in the orthorhombic space group  $Pna2_1$ , with  $Z = 4$ . The acid molecule has lost one of its transferable hydrogens to the base molecule leaving it mono-deprotonated (Figure 5.2.6.1), therefore a salt has formed.

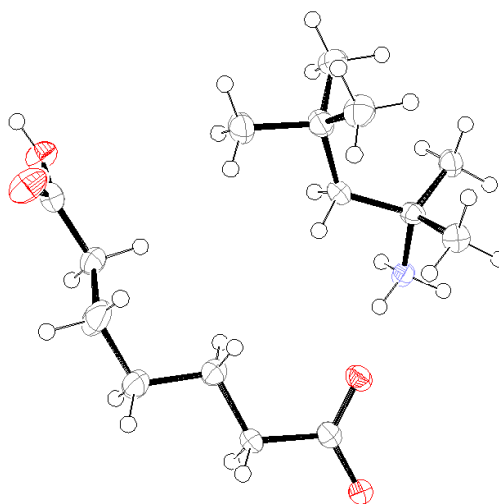


**Figure 5.2.6.1** Ortep diagram for the asymmetric unit of PmA and TMBA.

This structure also consists of tapes of alternately hydrogen bonded anions and cations with three hydrogen bonds from the cation and the monoanion. The longer chain of the anion adopts a twisted arrangement with the non-hydrogen groups on carbons 3 and 4 being in the *gauche* conformation to each other (torsion angle  $69.3(6)^\circ$ ).

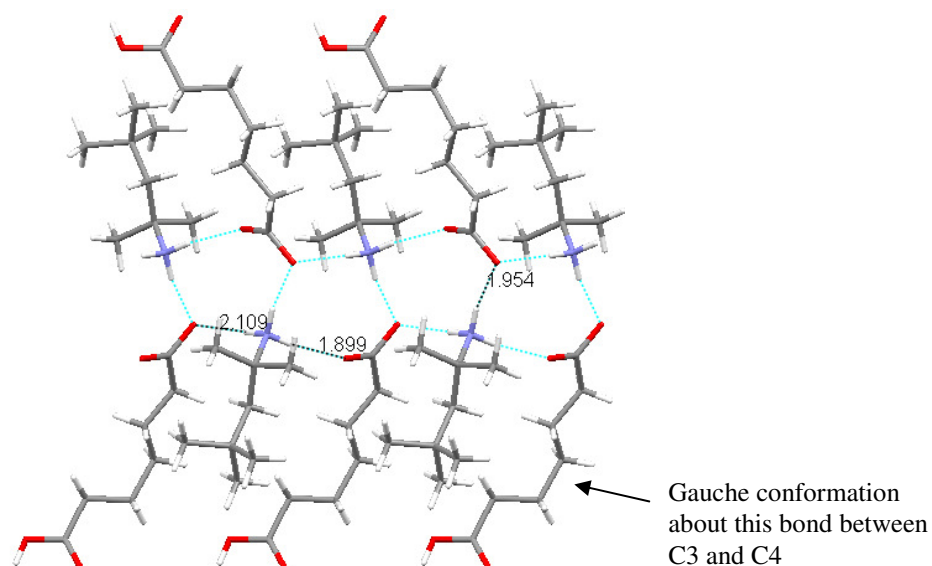


**Figure 5.2.6.2** Tape structure, hydrogen bond distances marked (error  $\pm 0.005$  Å).

The tapes are linked differently to the TMBA structures seen so far due to the anion having retained one of its hydrogens. The protonated end of the anion hydrogen bonds in the *syn-anti* conformation to the deprotonated end of an anion in an adjacent tape (1.76(4) Å), thus creating a 3-D network (Figure 5.2.6.3).

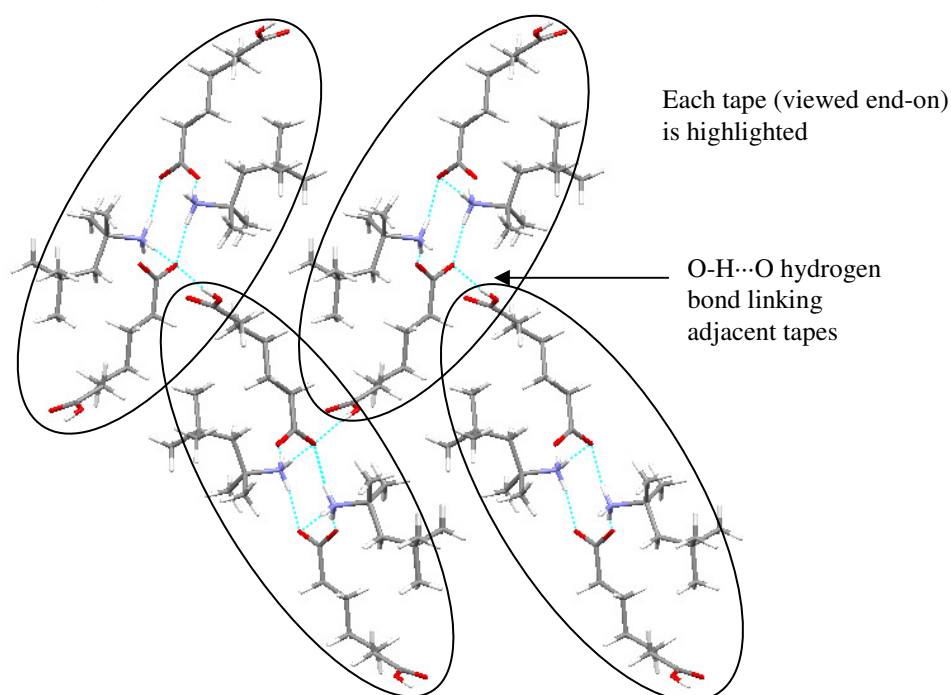


**Figure 5.2.6.3** 3-D network with each tape viewed end-on, viewed down the *c*-axis.

### 5.2.7 *DL*-Tartaric Acid and 1,1,3,3-Tetramethylbutylamine

These compounds crystallised together in the triclinic space group *P*-1, with *Z* = 2, in a 1:2 acid:base ratio with water also present in the structure, thus forming a salt dihydrate. The R-factor of the refined structure remained quite high (12.02%) and the ellipsoids for some of the cation

methyl groups are quite large. One of the water molecules is also disordered and it was not possible to locate the hydrogens. This is due to the water molecule occupying a cavity within the structure in which it was found in two positions (79.8% of the time in position *a*). Water molecules often rotate around their position, thus making it hard to find the hydrogens, and are even more prone to do so when in a cavity and disordered over two positions. Consequently, the hydrogens could not be located for the disordered water molecule.

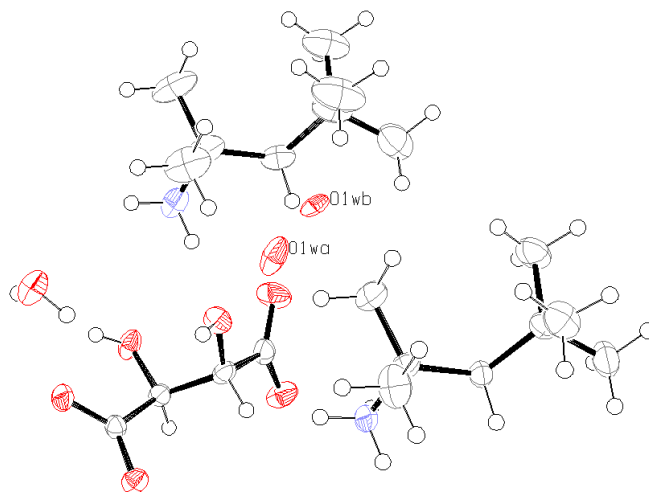


**Figure 5.2.7.1** Ortep diagram for the asymmetric unit of DLTA and TMBA.

The structure consists of a sheet of dianions and cations where the dianions are hydrogen bonded together in pairs (hydroxyl to carboxylate groups). Each of the cations is hydrogen bonded to two dianions: cation 2 hydrogen bonds to two anions, one in front of and one behind it along the *b*-axis; cation 3 hydrogen bonds to one anion in front of it and one behind it along the *a*-axis.

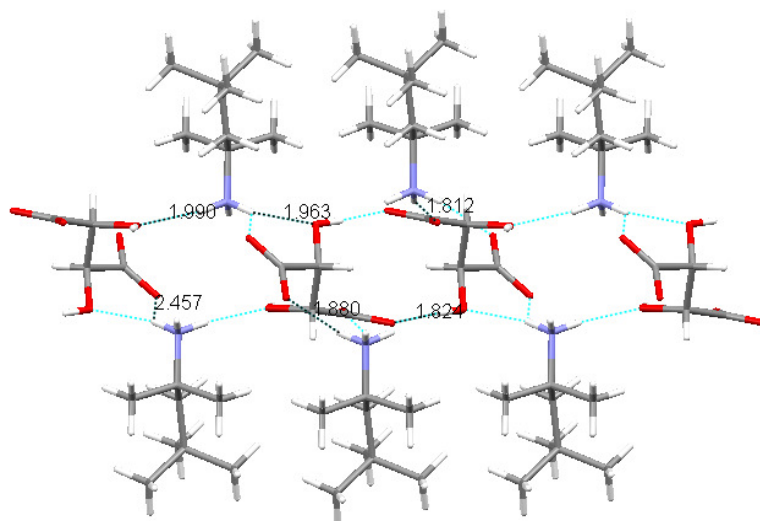


**Figure 5.2.7.2** Edge of the sheet, viewed down the *a*-axis; the water molecules are omitted for clarity (hydrogen bond distance error  $\pm 0.005$  Å).

The water molecules fill the voids between the anions and are involved in a number of hydrogen bonds which further bridge the ions in the sheet. In Figure 5.2.7.3a the water molecules are depicted as ‘space-filling,’ showing their positioning within the sheet when the sheet is viewed

side-on. The disordered water molecules appear as two spheres stuck together – this is the void which they fill. There is a separate set of hydrogen bonds for each of the positions of the disordered water molecule due to the availability of the hydroxyl and carboxylate groups next to the cavity they occupy (Figure 5.2.7.3b). The second non-disordered water molecule only has one possible set of hydrogen bonding contacts due to the orientation of the hydrogen bonding groups of the anion – this explains why this water molecule is not also disordered.

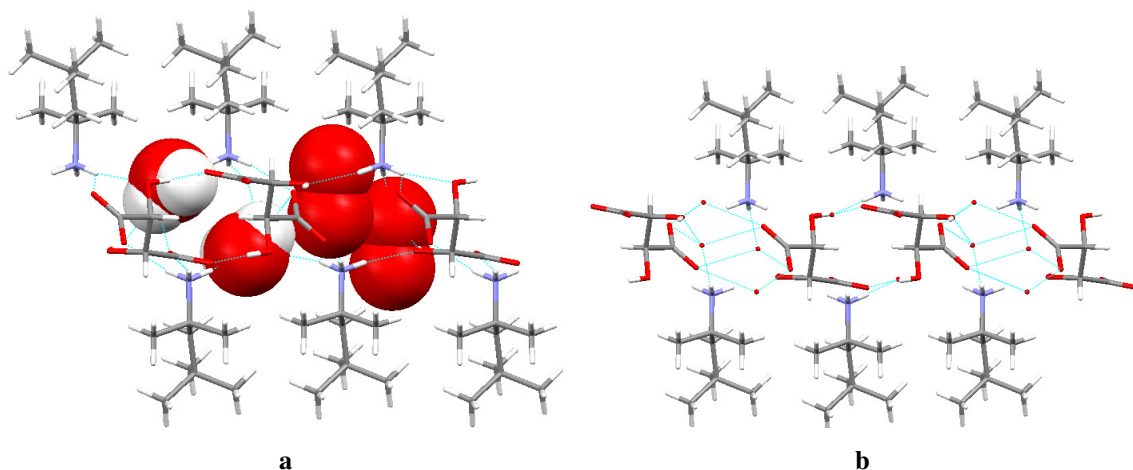


**Figure 5.2.7.3** a) Space-filling water molecules within the sheet; b) Possible short contacts between the water molecules

The sheets are stacked on top of each other so as the cations appear directly over each other but are actually staggered along the *a*-axis, due to the sheets being in a slipped arrangement. This increases the close-packing.

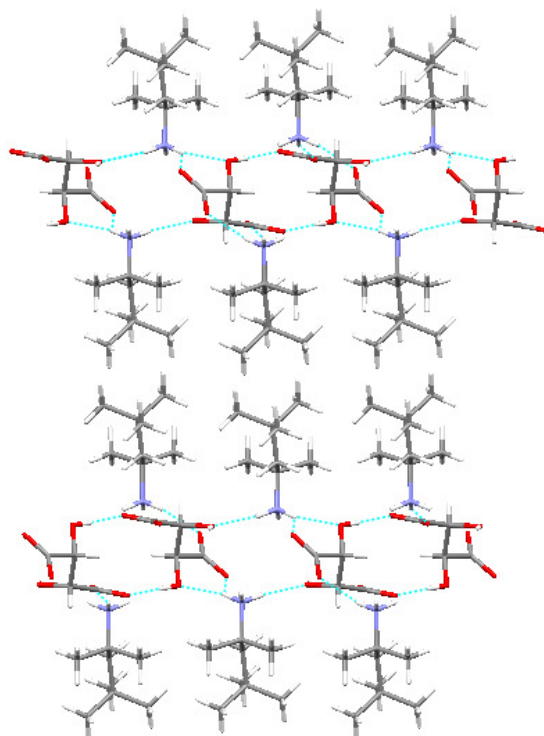


**Figure 5.2.7.4** Stacking of sheets viewed down the *a*-axis, water molecules omitted for clarity.



### 5.2.8 Maleic Acid and 1,1,3,3-Tetramethylbutylamine

The data for this crystal structure were collected using synchrotron radiation due to the very small size of the crystals. It was found that the components crystallised in a 1:1 ratio in the monoclinic space group  $P2_1/c$ , with  $Z = 8$ , to form a salt. The acid has also reacted with the methanol, resulting in one of the carboxyl groups on each anion being methylated (Figure 5.2.8.1).

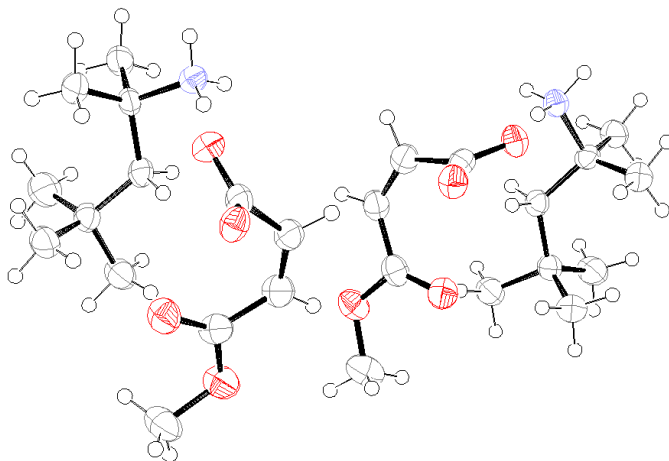


**Figure 5.2.8.1** Ortep diagram for the asymmetric unit of MeA and TMBA.

The structure consists of tapes of alternate anions and cations hydrogen bonded together. The anion has a flat carbon backbone (torsion angles  $-0.8(5)$  and  $1.5(5)^\circ$ ), however the planes of the free and methylated carboxylate groups are  $74.83$  and  $78.64^\circ$  to each other. The twisting of the carboxylate group enables the carbon backbone to fit between the cations, and the subsequent orientation of the methylated carboxyl group also enables closer packing. There are also weak  $C-H\cdots O$  hydrogen bonds within the tape between the methylene groups of the cations and the carbonyl of the methylated carboxyl group of the anion ( $2.552 \text{ \AA}$ ).

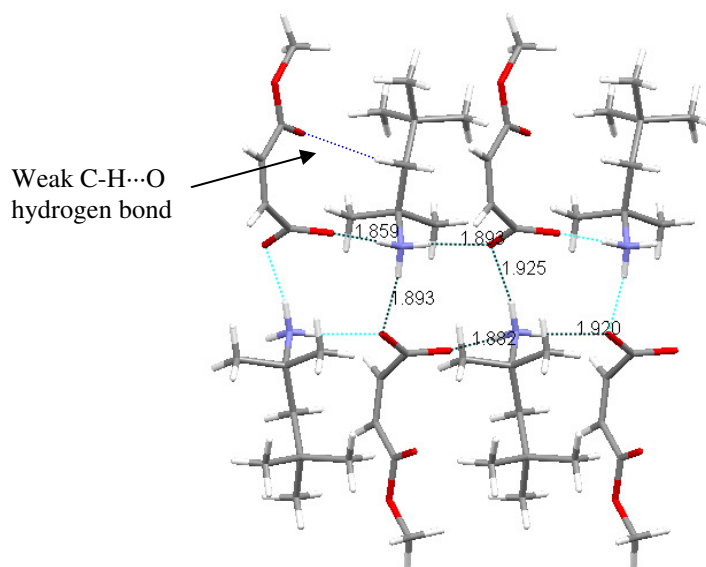


**Figure 5.2.8.2** Tape structure, hydrogen bond distances marked (error  $\pm 0.003 \text{ \AA}$ ).



Due to the methylation of the carboxyl group, the tapes are not linked together by the anions as seen in the other TMBA structures which adopt the tape arrangement. Instead the tapes are arranged so as adjacent tapes along the *c*-axis have like ions next to each other. This allows weak C-H...O hydrogen bonds between the aromatic hydrogens and the carboxylate group of adjacent anions. The arrangement is then slipped in the next 'layer' of tapes (Figure 5.2.8.3).

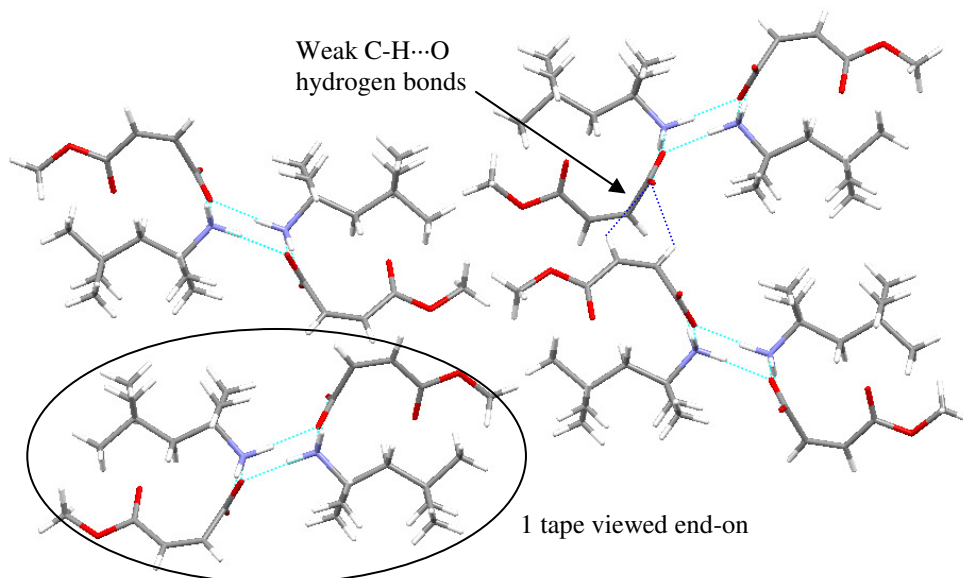


**Figure 5.2.8.3** Arrangement of tapes, viewed down the *a*-axis.

#### 5.2.9 *Fumaric Acid and 1,1,3,3-Tetramethylbutylamine*

The product from this crystallisation consists of very thin plates which gave poor data during analysis by SXRD. This resulted in the structure solution having a particularly high R-factor (19.26%) and the ellipsoids being larger than usual. In spite of this, the positions of the transferable hydrogens were easily located on the nitrogen. It was found that the components crystallised in a 1:2 acid:base ratio in the monoclinic space group  $P2_1/c$ , with  $Z = 2$ , to form a salt. The dianion lies across an inversion centre, with only half of the molecule shown in the asymmetric unit.

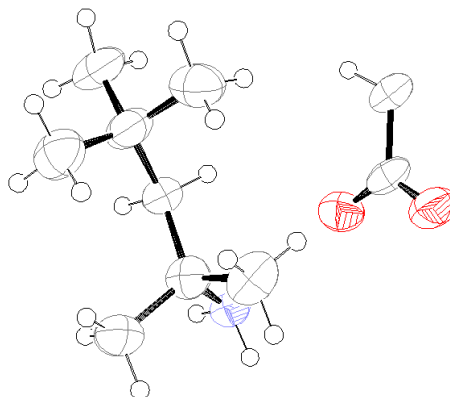


**Figure 5.2.9.1** Ortep diagram for the asymmetric unit of FmA and TMBA.

The structure consists of alternate anions and cations hydrogen bonded together to form tapes. The carbon backbone of the dianion is planar, however the carboxylate groups are twisted with respect to the plane of the carbon backbone (torsion angle =  $19.9(18)^\circ$ ).

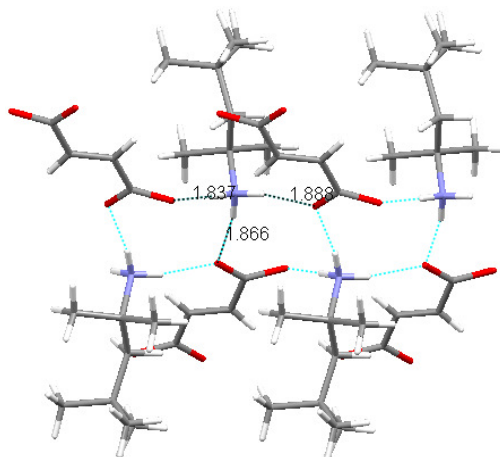


**Figure 5.2.9.2** Tape structure, hydrogen bond distances marked (error  $\pm 0.012$  Å).

The other carboxylate group of the dianion is also involved in the same tape structure and hence the tapes are linked across the dianions to form a sheet. The sheets are then stacked so as the bulky methyl groups of the cations fit between each other.

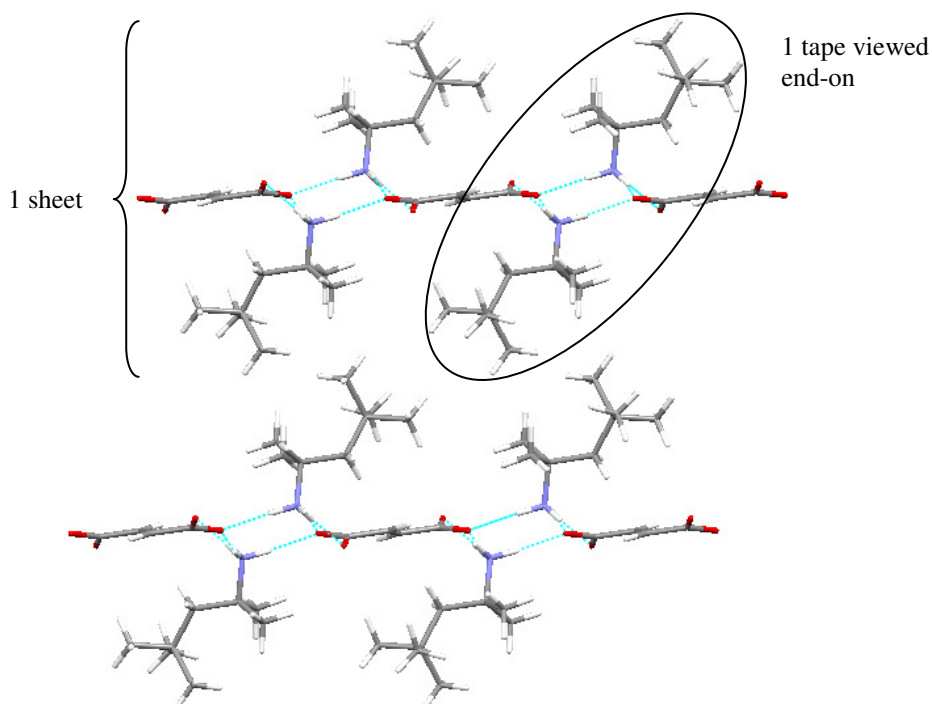


**Figure 5.2.9.3** Arrangement of sheets, each sheet viewed side-on.

#### 5.2.10 Discussion of 1,1,3,3-Tetramethylbutylamine Structures

From the well-plate crystallisations, only MnA-TMBA and ScA-TMBA did not form solid products and instead formed oils, however, both of these formed solid products when crystallised

using Method 3. The LTA-TMBA combination was found to have crystallised out separately. SbA-TMBA produced very small micro-crystals which were analysed by PXRD, however, the resulting pattern was inconclusive. Thermal analysis of SbA-TMBA using HSM showed partial melting at 66.7-80.5°C followed by complete melting at 130°C. The first melt suggests a new binary compound may have formed as the temperature is much lower than the melting point of the diacid, and higher than that of the base. The second melt may be diacid that has been left over from the binary compound formation.

Table 5.2.10 indicates various structural and physical parameters for the TMBA structures. Both OxA and MeA have been mono-deprotonated and the other carboxyl group has reacted with the methanol. The methylation may aid close packing by making the molecules a similar size to the base. ScA and PmA have both been mono-deprotonated while DLTA, FmA, GlA and AdA have all been di-deprotonated; the latter two also have a neutral acid molecule present in the structure. From the  $pK_a$  differences (Appendix, Table A2) double deprotonation of the acid is likely to occur as the minimum  $pK_a$  difference is 6.23 (SbA-TMBA).

	Contents of asymmetric unit	Structure type	Melting point/ °C	Density/ g cm <sup>-3</sup>	Packing index / %
OxA	4AMe <sup>-</sup> :4B <sup>+</sup>	Sheet	154.19	1.14	66.2
ScA	2A <sup>-</sup> :2B <sup>+</sup> :H <sub>2</sub> O	Sheet	57.76	1.12	64.8
GlA	½A:A <sup>2-</sup> :2B <sup>+</sup>	Tape→Sheet →3-D	83.7-89.3	1.11	66.6
AdA	½A: ½A <sup>2-</sup> :B <sup>+</sup>	Tape→Sheet →3-D	122.45	1.17	69.0
PmA	A <sup>-</sup> :B <sup>+</sup>	Tape →3-D	100.5	1.34	69.1
DLTA	A <sup>2-</sup> :2B <sup>+</sup> :2H <sub>2</sub> O	Sheet	159.4-167.7	1.13	66.4
MeA	2AMe <sup>-</sup> :2B <sup>+</sup>	Tape	96.43	1.12	65.2
FmA	½A <sup>2-</sup> :B <sup>+</sup>	Tape→Sheet	130.37	1.04	63.4

**Table 5.2.10** Various structural and physical parameters of the diacid-TMBA structures (Note: ‘Me’ in formula column indicates methylation of one of the carboxyl groups).

All of the structures except MeA-TMBA consist of sheets, though some also contain neutral acid molecules which link the sheets into 3-D arrays. ScA-TMBA is the only structure that has anions hydrogen bonded head-to-tail to form infinite chains. The structures that form tapes all have a similar hydrogen bonding motif linking the cations and anions. Of these, GlA-TMBA, AdA-TMBA and FmA-TMBA then form similar sheets, which are further linked by acid molecules in the first two instances. PmA-TMBA and MeA-TMBA also form similar tape structures, however the tapes are not linked to form sheets due to the mono-deprotonation of the acid molecule in the former and the methylation of one of the carboxyl groups in the latter. DLTA-TMBA forms sheets though the

arrangement of the molecules is slightly different as the diacid has more hydrogen bonding groups available. Although OxA-TMBA is methylated, the size of the anion affords two hydrogen bonds with the cation positioned to the side of the diacid as well as two with the cation facing its carboxylate group.

Although some of the structures are similar, the ratios of ions and neutral moieties are different for each case. The tape arrangement that is seen in five of the structures requires a 1:1 ion ratio (as in the case of PmA and MeA), however if the anion is double deprotonated then the second carboxylate group is also involved in another tape and hence the ratio changes to 1dianion:2cations (as in the case of GlA, AdA and FmA). As all the crystallisations were prepared in a 1:1 ratio, except DLTA which had excess base, it would appear that the deprotonation directs the ratio of the components rather than the other way round. Furthermore, the preferred structure type from the hydrogen bonding synthon appears to direct the deprotonation, as opposed to the components forming a structure in their crystallisation ratios and the deprotonation being dictated by the  $pK_a$  differences.

Analysis using PLATON found that the ScA and FmA structures contain discrete voids of volumes  $75.7 \text{ \AA}^3$  and  $67.1 \text{ \AA}^3$  respectively which could potentially be filled by solvent. These are in addition to the other small voids in the structure that are not accessible to solvent molecules. The large voids constitute 2.5% of the total unit cell volume for the ScA structure and 5.6% for the FmA structure. Voids of the sizes found here are easily capable of fitting a hydrogen bonded water molecule ( $40 \text{ \AA}^3$ ), however, the voids in the structures are surrounded by hydrophobic groups, preventing hydrogen bonding. To confirm there were no disordered solvent molecules present in the voids, the SQUEEZE command in PLATON was used. The presence of voids, as well as the chain structure, explains the low melting point of the ScA-TMBA structure. The FmA structure is similar to the other structures found in the series, and hence it can be inferred that in spite of the low packing index this supramolecular structure is fairly stable, as is reflected by the higher melting point.

The conformation of the anion/acid molecule appears to accommodate for the method of packing; there is more torsion in the longer chain diacids, not only because this is more possible as chain length increases, but also to accommodate the long chain into the structure. The *gauche* conformation is adopted at least once in three of the four structures with four or more carbons, to increase the close packing and orientate the hydrogen bonding groups appropriately. Hence, the long chain diacids have high densities compared to the rest of the group. The highest density structure is PmA-TMBA even though it only has a melting point of  $100.5^\circ\text{C}$ . This is because the increased density from the twisted alkyl chain does not contribute to the stability of the structure (and hence influence the melting point). In fact the highest melting point is for DLTA-TMBA, in spite of its low density. This is due to the extra hydrogen bonding interactions possible from the hydroxyl groups.

TMBA is able to freely rotate its methyl and ammonium groups as there are no restrictive bonds. Although there are actually three possible positions of the nitrogen with relation to the methylene backbone of the compound, two appear the same and hence there are two identifiable conformations. Thus the probability of the nitrogen pointing in the same direction as the backbone is 30%. Analysis of the TMBA conformations show that out of the fifteen instances described here, thirteen take a conformation with the nitrogen pointing in the same direction as the methylene backbone (Figure 5.2.10.1) whereas the remaining two point down and sideways from the methylene backbone.

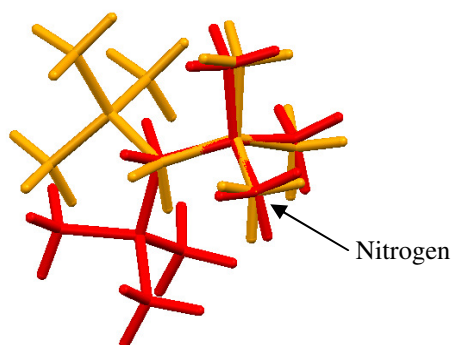


**Figure 5.2.10.1** Overlay of the two TMBA molecules from the ScA-TMBA structure to show the two conformations of the cation; 13 in the yellow conformation, 2 in the red.

There are also a number of weak C-H...O hydrogen bonds present in each of the structures, these are from the cation methyl and methylene groups and also from the anion alkyl or alkene groups. On average the interactions are 2.606 Å in length; the strongest of these interactions are in the MeA structure from the aromatic hydrogens of the anions to the carboxylate group (2.493 Å).

### 5.3 1,2-DIAMINOETHANE

#### 5.3.1 Oxalic Acid and 1,2-Diaminoethane (PEPMOM)

Crystals of ethylenediammonium bis(monohydrogen oxalate) monohydrate were obtained by Barnes *et al.*<sup>3</sup> by slow evaporation of an aqueous mixture of OxA and DAE at room temperature. The components crystallised in a 2:1 acid:base ratio with water to form a salt monohydrate in the monoclinic space group  $C2/c$ , with  $Z = 4$ ; this structure was found to crystallise regardless of the ratio of the components during crystallisation. The dication lies across an inversion centre, making it centrosymmetric, and the water molecule lies across a 2-fold rotation axis. The structure consists of parallel linear chains of monoanions hydrogen bonded together in the *syn-syn* conformation (Figure 5.3.1.1).

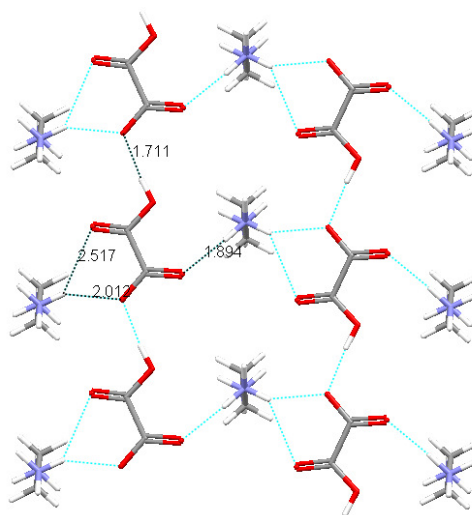


**Figure 5.3.1.1** Anion chains linked by hydrogen bonding across the cations (hydrogen bond distance error  $\pm 0.003$  Å).

Pairs of anti-parallel anion chains are linked by hydrogen bonding across the dications that are perpendicular to the chain, thus forming a sheet. Tetrahedral hydrogen bonding of the water molecules links the adjacent sheets to form a 3-D array.

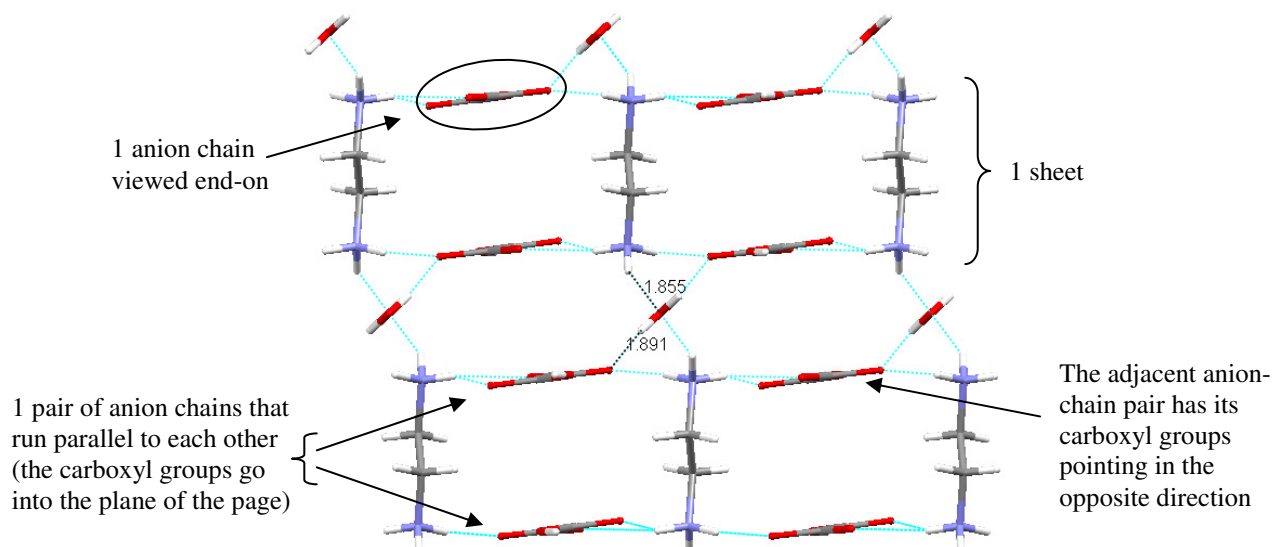


**Figure 5.3.1.2** The 3-D network, viewed down the *b*-axis (hydrogen bond distance error  $\pm 0.003$  Å).

### 5.3.2 Malonic Acid and 1,2-Diaminoethane (WOBXIU)

This crystal structure was obtained by Barnes *et al.*<sup>4</sup> through the slow evaporation of an equimolar aqueous mixture of MnA and DAE. The components crystallised in a 2:1 acid:base ratio with water to form a salt monohydrate in the monoclinic space group *P2<sub>1</sub>/n*, with *Z* = 2; this structure was found to crystallise regardless of the ratio of the components during crystallisation.

In this compound the monoanion has a strong intramolecular O-H...O hydrogen bond of 1.33(2) Å (the O-H distance is 1.13(2) Å). The anions are connected into pairs through hydrogen bonds of

1.889(19) Å from the water molecule which is positioned on a two-fold rotation axis. The dication is centrosymmetric as it lies across an inversion centre; each ammonium ion is involved in hydrogen bonding to three anions and a water molecule thereby resulting in a 3-D network.

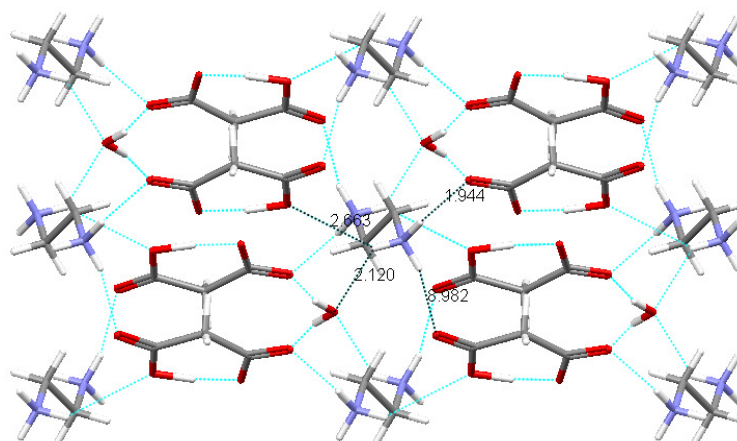


**Figure 5.3.2.1** 3-D network with N-H...O hydrogen bond distance marked, viewed down the *a*-axis (hydrogen bond distance error  $\pm 0.020$  Å).

### 5.3.3 Succinic Acid and 1,2-Diaminoethane (PINNIJ)

This crystal structure was obtained by Schreuer *et al.*;<sup>5</sup> it was found that the components crystallised in a 2:1 acid-base ratio in the monoclinic space group  $P2_1/c$ , with  $Z = 2$ , to form a salt. The dication lies across an inversion centre making the two nitrogen atoms equivalent.

The structure consists of chains of monoanions hydrogen bonded together in the *syn-syn* conformation (1.696 Å). Dications are further hydrogen bonded to the carboxylate groups of the monoanions thus linking the adjacent anion chains. The orientation of the cation enables it to link anion chains, which are stacked on top of each other, along the *b*-axis as well as the *c*-axis thereby forming a 3-D network. The free oxygen of the carboxyl group is involved in weak C-H...O hydrogen bonds with the methylene groups of adjacent anions and cations (2.595 and 2.476 Å respectively).

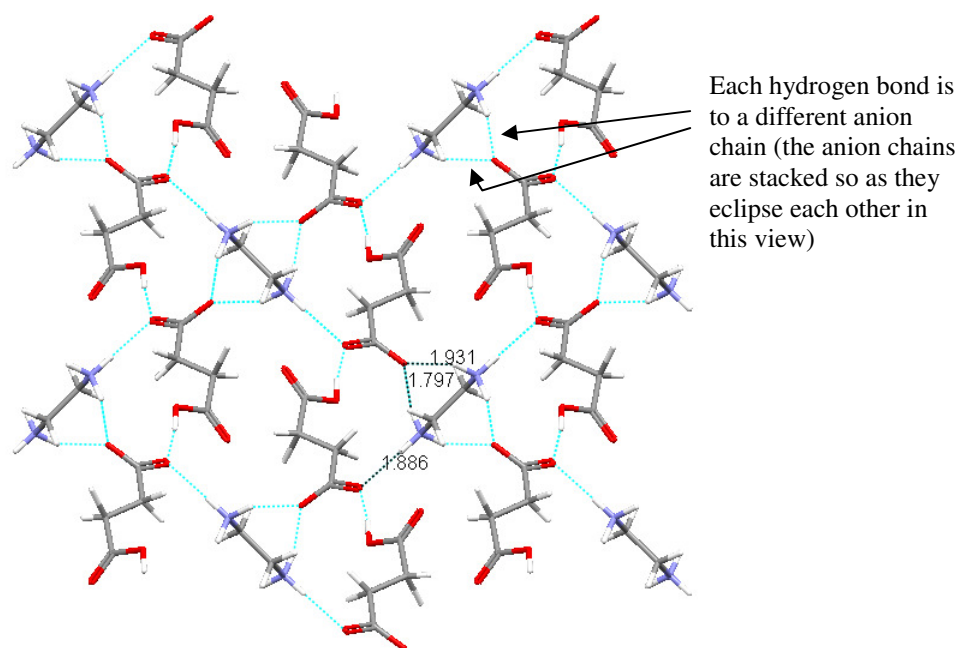


**Figure 5.3.3.1** 3-D structure, viewed down the *a*-axis.

#### 5.3.4 Glutaric Acid and 1,2-Diaminoethane

These compounds crystallised together in the monoclinic space group  $P2_1/n$ , with  $Z = 4$ , in a 1:1 ratio to form a salt.

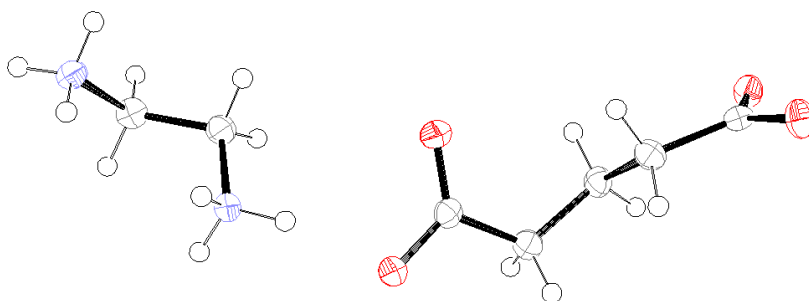


**Figure 5.3.4.1** Ortep diagram for the asymmetric unit of GIA and DAE.

This structure consists of alternate dianions and dications hydrogen bonded together to form a 3-D network. The dianions are twisted and adopt a *gauche* conformation across carbons 3 and 4 (torsion angle  $72.0(3)^\circ$ ), in addition, their carboxylate groups are in different planes ( $86.04^\circ$  between  $\text{COO}^-$  planes). Each carboxylate group is involved in four hydrogen bonds to three different dications. The dications also adopt a *gauche* conformation (torsion angle  $74.1(3)^\circ$ ); the dication is positioned facing one of the carboxylate groups so as each nitrogen hydrogen bonds with one of the oxygens to create a seven-membered ring (1.78(1) and 1.86(1) Å). The other carboxylate group is involved in a bifurcated hydrogen bond to one ammonium group of the dication (1.82(1) and 2.67(1) Å). These and the other N-H...O hydrogen bond distances are shown in Figure 5.3.4.2.



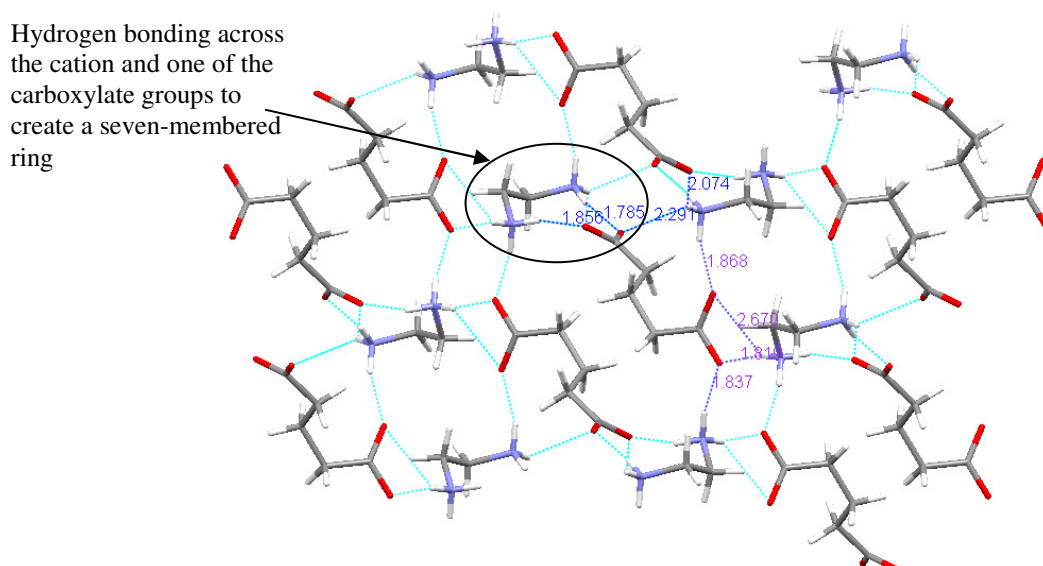


**Figure 5.3.4.2** 3-D network, hydrogen bond distances (error  $\pm 0.003$  Å) from one carboxylate group are shown in blue, those from the other are shown in purple; viewed down the  $c$ -axis.

### 5.3.5 Adipic Acid and 1,2-Diaminoethane (ZZZGYW)

Although this structure is noted on the CSD, there are no co-ordinates or cif file available for it. Some details with regards to the crystal synthesis and the unit cell were obtained from the literature. The compound was prepared by slow cooling of a hot methyl alcohol solution of the acid and the base to give thin needle crystals. The components were found to crystallise in a 1:1 ratio in the monoclinic space group  $P2_1/a$ , with  $Z = 2$ , to form a salt with both of the acidic hydrogens having been transferred to the base. Attempts to crystallise this product to repeat the SXRD analysis have been unsuccessful, only producing very small crystals that are unsuitable for the analysis.

### 5.3.6 D-Tartaric Acid and 1,2-Diaminoethane (EDATAR10)

This crystal structure was first characterised by Perez<sup>6</sup> in 1976; the crystals were obtained through the slow evaporation at 41°C of an equimolar aqueous mixture of the acid and base. The components were found to crystallise in a 1:1 ratio in the monoclinic space group  $P2_1$ , with  $Z = 2$ , to form a salt.

The structure consists of a dianion sheet where the dianions are linked by hydrogen bonding between the hydroxyl and carboxylate groups (Figure 5.3.6.1). The dications are linked to the hydroxyl and carboxylate oxygen atoms of adjacent anion sheets by three hydrogen bonds from one of the ammonium groups and five from the other.

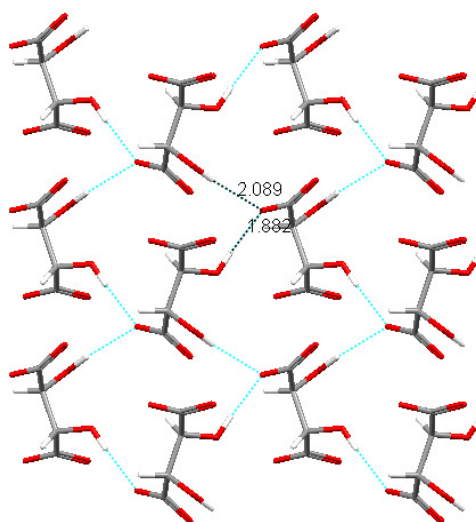


**Figure 5.3.6.1** Hydrogen bonded dianion sheet.

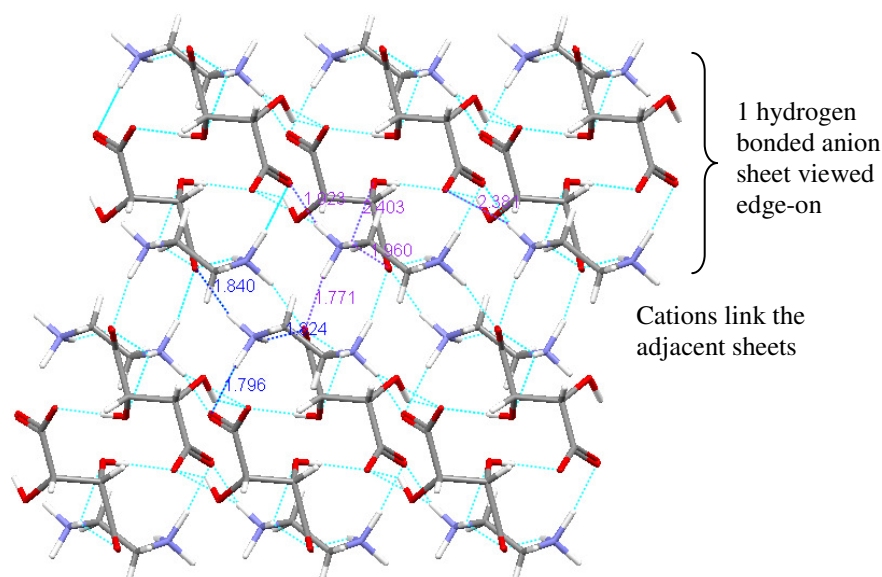


**Figure 5.3.6.2** 3-D network, hydrogen bond distances from one of the ammonium groups is shown in blue, those from the other are shown in purple; viewed down the *b*-axis.

### 5.3.7 *DL-Tartaric Acid and 1,2-Diaminoethane*

The crystalline product from this acid-base combination was analysed by SXRD and was found to have the same unit cell as that of ethylenediamine ditartrate dihydrate (ENHTAR) which only contains one of the TA isomers. Thus the DLTA has undergone spontaneous resolution in the presence of DAE to result in the D and L forms crystallising out separately with the DAE.

The crystal structure was first obtained by Pérez<sup>7</sup> during a study of the critical temperature of the crystal growth of anhydrous ethylenediamine D-tartrate (EDATAR10); it was found that by cooling a supersaturated solution of DAE-DTA at a rate of 0.025°C per day from 41.5 to 40°C a dihydrate form crystallised. The components crystallised in a 2:1 acid:base ratio in the tetragonal space group

$P4_12_12$ , with  $Z = 4$ , to form a salt hydrate. The dication lies on a special position making the two nitrogens equivalent.

The structure consists of monoanions hydrogen bonded head-to-tail in the *syn-syn* conformation (1.45(4) Å) to form a chain. The chains are then linked by hydrogen bonding with each other between the hydroxyl and carboxylate groups (2.01(4) and 2.49(4) Å) to form a layer. The dications are subtended from the layer by hydrogen bonds to the carboxyl (1.85(3) and 2.71(4) Å), carboxylate (1.94(4) Å) and hydroxyl groups (2.49(4) Å) and act to link adjacent anion layers, thus creating a 3-D network. The cations adopt the *gauche* conformation (torsion angle  $-71.34^\circ$ ). Adjacent anion layers are orientated so as the head-to-tail linked chains are parallel to the *a*-axis in one layer and the *b*-axis in the adjacent layer. Water molecules are also involved in three hydrogen bonds, two to anions and one to a cation, further stabilising the structure.

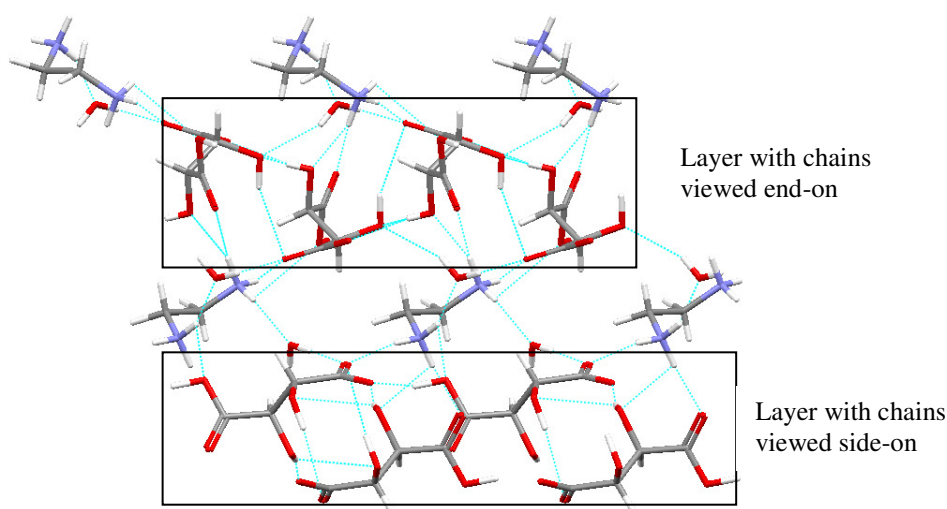


**Figure 5.3.7.1** 3-D network made up of layers of anions with cations and water molecules linking the layers, viewed down the *a*-axis.

### 5.3.8 Maleic Acid and 1,2-Diaminoethane (ROHKUU)

This crystal structure was obtained by Barnes *et al.*<sup>8</sup> by mixing together ethanolic solutions of 2 mmol MeA and 1 mmol DAE hydrate and then re-crystallising the precipitate from water. It was found that the components crystallised in a 2:1 acid-base ratio in the triclinic space group  $P-1$ , with  $Z = 1$ , to form a salt. The dication occupies an inversion centre making the two nitrogen atoms equivalent. There is also a strong intramolecular bond between the carboxyl and carboxylate groups of the monoanion (1.42(3) Å).

The monoanions are arranged in layers; the carboxylate group of the anion is involved in hydrogen bonding with three dications and the free oxygen of the carboxyl group is hydrogen bonded to one dication. The cations span a pair of layers, with the ammonium groups not only linking the anions

to form layers, but also linking adjacent pairs of layers, thus creating a 3-D network. There are also weak C-H...O hydrogen bonds between the anions (2.575 and 2.662 Å) and between the cations and anions (2.645 and 2.675 Å) which further stabilise the structure.

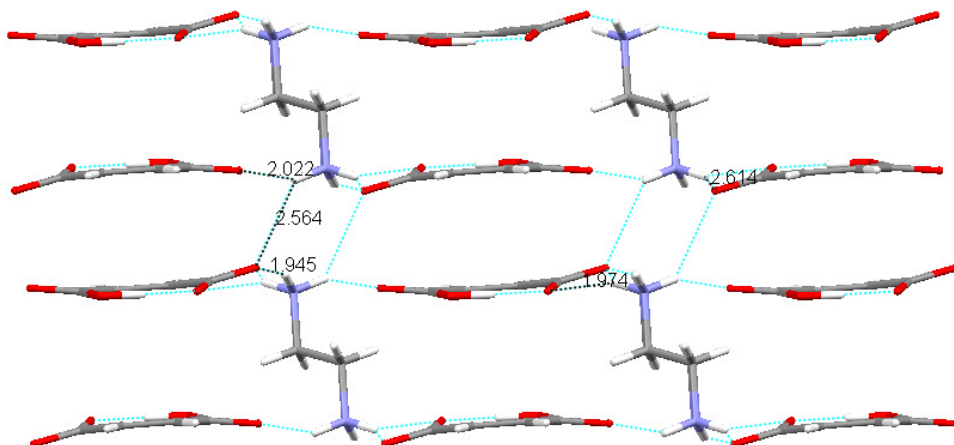


**Figure 5.3.8.1** 3-D network viewed down the *a*-axis, hydrogen bond distances marked (error +/-0.002 Å).

### 5.3.9 Fumaric Acid and 1,2-Diaminoethane

These compounds crystallised in a 1:1 ratio in the triclinic space group *P*-1, with *Z* = 1, to form a salt. Both of the components lie across inversion centres, therefore the two nitrogens of the dication are equivalent, as are the carboxylate groups of the dianion.

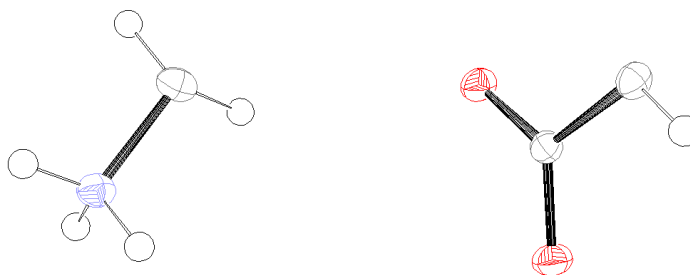


**Figure 5.3.9.1** Ortep diagram for the asymmetric unit of FmA and DAE.

The structure consists of a 3-D array of alternate anions and cations hydrogen bonded together. Each ion is surrounded by 8 ions of the opposite charge; each carboxylate group is hydrogen bonded to four cations. There are also weak C-H...O hydrogen bonds between the anions (2.513 Å), and between the methylene groups of the cations and the anions (2.709 Å) which further stabilise the structure.

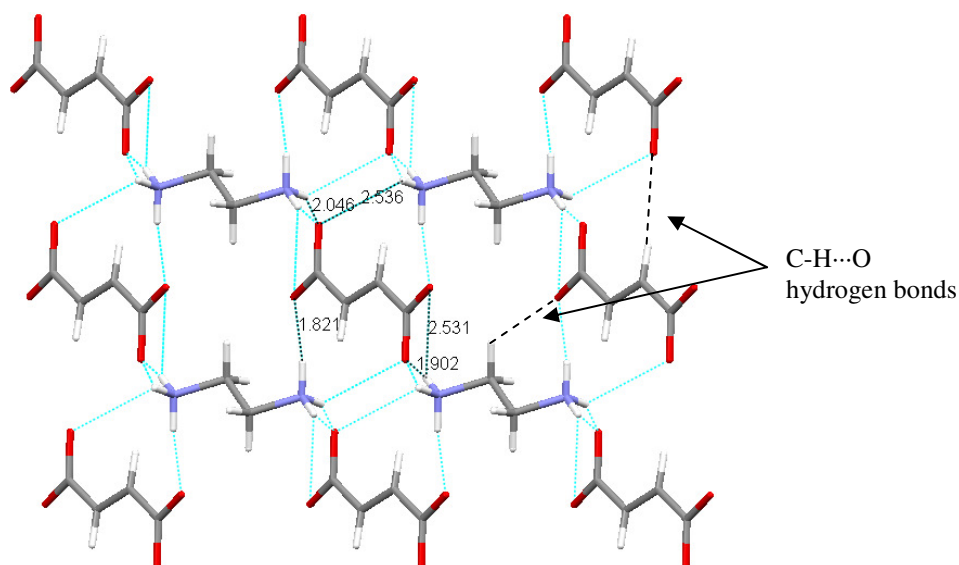


**Figure 5.3.9.2** Hydrogen bonded 3-D network of alternate anions and cations (hydrogen bond distance error  $\pm 0.002$  Å), viewed down the  $a$ -axis.

Two morphologies were found in the FmA-DAE well - a powder was present in the bottom of the well and block crystals were found at the top of the well. PXRD of the powder was found to be consistent with the powder pattern generated from this crystal structure.

### 5.3.10 Discussion of 1,2-Diaminoethane Structures

Some of the structural and physical parameters of the DAE salts are given in Table 5.3.10.

	Contents of asymmetric unit	Structure type	DAE cation conformation	Density/ g cm <sup>-3</sup>
OxA	$A^-:\frac{1}{2}B^{2+}:\frac{1}{2}H_2O$	3-D (layers)	Anti	1.508
MnA	$A^-:\frac{1}{2}B^{2+}:\frac{1}{2}H_2O$	3-D	Anti	1.483
ScA	$A^-:\frac{1}{2}B^{2+}$	3-D	Anti	1.483
GlA	$A^{2-}:B^{2+}$	3-D	Gauche	1.32
DTA	$A^{2-}:B^{2+}$	3-D (layers)	Anti	1.526
D/LTA	$A^-:\frac{1}{2}B^{2+}$	3-D (layers)	Gauche	1.529
MeA	$A^-:\frac{1}{2}B^{2+}$	3-D (layers)	Anti	1.538
FmA	$\frac{1}{2}A^{2-}:\frac{1}{2}B^{2+}$	3-D	Anti	1.49

**Table 5.3.10** Various structural and physical parameters of the diacid-DAE structures.

All of the diacids except PmA and SbA crystallised with DAE to produce salts or salt hydrates. The PmA and SbA products were instead analysed by PXRD; both produced weak patterns from which it could not conclusively be determined if a binary product had formed. The melting points of the PmA and SbA products were found using DSC; both are quite close to the melting points of the diacid starting materials suggesting that the components may have crystallised out separately.

Although the DAE molecule in each of the structures is diprotonated, the deprotonation of the diacid molecules changes throughout the series. From the  $pK_a$  differences (Appendix, Table A2) it can be seen that loss of the second hydrogen of the diacid to the second nitrogen of the dibase is not likely as the  $pK_a$  difference is less than 3 (maximum 2.58 for OxA and minimum 0.70 for MeA). For the first ionisation, the  $pK_a$  differences are between 8.66 and 5.37 units and therefore a salt is expected to form. In five out of the eight structures the components crystallised in a 2:1 acid:base ratio i.e. a second diacid molecule loses a proton to a monoprotonated diamine, the  $pK_a$  differences for which are between 5.54 and 2.25 units. This concurs with other studies that show that a rule of two may be more appropriate in predicting proton transfer (discussed in Section 2.4.2). The diacids with the smallest  $pK_a$  difference, PmA and SbA, did not form crystals suitable for SXRD analysis and hence the ratios of their components, if binary, are unknown. The protonation of a DAE monocation by a second ScA molecule further concurs with a rule of two as the  $pK_a$  difference is 2.57 units. The 2:1 acid:base ratio found here may be due to the strong O-H...O hydrogen bonded anion chain that can form between monoanions directing the stoichiometry. The 1:1 ratio of the components in the GlA-DAE structure is unlikely as the  $pK_a$  differences are 5.58 and 1.36 units; this stoichiometry is in keeping with that from crystallisation which may, together with the strong hydrogen bonds that are formed, drive the formation of this structure. This further demonstrates that there are more factors influencing the deprotonation than just the  $pK_a$ . DTA and FmA also have a 1:1 component ratio, however, the  $pK_a$  differences are all greater than two units.

It is interesting to note that in DLTA-DAE the TA was spontaneously resolved to form binary compounds of each of its optical components with DAE. These structures differ in their stoichiometry and also in that one contains the solvent the crystallisation was prepared with. From the  $pK_a$  differences, a 2:1 acid:base ratio is more likely than a 1:1 ratio. Perhaps the inclusion of water in the structure affects the deprotonation of the diacid. It should be noted, however, that all the structures that contain water have a  $pK_a$  difference greater than three.

In all of the 2:1 acid:base ratio structures, the anions form a hydrogen bonded chain, except in the MnA-DAE and MeA-DAE structures which both have a strong intramolecular hydrogen bond. It should be noted that the simple even diacids form anion chains whereas the odd diacids do not. DTA-DAE (EDATAR10) also forms an anion chain even though it is di-deprotonated; this is possible as the hydroxyl groups on the anion can act as hydrogen bond donors also. The presence of water in the OxA-DAE extends the layer structure in to a 3-D array. The layers formed are similar to those in MeA-DAE. The other structures also consist of 3-D arrays, however, they do not form the same layer arrangement as OxA and MeA.

All the DAE cations in the above structures are in the *anti* conformation (average torsion angle = 178.67°) except in the GlA and DTA (ENHTAR) structures which are in the *gauche* conformation

(torsion angles of  $74.1(3)^\circ$  and  $-71.34^\circ$  respectively). The carbon-carbon distances in the centre of the DAE molecule are slightly longer in the *anti* conformations (range 1.503–1.518 Å) than in the *gauche* conformation (1.500(4) Å and 1.503 Å). In a study by Chang *et al.*<sup>9</sup> it was found that the *gauche* conformation of neutral DAE is more stable than the *anti* conformation by 0.84 kcal mol<sup>-1</sup> due to intramolecular hydrogen bonding, however all the SXR D structural analyses show the ion in the *anti* conformation. The adoption of the higher energy configuration may therefore be due to packing and intermolecular interactions. A search of the CSD for the neutral DAE molecule gives only one instance of the *gauche* conformation out of 13 distinct structures. When the CSD was searched for diprotonated DAE, 27 structures were found to contain the compound in the *gauche* conformation and 75 in the *anti* conformation; a further 5 structures contained both of the conformations. The results from the CSD indicate a 1 in 4 frequency of the *gauche* conformation occurring which is similar to the frequency seen here. The anions are predominantly quite flat, with only GlA adopting a *gauche* conformation in its alkyl chain. The presence of this conformation may be to increase the close packing of the molecules. The conformation also enables the seven-membered hydrogen bonded ring to form across the cation and the carboxylate group – a hydrogen bond motif that is not possible when the cation is in the *anti* conformation.

Although there are only a couple of melting points available for these structures, these decrease as chain length increases (Appendix, Table A6). The densities of the structures on the CSD are available from the literature and it can be seen that the density decreases as chain length increases; DTA, MeA and FmA binary compounds all have high density, with MeA-DAE being the highest.

## 5.4 2-AMINOETHANOL

### 5.4.1 Oxalic Acid and 2-Aminoethanol (QAMRIF)

Bis(2-hydroxyethylammonium) oxalate was obtained by Jordanovska *et al.*<sup>10</sup> by neutralisation of an aqueous solution of OxA with aqueous AEI at pH 8; crystallisation occurred after cooling the solution to room temperature. The components were found to crystallise in a 1:2 acid:base ratio in the monoclinic space group *C2/c*, with *Z* = 4, to form a salt.

The structure consists of layers of hydrogen bonded molecules where the monocations are positioned above and below a central core of dianions to form a bilayer (Figure 5.4.1.1). The bilayer extends down the *b*- and *c*-axes due to the hydroxyl and ammonium groups of the cation forming hydrogen bonds with different dianions. The methylene groups of the cation point outwards from the bilayer due to the nitrogen and the oxygen being involved in hydrogen bonding.

Adjacent layers are arranged so as the methylene groups fit between those of the adjacent layer, enabling closer packing.

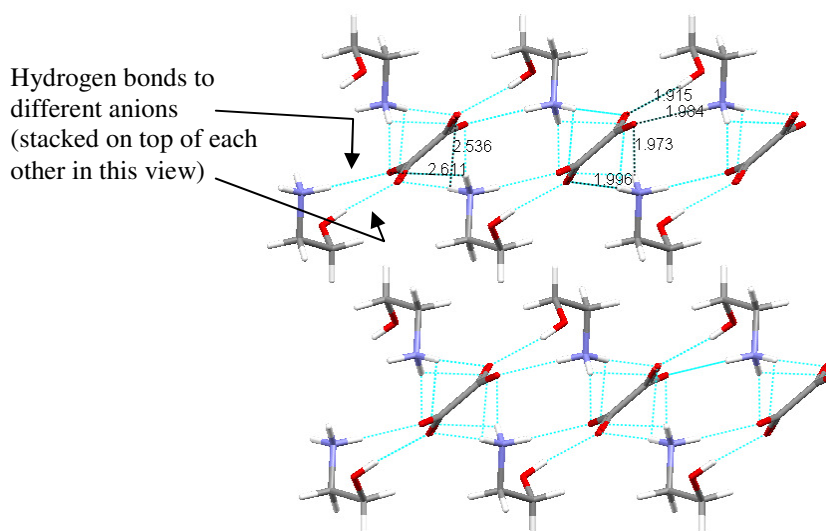


**Figure 5.4.1.1** Bilayer structure viewed side-on, down the *b*-axis (hydrogen bond distance error  $\pm 0.003$  Å).

#### 5.4.2 Succinic Acid and 2-Aminoethanol

These compounds crystallised together in a 1:1 ratio in the triclinic space group *P*-1, with *Z* = 2, to form a mixed system. In the asymmetric unit the acid molecule is present in two halves, both of which lie on inversion centres; only one half has retained its proton therefore resulting in a neutral acid molecule and a dianion.

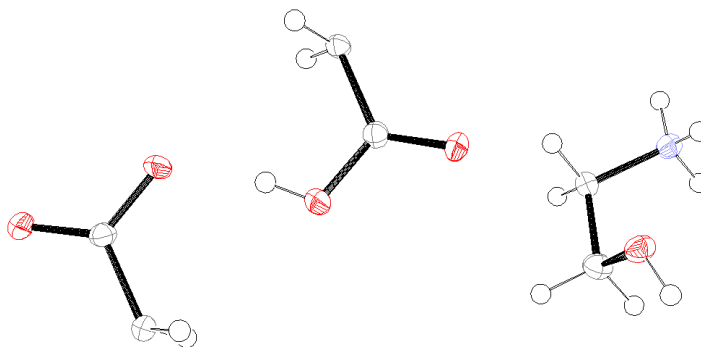


**Figure 5.4.2.1** Ortep diagram for the asymmetric unit of ScA and AEI.

The structure consists of chains of alternate dianions and acid molecules hydrogen bonded together in the *anti-anti* conformation. The cations are then subtended from this chain, above and below the central acid-anion core.



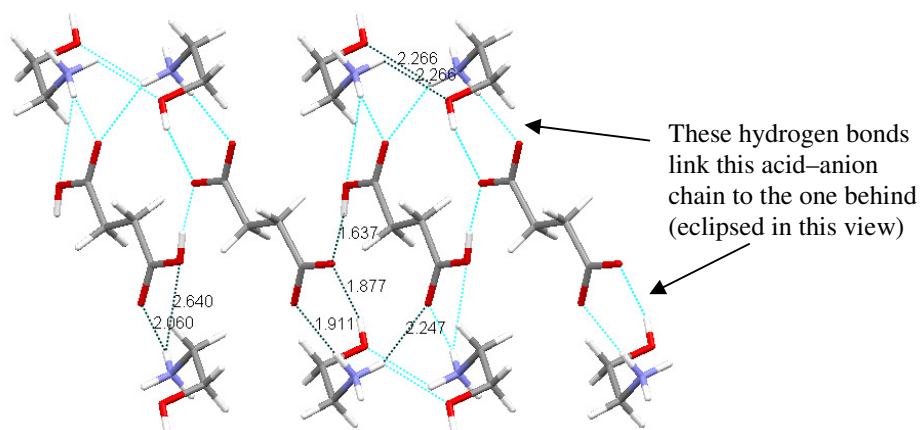


**Figure 5.4.2.2** Bilayer type chain structure, viewed down the *a*-axis (hydrogen bond distance error  $\pm 0.003$  Å).

Due to the orientation of the cations, the ammonium and hydroxyl groups do not hydrogen bond to the same acid-anion chain, and instead hydrogen bond to adjacent chains, thus creating a 3-D network.

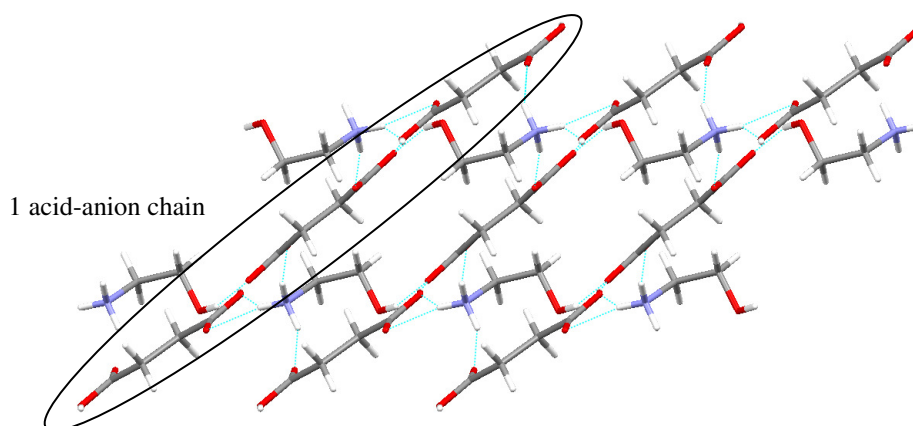


**Figure 5.4.2.3** 3-D network with acid-anion chains linked by hydrogen bonding across the cations, viewed down the *c*-axis.

#### 5.4.3 Suberic Acid and 2-Aminoethanol

These compounds crystallised in a 1:1 ratio in the triclinic space group *P*-1, with *Z* = 8, to form a mixed system. The R-factor of the refined structure remained quite high (11.52%) however all of the transferable hydrogens were located and their positions were confirmed by the C-O and C=O bond distances. Some of the ellipsoids are slightly larger than usual due to the poor quality of the crystal and the resulting data.

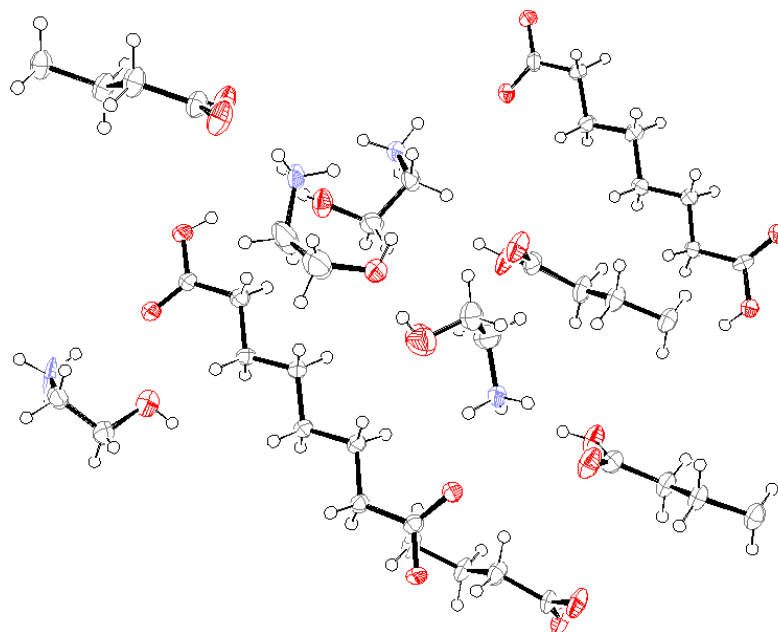


**Figure 5.4.3.1** Ortep diagram for the asymmetric unit of ScA and AEI.

This structure consists of a number of anion chain configurations:

- Molecule 1 is a monoanion that forms a chain with itself through hydrogen bonding in the *anti-anti* conformation (1.65(1) Å). Cations are linked to the chain by hydrogen bonds from the ammonium and hydroxyl groups to the carboxylate and free oxygen of the carboxyl groups.

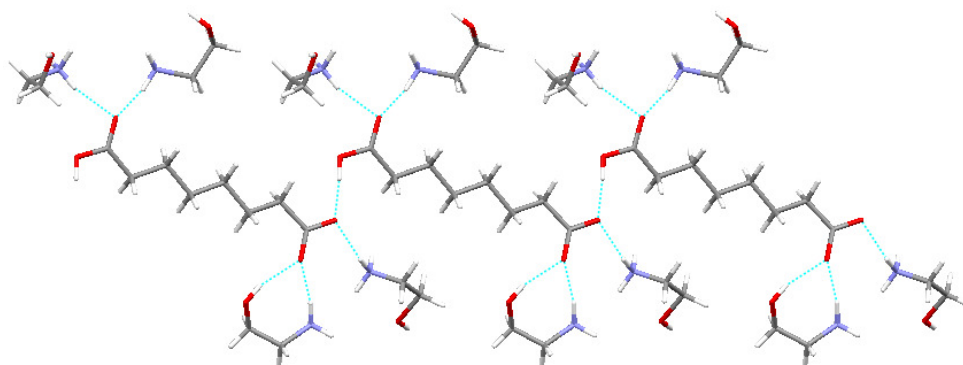


**Figure 5.4.3.2** Chain structure involving monoanion 1.

- Molecules 3 and 5 are an acid molecule and a dianion respectively and are hydrogen bonded together in the *syn-syn* conformation to form another chain (1.72(1) Å). Cations are then subtended from this chain via hydrogen bonds from the ammonium group only, to the carboxylate group and the free oxygen of the carboxyl group (Figure 5.4.3.3).

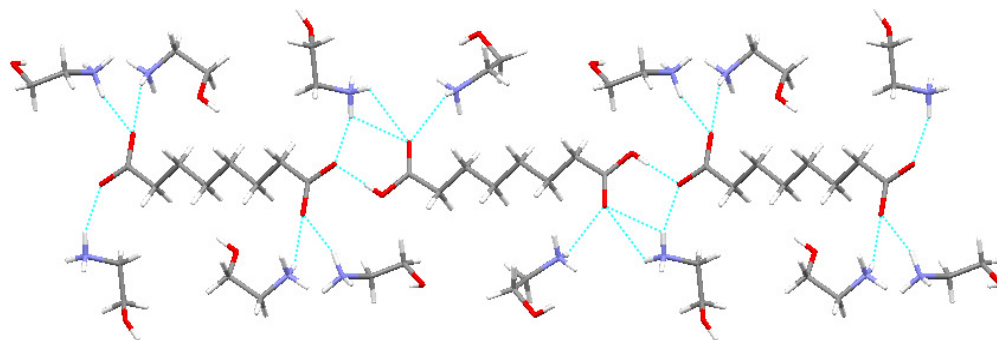


**Figure 5.4.3.3** Chain structure involving acid molecule 3 and dianion 5.

- Molecule 7 is also a monoanion and hydrogen bonds with itself in the *anti-anti* conformation to form a chain (1.65(1) Å), similar to that formed by molecule 1. Again the cations are subtended from this chain by hydrogen bonds from both the ammonium and hydroxyl groups to the carboxylate and carboxyl groups of the monoanion. However, there are fewer of cations hydrogen bonded to the anion chain than seen in the other two chain structures. This is because the hydrogen bond acceptors are more often involved in either bifurcated hydrogen bonds or hydrogen bonds to the same cation.

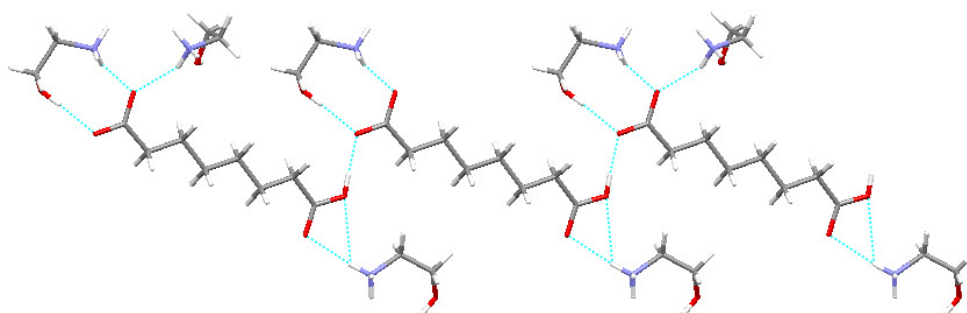


**Figure 5.4.3.4** Chain structure involving monoanion 7.

- Molecules 9 and 10 are an acid molecule and a dianion respectively, which are hydrogen bonded together in the *syn-syn* conformation (1.69(1) Å) similar to the chains formed by molecules 3 and 5. Cations are hydrogen bonded to the chain alternately via the ammonium and hydroxyl groups so as each carboxyl-carboxylate unit is hydrogen bonded to one of each.

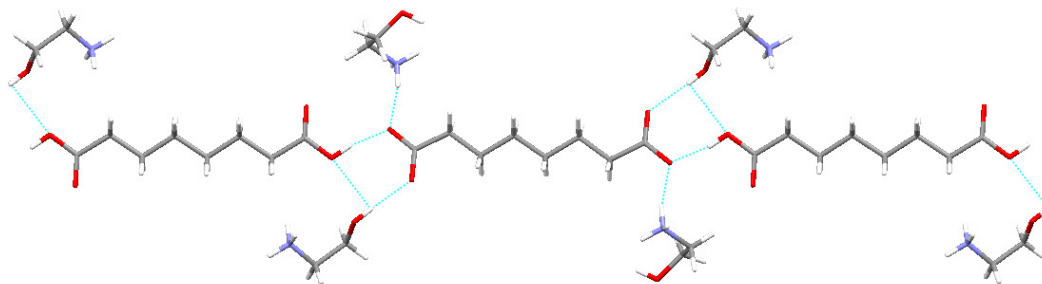


**Figure 5.4.3.5** Chain structure involving acid molecule 9 and dianion 10.

As most of the cations have one of their hydrogen bond donor groups linked to one chain, and the other linked to another type of chain, they act to link the chains together to form a 3-D network. In

this network, the similar types of chains are arranged in pairs with the plane of the carbon backbone of the adjacent pairs approximately perpendicular to each other. The different pairs of chains are not parallel; instead there is an angle of  $42^\circ$  between them.

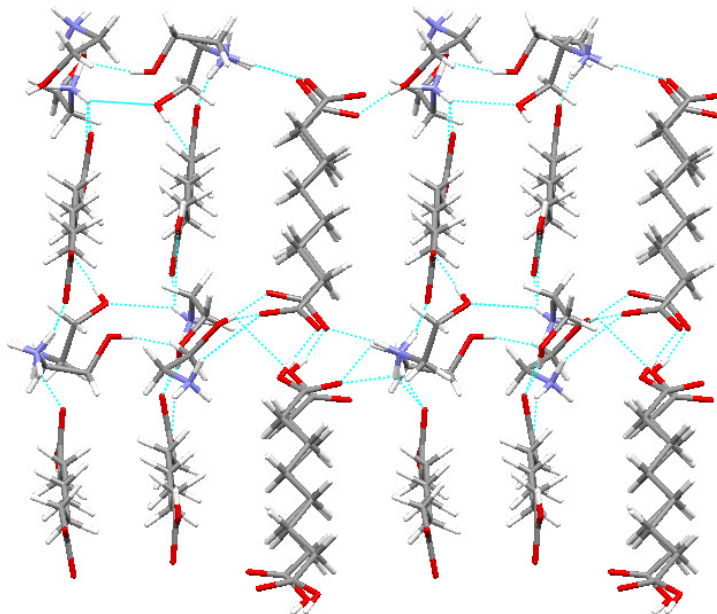


**Figure 5.4.3.6** 3-D network comprising of pairs of chains linked by the cations, viewed down the *a*-axis.

#### 5.4.4 *L*-Tartaric Acid and 2-Aminoethanol (XAGDAK)

This crystal structure was obtained by Akkurt *et al.*<sup>11</sup>; the crystals were prepared through the evaporation of an aqueous solution containing equimolar amounts of AEI and LTA at room temperature. The components were found to crystallise in a 1:1 ratio with water in the monoclinic space group  $P2_1$ , with  $Z = 2$ , to form a salt monohydrate.

The monoanions are hydrogen bonded together head-to-tail to form a chain (1.417 Å); the monocations and water molecules are then subtended from this chain by hydrogen bonding with the carboxyl, carboxylate and hydroxyl groups (Figure 5.4.4.1).

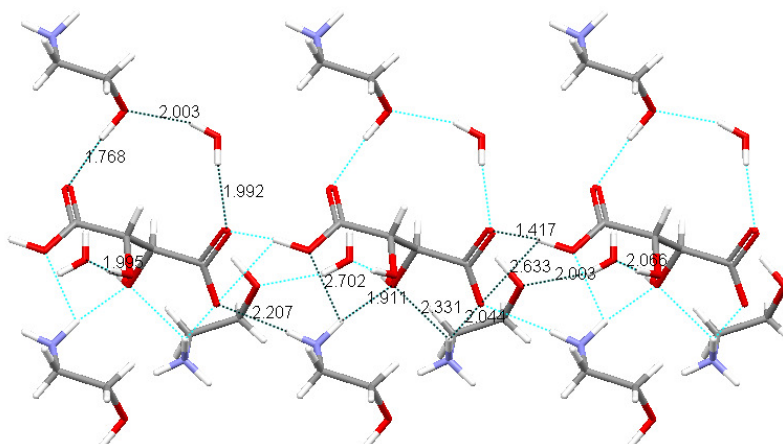


**Figure 5.4.4.1** Hydrogen bonded anion chain with subtended cations and water molecules, viewed down the *a*-axis.

Each anion is hydrogen bonded to two cations via the ammonium group, one cation via the hydroxyl group, and three water molecules. Further hydrogen bonding across the cations and water molecules links adjacent anion chains to form a 3-D network (Figure 5.4.4.2). This crystal structure is isostructural with the DTA-AEI salt monohydrate<sup>12</sup> (ZZZIEI).

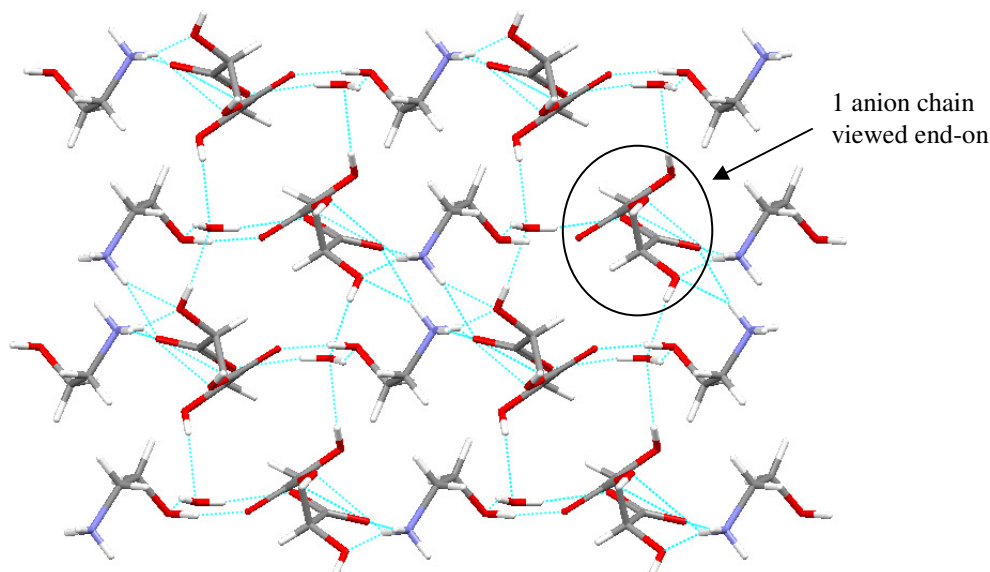
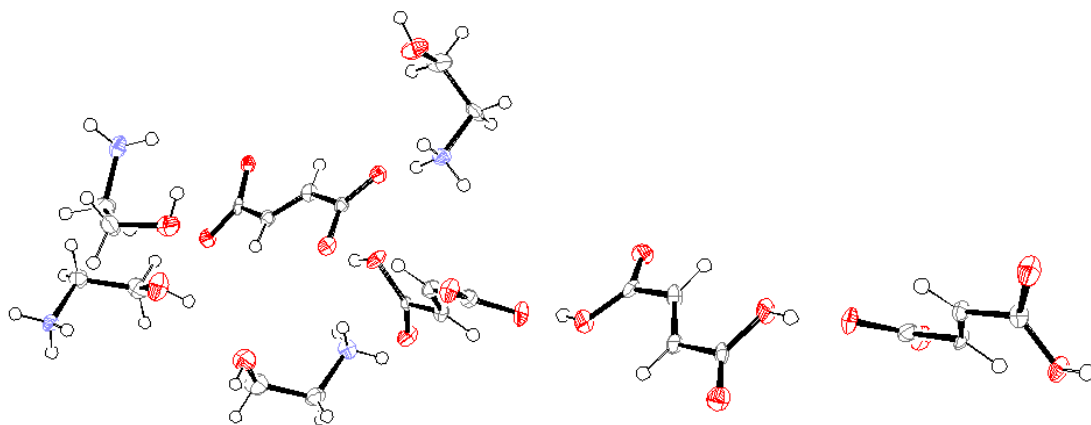


Figure 5.4.4.2 3-D network, viewed down the *b*-axis.

#### 5.4.5 Fumaric Acid and 2-Aminoethanol

These compounds crystallised in a 1:1 ratio in the triclinic space group *P*-1, with *Z* = 8. The data was quite poor however, due to the crystals containing of a number of component regions and, although the data was processed as a twin, the R-factor of the refined structure remained quite high (14.72%). The oxygen and nitrogen atoms of the base molecule were assigned according to the relative size of the electron density peaks and then checked by comparing the sizes of the ellipsoids and by viewing the number of potential hydrogen bonds each atom is involved in. Electron density peaks could not be found for all the hydrogens, including the transferable hydrogens, due to the poor quality of the data. The hydrogens were therefore assigned according to the arrangement of the molecules in the structure and the relevant bond distances; the acid molecules form a chain where they are arranged head-to-tail, with the carboxyl/carboxylate groups of adjacent molecules twisted with respect to each other. This suggests that four of the eight possible transferable hydrogens have protonated the base molecules, which concurs with the number of potential hydrogen bonds from the nitrogen atom of the monocations. The positions of the hydrogens within the acid chain were assigned according to the C-O and C=O bond distances of the acid molecules; this results in one acid molecule, two monoanions and one dianion and creating a mixed system.



**Figure 5.4.5.1** Ortep diagram for the asymmetric unit of FmA and AEI.

As mentioned earlier, the structure consists of a hydrogen bonded chain of acid molecules and anions in the *syn-syn* conformation (1.69(1), 1.61(1), 1.65(1) and 1.63(1) Å) with the plane of the carboxyl and carboxylate groups involved in a hydrogen bond being, on average, 61° to each other. The cations are then subtended from this chain by hydrogen bonds from the ammonium group which range in length from 2.71(1) to 1.89(1) Å.

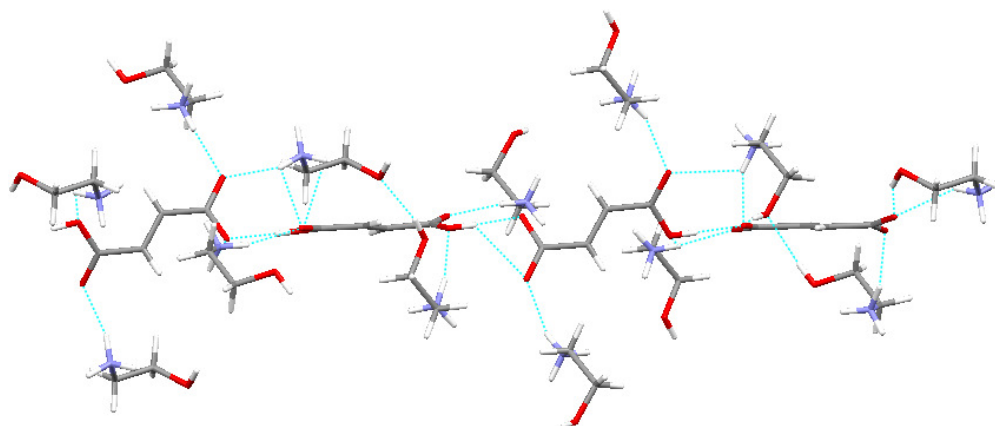


**Figure 5.4.5.2** Acid-anion chain structure with cations subtended.

The cations thus link adjacent acid-anion chains to form a 3-D network. The hydroxyl groups of the cations also contribute to the stability of the structure; two of the hydroxyl groups act as both hydrogen donors and acceptors, and the other two act only as hydrogen bond donors. The chains are arranged so as the acid/anions that are in a similar orientation stack on top of each other.



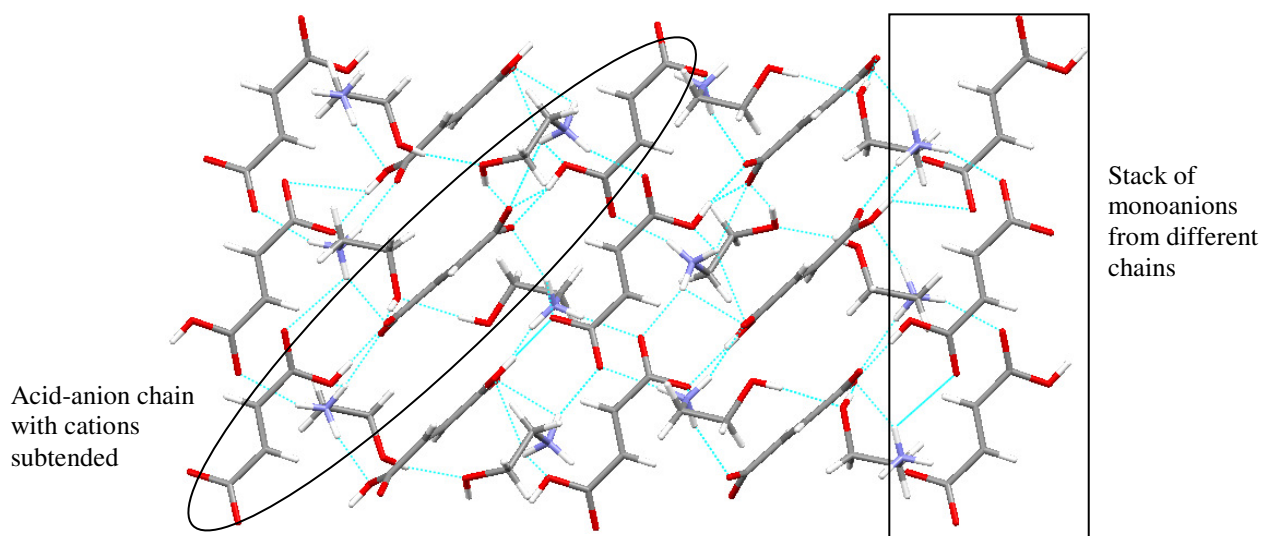


**Figure 5.4.5.3** Arrangement of acid-anion chains, linked by hydrogen bonds from the cations.

#### 5.4.6 Discussion of 2-Aminoethanol Structures

It is interesting to note that all the odd diacids formed oils whereas the even diacids all formed solid products. Of these, the AdA product was not suitable for SXRD and was instead analysed by PXRD. The resulting pattern was very weak and inconclusive as to whether or not a binary compound has formed. The low melting point of 39.33°C of the AdA-AEI product suggests that a binary compound may have formed as the melting point is much lower than that of the diacid and higher than that of the base. MeA-AEI produced an amorphous compound; amorphous solids are not crystalline as they have a disordered, random arrangement of molecules, similar to those in a liquid. As the amorphous state is thermodynamically unstable it is generally undesirable for a pharmaceutical compound. Amorphous substances are usually hygroscopic and less stable chemically and physically due to their molecular mobility, thus tending to transform into crystalline forms upon storage, humidification and heating.

Some of the structural and physical parameters of the AEI salts are given in Table 5.4.6.

	Contents of asymmetric unit	Structure type	AEI cation conformation	Density/ g cm <sup>-3</sup>
OxA	A <sup>2-</sup> :2B <sup>+</sup>	Bilayer	Gauche	1.502
ScA	½A:½A <sup>2-</sup> :B <sup>+</sup>	3-D (acid-anion chains)	Gauche	1.45
SbA	A:2A <sup>-</sup> :A <sup>2-</sup> :4B <sup>+</sup>	3-D (acid-anion chains)	Gauche	1.26
LTA	A <sup>-</sup> :B <sup>+</sup> :H <sub>2</sub> O	3-D (acid-anion chains)	Gauche	1.519
FmA	A:2A <sup>-</sup> :A <sup>2-</sup> :4B <sup>+</sup>	3-D (acid-anion chains)	Gauche	1.46

**Table 5.3.10** Various structural and physical parameters of the diacid-AEI structures.

It is unclear why the odd diacid-AEI combinations do not form solid products or even crystallise out separately, while the even diacids form binary compounds. As the components have not crystallised out separately, this suggests that although the components interact it is not sufficient to form a solid at 4°C or above. The lower melting points of the pure odd diacids indicate a higher solubility than the pure even diacids therefore perhaps the solubility of the odd diacids is too high in methanol to induce crystallisation. The orientation of the carboxyl(ate) groups in the odd diacids may also be inappropriate for salt or co-crystal formation.

The structures mainly have a 1:1 stoichiometry with the anion (and acid) molecules forming hydrogen bonded chains. OxA-AEI is the exception with a 1:2 acid:base ratio; the structure consists of a bilayer where the cations link the dianions together. From the  $pK_a$  differences, the first and second ionisation of all of the diacids is expected, thus resulting in a salt. In particular, OxA-AEI has the largest  $pK_a$  differences which may explain why the structure formed in a 1:2 acid:base ratio. Maybe the size of the OxA molecule and the various hydrogen bonding motifs it can form, such as bifurcated hydrogen bonds to both of the carboxylate groups, also contribute to the formation of this structure. The presence of neutral diacids together with anions in the ScA-AEI, SbA-AEI and FmA-AEI structures is probably due to the strong hydrogen bonds in the acid-anion chains making the hydrogen more likely to be shared between the carboxylate groups.

The melting points of the crystalline products are shown in Appendix Table A6; although the melting point for the OxA-AEI combination is not known, it can be seen that the melting points of the crystalline products described here decrease as the chain length of the diacid increases. The melting point for both of the stereoisomers of TA cannot be found in the literature, however, in one paper the AEI-DTA product is heated to 105°C for 1 hour to obtain the anhydrous form<sup>12</sup> therefore it can be assumed that the melting point is higher than this.

By measuring the torsion angle of the cation in each of the structures it was found that in all cases the cations are in the *gauche* conformation (angles in Appendix, Table A12) with an average torsion angle of 64.81°. The possible conformations of AEI as a neutral molecule have been studied by Chang *et al.*<sup>9</sup> in order to determine the most energetically favourable conformation. This was found to be the *gauche* conformation which was hypothesised by the authors to be stabilised by an O-H...N intramolecular hydrogen bond. The O-H...N hydrogen bond was found to be stronger than the N-H...O hydrogen bond due to the increased strain on the conformational structure in the latter case. The most important factors in determining the conformation were therefore deemed to be intramolecular hydrogen bonding >CH<sub>2</sub> electrostatic interaction >*gauche* interaction. A search of the CSD for neutral AEI gave the pure compound and a co-crystal, both of which contained AEI in the *gauche* conformation. A search for the protonated form of AEI found 16 unique structures, all of which were in the *gauche* conformation except for one (IJOTIK<sup>13</sup>) which contains a disordered AEI



molecule with electron density for the oxygen found both in the *anti* and *gauche* positions. As the intramolecular O-H...N hydrogen bond is not found in the AEI binary compounds described here, the reason for the cation's *gauche* conformation must be attributed to another cause.

Although the ammonium and hydroxyl groups of most of the cations are hydrogen bonded to different molecules, some of the cations in SbA-AEI and FmA-AEI create a ring system by each end of the cation being hydrogen bonded with the same carboxylate group. In two of the cases both the ammonium and hydroxyl group of the cation are hydrogen bonded to the same oxygen, creating a five-membered ring. In the other case the groups are hydrogen bonded to different oxygens of the same carboxylate group, thus creating a seven-membered ring. These ring systems are possible due to the *gauche* conformation of the cation. The torsion angles and C-C bond distances for the cations are not affected by the type of hydrogen bonding arrangement that is being participated in.

## 5.5 TETRAMETHYLEthylenEDIAMINE

### 5.5.1 Oxalic Acid and Tetramethylethylenediamine

These compounds crystallised in a 1:1 ratio with water in the monoclinic space group  $P2_1/c$ , with  $Z = 2$ . The asymmetric unit contains half of each of the acid and base components, the other half of each of the molecules is generated by symmetry to create a dication and a dianion, thus forming a salt dihydrate.

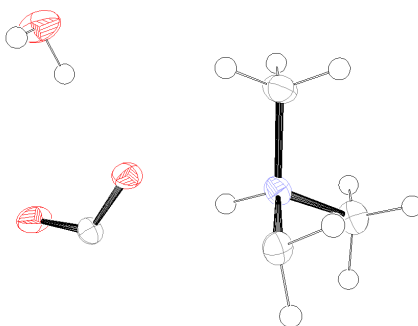


**Figure 5.5.1.1** Ortep diagram for the asymmetric unit of OxA and TEMED.

The structure consists of alternate dianions and dications hydrogen bonded together to form a chain. The chain is stepped due to the position of the nitrogens in the cation and the subsequent orientation of the molecules. The hydrogen bonds from each nitrogen on the cation are bifurcated and link to one oxygen on each of the carboxylate groups on the anion. Each of these oxygen atoms are further hydrogen bonded to a water molecule.

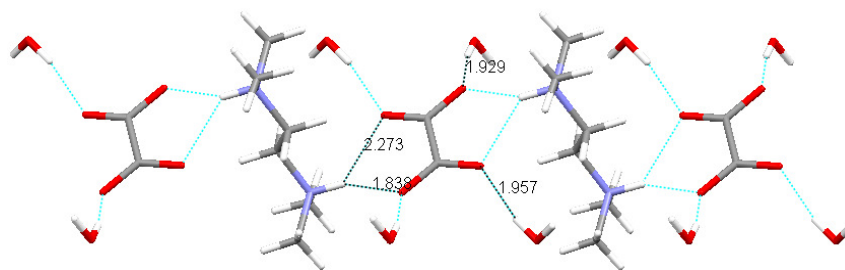


**Figure 5.5.1.2** Chain structure, viewed down the *b*-axis (hydrogen bond distance error  $\pm 0.018$  Å).

Adjacent chains are linked via hydrogen bonding across the water molecules to form sheets parallel to the *bc*-plane. Adjacent chains are orientated differently to each other due to the molecules being related by the  $2_1$  screw axis.

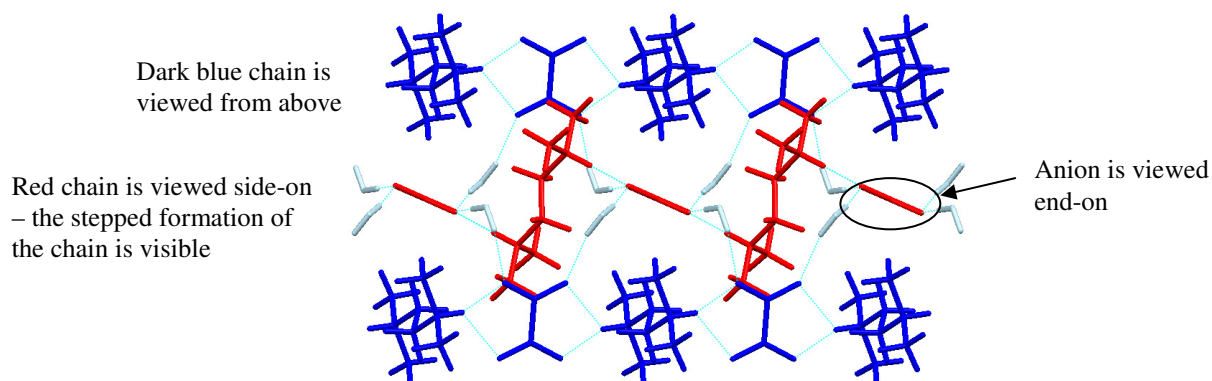


**Figure 5.5.1.3** Sheet viewed from above; the central chain is coloured red (the anions are viewed end-on) and the adjacent chains are blue; the linking water molecules are shown in light blue.

The sheets are then stacked on top of each other with weak C-H...O hydrogen bonds from the cation methyl groups and the carboxylate and water molecules (2.538 and, 2.330 and 2.496 Å). Other C-H...O hydrogen bonds between the components also further stabilise the sheet structure.

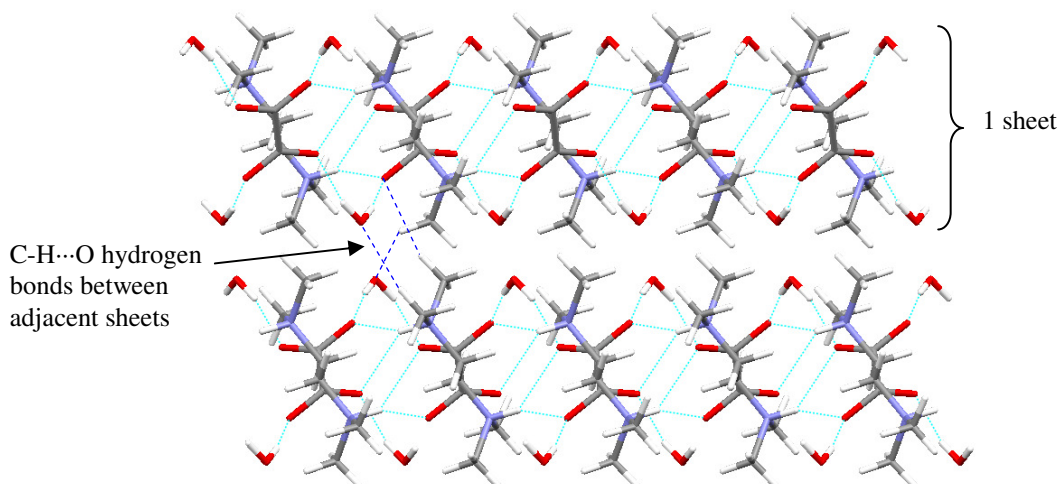


**Figure 5.5.1.4** Stacking of sheets.

### 5.5.2 Malonic Acid and Tetramethylethylenediamine (QAFVID)

This crystal structure was characterised by Adam *et al.*<sup>14</sup> crystals were prepared by slow evaporation of an equimolar aqueous acid-base solution, resulting in colourless prisms. The components crystallised in a 2:1 acid:base ratio to form a salt in the triclinic space group *P*-1, with *Z* = 1. Each of the anions has an intramolecular hydrogen bond, which the authors note, results in a “stable, approximately planar six-membered ring.” Two anions are hydrogen bonded to one cation via the anionic carboxylate groups producing a tertiary unit (Figure 5.5.2.1).

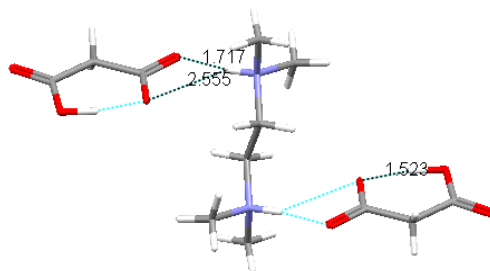


**Figure 5.5.2.1** Hydrogen bonded tertiary unit.

The units are arranged so as there are weak C-H...O hydrogen bonds between the carboxyl groups and methyl groups (2.470 and 2.650 Å) and also between the carboxylate and methylene groups (2.514 and 2.637 Å). These weak interactions link the units to form sheets where the cation is positioned nearly perpendicular to the plane of the sheets and the anions are positioned at the top and the bottom of the sheet.

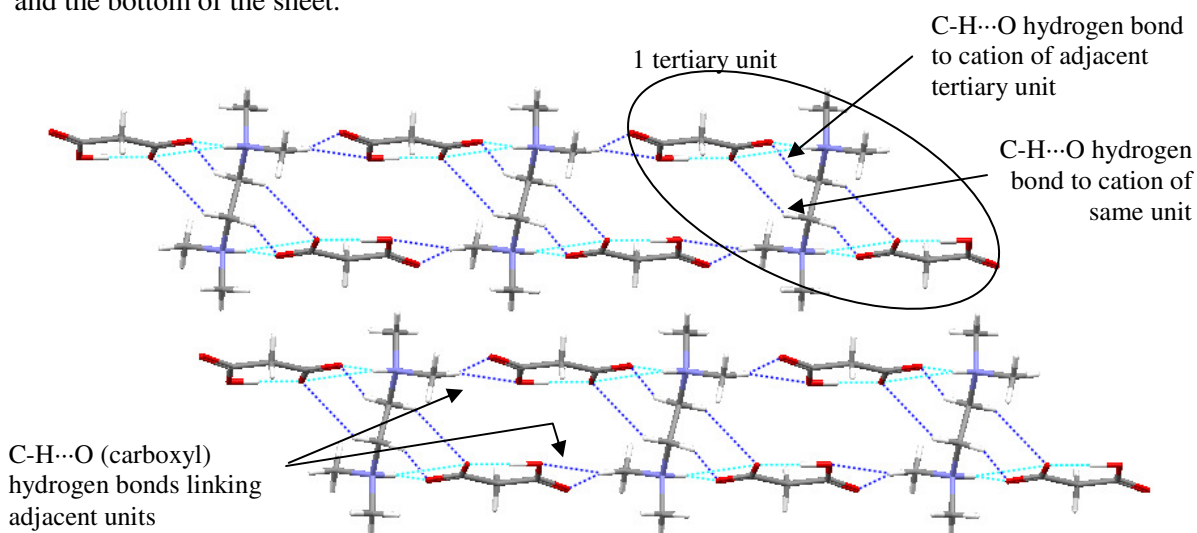


**Figure 5.5.2.2** Arrangement of tertiary units to form sheets; N-H...O hydrogen bonds shown in light blue, C-H...O hydrogen bonds shown in dark blue.

### 5.5.3 Succinic Acid and Tetramethylethylenediamine (ISUTEV)

This crystal structure was obtained by Bruno *et al.*<sup>15</sup>; an equimolar aqueous solution of the acid and the base was prepared at room temperature which was then filtered and the resulting crystals dried.

The asymmetric unit was found to contain half a dianion, half a dication and half an acid molecule with each of the components on a special position. Thus the components formed a mixed system in the triclinic space group  $P-1$ , with  $Z = 1$ .

The structure consists of chains of alternate planar dianions and planar acid molecules hydrogen bonded together head-to-tail ( $1.70(1)$  Å) in the *anti-anti* conformation. Dications link the adjacent chains by hydrogen bonding to the dianions ( $1.82(1)$  and  $2.45(1)$  Å) thereby forming a sheet (Figure 5.5.3.1). The sheet is stepped due to the perpendicular orientation of the dications with respect to the plane of the dianion-acid molecule chains.

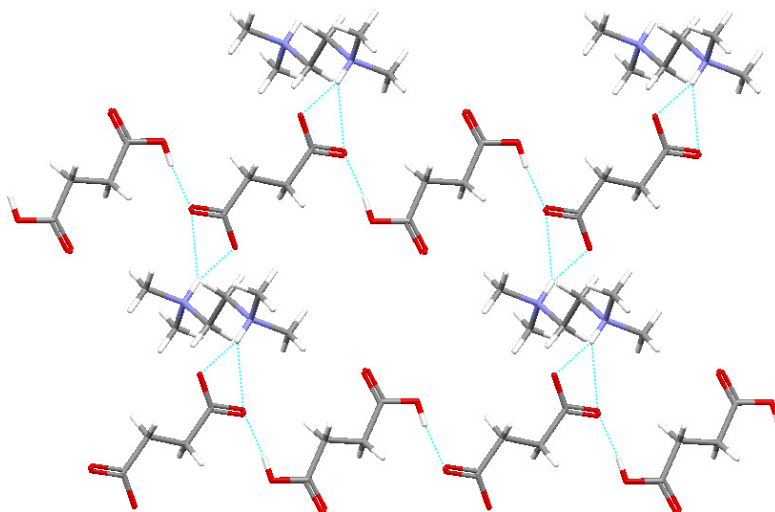


**Figure 5.5.3.1** Sheet structure with anion-acid chains linked by cations.

Adjacent sheets are positioned so as the methyl groups of the cations of one sheet fill the gaps between the acid molecules of another sheet. Weak C-H...O hydrogen bonds between the carboxyl groups and the methyl groups of the cations in the adjacent sheets ( $2.481$ ,  $2.782$  and  $2.606$  Å) result in a 3-D network.

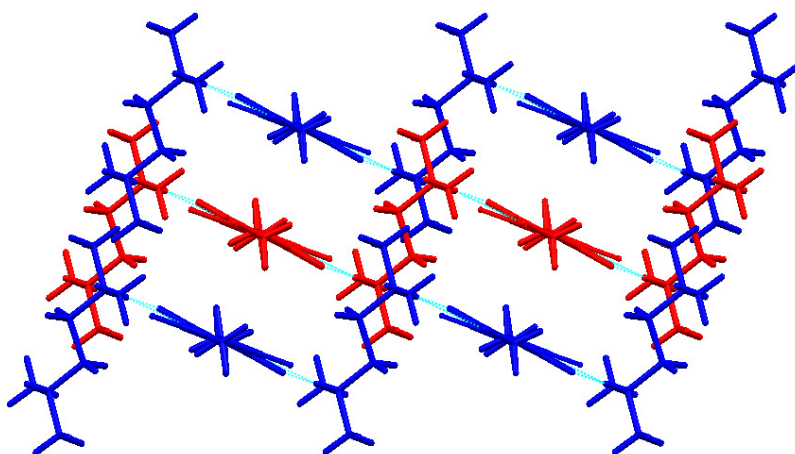


**Figure 5.5.3.2** Interlinking of cations of adjacent sheets, alternate sheets are coloured red and blue.

#### 5.5.4 Glutaric Acid and Tetramethylethylenediamine

These two compounds crystallised in a 2:1 acid:base ratio in the monoclinic space group  $P2_1/n$ , with  $Z = 6$ , to form a salt. One of the dications is on a special position and hence only half of it is present in the asymmetric unit (Figure 5.5.4.1). In spite of the poor data, all of the transferable hydrogens were found, except for one that would either be on O5b or O51a (as all the hydrogens on the base molecules had already been located). Due to the hydrogen bonding arrangement of the anions and the fact that the other anions in the structure are mono-deprotonated, the hydrogen was fixed to O5b in the *anti* orientation in concurrence with the other anion-anion hydrogen bonds present in the structure. The R-factor remained quite high (14.72%) and some of the ellipsoids are larger than usual.

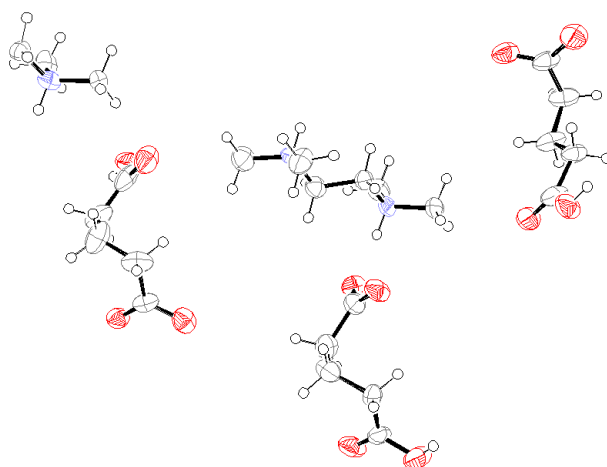


**Figure 5.5.4.1** Ortep diagram for the asymmetric unit of GlA and TEMED.

The structure consists of chains of monoanions hydrogen bonded together head-to-tail in the *anti-anti* conformation. The chains are twisted with each half taking the *gauche* conformation (torsion angles approximately  $70^\circ$ ); the angles between the planes of the carboxyl and carboxylate groups are  $82.93^\circ$ ,  $88.85^\circ$  and  $77.12^\circ$ . The cations link pairs of anion chains by hydrogen bonding with the carboxylate groups to form a tape (Figure 5.5.4.2).

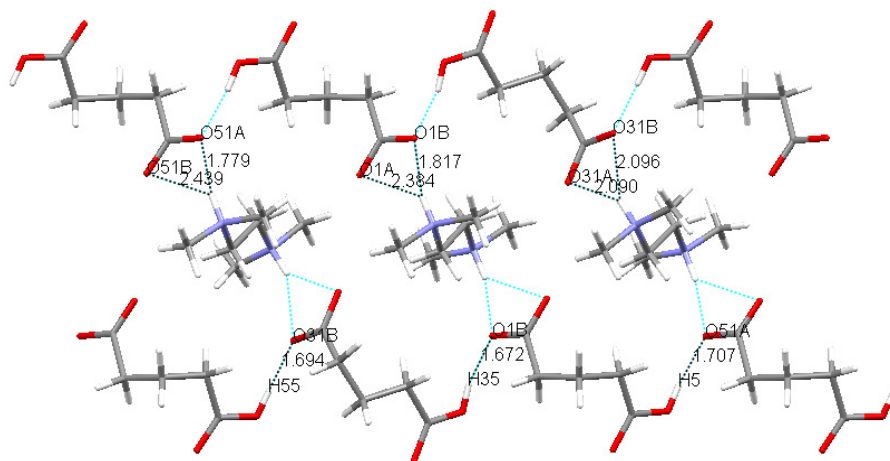


**Figure 5.5.4.2** Tape structure with cations linking anionic chains, hydrogen bond distances marked (hydrogen bond distance error  $\pm 0.008$  Å).

The tapes are linked via C-H...O hydrogen bonds between the carboxyl groups of the anions and the methyl groups of the cations to form a 3-D network.

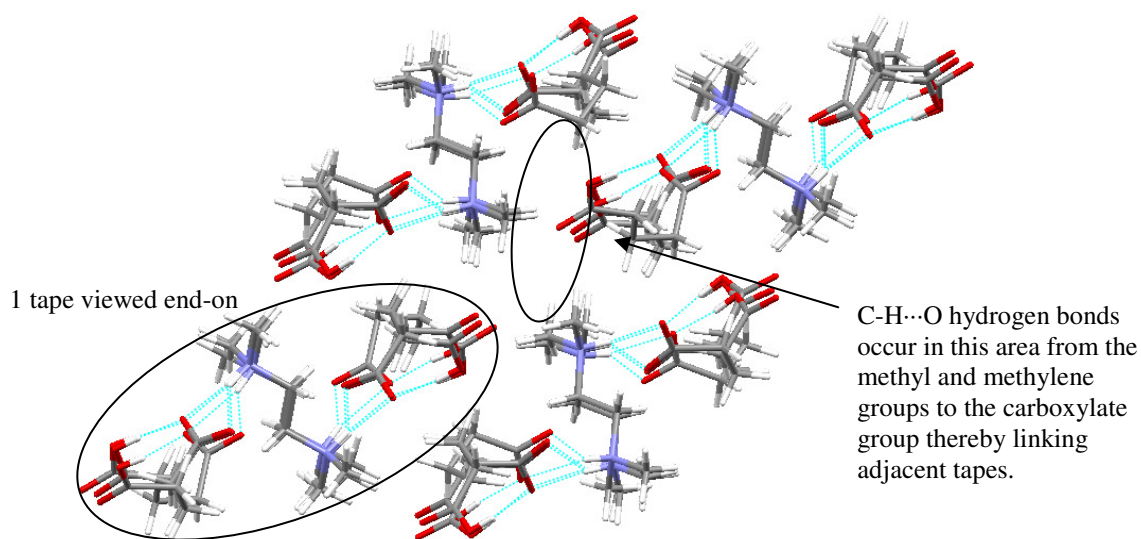


**Figure 5.5.4.3** Tapes viewed end-on, C-H...O hydrogen bonds link tapes to form a 3-D network.

#### 5.5.5 *DL-Tartaric Acid and Tetramethylethylenediamine*

These compounds crystallised in a 1:1 ratio with water in the triclinic space group *P*-1, with *Z* =2, to form a salt trihydrate. Both of the protons have been transferred from the diacid to the diamine to form a dianion and dication.

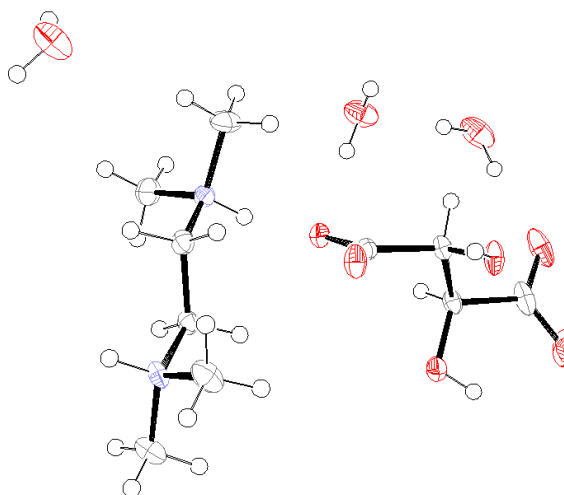


**Figure 5.5.5.1** Ortep diagram for the asymmetric unit of DLTA and TEMED.

The structure consists of anions hydrogen bonded from the hydroxyl to the carboxylate groups to form a tape (2.10(1) and 2.15(1) Å). The cations are then hydrogen bonded to each of the carboxylate groups of the anions (Figure 5.5.5.2).



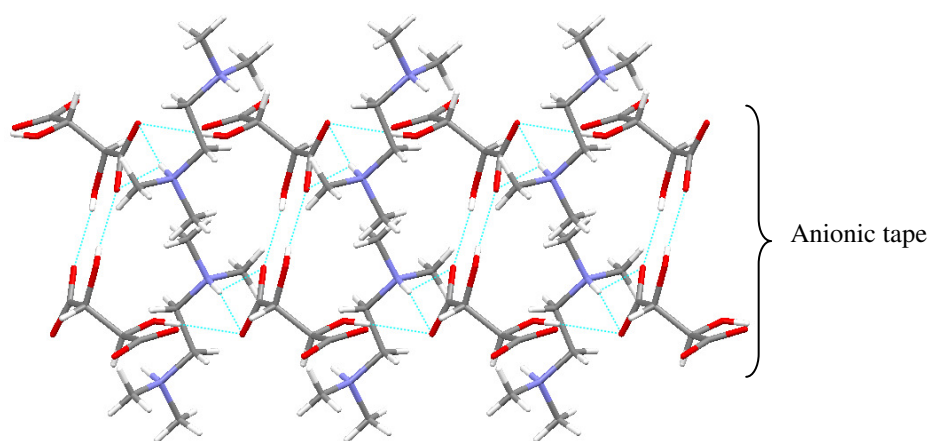


**Figure 5.5.5.2** Anionic tape structure with hydrogen bonded cations.

As the cations possess two protonated amine groups, they are able to hydrogen bond the carboxylate groups of an adjacent tape, thus forming a sheet.

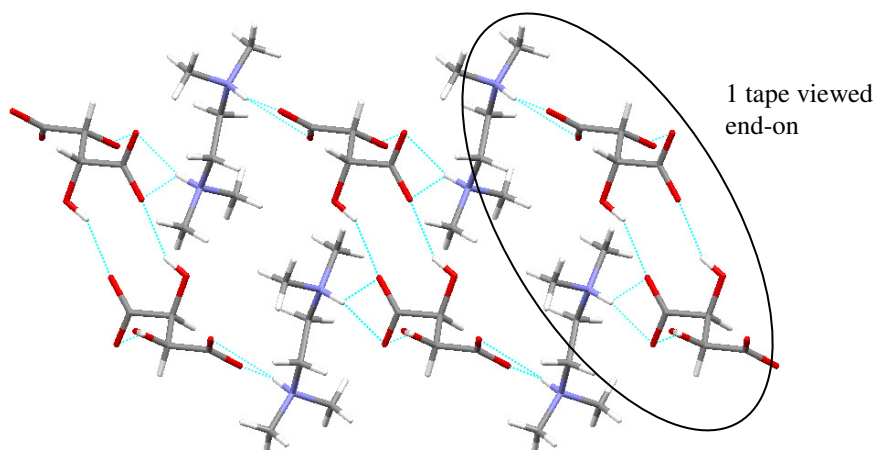


**Figure 5.5.5.3** Linking of tapes to form a sheet (edge of sheet is viewed here).

Water molecules are hydrogen bonded to the carboxylate groups of the anions and further hydrogen bonds across more water molecules link the adjacent sheets to form a 3-D network.

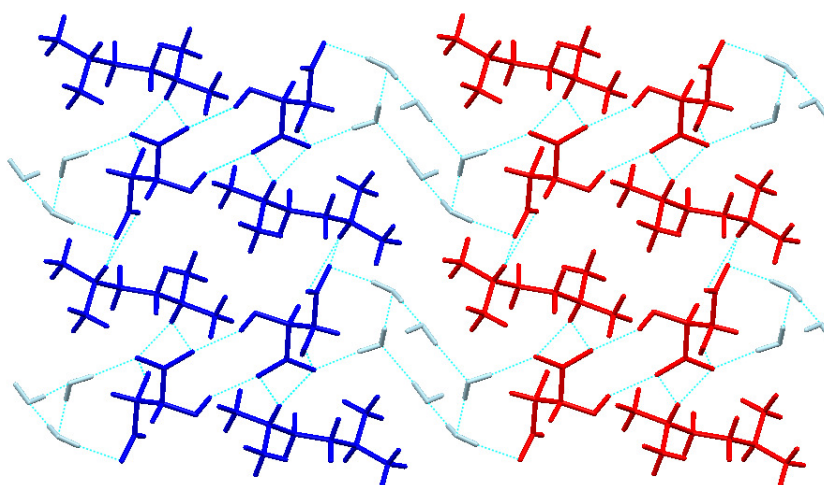


**Figure 5.5.5.4** The 3-D structure with the sheets viewed side-on; the adjacent layers are coloured blue and red, the connecting water molecules are light blue.

### 5.5.6 Maleic Acid and Tetramethylethylenediamine

These compounds crystallised in a 2:1 acid:base ratio in the monoclinic space group  $P2_1/c$ , with  $Z = 2$ , to form a salt. Although the R-factor remained quite high (10.29%) all the transferable hydrogens were located easily.

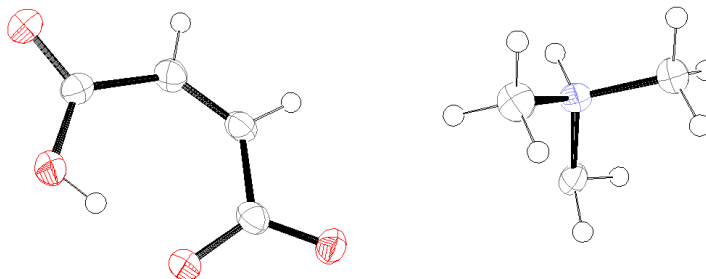


**Figure 5.5.6.1** Ortep diagram for the asymmetric unit of MeA and TEMED.

This structure is similar to the MnA-TEMED structure as the planar monoanion has a strong intramolecular bond between its carboxyl and carboxylate groups (1.61(1) Å). The carboxylate group is also involved in hydrogen bonding with the cation which is further linked to a second anion to form a triplet (Figure 5.5.6.1)

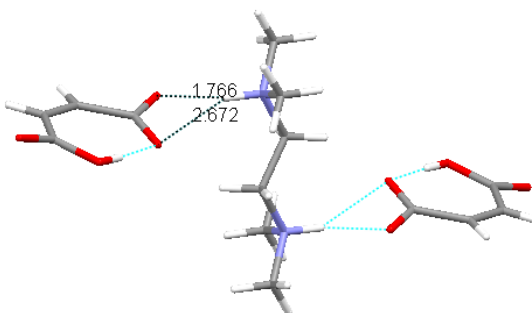


**Figure 5.5.6.2** Hydrogen bonded triplet (hydrogen bond distance error  $\pm 0.004$  Å).

The units are arranged into layers with the anions of adjacent units positioned next to each other. Weak C-H...O hydrogen bonds from the cationic methyl groups to the carboxyl and carboxylate groups of the anion link the adjacent units. There are also weak C-H...O hydrogen bonds from the aromatic hydrogens on the anion to the carboxyl and carboxylate groups of an adjacent anion, thus creating a 3-D network.



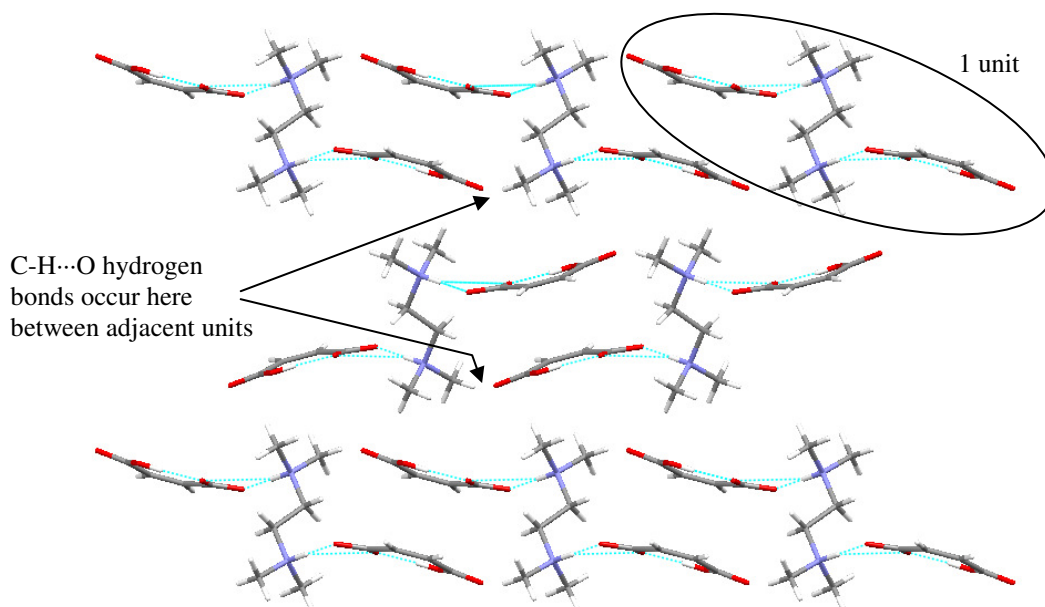


**Figure 5.5.6.3** 3-D network – units linked by C-H...O hydrogen bonds.

#### 5.5.7 Fumaric Acid and Tetramethylethylenediamine (QAFVEZ)

This structure was characterised by Adam *et al.*<sup>14</sup>; the crystals were produced by the slow recrystallisation of an aqueous solution of the acid and base in a 1:1 ratio to give colourless needles. The asymmetric unit was found to contain half a dianion, half a dication and half an acid molecule with each of the components on a special position. Thus the components formed a mixed system in the triclinic space group *P*-1, with *Z* = 1. This assembly is isostructural with the ScA-TEMED binary product (ISUTEV) described previously.

The structure again consists of chains of alternate dianions and acid molecules hydrogen bonded together in the *anti-anti* conformation (1.546 Å). The chains are linked by hydrogen bonding across the dication (1.731 and 2.555 Å) to form a stepped sheet.

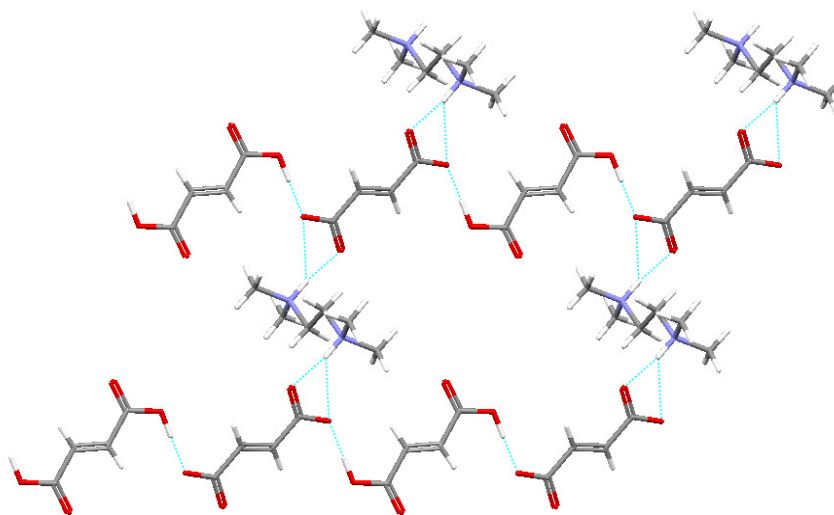


**Figure 5.5.7.1** Hydrogen bonded chains of anions and acid molecules linked by hydrogen bonding across the cations to form a sheet.

The sheets are arranged in the same manner as the ScA-TEMED structure (Figure 5.5.3.2) with the methyl groups of the cations filling the gaps between the acid molecules of the adjacent sheets. Weak C-H...O hydrogen bonds stabilise the 3-D network (2.448, 2.718 and 2.559 Å).

#### 5.5.8 Discussion of Tetramethylethylenediamine Structures

The AdA, PmA and SbA combinations formed oils, however the shorter chain diacids formed crystalline products. In this group, whether the diacid has an odd or even number of carbons does not seem to influence the products.

Some of the structural and physical parameters of the TEMED salts are given in Table 5.5.8.

	Contents of asymmetric unit	Structure type	Density/ g cm <sup>-3</sup>	Melting point/ °C
OxA	$\frac{1}{2}A^{2-}:\frac{1}{2}B^{2+}:H_2O$	Sheets	1.29	71.4
MnA	$A^-:\frac{1}{2}B^{2+}$	Tertiary units	1.317	
ScA	$\frac{1}{2}A:\frac{1}{2}A^{2-}:\frac{1}{2}B^{2+}$	Sheets	1.372	
GlA	$3A^-:1\frac{1}{2}B^{2+}$	Tapes	1.33	72.7
DLTA	$A^{2-}:B^{2+}:3H_2O$	3-D (layers)	1.34	71.8
MeA	$A^-:\frac{1}{2}B^{2+}$	Tertiary units	1.35	71.2
FmA	$\frac{1}{2}A:\frac{1}{2}A^{2-}:\frac{1}{2}B^{2+}$	Sheets	1.388	

**Table 5.5.8** Various structural and physical parameters of the diacid-TEMED structures.

The first ionisation of the molecules has a  $pK_a$  difference of between 7.63 and 4.34 units (Appendix, Table A2) and hence salt formation is expected. Protonation of a second TEMED molecule by the same diacid monoanion ( $pK_a$  difference range 4.67 to 2.79) is more likely than protonation of the same TEMED monocation by a different diacid molecule ( $pK_a$  difference range 4.35 to 1.06). The second ionisation of both of the molecules also yields very small  $pK_a$  differences (range 1.39 to -0.49) and is therefore even more unlikely. From the results however, it can be seen that the assemblies have not followed these rules and instead the TEMED molecule is diprotonated in every instance. Both ScA-TEMED and FmA-TEMED have a dianion and an acid molecule present in the structure; the second  $pK_a$  difference for the dianion to form is -0.03 and 1.14 respectively and hence formation is unexpected. The short O...O distance (2.514 and 2.516 Å respectively) in the dianion-acid chains may indicate a low barrier hydrogen bond which could explain the presence of the dianion. The second  $pK_a$  difference for OxA-TEMED is less than 1.39 units and hence its di-deprotonation is also rather unexpected.

MnA-TEMED and MeA-TEMED form similar structures with discrete units which are extended only by weak C-H...O hydrogen bonds. This is due to the size of the monoanion and the orientation

of the carboxyl/carboxylate groups which promote a strong intramolecular hydrogen bond. The ScA, FmA, GlA and DLTA structures all contain anion chains, however the chains in DLTA are not hydrogen bonded head-to-tail and instead involve the hydroxyl group of the dianion. The structures predominantly consist of sheets which, in the case of DLTA, can be extended in to a 3-D array through hydrogen bonding across water molecules. GlA-TEMED is an exception as it forms a tape structure. It should also be noted that the ScA and FmA assemblies are isostructural.

The TEMED cation is always in the same conformation with an average torsion angle of 178.47°C. The hydrogens on the nitrogens are also always pointing in opposite directions.

There is insufficient melting point data to draw conclusions across this group, however the highest and lowest melting point structures are DLTA-TEMED and GlA-TEMED respectively. The densities of the structures (some obtained from the literature) can be seen to increase from OxA to ScA (1.29 to 1.372 g cm<sup>-3</sup>) and then drop for GlA (1.33 g cm<sup>-3</sup>); as usual the TAs and alkene diacids are in the upper range of the densities for the group.

## 5.6 DISCUSSION OF ALIPHATIC AMINES

The most interesting point in this group of bases, is that all the dibases have been diprotonated whilst the deprotonation of the acid varies. This is often in spite of the pK<sub>a</sub> values which suggest that the manner of deprotonation occurs to optimise the hydrogen bonding interaction. This is concurrent with a study by Barnes *et al.*<sup>4</sup> which notes that ‘frequently the dominant compound contains a partially ionised acid group ... to optimise the hydrogen bonding.’ In the case of dibases, this explains why even though the base is diprotonated, the acid is often mono-deprotonated or there are neutral acid molecules as well as dianions present in the structure which can link to form chains. Some of the crystals were prepared from a number of different stoichiometric mixtures which all gave the same product, indicating the preference for the structure.

It is interesting that the pK<sub>a</sub> differences in methanol do not predict the proton transfer in the binary compounds in spite of this being the crystallisation solvent used in the well-plate crystallisations (except for the TAs). Indeed, the second ionisations almost always have a pK<sub>a</sub> difference of less than two units and many of the first ionisations are also less than two units. According to the ‘rule of three’ this should result in co-crystal formation, however all of the binary compounds synthesised are salts, salt hydrates or mixed systems. It would appear that the ‘rule of three’ only applies to the pK<sub>a</sub> values in water, irrespective of the crystallisation solvent used. This needs to be further investigated using a range of solvents to ensure the case with methanol is not an anomaly.

As the bases in this chapter are mainly the most basic, and methanol decreases the acidity of the diacids by approximately 5 units, the pK<sub>a</sub> values measured in water will be discussed herein as they

appear to be most applicable to the products formed. Any important notes regarding the methanol values will be noted.

## References

1. C. K. Johnson, ORTEP, C. K. Johnson, Report ORNL-3794, Oak Ridge National Laboratory, Tennessee, USA, 1965.
2. A. J. M. Duisenberg, L. M. J. Kroon-Batenburg, A. M. M. Schreurs, *J. Appl. Crystallogr.*, 2003, **36**, 220-229.
3. J. C. Barnes, R. W. Longhurst, T. J. R. Weakley, *Acta Crystallogr., Sect. C*, 1998, **C54**, 1347-1351.
4. J. C. Barnes, T. J. R. Weakley, *Acta Crystallogr., Sect. C*, 2000, **C56**, e346-e347.
5. J. Schreuer, T. Munch, *Z. Kristallogr.*, 1994, **209**, 32-35.
6. S. Pérez, *Acta Crystallogr., Sect. B*, 1976, **B32**, 2064-2070.
7. S. Pérez, *Acta Crystallogr., Sect. B*, 1977, **B33**, 1083-1087.
8. J. C. Barnes, T. J. R. Weakley, *Acta Crystallogr., Sect. C*, 1997, **53**, 9700018.
9. Y.-P. Chang, T.-M. Su, T.-W. Li, I. Chao, *J. Phys. Chem. A*, 1997, **101**, 6107-6117.
10. V. Jordanovska, P. Naumov, M.-J. Kim, H.-J. Lee, S. W. Ng, *Acta Crystallogr., Sect. E*, 2001, **E57**, o45-o47.
11. M. Akkurt, I. Celik, S. Ozbey, E. Kendi, *Z. Kristallogr.-New Cryst. Struct.*, 2000, **215**, 71-72.
12. D. W. Moore, J. H. Bryden, *Acta Crystallogr.*, 1954, **7**, 602.
13. N. W. Alcock, *CSD Private Communication*, 2003,
14. K. R. Adam, I. M. Atkinson, L. F. Lindoy, B. J. McCool, T. Rambusch, *J. Supramol. Chem.*, 2001, **1**, 201-205.
15. G. Bruno, A. Rotondo, L. De Luca, S. Sammartano, F. Nicoló, *Acta Crystallogr., Sect. C*, 2004, **C60**, o287-o289.

## CHAPTER 6

### Results and Discussion – Nitrogen-Containing Heterocycles.

#### 6.1 INTRODUCTION

In this chapter the products from the various crystallisation procedures of the acid-base combinations containing a heterocyclic ring are described and discussed. The well-plate observations and the type of characterisation performed for the products of this chapter are summarised in Table 6.1.

	2-Pyrrolidinone (Pyr)	2-Imidazolidinone (Idn)	1,3-dimethylimidazol- idinone (DMI <sub>Idn</sub> )	Morpholine (Mo)
OxA	Oil	Plates SXR	Powder	Blocks SXR
MnA	Oil	Blocks SXR	Oil	Oil
ScA	Blocks SXR	Micro-blocks Synchrotron	Blocks SXR	Blocks SXR
GlA	Oil	Blocks SXR	Blocks SXR	Oil
AdA	Powder	Blocks SXR	Blocks SXR	Blocks SXR
PmA	Oil*	Plates SXR	Blocks SXR	Oil
SbA	Powder	Powder	Powder	Powder
LTA	Oil	Micro-crystals Synchrotron	Oil	Oil
DLTA	Blocks SXR	Micro-crystals Synchrotron	Powder	Blocks SXR
MeA	Oil	Oil*	Oil	Needles + powder SXR
FmA	Blocks SXR	Powder	Powder	Rods SXR

**Table 6.1** Observations of the well-plate products for the acid-base combinations involving nitrogen-containing heterocycles and their appropriate method of analysis.

Unless stated it should be assumed that the crystallisation procedure used was Method 1, or Method 2 for tartrates. Further crystallisation experiments using Method 3 were performed for the acid-base combinations containing Pyr, Idn and Mo with OxA, MnA, GlA, PmA and MeA that produced oils. The products again consisted of oils except for two combinations PmA-Pyr and MeA-In (marked \*) which gave crystals suitable for analysis by SXRD. Powder products were analysed on a small scale by PXRD to ascertain if the product was either of the starting materials.

In the following sections the outcomes of each of the XRD studies will be discussed along with the thermal analysis results. Unless stated, the transferable hydrogen atom positions were found in the electron density difference map, and their correct assignment was confirmed not only by the difference between the C-O and C=O bond lengths, but also by moving them to their other possible position and seeing where the hydrogen atom refined to. The Ortep<sup>1</sup> diagrams for each of the structures display the molecules present in the asymmetric unit, the numbering scheme and 50% probability displacement ellipsoids; hydrogen atoms are shown as spheres.

The cell dimensions for each of the products are listed in Appendix, Table A5. For reference, the types of binary compounds formed and some of their properties are displayed in Appendix, Tables A3 and A6 respectively. The crystal structure data is available on the Appendix CD.

## 6.2 2-PYRROLIDINONE

### 6.2.1 Succinic Acid and 2-Pyrrolidinone

This combination was found to crystallise in a 1:2 acid:base ratio in the triclinic space group *P*-1, with *Z* = 1, to form a co-crystal. The ellipsoids are larger than usual (Figure 6.2.1.1) due to the small size of the crystals and the subsequent weak data. In spite of this, the hydrogens were found easily; the R-factor for the refined structure is 7.36%. The ScA molecule lies across an inversion centre and hence only half of it is seen in the asymmetric unit.

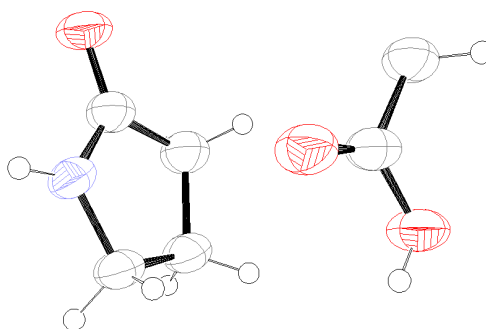


**Figure 6.2.1.1** Ortep diagram for the asymmetric unit of ScA and Pyr.

The structure comprises chains of molecules where hydrogen bonded base dimers (N-H...O 2.07(1) Å) are linked by hydrogen bonding across the acid molecules (O-H...O 1.77(1) Å). The chains are arranged so as to form 'sheets.'

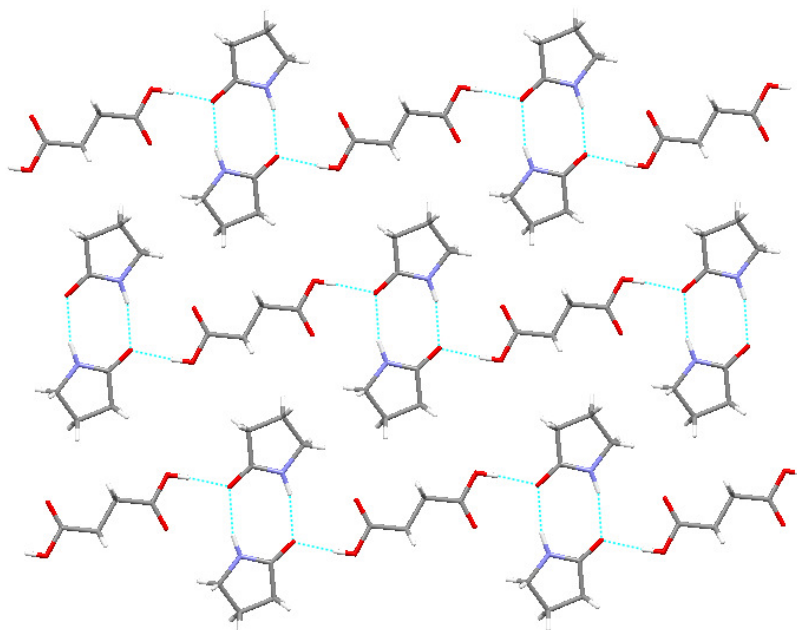


**Figure 6.2.1.2** Hydrogen bonded chains are arranged into flat 'sheets.'

Adjacent 'sheets' are stacked on top of one another in an offset manner with the molecules filling the gaps between the molecules in the sheet below. There are weak base-acid C-H...O hydrogen bonds (2.642 Å) between adjacent sheets. The chains are not quite flat with a small torsion in the base molecules:

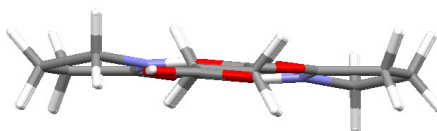


**Figure 6.2.1.3** Chain viewed end-on.

### 6.2.2 Fumaric Acid and 2-Pyrrolidinone

These two compounds crystallised together in a 1:2 acid:base ratio in the monoclinic space group  $P2_1/n$ , with  $Z = 2$ , to form a co-crystal. The asymmetric unit contains one base molecule and half an acid molecule (Figure 6.2.1.1); the acid molecule lies across an inversion centre therefore the remainder of the molecule is generated by symmetry.



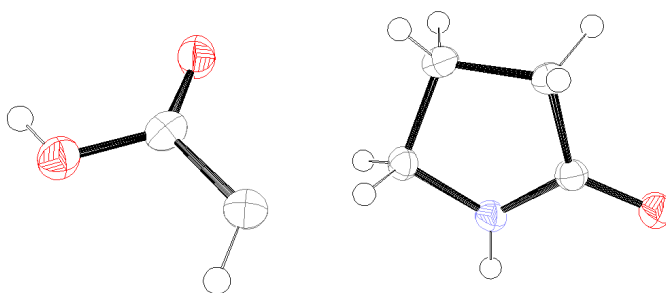


**Figure 6.2.2.1** Ortep diagram for the asymmetric unit of FmA and Pyr.

The components also form the same chain structure as is found in the ScA-Pyr structure (Figure 6.2.1.2). The hydrogen bond distances are approximately the same; O-H...O 1.71(1) Å and N-H...O 2.08(1) Å.

The chains are stacked along their length, with the plane of each chain tilted 42° to the direction of the stack. The adjacent stacks of chains are not only in a different orientation but also in a non-parallel arrangement (Figure 6.2.2.2). There are weak C-H...O hydrogen bonds (2.718 Å) between the aromatic carbons of the acid and the carboxyl group of the acid molecule of adjacent chains within the same stack. The presence of CH- $\pi$  interactions between the base and the acid molecules in adjacent stacks is confirmed by the ‘wing’ features in the fingerprint plots (Appendix, Table A10.1).

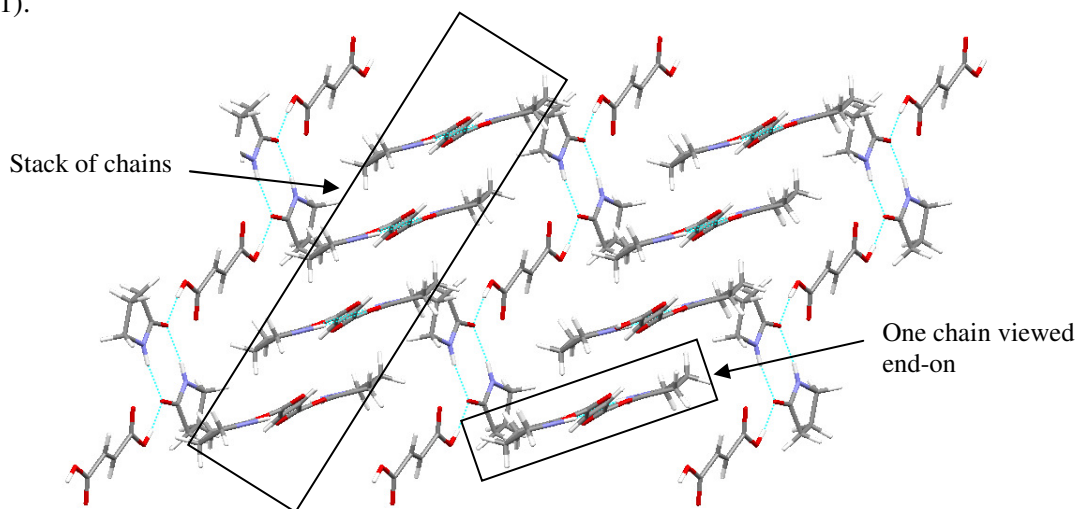


**Figure 6.2.2.2** Arrangement of chains into stacks that are at a different orientation to each other and non-parallel.

When the chains are viewed end-on it can be seen that the chains are not quite flat and that the base molecules adopt a chair conformation.

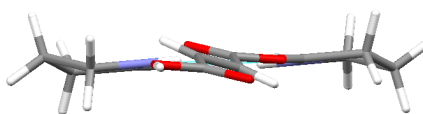


**Figure 6.2.2.3** Hydrogen bonded chain viewed end-on.

### 6.2.3 Discussion of 2-Pyrrolidinone structures

Although five solid products were formed from the well-plate crystallisations, the DLTA combination was found DLTA starting material. AdA-Pyr and SbA-Pyr produced powders which on analysis using PXRD gave weak patterns that do not resemble those of either of the starting materials. Further crystallisations (using Method 3) of OxA, MnA, and GlA again produced oils, however, the PmA combination formed crystals that were found to be the PmA starting material (PIMELA04).

Although only two diacids, ScA and FmA, formed co-crystals with Pyr, they are interesting as they formed the same chain structure but with a different subsequent arrangement of the chains. Indeed, the chains are so similar that there is a maximum difference of 0.055 Å between the hydrogen bond distances for the structures. ScA and FmA have a very similar molecular structure with the only difference being a single or double bond between the second and third carbons. The different interactions from the FmA aromatic CH and the ScA methylene group may cause the different chain arrangement in each of the structures.

Various structure properties are detailed in Table 6.2.3; the similarity of the melting points indicates the structures are equally stable. The slight differences in packing index and melting point are too small to draw conclusions from.

	Melting point/ °C	Packing Index/ %	Torsion angle of base/ °	Density/ g cm <sup>-3</sup>	Torsion angle of acid/ °
ScA	69.98	72.3	9.6(5)	1.39	180.00
FmA	71.10	71.6	-23.08(19)	1.39	180.00

**Table 6.2.3** Various structural properties of the ScA-Pyr and FmA-Pyr co-crystals.

The bond lengths within the ring of the base molecules are approximately equivalent (both co-crystals have an average of 1.47 Å), however, in the FmA structure Pyr has a greater torsion angle than in the ScA structure. The increased planarity in the ScA structure may be due to repulsion between the hydrophobic groups of the closely packed base molecules. The base molecules are also involved in C-H...O hydrogen bonds which may also induce a more planar conformation.

Although the torsion angle of each of the acid molecules is 180°, the alkene backbone of the FmA molecule is 12.5° to the plane of the carboxyl groups. This is a small torsion however, compared to a flat chain, it strengthens the weak hydrogen bonds from the aromatic hydrogens of the acid and also further exposes the double bond for  $\pi$ -interactions with the base.

## 6.3 2-IMIDAZOLIDINONE

### 6.3.1 Oxalic Acid and 2-Imidazolidinone

These two compounds crystallised in a 1:2 acid:base ratio in the monoclinic space group  $P2_1/c$ , with  $Z = 4$ , to form a co-crystal. The R-factor of the refined structure is quite high (15.97%) however, unusually, the ellipsoids are small and the hydrogens were found easily.

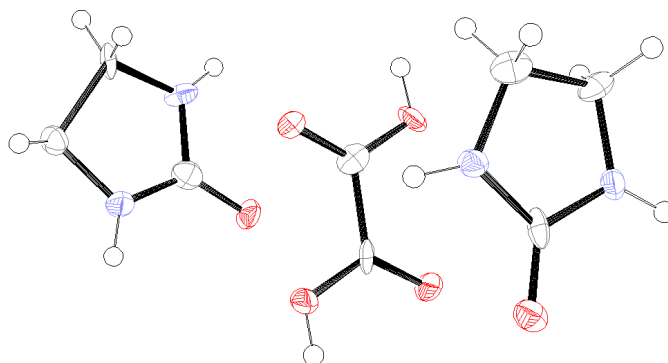


**Figure 6.3.1.1** Ortep diagram for the asymmetric unit of OxA and Idn.

The structure consists of hydrogen bonded acid-base triplets; further acid-base hydrogen bonding results in a nearly planar sheet structure (Figure 6.3.1.2).

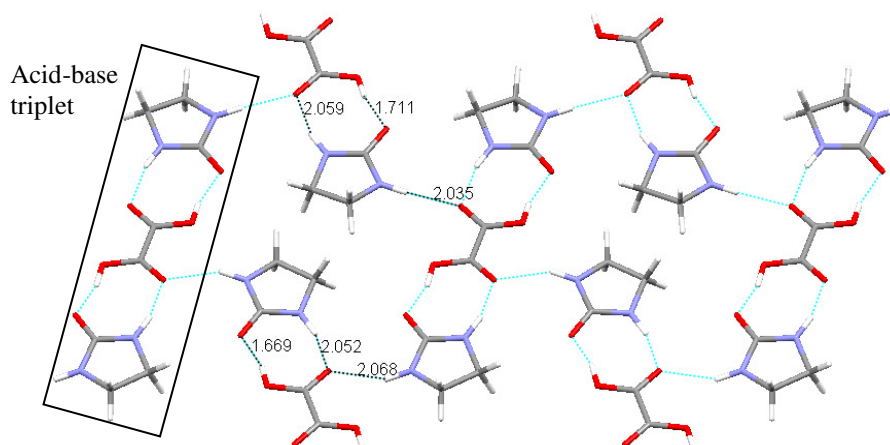


**Figure 6.3.1.2** Hydrogen bonded sheet structure made up of acid-base triplets (error  $\pm 0.008$  Å).

The sheets are then stacked on top of each other in an offset manner so as the molecules fill the gaps between the molecules of the sheet below (Figure 6.3.1.3).

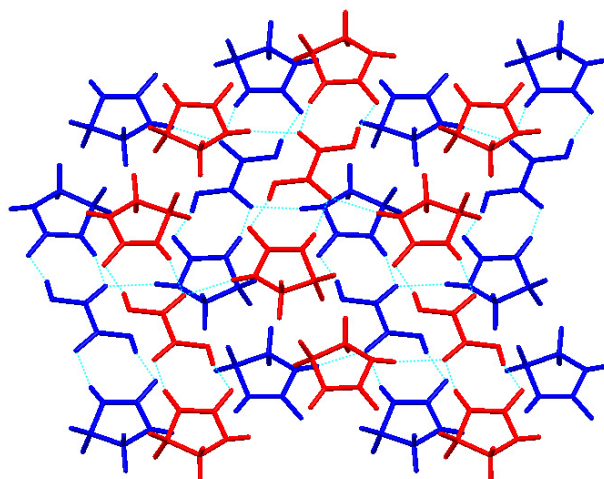


**Figure 6.3.1.3** Stacking of sheets – bottom sheet is coloured blue, top sheet is red.

### 6.3.2 Malonic Acid and 2-Imidazolidinone

These two compounds crystallised in a 1:3 acid:base ratio in the monoclinic space group  $C2/c$ , with  $Z = 8$ , to form a co-crystal. The R-factor is quite high (11.15%) however the ellipsoids are small and the hydrogens were located easily.

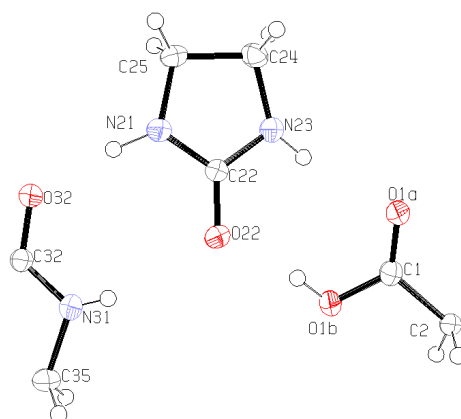


**Figure 6.3.2.1** Ortep diagram for the asymmetric unit of MnA and Idn.

The components form a hydrogen bonded chain structure where three base molecules are hydrogen bonded together to form a trimer. These units are then linked by hydrogen bonding across the acid molecule (Figure 6.3.2.2). The chains are arranged in non-hydrogen bonded 'sheets' parallel to the  $ab$ -plane.

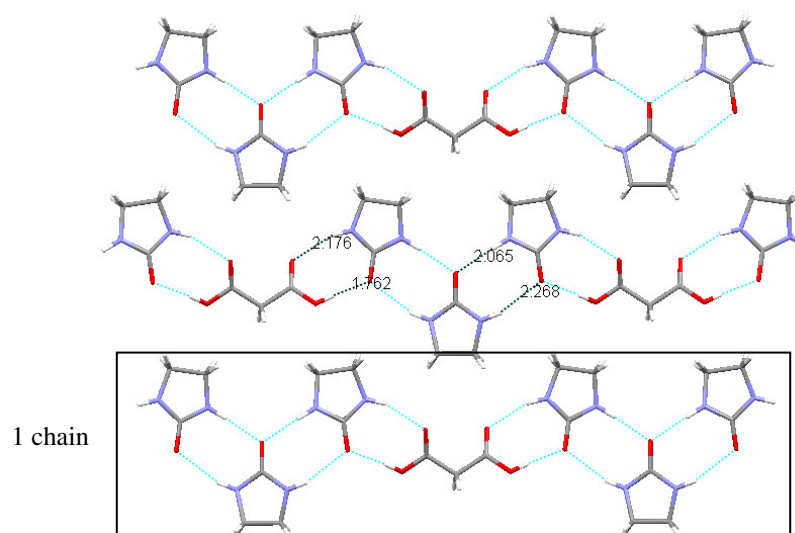


**Figure 6.3.2.2** Arrangement of chains to form a non-hydrogen bonded 'sheet' (error  $\pm 0.007$  Å).

The 'sheets' are stacked in an offset manner with C-H...O hydrogen bonds between the methylene groups of the base and the carboxyl groups of the acid molecules of adjacent sheets (2.641 Å).

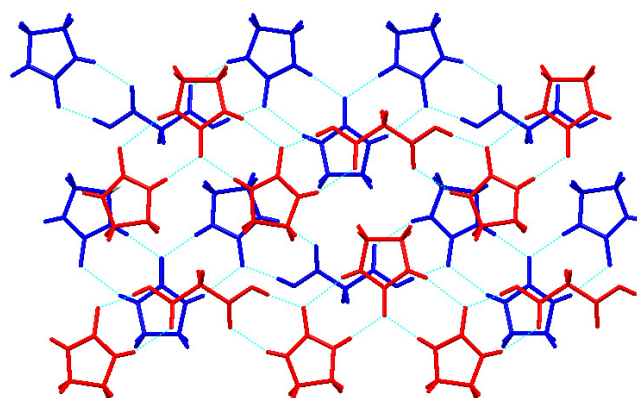


**Figure 6.3.2.3** Stacking of 'sheets.'

### 6.3.3 Succinic Acid and 2-Imidazolidinone

This crystal structure was obtained using synchrotron data due to the very small size of the crystals. It was found that the components crystallised in a 1:2 acid:base ratio in the triclinic space group  $P\bar{1}$ , with  $Z = 2$ , to form a co-crystal. The two halves of the acid molecules present in the asymmetric unit form two distinct acid molecules in the crystal structure, where the other half of each molecule having is generated by inversion symmetry.

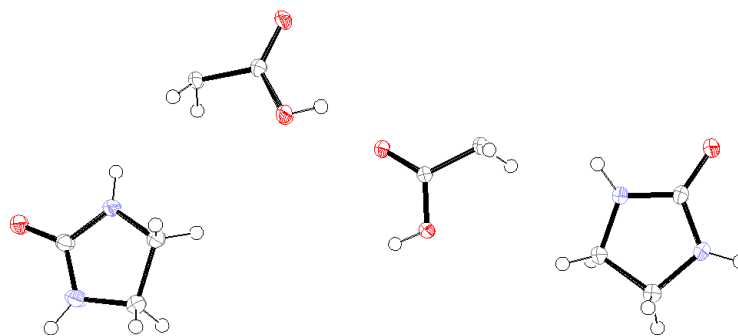


**Figure 6.3.3.1** Ortep diagram for the asymmetric unit of ScA and Idn.

This crystal structure is very similar to the OxA-Idn structure, forming hydrogen bonded triplets containing one acid and two base molecules that are further hydrogen bonded to form planar sheets (Figure 6.3.3.1). As there are two sets of acid-base units in the asymmetric unit, there are two sets of hydrogen bond values.

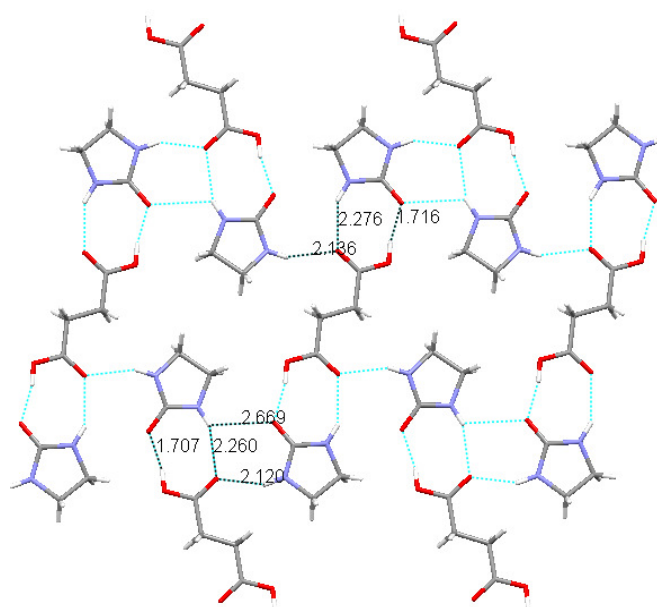


**Figure 6.3.3.2** Hydrogen bonded sheet structure (error  $\pm 0.002$  Å).

The sheets are stacked in an offset manner with weak C-H...O hydrogen bonds between the base oxygen and the base methylene group of adjacent sheets (2.551 Å).

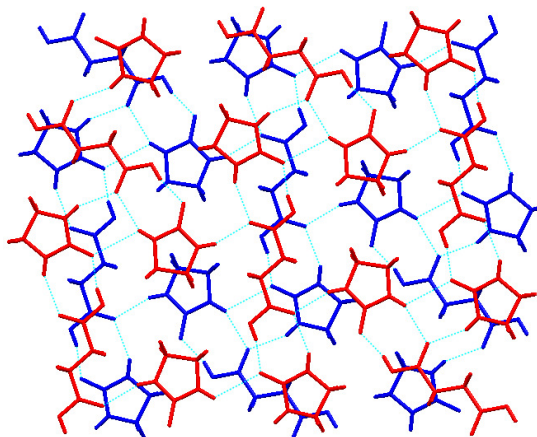


**Figure 6.3.3.3** Stacking of sheets; one sheet coloured blue, adjacent coloured red.

### 6.3.4 Glutaric Acid and 2-Imidazolidinone

These compounds crystallised in a 1:1 ratio in the monoclinic space group *Cc*, with  $Z = 4$ , to form a co-crystal.

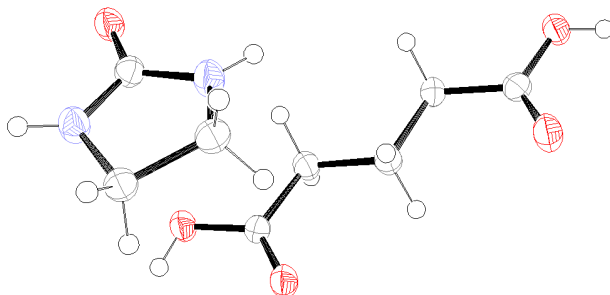


**Figure 6.3.4.1** Ortep diagram for the asymmetric unit of GIA and Idn.

The structure consists of a hydrogen bonded chain of alternate acid and base molecules (Figure 6.3.4.2); there are two sets of hydrogen bond distances as the two carboxyl groups of the GIA molecule are not equivalent.

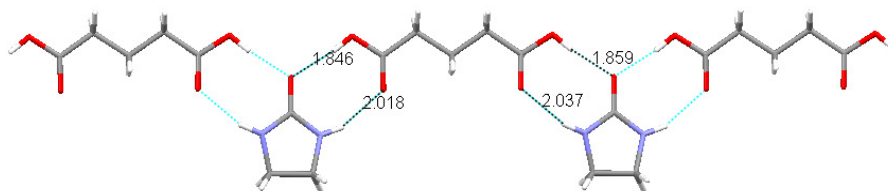


**Figure 6.3.4.2** Hydrogen bonded chain of alternate acid and base molecules (error  $\pm 0.003$  Å).

The chains are arranged into pairs to form a V-shape with the base molecules of each chain in the pair interdigitating. The pairs of chains are then stacked, with adjacent stacks being slightly offset. There are weak C-H $\cdots$ O hydrogen bonds between base and acid molecules of adjacent chains within a pair (2.516 and 2.603 Å). Other weak C-H $\cdots$ O hydrogen bonds between acid molecules link pairs in the same and adjacent stacks (2.559 and 2.660 Å respectively).

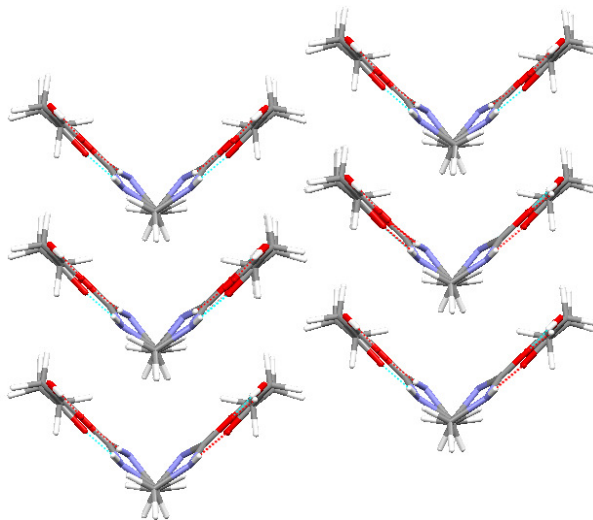


**Figure 6.3.4.3** V-shaped pairs of chains form stacks.

### 6.3.5 Adipic Acid and 2-Imidazolidinone

These components crystallised in a 1:2 acid:base ratio in the monoclinic space group  $P2_1/c$ , with  $Z = 4$ , to form a co-crystal.

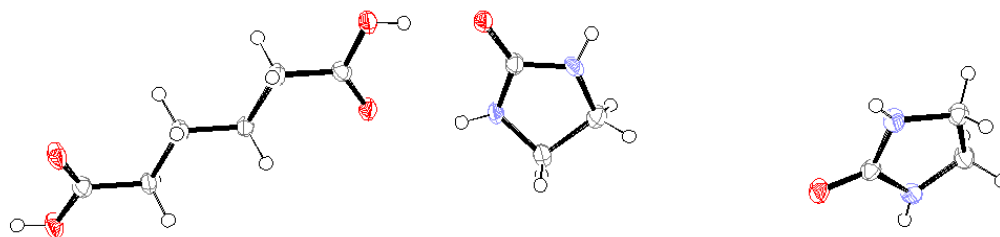


**Figure 6.3.5.1** Ortep diagram for the asymmetric unit of AdA and Idn.

This combination also forms the same sheet structure as that of OxA and ScA structures (Figure 6.3.5.2). However, this sheet is not as flat as the previous two, which can be seen when the sheet is viewed side-on (Figure 6.3.5.3).

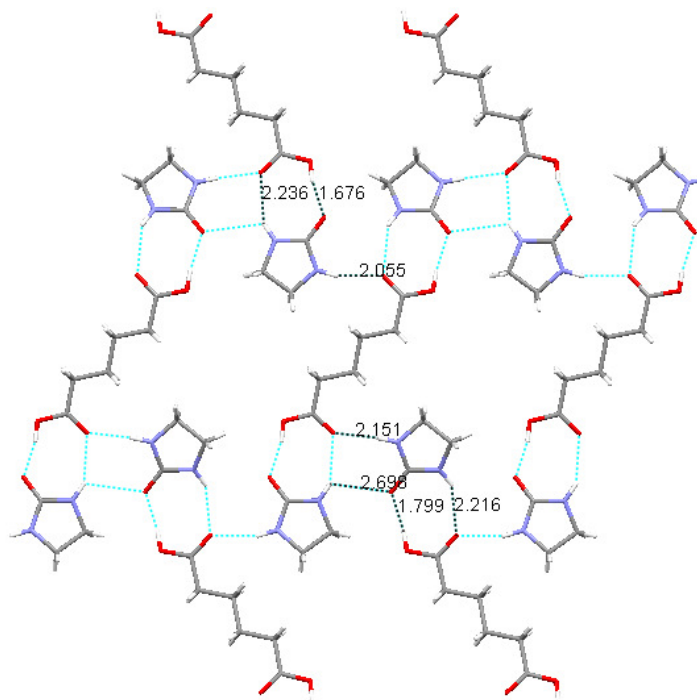


**Figure 6.3.5.2** Sheet structure, hydrogen bond distances marked (error  $\pm 0.004$  Å).

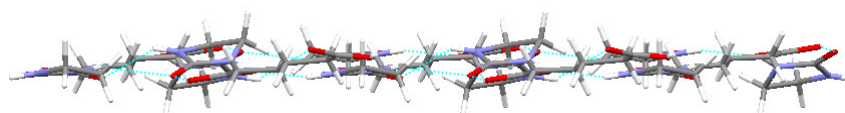


**Figure 6.3.5.3** Sheet viewed side-on.

The sheets are stacked on top of each other in an offset manner with weak C-H $\cdots$ O hydrogen bonds from the base oxygen to the acid methylene group of adjacent sheets (2.642 Å).



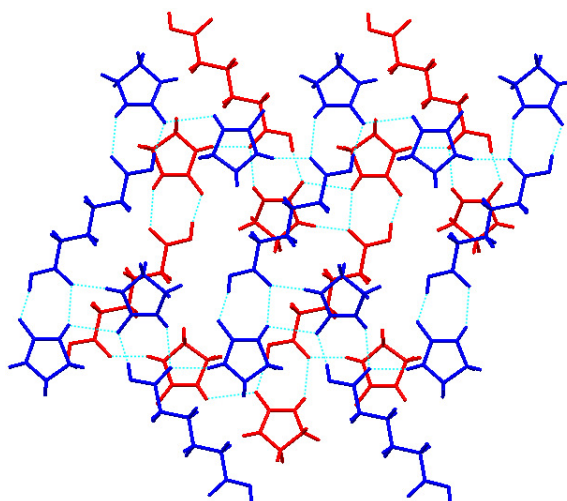


**Figure 6.3.5.4** Stacking of sheets, one coloured red, adjacent coloured blue.

### 6.3.6 *Pimelic Acid and Imidazolidinone*

These compounds crystallised in a 1:1 ratio in the orthorhombic space group *Cmcm*, with  $Z = 8$ , to form a co-crystal. The asymmetric unit contains only half of each of the acid and base molecules, with the other halves being generated by 2-fold rotation symmetry (Figure 6.3.6.1).

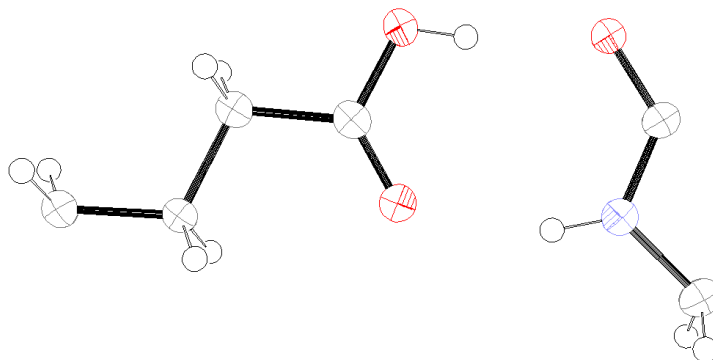


**Figure 6.3.6.1** Ortep diagram for the asymmetric unit of PmA and Idn.

The two components are hydrogen bonded alternately to form planar a chain similar to that seen in the GLA-Idn structure; the hydrogen bond distances are shown in Figure 6.3.6.2.

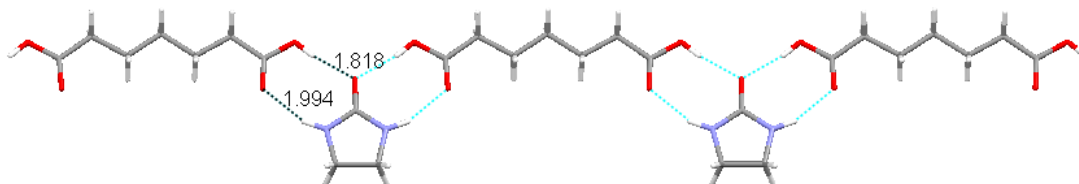


**Figure 6.3.6.2** Hydrogen bonded chain of alternate acid and base molecules (error +/-0.003 Å).

The arrangement of the chains is slightly different to the GLA-Idn structure; the chains stack over each other so as each acid molecule is centred over a base molecule and vice versa (Figure 6.3.6.3).

The chains are arranged into ‘sheets,’ however there are no hydrogen bonds between adjacent chains within a ‘sheet.’ There are also no weak C-H...O hydrogen bonds stabilising the structure.

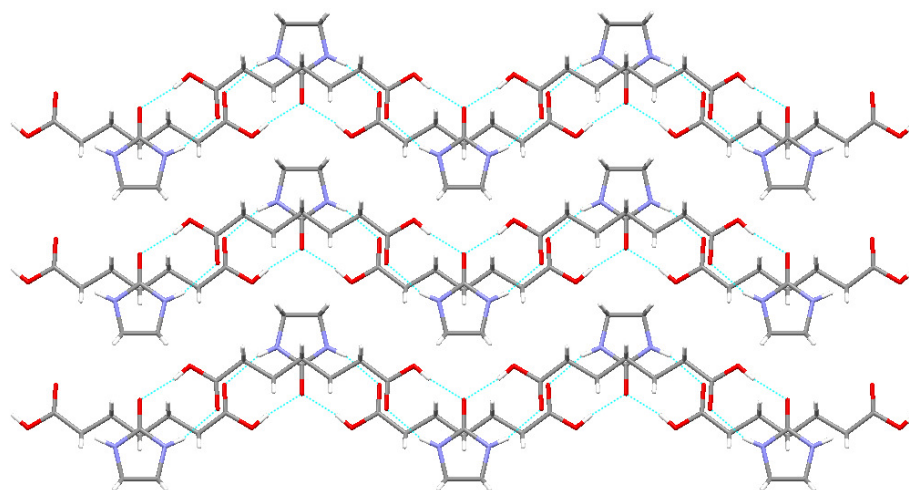


**Figure 6.3.6.3** Stacking of chains so as acid and base molecules are adjacent.

### 6.3.7 *L*-Tartaric Acid and 2-Imidazolidinone

This crystal structure was obtained from synchrotron data due to the small size of the crystals. It was found that the components crystallised in a 1:1 ratio in the orthorhombic space group  $P2_12_12_1$ , with  $Z = 4$ , to form a co-crystal.

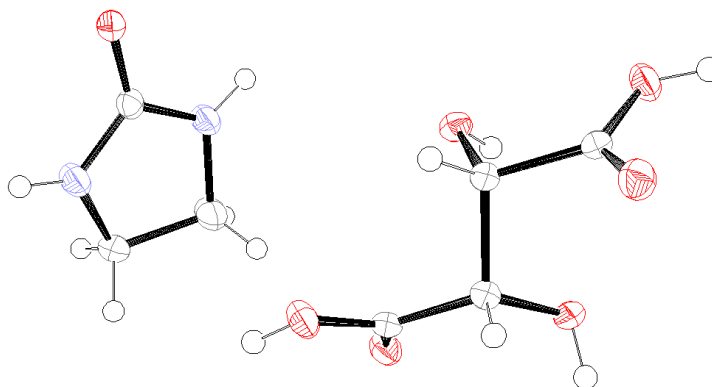


**Figure 6.3.7.1** Ortep diagram for the asymmetric unit of LTA and Idn.

This structure consists of LTA molecules hydrogen bonded across their carboxyl and hydroxyl groups to create a tape (Figure 6.3.7.2). The base molecules are then subtended from this tape by hydrogen bonding to the carboxyl groups of the acid molecules (Figure 6.3.7.3).

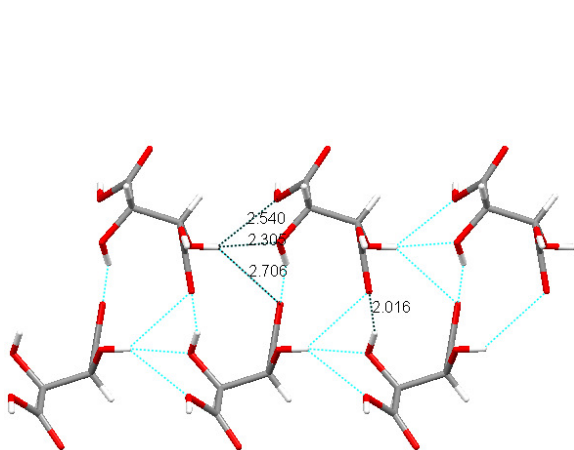


**Figure 6.3.7.2** Acid tape structure, hydrogen bond distances marked (error  $\pm 0.002$  Å).

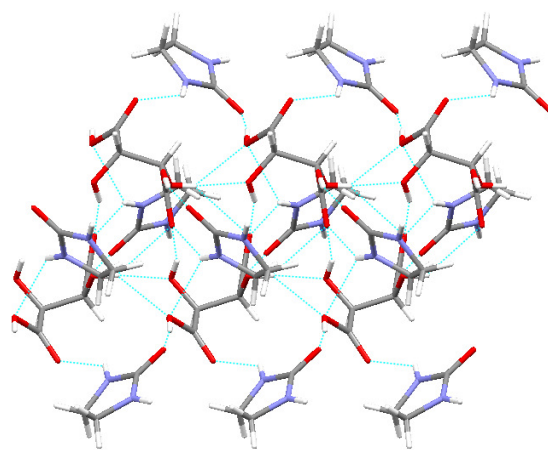


**Figure 6.3.7.3** Base molecules subtended from the acid tape.

As there is a second nitrogen on the base available for hydrogen bonding, the base molecules link adjacent tapes to create a 3-D network (Figure 6.3.7.4). The hydrogen bond distances involving the base and four acid molecules are 1.82(1) and 1.78(1) Å for O-H...O, and 2.17(1), 2.24(1) and 2.71(1) Å for N-H...O. This arrangement also enables C-H...O hydrogen bonds between adjacent base and acid molecules, and adjacent base molecules (2.628 and 2.695, and 2.604 Å respectively).

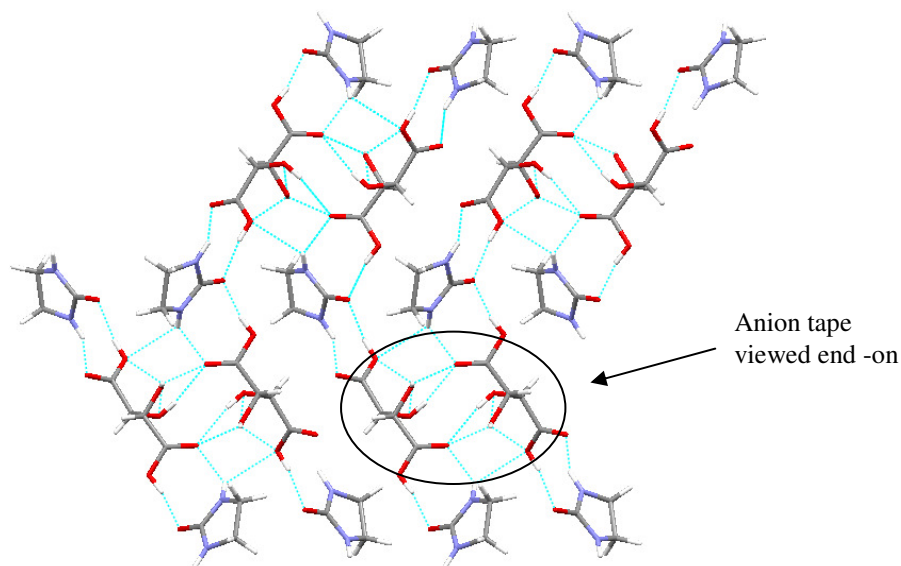


**Figure 6.3.7.4** Hydrogen bonded 3-D network consisting of acid tapes linked by base molecules.

### 6.3.8 *DL-Tartaric Acid and 2-Imidazolidinone*

This crystal structure was obtained from synchrotron data due to the small size of the crystals. The components were found to crystallise in a 1:1 ratio in the monoclinic space group  $P2_1/c$ , with  $Z = 4$ , to form a co-crystal.

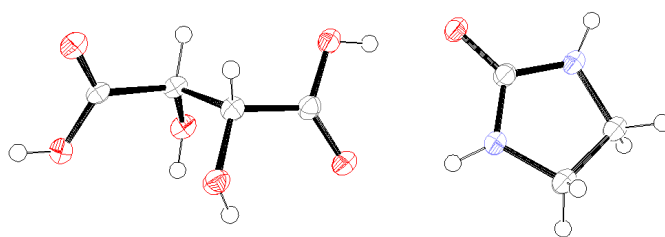


**Figure 6.3.8.1** Ortep diagram for the asymmetric unit of DLTA and Idn.

The acid molecules are hydrogen bonded via the carboxyl and hydroxyl groups to form a chain. One side of the base molecules is hydrogen bonded to the acid carboxyl groups thus creating a tape. The other carboxyl group that is involved in forming the acid chain also hydrogen bonds to the free side of the base thereby forming a zigzag sheet.

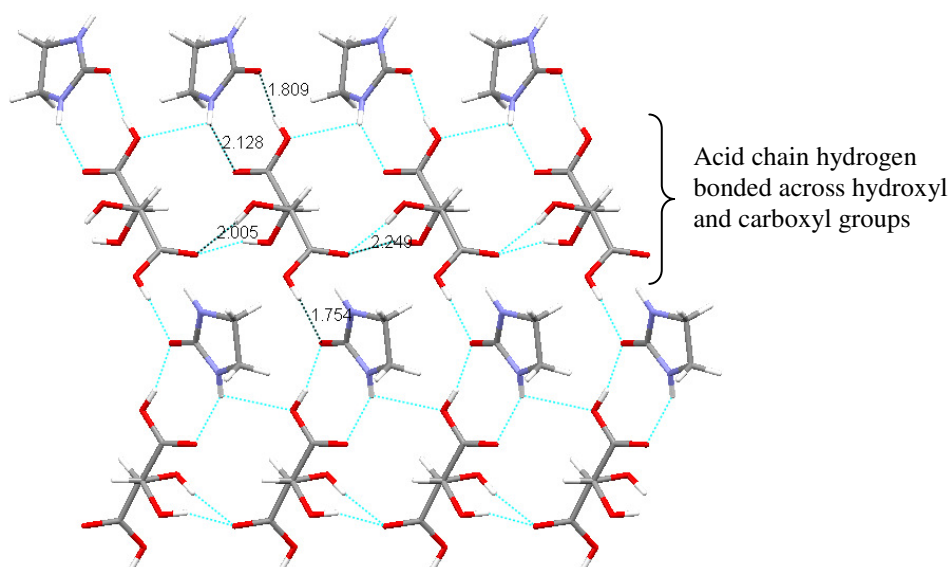


**Figure 6.3.8.2** Acid chains linked by hydrogen bonding across the base molecules, hydrogen bond distances marked (error  $\pm 0.002$  Å).

The nitrogen of the base molecule that is not involved in hydrogen bonding in this sheet, hydrogen bonds to an acid molecule in an adjacent sheet, thereby creating a 3-D network. There are also weak C-H $\cdots$ O hydrogen bonds between the base molecules and the carboxyl groups of the acid molecules (2.555, 2.596 and 2.611 Å) which further stabilise the 3-D array.

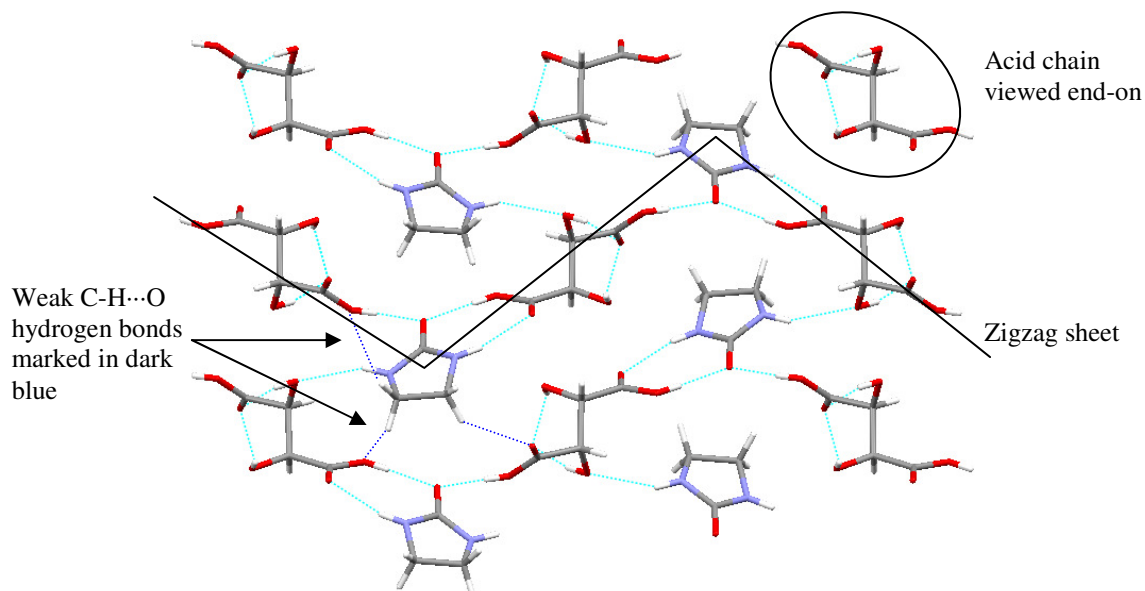


**Figure 6.3.8.3** 3-D network – acid molecules in chains are positioned directly over each other; viewed down the *a*-axis.

### 6.3.9 Maleic Acid and 2-Imidazolidinone

Initially these two compounds formed an oil when combined using Method 1 however, using Method 3, block crystals formed. These were found to contain the components in a 2:1 acid:base ratio, having crystallised in the monoclinic space group  $P2_1/c$ , with  $Z = 8$ , to form a co-crystal. The R-factor of this structure remained quite high (11.81%) even though the transferable hydrogens could be found easily and the ellipsoids are quite small (Figure 6.3.9.1). The structure was tested for merohedral twinning using ROTAX,<sup>2</sup> however none of the suggested matrices reduced the R-factor.

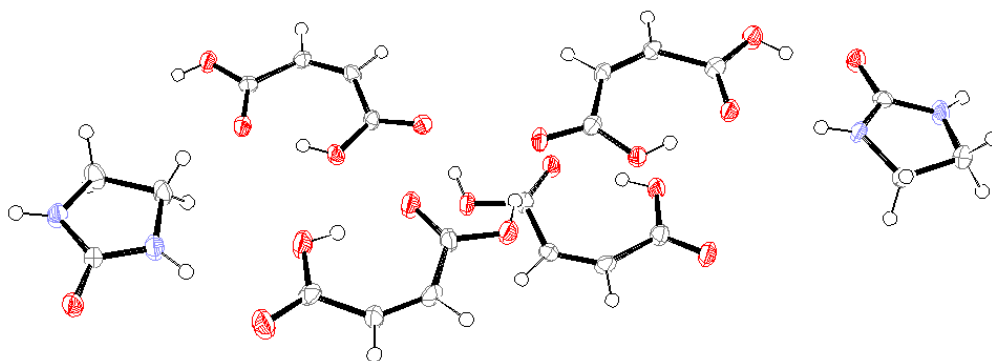


**Figure 6.3.9.1** Ortep diagram for the asymmetric unit of MeA and Idn.

There are strong intramolecular hydrogen bonds between the carboxyl groups of the acid molecules (1.718, 1.700, 1.619 and 1.620 Å). The structure consists of hydrogen bonded chains of acid and base molecules, in a ...A...A...B...A...A...B... arrangement. As there are two sets of acid-acid-base units in the asymmetric unit, there are two sets of hydrogen bond distances within the chain; these are marked in Figure 6.3.9.2. One side of each base molecule is linked to the adjacent acid

molecule as both a hydrogen bond acceptor and donor. The other side of the base molecule acts only as a donor with a bifurcated hydrogen bond to each of the oxygen atoms in the carboxyl group. The chains are arranged to form a reasonably flat ‘sheet’ with C-H...O hydrogen bonds between acid molecules in adjacent chains (range = 2.336-2.527 Å).

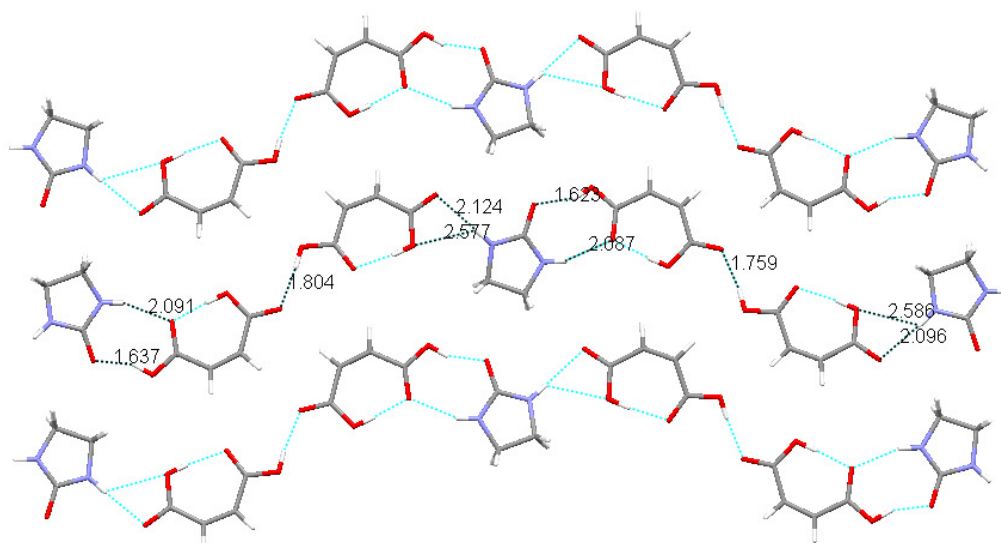


**Figure 6.3.9.2** ‘Sheet’ arrangement of hydrogen bonded chains with hydrogen bond distances marked on one chain (error  $\pm 0.006$  Å).

The ‘sheets’ are stacked so as the base molecules are positioned on top of each other in a parallel offset manner; the acid molecules are similarly arranged (Figure 6.3.9.3). There are C-H...O hydrogen bonds between the base molecules and acid molecules of adjacent sheets (2.668 and 2.680 Å).

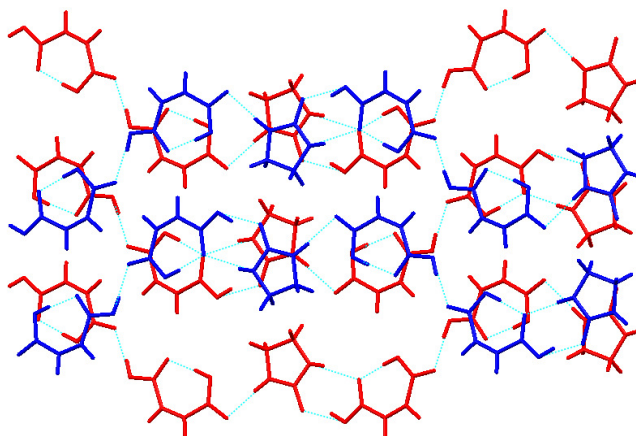


**Figure 6.3.9.3** Stacking of sheets, bottom sheet is coloured red, the top is coloured blue.

### 6.3.10 Discussion of 2-Imidazolidinone Structures

Although most of the diacids formed binary compounds, SbA-Idn and FmA-Idn produced powders; the SbA product will be discussed later. The powder pattern of the FmA-Idn product has three main peaks which do not fit either of the starting material patterns. This suggests that either a new binary

compound has formed, or possibly a new starting material polymorph. As ScA and FmA sometimes form similar structures (and in some cases are isostructural) the pattern was also compared with that generated from the ScA structure – this showed some similarity but insufficient for it to be assumed that the structures are the same. When the FmA-Idn product was heated using a hot-stage microscope, the product partially melted at 84-93°C and then completely melted at 108-116°C. Neither of these events concurs with the melting temperatures of the starting materials, further suggesting a new product has formed.

From the crystal structure descriptions it can be seen that for the simple diacids there is a pattern as the acid chain length increases; sheet structures form for the even diacids and chain structures form for the odd diacids. This is tabulated, along with various structure properties, in Table 6.3.10.

Diacid		Ratio in the asymmetric unit	Structure type	Melting point/ °C	Packing index/ %
Oxalic Acid	Even	A:2B	Planar sheet	128.2-131.5	74.6
Malonic Acid	Odd	0.5A:1.5B	Chain	73.0	71.9
Succinic Acid	Even	A:2B	Sheet	124.58	72.4
Glutaric Acid	Odd	A:B	chain	98.81	70.4
Adipic Acid	Even	A:2B	Sheet	83.78	69.3
Pimelic Acid	Odd	0.5A:0.5B	chain	92.25	69.5
Suberic Acid	Even	-	Crystals badly split	45.33	-

**Table 6.3.10** Table of the crystal structure descriptions and properties for the simple diacid co-crystals.

The sheet structures of the even diacids are all very similar with the same layout of atoms and hydrogen bonding motifs; only the chain length of the diacid, and hence the distance between the base molecules, increases. The distance between the centroids of the base molecules increases from 5.468 Å in OxA to 9.343 Å in AdA. The packing index in each of the structures decreases with chain length as the voids between the base molecules are enlarged. This is also highlighted by the disperse points and uneven top edge in the fingerprint plots for AdA-Idn (Appendix, Table A10.2). The decrease in melting point as the chain length increases is a result of the destabilisation caused by the expanding voids. The reduction in planarity of the sheet as the chain length increases may be to try to compensate for the increased chain length so as to reduce the size of the resultant voids.

As SbA has an even number of carbons it would be expected to form a sheet structure with Idn. If this is the case, the longer chain length would decrease the packing index further, making the potential sheet structure even less stable and hence very poor, small crystals are formed. The DSC trace of this product gave one trough with a melting point of 45.33°C, this is much lower than the published SbA melting point of 144.4°C suggesting a binary compound has formed. The powder pattern gave a number of weak peaks, two of which match SUBRAC04, however, none fit the Idn powder pattern further suggesting that a new binary compound has been formed.



The odd diacids give two types of chain structure; one contains a 1:3 acid:base ratio and the other contains a 1:1 stoichiometry. The crystal structure for MnA adopts the former ratio and the GlA and PmA crystal structures adopt the latter with very similar chain structures. The main difference between the GlA and PmA structures is the increase in chain length leading to a less close packed structure – this can be seen by the packing index decreasing by approx 1% and also the melting point of the products decreasing by approximately 6°C.

Figure 6.3.10.1 shows the melting points of each of the structures together with their packing indexes. The trends mentioned above can be seen and it can also be noted that the curve of the melting point for the acids of chain length 4-7 is the same shape as that of the packing index. OxA and MnA do not follow this curve to the same extent as the other members of the series; the melting point are lower than expected from the curve of the packing index, and the melting point for MnA is lower than expected.

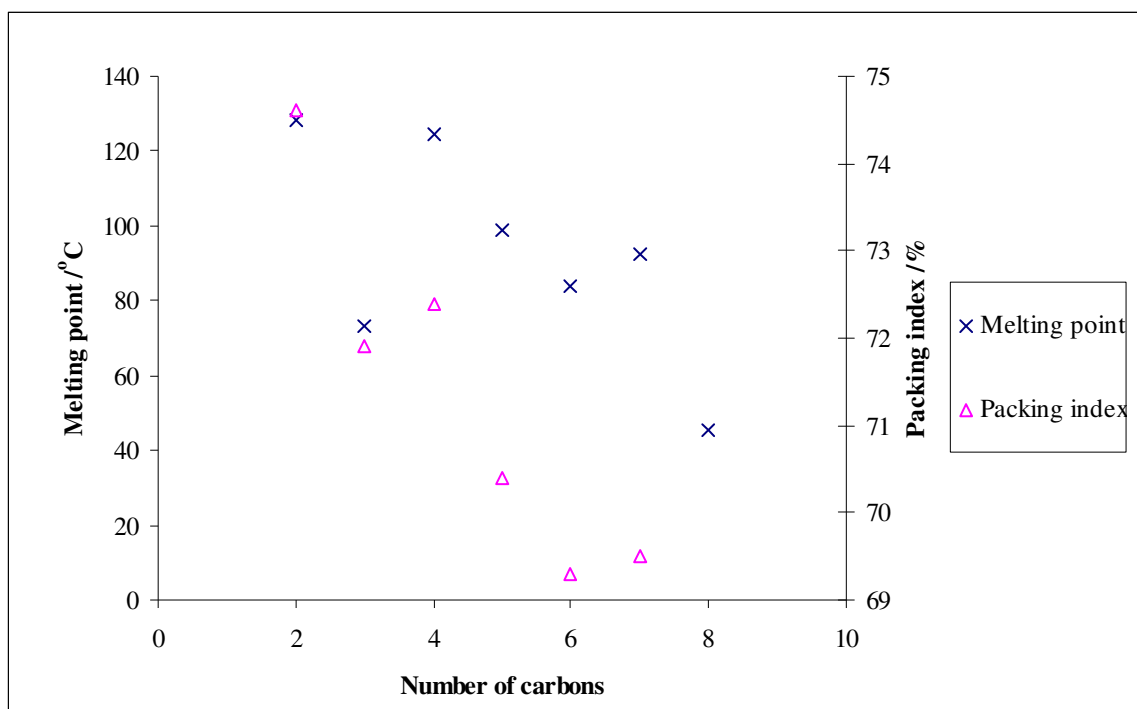


**Figure 6.3.10.1** Graph showing the melting point and packing indexes for the diacid-Idn co-crystals.

It was discussed earlier how across the series of pure diacids, the different odd and even diacid structures give rise to an alternation in melting point (Section 2.6.1). It is interesting that when co-crystallised with Idn this diacid property is reflected in the type of structure formed. This may be due to the different relative position of the acid groups on a chain with an even versus an odd number of carbons. It should also be noted that for all the even structures the acidic hydrogens are on opposite sides of the molecule (*anti* conformation), however in the odd structures they are on the same side of the molecule (*syn* conformation). The *anti* conformation is more stable than the *syn* conformation by less than 0.5 kcal mol<sup>-1</sup>.<sup>3</sup> The *syn* conformation is not prevalent in the literature with only three occurrences noted in a search by Vishweshwar *et al.*,<sup>4</sup> all of which are co-



crystals of OxA. The *anti* conformation of the odd diacid allows close packing of the molecules; the *syn* conformation would result in zigzag chains where the base molecule may make them more difficult to pack than straight chains.

In a study by Vishweshwar *et al.*,<sup>4</sup> where alkanedicarboxylic acids (carbon chain lengths 2-6) were co-crystallised with isonicotinamide, melting point alternation was noted in the co-crystals as well as alternation in crystal density and packing fraction. This was found to be in keeping with the melting point alternation of the diacid starting materials. It was further noted that the co-crystals had higher melting points than the starting materials due to strong hydrogen bonds and efficient packing stabilising the structures. An increase in melting point is not seen in the Idn co-crystals (Figure 6.3.10.2). The distribution of the even diacid co-crystal melting points follows that of the free even diacids, however the melting points of the GlA and PmA are much higher than expected if following the curve of the free odd diacids. This may be due to the changing stoichiometry of the odd diacid co-crystals which compensates for the increased chain length and hence produces structures of a relatively higher stability.

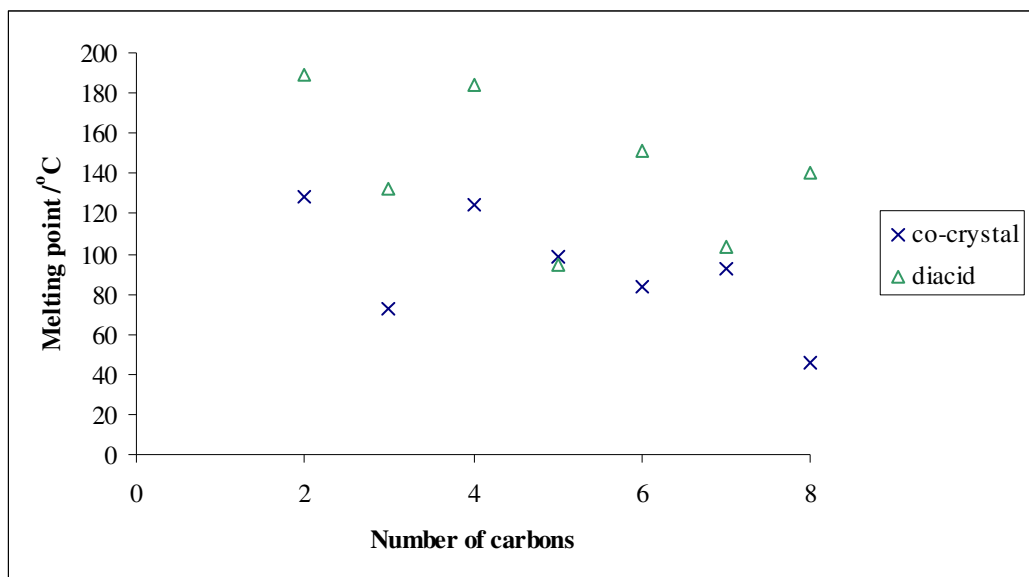


**Figure 6.3.10.2** Graph showing the melting points of the Idn co-crystals and the free diacids.

The LTA and DLTA co-crystal structures are different from the usual TA structures as the acid molecules do not hydrogen bond head-to-tail and instead link the hydroxyl and carboxyl groups to create a chain. This enables the carboxyl groups to form strong hydrogen bonds with both the nitrogen and the oxygen of the base. Both of the TAs form 3-D networks that have a similar basic structure where the acid chains are linked by the base molecules. In the DLTA-Idn structure, however, the acid molecules form a chain as all the hydroxyl groups are pointing in the same direction, whereas in the LTA structure the hydroxyl groups in a pair of chains point towards each other, thus creating a tape. Another similarity in these structures is the formation of a hydrogen bonded pair between one end of the acid and one side of the base, the other ‘ends’ of the molecules

then form hydrogen bonds to two different molecules each. This is not seen in any of the other Idn structures.

The MeA-Idn structure is different from the rest of the group as the acid molecules hydrogen bond to each other in pairs, in all of the other structures (except the TAs) the acid is only ever hydrogen bonded to the base molecule. In the MeA-Idn case, the intramolecular hydrogen bond prevents one end of the acid molecule from being a hydrogen bond donor. Therefore one acid molecule forms a hydrogen bonded pair with the amide group of the base whereas the other forms a bifurcated hydrogen bond to the base nitrogen.

## 6.4 1,3-DIMETHYLIMIDAZOLIDINONE

The MnA, MeA and LTA combinations all produced oils. The OxA, ScA, GlA, AdA, and PmA combinations were analysed by SXRD and were shown to be the acid starting material. PXRD showed the FmA and SbA combinations had each resulted in the starting materials crystallising out separately. DLTA was also analysed by PXRD and the pattern showed three peaks which could be from the DLTA starting material pattern (ZZZDUI01), however, the relative intensities do not correspond. The melting point of the DLTA-DMI<sub>dn</sub> product is 124.7°C which is significantly lower than the melting point of DLTA and significantly higher than that of DMI<sub>dn</sub> suggesting that a binary product may have formed.

As the starting materials predominantly crystallised out separately, DMI<sub>dn</sub> must be particularly poor at forming binary compounds. This is due to the lack of hydrogen bond donors and acceptors on the molecule which prevents it from forming hydrogen bonds with the diacids. There are three DMI<sub>dn</sub> binary compounds on the CSD, two of which are co-crystals (DIVTAD, XAWTUL). These consist of a lattice structure made by the co-crystal former from which DMI<sub>dn</sub> is subtended via hydrogen bonding to its carbonyl group. The third is a clathrate (DAGGAU).

## 6.5 MORPHOLINE

### 6.5.1 Oxalic Acid and Morpholine

These two compounds crystallised to form a salt with a 1:2 acid:base ratio in the monoclinic space group  $P2_1/c$ , with  $Z = 2$ , to form a salt. The dianion lies across an inversion centre, making the molecule centrosymmetric.

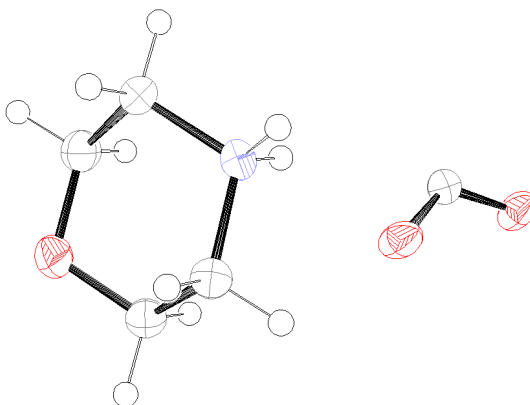


**Figure 6.5.1.1** Ortep diagram for the asymmetric unit of OxA and Mo.

Each dianion is hydrogen bonded to four adjacent cations, which are in turn hydrogen bonded to adjacent dianions to create a tape (Figure 6.5.1.2).

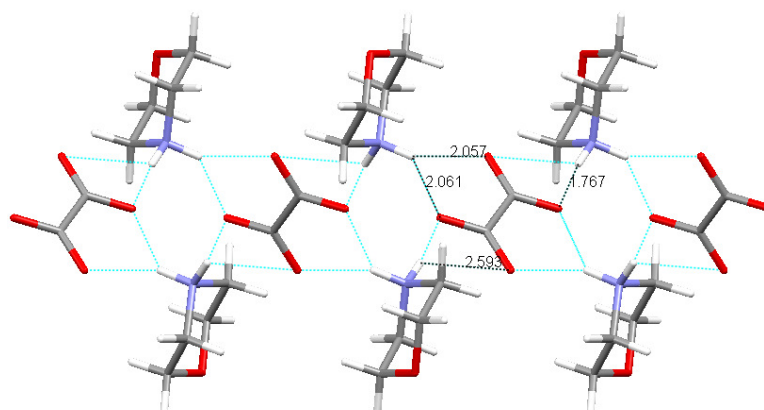


**Figure 6.5.1.2** Tape structure viewed down the *b*-axis, hydrogen bond distances marked (error  $\pm 0.002$  Å).

The anions and cations are hydrogen bonded to each other alternately in different planes (i.e. in front of and behind each ion) and hence the chain actually extends down the *b*-axis to create a sheet that runs parallel to the *bc*-plane (Figure 6.5.1.3). As the cations are positioned above and below the central anion core the sheet has a bilayer structure.

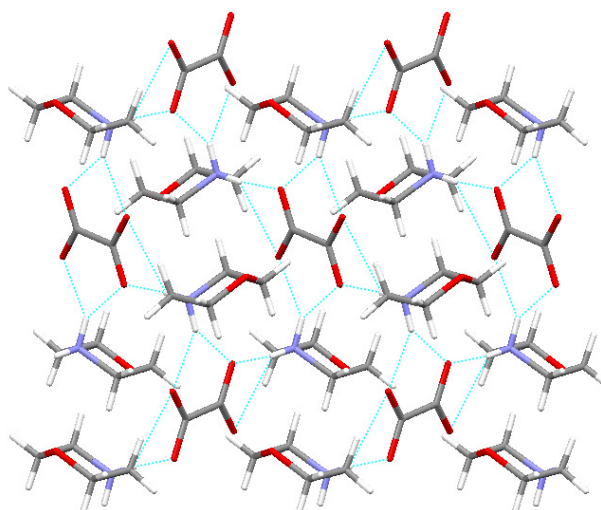


**Figure 6.5.1.3** The sheet layout, viewed down *a*-axis.

The sheets are stacked on top of each other so as the base molecules from the adjacent sheets are offset, allowing closer packing (Figure 6.5.1.4). There are also weak C-H...O hydrogen bonds between the cations of adjacent sheets (2.545 Å).

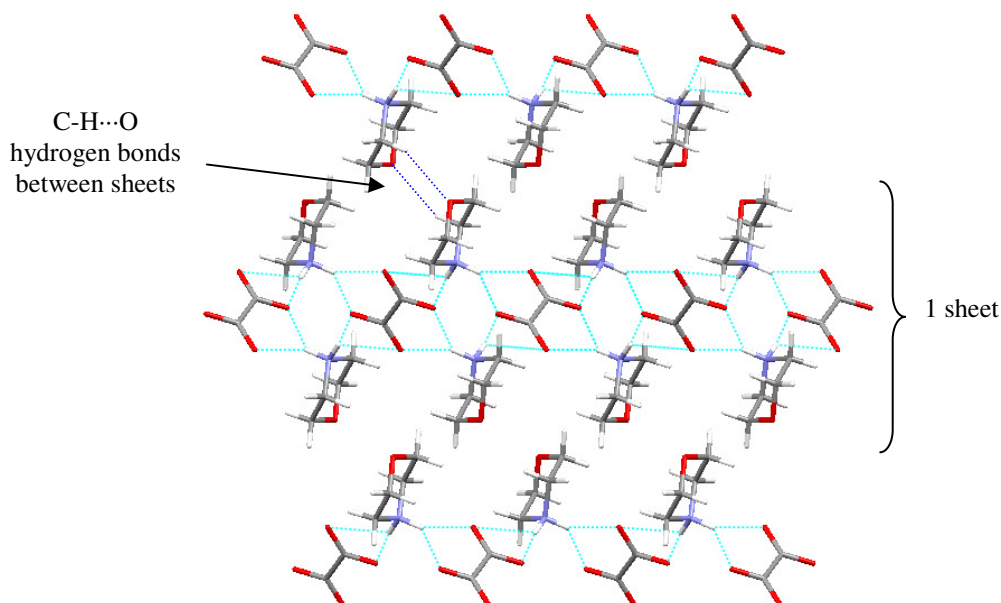


**Figure 6.5.1.4** Offset stacking of sheets, sheets viewed side-on down the *b*-axis.

### 6.5.2 Succinic Acid and Morpholine

These two compounds also crystallised a 1:2 acid:base ratio in the monoclinic space group  $P2_1/c$ , with  $Z = 2$ , to form a salt. The dianion lies across an inversion centre, making the carboxylate groups equivalent.

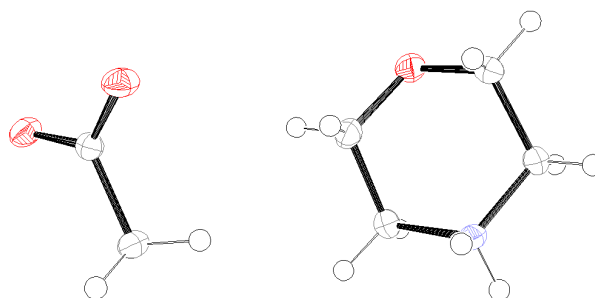


**Figure 6.5.2.1** Ortep diagram for the asymmetric unit of ScA and Mo.

This structure is similar to OxA-Mo in that each dianion is surrounded by four cations to which the dianion is linked by hydrogen bonds (Figure 6.5.2.2).

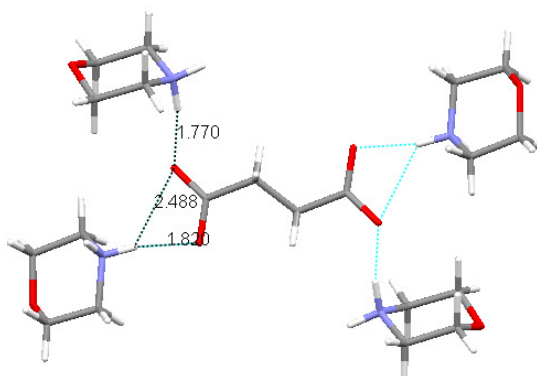


**Figure 6.5.2.2** Hydrogen bonded unit of anions and cations, hydrogen bond distances marked (error  $\pm 0.002$  Å).

Each cation is involved in three hydrogen bonds, with the anions and cations linked alternately to create a tape; each ion is hydrogen bonded to another in a different plane and hence the structure extends down the *b*- and *c*-axes creating a sheet. The cations are positioned above and below the central anion core, resulting in a bilayer structure.

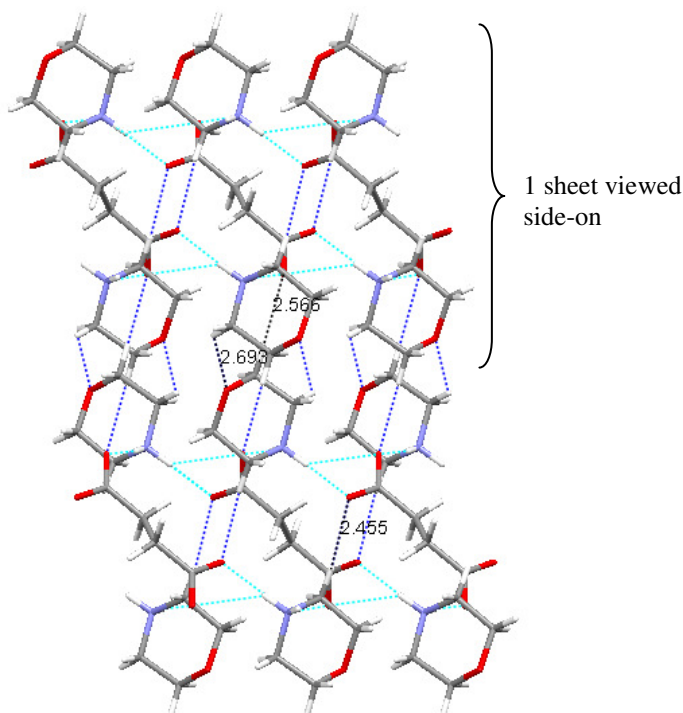


**Figure 6.5.2.3** Bilayer arrangement, sheet viewed side-on down the *b*-axis; C-H...O hydrogen bond distances marked (dark blue); N-H...O hydrogen bonds (light blue).

The sheets are arranged so as each section of the bilayer eclipses that of the sheet below. This still results in a close packed arrangement as the molecules in the bilayer are offset relative to the direction of stacking. There are C-H...O hydrogen bonds between the CH<sub>2</sub> groups and oxygens of the cations (2.693 and 2.566 Å).

### 6.5.3 Adipic Acid and Morpholine

These compounds crystallised in a 1:2 acid:base ratio in the triclinic space group *P*-1, with *Z* = 1, to form a salt. The dianion is centrosymmetric as it lies across an inversion centre. In spite of the high R-factor (14.03%), the transferable hydrogens were found easily.

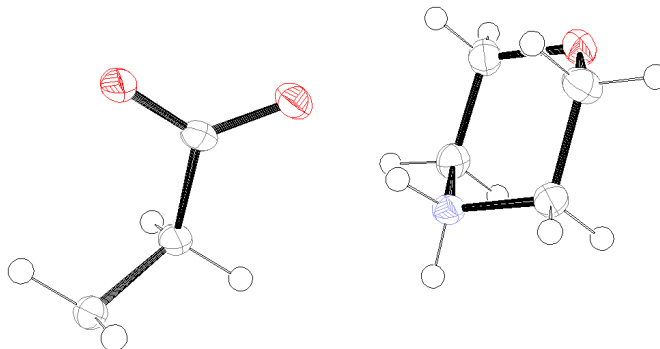


**Figure 6.5.3.1** Ortep diagram for the asymmetric unit of AdA and Mo.

The structure, again, consists of a tape of alternately hydrogen bonded dianions and cations with the cations positioned above and below the central anion core (Figure 6.5.3.2). This structure differs from the OxA and ScA structures however, as all of the ions within the tape are in the same plane and therefore the structure does not extend into a sheet through N-H...O hydrogen bonding.

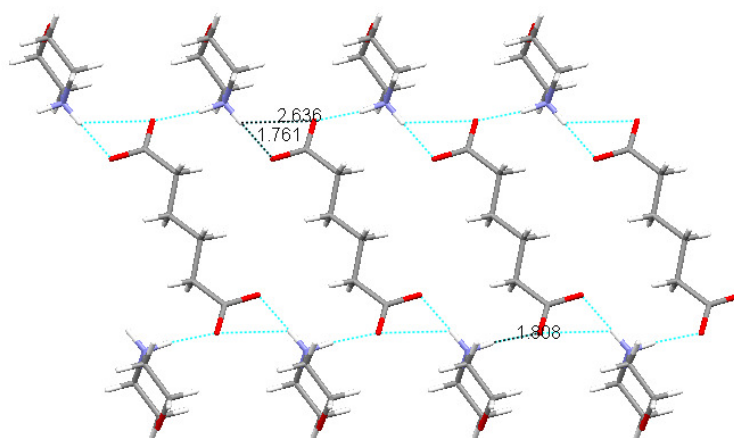


**Figure 6.5.3.2** The hydrogen bonded tape structure (error  $\pm 0.006$  Å), viewed down the *c*-axis.

The tapes are parallel to the *a*-axis with adjacent tapes arranged in an offset manner so as to enable weak C-H...O hydrogen bonds between adjacent tapes (Figure 6.5.3.3).

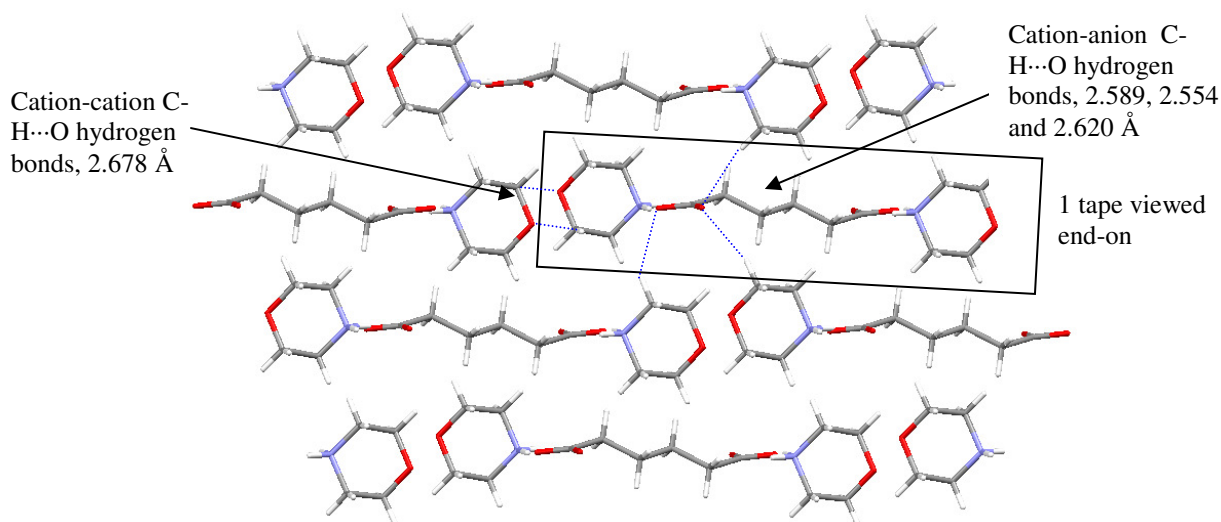


**Figure 6.5.3.3** The arrangement of tapes viewed down  $a$ -axis; C-H...O hydrogen bonds marked.

#### 6.5.4 *DL-Tartaric Acid and Morpholine*

These compounds crystallised in a 1:1 ratio with water in the triclinic space group  $P-1$ , with  $Z = 2$ , to form a salt monohydrate.

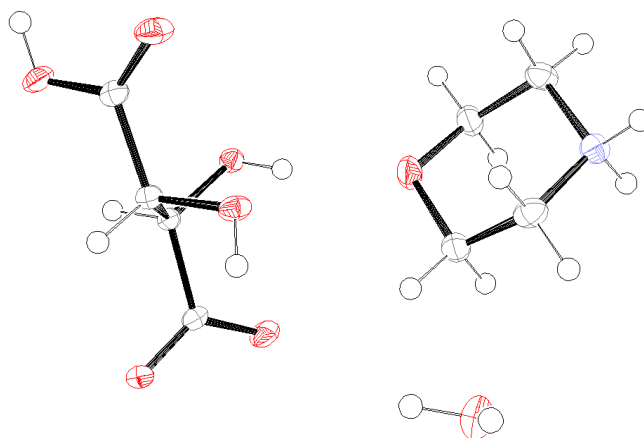


**Figure 6.5.4.1** Ortep diagram for the asymmetric unit of DLTA and Mo.

The structure consists of monoanions hydrogen bonded head-to-tail to form a chain (1.70(1) Å). The cations are linked to a pair of anion chains by hydrogen bonds from the hydroxyl group of the anion to the oxygen of the cation (1.93(1) Å), and from the cation nitrogen to the carboxyl and hydroxyl group of the anion (2.231(17) and 2.018(19) Å respectively). This results in the cations being sandwiched between a pair of anion chains (Figure 6.4.4.2).

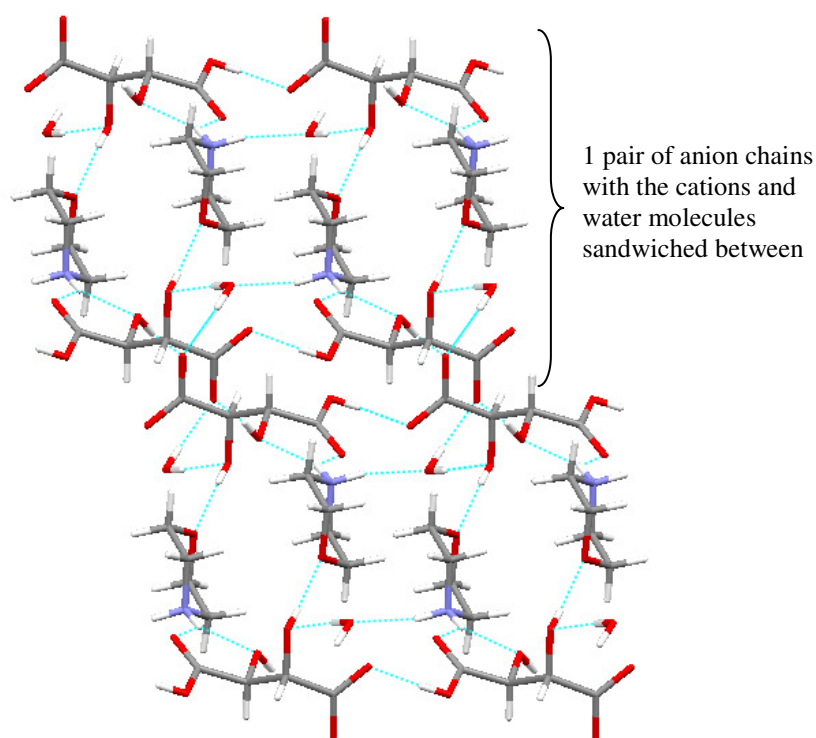


**Figure 6.5.4.2** Sandwich structure.

The water molecules are also sandwiched between the anion chains and are hydrogen bonded to the second hydrogen of the nitrogen on the cation and the anion hydroxyl group. In addition, the water molecule is also hydrogen bonded to the carboxylate group of an anion in an adjacent anion pair. This, together with hydrogen bonding between the hydroxyl and carboxylate groups of anions in adjacent pairs, creates a 3-D network (Figure 6.5.4.3). There are weak C-H...O hydrogen bonds between cations and anions (2.603 and 2.657 Å), cations and water molecules (2.691 Å) and between anions (2.598 Å) which further stabilise the structure.

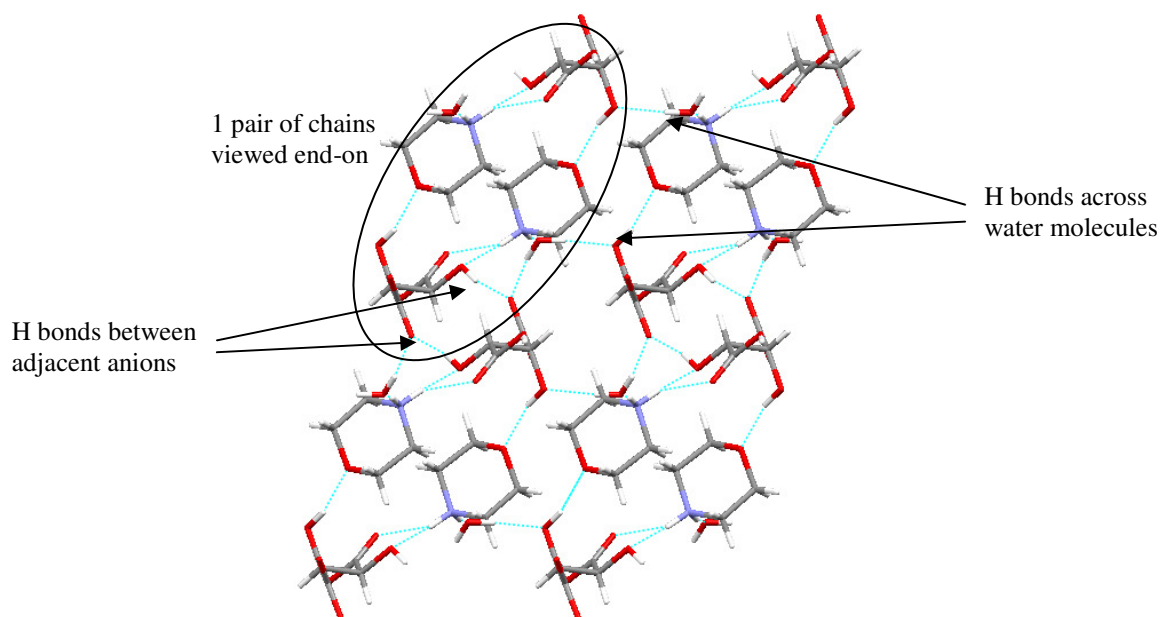


**Figure 6.5.4.3** 3-D network, pairs of chains viewed end-on.



### 6.5.5 Maleic Acid and Morpholine

These two compounds reacted with each other via a 1,4-Michael addition reaction. The diacid also reacted with the solvent used in the crystallisation to become dimethylated. The product is shown in Figure 6.5.5.1.

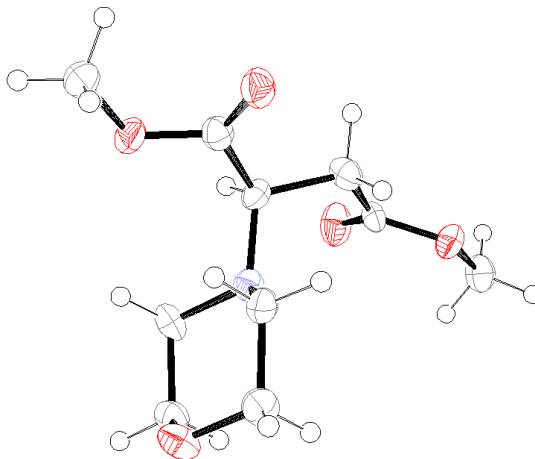


**Figure 6.5.5.1** Ortep diagram of the product from crystallisation of MeA and Mo in methanol.

### 6.5.6 Fumaric Acid and Morpholine

These two compounds crystallised in a 1:2 acid:base ratio in the monoclinic space group  $P2_1/c$ , with  $Z = 2$ , to form a salt which is isostructural with that of ScA-Mo. The dianion again lies across an inversion centre, making the carboxylate groups equivalent.

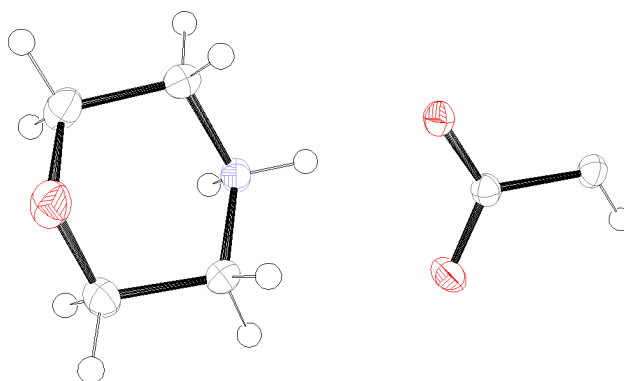


**Figure 6.5.6.1** Ortep diagram for the asymmetric unit of FmA and Mo.

Although the hydrogen bond distances and other weak intermolecular interactions are slightly altered, the presence of the double bond does not appear to have a significant affect on the structure:

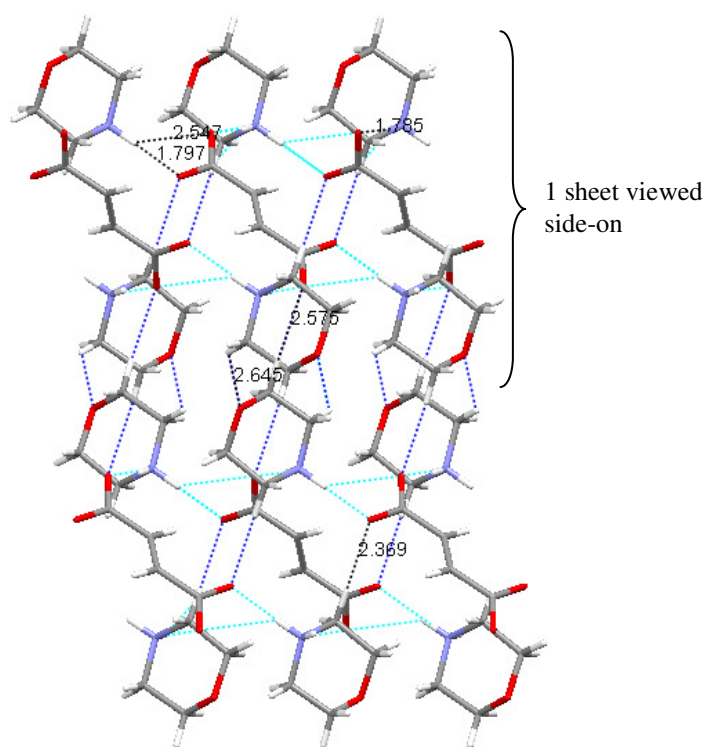


**Figure 6.5.6.2** Bilayer arrangement, sheet viewed side-on down the *b*-axis; N-H...O and C-H...O hydrogen bond distances marked (light blue and dark blue respectively; error  $\pm 0.002$  Å).

#### 6.5.7 Discussion of Morpholine Structures

This group is similar to the Idn group as all the odd diacids formed different products to the even diacids – in this case oils instead of crystalline products. Further crystallisation experiments (Method 3) with the odd diacid-Mo combinations also resulted in oils. The odd diacids may have formed binary products that are not sufficiently stable to be solid at room temperature. Although all the even diacids formed crystalline products, SbA formed micro-crystals which could not be analysed by SXRD or synchrotron radiation due to their small size and poor quality and instead they were assessed using PXRD. This gave a weak powder pattern that did not fit the SbA pattern, suggesting that a binary product may have formed. This is confirmed by the melting events of the SbA-Mo combination seen using HSM. Two melting events occur, one at 93.1-96.6°C and another at 130.6°C. The first event may be a binary compound as the temperature is much lower than the melting point of SbA and higher than that of Mo. The second event could be the melting of some SbA that has been left over from forming the binary compound. This would also be in keeping with the formation of a 1:2 acid:base structure as seen with the other even diacids.

The even diacid OxA, ScA, AdA and FmA combinations all formed similar crystal structures, with a 1:2 acid:base ratio and the consequential bilayer arrangement of the molecules. Indeed, the ScA and FmA salts are isostructural; there are small changes in the hydrogen bonding distances but the presence of the double bond does not significantly affect the structure. The double deprotonation of

the acids is a consequence of the  $pK_a$  value (Appendix Table A2); the  $pK_a$  difference is greater than 2.9 units for both the first and second ionisation of the acid molecule therefore it can be expected that the proton will have transferred. (The smallest difference is for the second ionisation of MeA, however this diacid reacted with the base and solvent.) DLTA, however, is only mono-deprotonated – the  $pK_a$  values for this diacid suggest that double deprotonation is possible, however in this case, the strong carboxyl-carboxylate hydrogen bond is preferred in order to form anion chains. The N-H...O hydrogen bond is not as strong and hence does not form preferentially over the O-H...O interaction. This is further supported by the crystal structure being obtained from a crystallisation procedure that contained excess base.

The melting points and packing indexes of each of the structures are shown in Table 6.5.7. The melting points for the simple diacid structures are quite similar showing that they are of a comparable stability. The packing index for the OxA-Mo structure is the lowest – probably due to the small size of the anion being difficult for the larger cation to pack around. However, the melting point is as high as the other structures that have a higher packing index and would theoretically be more stable. The hydrogen bond interactions in the OxA-Mo structure are more numerous than in the other structures due to the small size of the anion. This would further stabilise the structure in spite of the packing index and density.

diacid	Stoichiometry Acid:base	Structure type	Melting point/ °C	Packing index/ %	Density/ g cm <sup>-3</sup>
OxA	1:2	Sheet	137.64	67.7	1.31
ScA	1:2	Sheet	143.91	74.1	1.39
AdA	1:2	tape	135.57	71.6	1.31
SbA	-	-	93.1-96.6,130.6	-	
DLTA	1:1 +water	3-D	86.5-97.3	72.6	1.49
FmA	1:2	sheet	138.1-143.8	72.1	1.37

**Table 6.5.7** Some of the structure properties for each of the salt structures and the possible binary product with SbA.

The ScA structure has the highest packing index and also the highest melting point. This may be due to the similar relative size of the anions and cations allowing close packing, and the close proximity of potential hydrogen bonding groups. The FmA salt is isostructural with the ScA salt, however the packing index is lower and the melting point is slightly lower. This must be due to the presence of the alkene double bond in FmA instead of the alkyl group. The melting point for DLTA-Mo is lower than expected for the TAs, this may be due to water molecules being present in the structure.

The change in structure type from OxA and ScA to AdA is probably due to the sheet structure becoming less stable as the acid chain length is increased past an optimum of 4 carbons. The

orientation of the base molecules differs slightly in the OxA and ScA to accommodate the different carbon chain lengths. The orientation of the base in the AdA structure leaves the nitrogen in the optimal position for hydrogen bonding within one tape, rotating the molecule would result in weaker hydrogen bonds between all of the chains. The arrangement of the tapes in the AdA structure enables a number of C-H...O hydrogen bonds, which although weaker than the N-H...O hydrogen bonds, will contribute to the stability of the 3-D network they create.

The fingerprint plots for the Mo cations are all quite similar showing the interactions are similar within the group. The DLTA plot has additional feature as the oxygen acts as a stronger hydrogen bond acceptor in this structure.

## 6.6 DISCUSSION OF NITROGEN-CONTAINING HETEROCYCLES

The results from this group have shown that the crystal structures and properties of the starting materials affect not only whether a solid product forms, but also the supramolecular structure created and the melting point.

It is interesting that even though Pyr, Idn and DMIdn are so similar in structure, the small differences in their structures are crucial when forming binary compounds. The methylation of the nitrogens in DMIdn prevented the formation of any binary compounds in this acid series. The presence of only one nitrogen in Pyr also resulted in fewer binary products due to the difficulties in forming infinite structures with only one amide group. In fact the structures formed by ScA and FmA leave one oxygen on each of the carboxyl groups unable to participate in N-H...O hydrogen bonding, and instead it only participates in a weak C-H...O hydrogen bond. Idn has two available nitrogens and therefore can form a number of supramolecular arrangements with a range of stoichiometries.

In the even diacid structures, the carboxyl-amide interaction is dominant whereas in the MnA-Idn structure the amide-amide interaction is also important. Head-to-tail hydrogen bonded acid/anion chains are found in none of the structures. This is unexpected as O-H...O hydrogen bonds are stronger than N-H...O hydrogen bonds. This can be seen in Figure 6.6.1 where the acid-base and acid-acid hydrogen bonds generally have shorter  $D\cdots A$  distances and  $DHA$  angles closer to  $180^\circ$  than the base-base and base-acid hydrogen bonds.

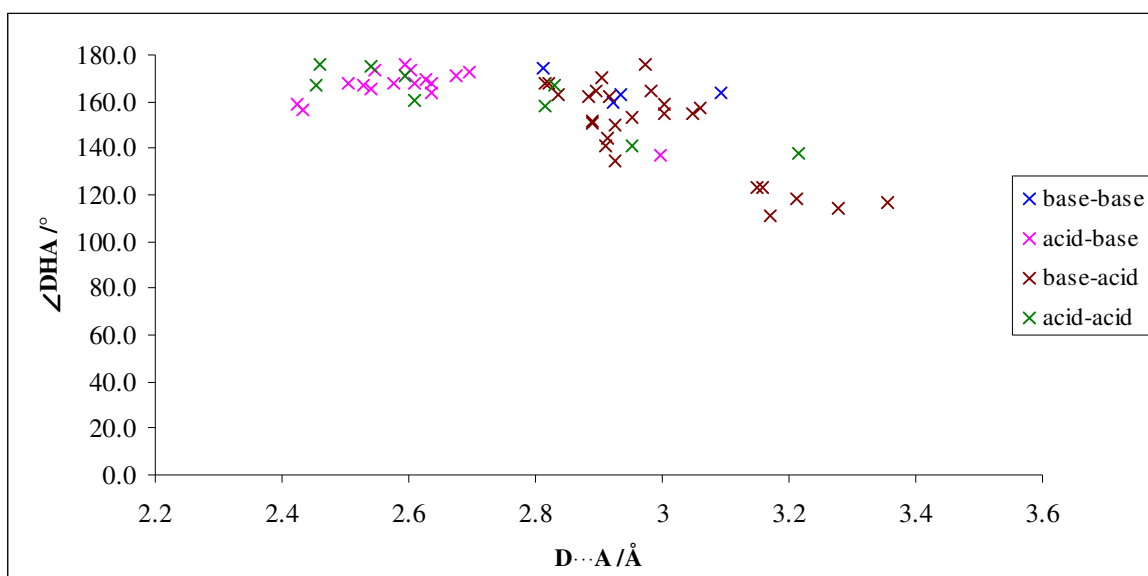


**Figure 6.6.1** Graph to show distance and angle between donor and acceptor of base-base, acid-base, base-acid and acid-acid hydrogen bonds in Pyr and Idn structures.

Four of the weakest base-acid hydrogen bonds are from the even diacid-Idn structures and, together with the strongest hydrogen bonds, they act to hold the adjacent base-acid-base units together in a sheet. The remaining two weakest base-acid hydrogen bonds are from the MeA-Idn structure and are the weaker part of a bifurcated hydrogen bond linking the base to each of the oxygen atoms of a carboxylate group. The surprisingly weak acid-acid hydrogen bond is between a disordered hydroxyl and carboxyl group on adjacent LTA anions and is also part of a stronger bifurcated hydrogen bond. It is interesting that the hydrogen bonds are split into three sections rather than evenly distributed across the range.

The  $pK_a$  differences in water were useful for the Mo structures, however, appear to be irrelevant in the formation of binary compounds with amides. The large  $pK_a$  values for Pyr and Idn suggest they will be protonated easily, however, this has not been the case. In a review of amide chemistry Horner and Johnson<sup>5</sup> note that the amide group is readily protonated in strong acidic solutions; obviously the diacid solutions are not sufficiently acidic. Although the stoichiometry of the Mo salts can mainly be predicted from the  $pK_a$  differences, DLTA forms a 1:1 acid-base structure highlighting that preferred hydrogen bond patterns of the components appear to take precedence over deprotonation and hence stoichiometric effects.

**References**

1. C. K. Johnson, ORTEP, C. K. Johnson, Report ORNL-3794, Oak Ridge National Laboratory, Tennessee, USA, 1965.
2. R. I. Cooper, R. O. Gould, S. Parsons, D. J. Watkin, *J. Appl. Cryst.*, 2002, **35**, 168-174.
3. P. D. Godfrey, M. J. Mirabella, R. D. Brown, *J. Phys. Chem. A*, 2000, **104**, 258-264.
4. P. Vishweshwar, A. Nangia, V. M. Lynch, *Cryst. Growth Des.*, 2008, **3**, 783-790.
5. R. B. Horner, C. D. Johnson, in *The Chemistry of Amides*; J. Zabicky (Ed.), Interscience: London, 1970, 187.

## CHAPTER 7

### Results and Discussion – Aromatic Amines

#### 7.1 INTRODUCTION

In this chapter the products from the various crystallisation procedures of the acid-base combinations containing the imidazole derivatives are described and discussed. The well-plate observations and the type of characterisation performed for the products of this chapter are summarised in Table 7.1.

	Imidazole (Im)	1-Methyl-imidazole (1MI)	2-Methyl-imidazole (2MI)	4-Methyl-imidazole (4MI)	1,2-Dimethyl-imidazole (DMI)
OxA	MEQPAZ	Laths SXR	Small blocks SXR	Blocks SXR	Oil
MnA	UMURAV/ VARHOM	Oil	Oil*	Oil*	Oil
ScA	MEQPON	Blocks SXR	Laths SXR	Small blocks SXR	Blocks SXR
GlA	Poor micro crystals	Laths SXR	Laths SXR	Laths SXR	Blocks SXR
AdA	MEQQEE	Powder	Micro crystals Synchrotron	Oil	Oil
PmA	Oil	Oil	Oil	Oil	Oil
SbA	Blocks SXR	Powder	Fragments SXR	Shards SXR	Oil
LTA	HAZHEV	ZAMXIU	ZELRIR	Micro crystals Synchrotron	Large laths SXR
DLTA	Blocks SXR	Small blocks SXR	Laths SXR	Blocks SXR	Blocks SXR
MeA	IMZMAL	Micro crystals Synchrotron	Powder	Oil*	Oil
FmA	MEQPED	Powder	Plates SXR	Powder	Thin small plates SXR

**Table 7.1** Observations of the well-plate products for the acid-base combinations containing Im derivative bases and their appropriate method of analysis.

Where a CSD reference code is given in Table 7.1, the crystallographic data for the compound was obtained from the CSD. Any further information about the compound was gathered from the literature. Unless stated it should be assumed that the crystallisation procedure used was Method 1, or Method 2 for the TAs. Further crystallisation experiments, using Method 3, were performed for the acid-base combinations that produced oils; these again resulted in oils except for 2MI-MnA and 4MI-MeA (marked \* ) which gave crystals suitable for analysis by SXRD. MnA-4MI produced small crystals that were badly split and unsuitable for SXRD. These and the powder products were analysed on a small scale by PXRD to ascertain if the product was either of the starting materials.

In the following sections the outcomes of each of the XRD studies will be discussed along with the thermal analysis results. Unless stated, the transferable hydrogen atom positions were found in the electron density difference map, and their correct assignment was confirmed not only by the difference between the C-O and C=O bond lengths, but also by moving them to their alternative possible position and seeing where the hydrogen atom refined to. The Ortep<sup>1</sup> diagrams for each of the structures display the molecules present in the asymmetric unit, the numbering scheme and 50% probability displacement ellipsoids; hydrogen atoms are shown as spheres.

The cell dimensions for each of the products are listed in Appendix, Table A5. For reference, the types of binary compounds formed and some of their properties are displayed in Appendix, Tables A3 and A6 respectively. The crystal structure data is available on the Appendix CD.

## 7.2 IMIDAZOLE

### 7.2.1 Oxalic Acid and Imidazole (MEQPAZ)

This structure was obtained by MacDonald *et al.*<sup>2</sup>; crystals were prepared through the slow evaporation of an equimolar acid-base solution (2:1 ethanol/water). The components crystallised in a 1:1 ratio to form a salt in the monoclinic space group  $P2_1/n$ , with  $Z = 4$ . The structure consists of chains of alternate monoanions and cations hydrogen bonded together; each of the hydrogen bond donors on the cations is bifurcated. Further hydrogen bonding between the anions links the chains to form sheets; the hydrogen bond distances are given in Figure 7.2.1.1.



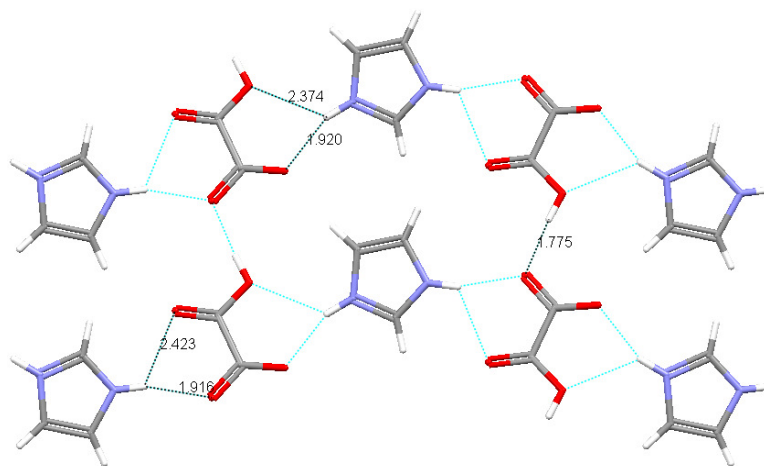


**Figure 7.2.1.1** The hydrogen bonded sheets of OxA-Im, viewed down the *c*-axis.

The sheets are arranged so as the cations are positioned on top of each other in an offset manner to form a stack with the positively charged nitrogen and its hydrogen positioned over the inside of the ring of the adjacent cation (N-H...centroid 3.319 Å). The presence of  $\pi$ - $\pi$  interactions is also confirmed on the fingerprint plot (Appendix, Figure A11.1). Weak C-H...O hydrogen bonds further stabilise the sheet structure (2.419 and 2.507 Å) and also link adjacent sheets (2.628 Å).

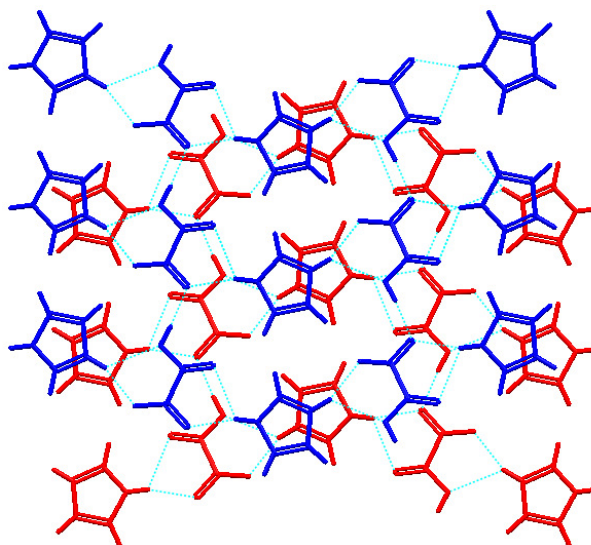


**Figure 7.2.1.2** Stacking of the sheets with each sheet coloured alternately red and blue for clarity.

When the sheets are viewed side-on it can be seen that they are slightly undulating with the cations tilted slightly with respect to the plane of the anions:

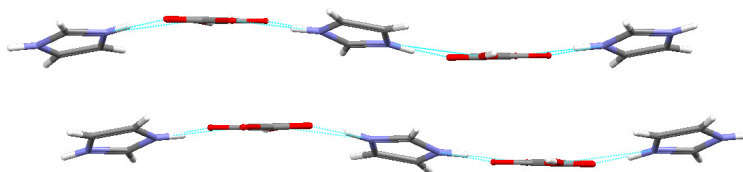


**Figure 7.2.1.3** Undulation of the sheets with cations slightly protruding above and below the plane of the anions.

### 7.2.2 Malonic Acid and Imidazole

Crystals of this structure were first obtained by Pogorzelec *et al.*<sup>3</sup> (UMURAV); a later characterisation by Trivedi *et al.*<sup>4</sup> (VARHOM) was found to have similar cell dimensions (Appendix, Table A5). Comparison of the two structures shows that the supramolecular structure is the same and indeed the two crystal structures can be overlaid exactly except that the water molecules in VARHOM are in the position of the disordered Im in UMURAV. This coincidence causes some concern as the oxygen atoms of the water molecules are in the same position as the nitrogen atoms of the disordered base, and the disordered oxygen atoms (again of VARHOM) are in the positions of two of the carbons of the Im ring in UMURAV. Although the positions of disordered water molecules in this way are possible, the coincidence suggests the structures are the same and one has been poorly determined. The R-factors for the structures are 10.53% for VARHOM and 4.07% for UMURAV suggesting that the data for VARHOM may be poor resulting in some electron density peaks being missed. Trivedi *et al.* note that the extra electron density found around a centre of symmetry was assigned as disordered oxygen atoms that must have come from the solvent. One of the acidic hydrogens could also not be located in VARHOM further making the structure incomplete.

There is a small concern about both of the structures, however, in that a base molecule in a position with strong hydrogen bonds to a carboxylate group is unlikely to be disordered. To really understand this structure the combination should be re-crystallised and the data re-collected, however this was not possible due to time constraints. Instead the data from the literature will have to be used to assess the structure. Although the two structures overlay and therefore the contact distances will be very similar, the geometries of the interactions will be obtained from the UMURAV structure as it appears to be more complete. Due to the way in which Mercury<sup>5</sup> displays disorder (by only showing one example disordered molecule), the VARHOM structure will be used in the diagrams as the position of the non-disordered water molecules are shown. These will symbolise the position of the disordered base as they are equivalent to the nitrogen atoms in the Im ring.

The components were found to have crystallised in the triclinic space group *P*-1, with *Z* = 2, to form a salt. The stoichiometry of the components is unclear due to the disordered Im, which also complicates the deprotonation – only two of the transferable hydrogens are accounted for in the structure.

The structure consists of catemeric hydrogen bonded chains involving one of the anion carboxylate groups and the cation. The other end of the anion is involved in a hydrogen bond to an adjacent catemeric chain in the same manner thus creating a ribbon (Figure 7.2.2.1).

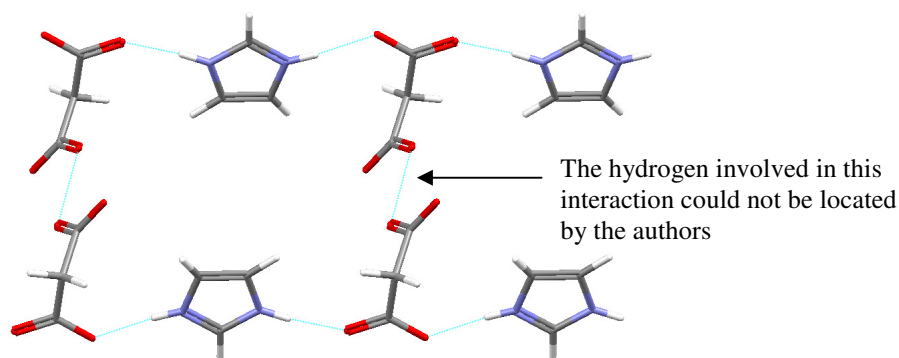


**Figure 7.2.2.1** Ribbon structure, hydrogen bond distances N-H...O = 1.710 and 1.706 Å.

The adjacent ribbons are linked by hydrogen bonding across the disordered Im cation to create a stepped sheet (1.763 and 1.931 Å). There are also weak C-H...O hydrogen bonds from each of the CH groups in the cation ring (including the disordered cation) and the anion carboxylate groups which create a 3-D network (range 2.403-2.597 Å).

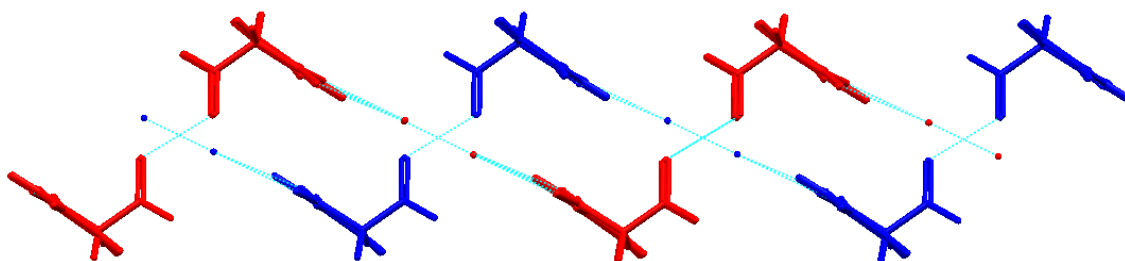


**Figure 7.2.2.2** Stepped sheets viewed from the side (ribbons are viewed end-on and extend into the plane of the page); one sheet is coloured red and the other blue to show their interpenetration.

### 7.2.3 Succinic Acid and Imidazole (MEQPON)

This structure was characterised by MacDonald *et al.*<sup>2</sup>; crystals were prepared by slow evaporation of an equimolar acid-base solution (1:1 methanol/acetonitrile). This crystallised in a 1:1 acid base ratio to form a salt in the triclinic space group *P*-1, with *Z* = 2. The structure consists of hydrogen bonded chains of monoanions but, unusually, they adopt the *anti-anti* conformation. The *syn* positions on the carboxyl and carboxylate groups are then left free for bifurcated hydrogen bonding with the cation. The cations thereby act to link the anion chains to form a 2-D sheet (Figure 7.2.3.1).

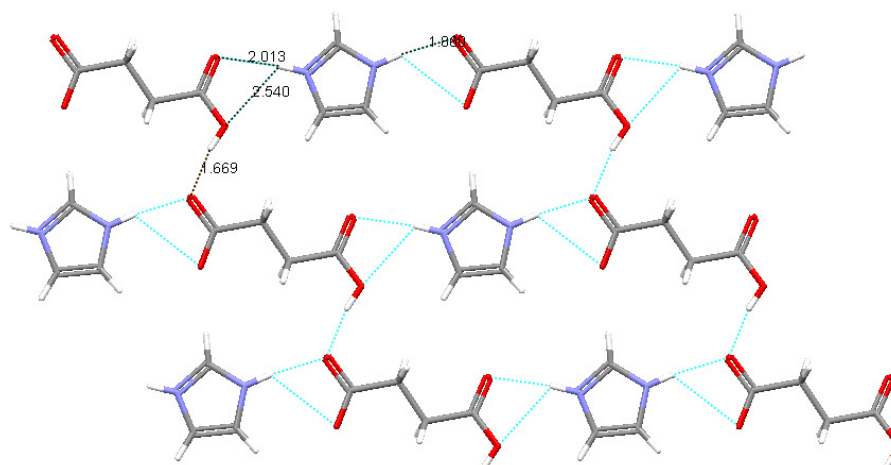


**Figure 7.2.3.1** Sheet structure with cations linking chains of anions.

There are also weak C-H...O hydrogen bonds between the cations and anions which further stabilise the sheet structure (2.153, 2.599 and 2.640 Å). The sheets are stacked on top of each other so as the cations are positioned over the hydroxyl part of the anion carboxyl groups.

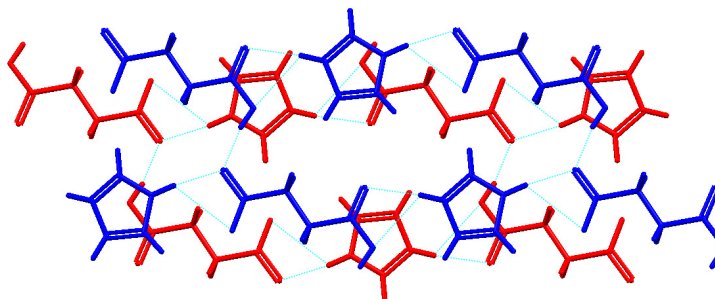


**Figure 7.2.3.2** Stacking of sheets – the central sheet is coloured red and the sheets above and below are blue.

#### 7.2.4 Adipic Acid and Imidazole (MEQQEE)

This structure was also characterised by MacDonald *et al.*<sup>2</sup> and prepared by slow evaporation of an equimolar acid-base solution in methanol. The components crystallised in a 1:1 acid-base ratio in the orthorhombic space group  $Pna2_1$ , with  $Z = 8$ , to form a salt. The structure consists of monoanions hydrogen bonded head-to-tail in the *syn-syn* arrangement to form chains; cations bridge the adjacent chains via hydrogen bonds to form a sheet (Figure 7.2.4.1).

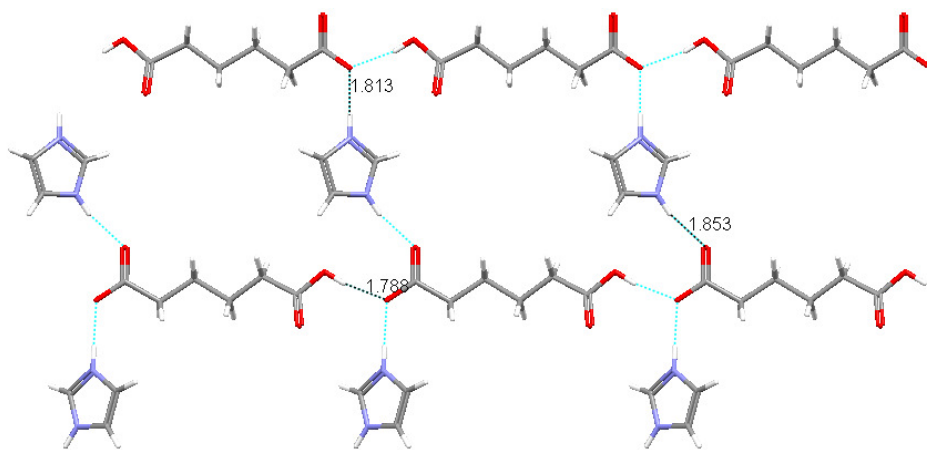


**Figure 7.2.4.1** Sheet structure of AdA-Im with hydrogen bond distances marked, viewed down the *c*-axis.

When the sheets are viewed down the *a*-axis it can be seen that the cations protrude above the plane of the anion chains (Figure 7.2.4.2). The sheets are arranged in pairs with the anion chains in the centre of each pair; adjacent pairs are translated half a unit along the *b*-axis so as the protruding cations are between those of the adjacent pair.

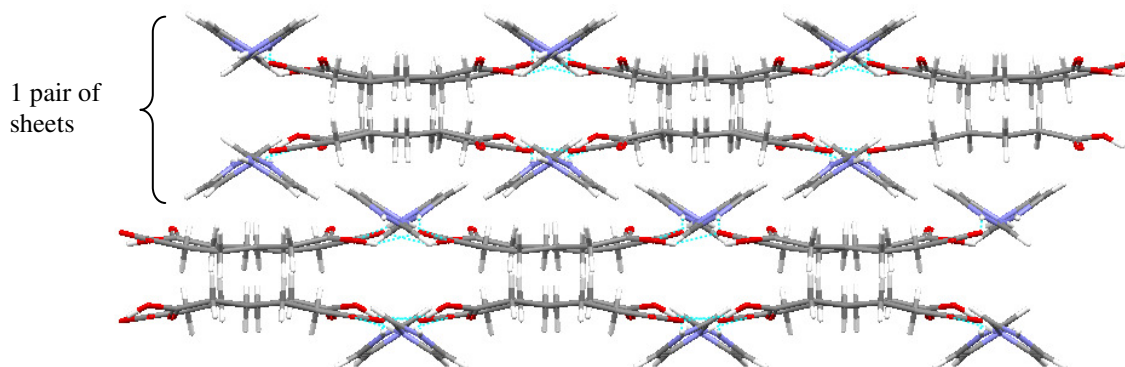


**Figure 7.2.4.2** Arrangement of sheets into pairs, viewed down the *a*-axis.

Within a pair of sheets, the sheets are further offset half a unit along the *a*-axis so as the anion chains are above and below the cations within the pair (Figure 7.2.4.3). There does not appear to be any  $\pi$ -interactions between the molecules, however, there are weak C-H $\cdots$ O hydrogen bonds between adjacent pairs of sheets and also further stabilising the sheets (2.476, 2.540, 2.322, 2.602 and 2.691 Å).

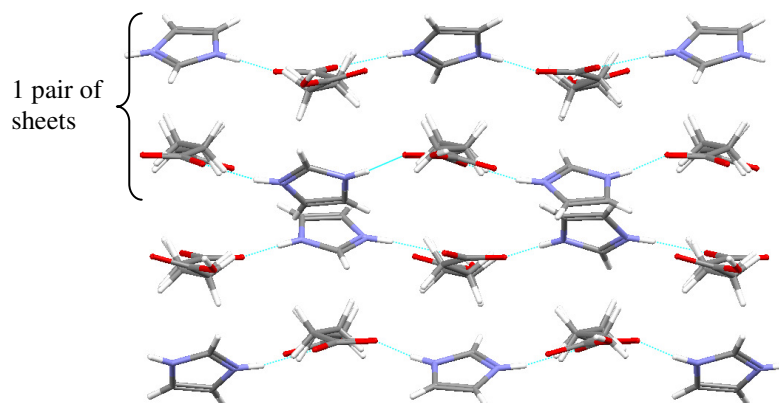


**Figure 7.2.4.3** Arrangement of sheets, viewed down the *b*-axis.

### 7.2.5 Suberic Acid and Imidazole

These components crystallised in the triclinic space group *P*-1, with *Z* = 2, with a 3:2 acid:base ratio. A mixed system was found to have formed with single proton transfer having occurred in two of the acid-base units, however there is also another acid molecule present which has not been deprotonated (Figure 7.2.5.1).

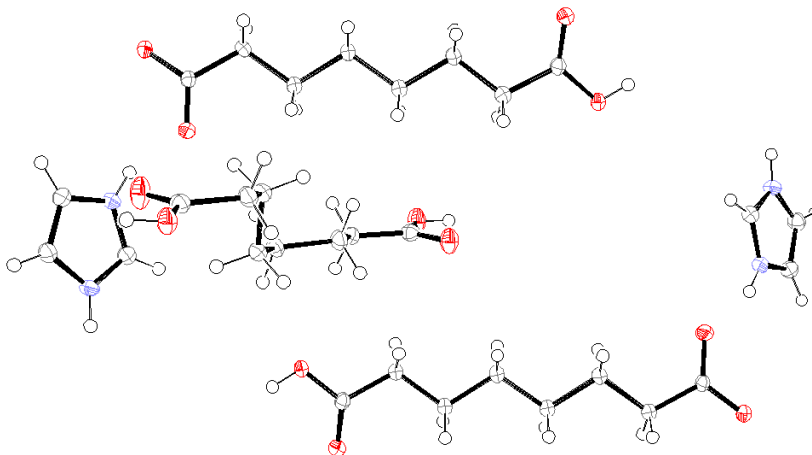


**Figure 7.2.5.1** Ortep diagram for the asymmetric unit of SbA and Im.

The monoanions are connected head-to-tail via hydrogen bonding in the *syn-syn* conformation to form infinite planar chains; the hydrogen bond distances are depicted in Figure 7.2.5.2. Adjacent anion chains are linked by hydrogen bonding across the cations to form an infinite sheet.

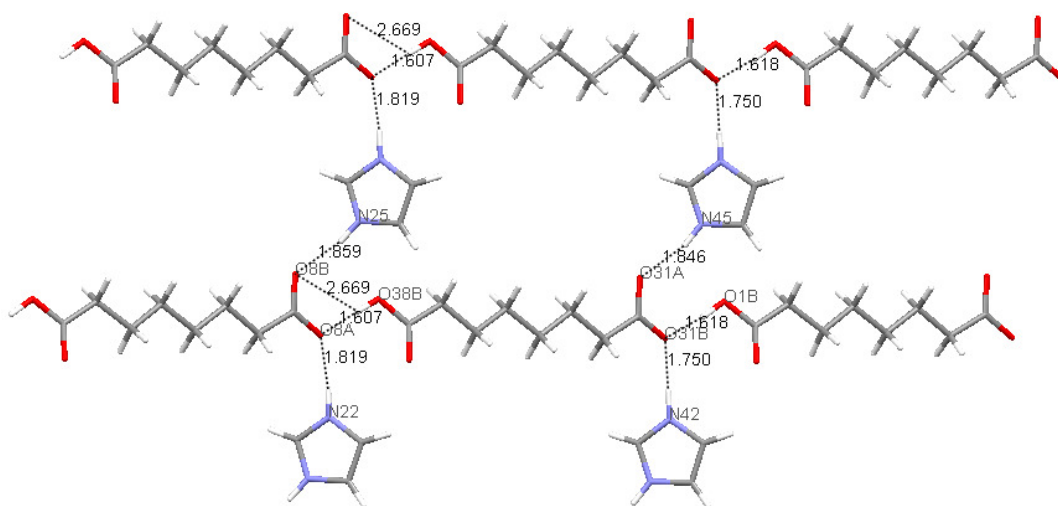


**Figure 7.2.5.2** The hydrogen bonded sheets of SbA-Im consisting of anion chains linked by cations (hydrogen bond distance error  $\pm 0.002$  Å).

There are two sets of hydrogen bonding interactions as there are two sets of acid-base units in the unit cell that are not related by symmetry. When the sheets are viewed side-on it can be seen that they are stacked in a slightly offset manner so as the anions are not directly over each other (Figure 7.2.5.3). A similar translation is not present along the *a*-axis. The cation rings are also positioned at

an angle to the plane of the sheets. The adjacent sheets are arranged in pairs where the cations protrude towards the centre of the pair. There are also weak C-H...O hydrogen bonds between cations and anions, further strengthening the sheet structure (2.390, 2.383, 2.465 and 2.399 Å).

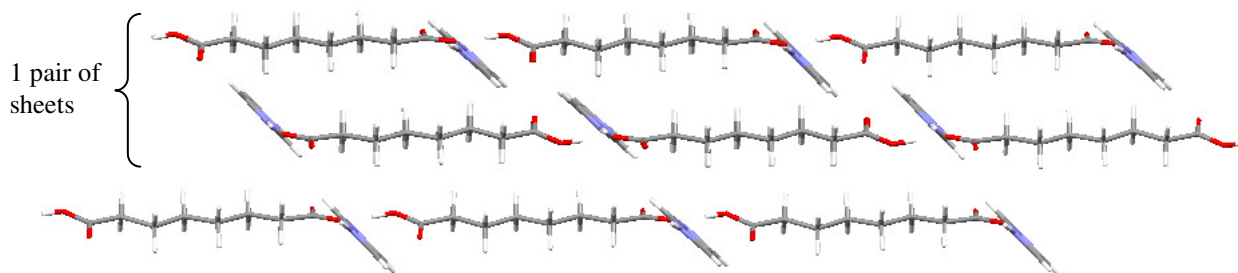


**Figure 7.2.5.3** Arrangement of the sheets leads to the anion chains being stacked but with the molecules slightly offset along their length, viewed down the *a*-axis.

There is also another chain present in the structure made up of neutral SbA molecules which are hydrogen bonded together head-to-tail in the *syn-syn* conformation. The acid molecules are bent with the alkyl chain adopting a *gauche* conformation across carbons C54-C55 and C56-C57 (torsion angles 72.1(2)° and -75.2(2)° respectively).

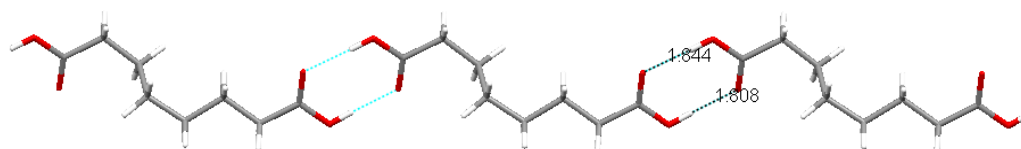


**Figure 7.2.5.4** Second type of chain present in the structure (hydrogen bond distance error +/-0.002 Å).

As these acid molecules are bent, the 1-D chain stepped and hence can fit into the aforementioned sheets through the gaps between the cations (Figure 7.2.5.5). They are linked to the sheets by weak C-H...O hydrogen bonds from the cations (2.707 Å). The bent acid chains are shown in red and the anion-cation sheets are shown in grey for clarity:

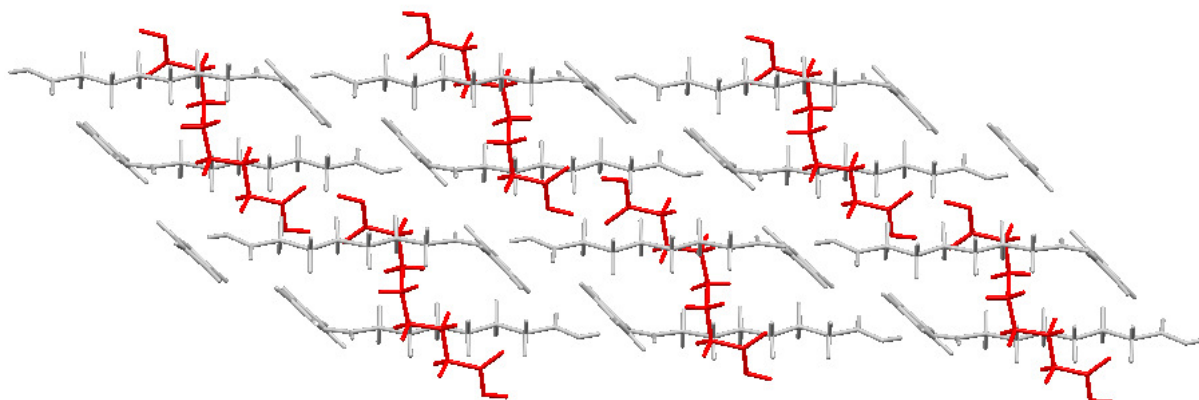


**Figure 7.2.5.5** The arrangement of the stepped SbA chain and the anion-cation sheets.



### 7.2.6 *L*-Tartaric Acid and Imidazole (HAZHEV)

This structure was characterised by Aakeröy *et al.*<sup>6</sup> in a study into the hydrogen bonded layers of hydrogentartrate anions; crystals were prepared by warming an equimolar aqueous solution of the two components. This crystallised in a 1:1 acid-base ratio in the monoclinic space group  $P2_1$ , with  $Z = 2$ , to form a salt that is isostructural with the DTA analogue<sup>7</sup> (ZELQUC). Aakeröy notes that the cation and monoanion ‘do not exhibit any unusual features with the anion displaying the expected zigzag configuration (C-C-C-C torsion angle  $\sim 180^\circ$ ).’ The monoanions are hydrogen bonded head-to-tail (1.387 and 2.506 Å) to form an infinite chain along the  $a$ -axis. Adjacent chains are then linked along the  $ab$ -plane via further hydrogen bonding involving the anion hydroxyl groups (2.468 and 2.289 Å) to create an infinite 2-D sheet. The base molecules are then subtended from this sheet structure via hydrogen bonds (1.806 and 1.978 Å) (Figure 7.2.6.2).

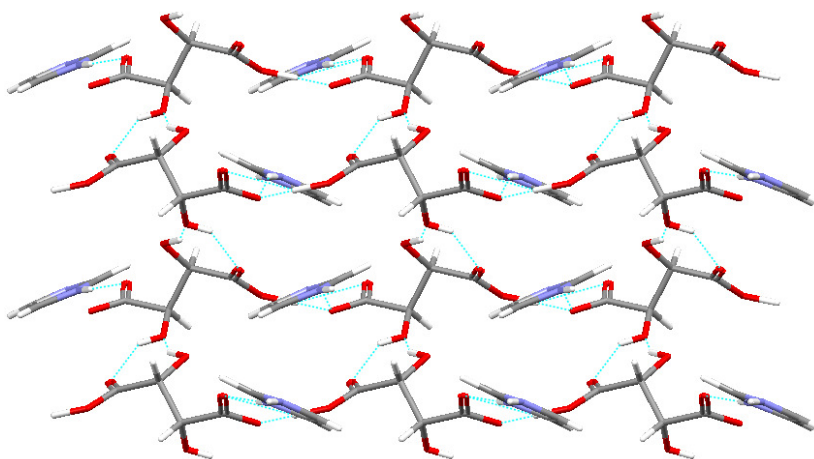


**Figure 7.2.6.1** The 2-D anion network that creates a sheet with cations subtended; strong hydrogen bonds occur between the chains of anions running from left to right across the page; viewed down the  $c$ -axis.

As the cations have two hydrogen bond donor sites they act as bridges connecting adjacent sheets, thus creating an infinite 3-D network (Figure 7.2.6.3). The authors note that ‘although it is impossible to predict *a priori* the exact arrangement of the cations within this salt, their spatial freedom has been severely restricted by the presence and geometry of the anionic sheets, thereby locking them into the structural framework in the anticipated fashion.’ It should also be noted that there are no  $\pi$ -interactions between the cations, however, there are a number of weak C-H $\cdots$ O hydrogen bonds between cations and anions (range 2.285-2.666 Å), and anions (2.686 Å).



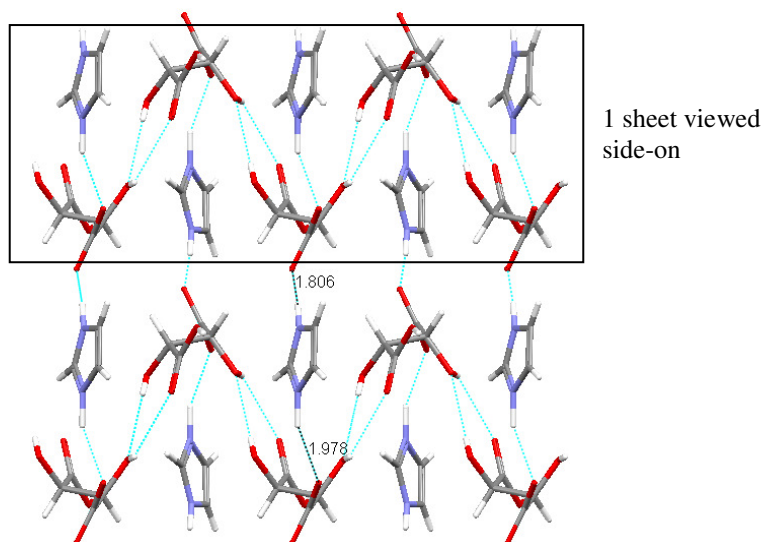


**Figure 7.2.6.2** 3-D network created as sheets are linked via hydrogen bonding across the cations, hydrogen bond distances shown; viewed down the *a*-axis.

### 7.2.7 *DL-Tartaric Acid and Imidazole*

These components crystallised in a 1:1 ratio in the monoclinic space group *C2/c*, with *Z* = 8, to form a salt. The cation was found to be disordered across two positions – this can be seen in Figure 7.2.7.1. The cation is in position *a* 45.5% of the time and is in position *b* for the rest. In the following diagrams only the dominant position of the cation is shown. Due to the disorder there were some problems in solving and refining the structure and the R-factor remained quite high (9.34%). In spite of this, all the hydrogens were found and their positions checked. There is also disorder across the acidic hydrogens, with a half occupancy hydrogen found on each carboxyl group, hence forming a monoanion.

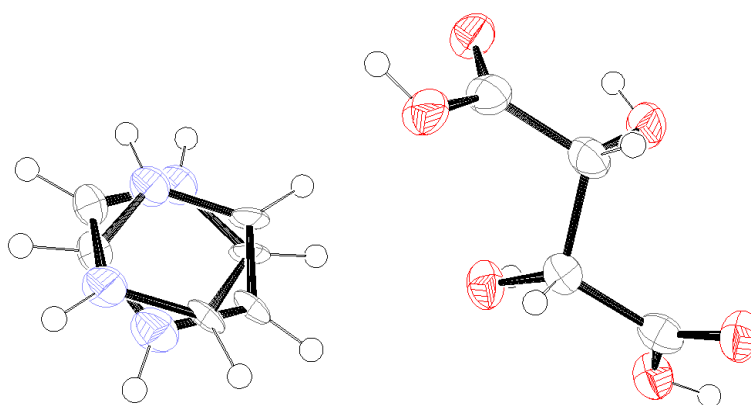


**Figure 7.2.7.1** Ortep diagram for the asymmetric unit of DLTA and Im.

The anions are hydrogen bonded head-to-tail to form infinite 1-D chains which are further linked to adjacent chains by hydrogen bonding between the carboxyl and hydroxyl groups of the anions (Figure 7.2.7.2). This forms a 2-D sheet from which the cations are subtended. The sheet is actually

a 3-D network as the hydrogen bonds involving the hydroxyl groups are between anions in different planes (1.92(1) and 2.37(1) Å).

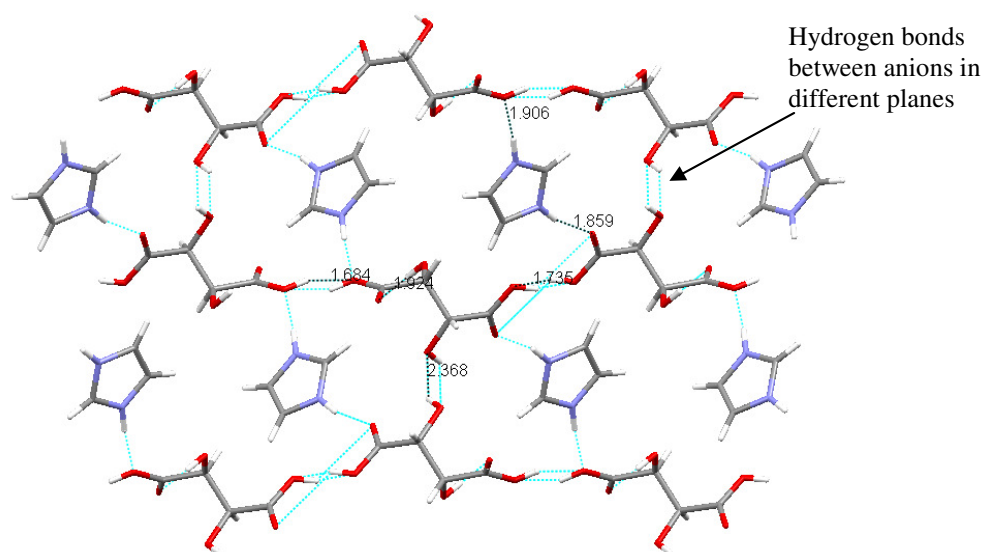


**Figure 7.2.7.2** Hydrogen bonded anion network (O-H...O error  $\pm 0.007$  Å, N-H...O error  $\pm 0.016$  Å); the N-H...O hydrogen bond distances for the *b* position of the cation are 2.00(2), 2.15(2) and 2.31(2) Å.

The chains of adjacent sheets are at a 20° angle to each other; this is shown in Figure 7.2.7.3 where the central sheet is coloured red and the sheets above and below are coloured blue. As the cations bridge the sheets they have not been coloured. There are also weak C-H...O hydrogen bonds between the cations and anions which further stabilise the structure (range 2.294-2.638 Å across both of the cation positions).

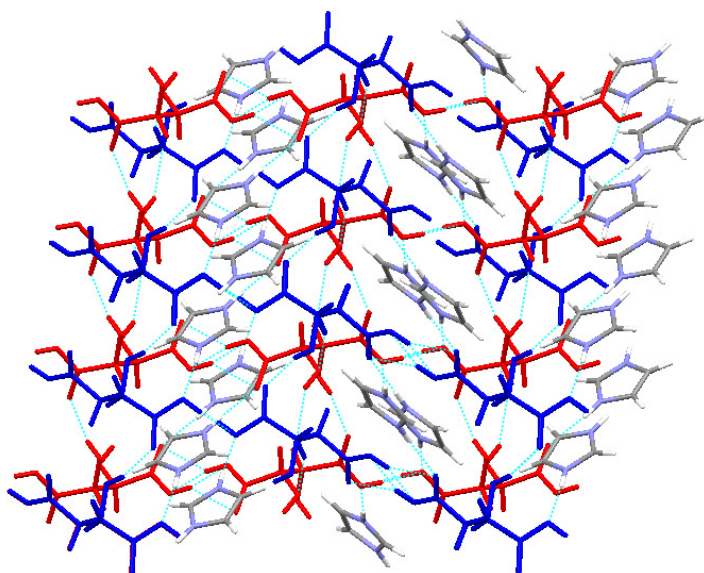


**Figure 7.2.7.3** Different directions of the chains of adjacent sheets.

### 7.2.8 Maleic Acid and Imidazole (IMZMAL10)

These components were first reported crystallised together in 1976 by James *et al.*<sup>8</sup> who prepared the binary product by slow evaporation of an equimolar acid-base solution in methanol. The components crystallised in a 1:1 acid-base ratio in the monoclinic space group  $P2_1/c$ , with  $Z = 4$ , to form a salt. The structure consists of acid-base quadruplets containing two monoanions and two cations which are related by inversion symmetry (Figure 7.2.8.1). The *cis* conformation of the anion and the position of the hydrogen bond donors on the cation enable this unit to form. The *cis* conformation of the anion also results in a strong intramolecular hydrogen bond between the carboxyl and carboxylate groups. When viewed side-on it can be seen that the unit is not planar (Figure 7.2.8.2); the anions are tilted above and below the plane of the cations. Bifurcated hydrogen bonding from each of the hydrogen bond donors links the molecules together.

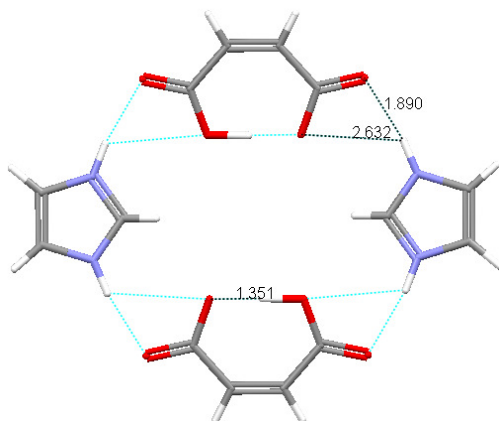


**Figure 7.2.8.1** MeA-Im quadruplet,  
hydrogen bond distances marked.

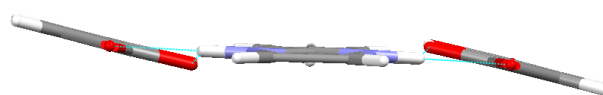


**Figure 7.2.8.2** Tilted arrangement of the acid molecules  
in the quadruplet.

The arrangement of the cations allows weak  $C-H\cdots\pi$  interactions between pairs of cations in the edge-face conformation ( $d(H\cdots\text{centroid}) = 3.037 \text{ \AA}$ ,  $D(C-H\cdots\text{centroid}) = 3.771 \text{ \AA}$ ). This arrangement is not classical as the angle between the cations is  $136.23^\circ$  instead of  $180^\circ$  and the CH donor does not point to middle of ring. The presence of the interaction, however, is supported by the ‘wing’ features in the fingerprint plot (Appendix, Table A11.1). This leads to layers being formed where the quadruplets are stacked on top of each other at an angle to form columns. Adjacent columns are stacked at  $70^\circ$  to each other and the units within the column are offset:

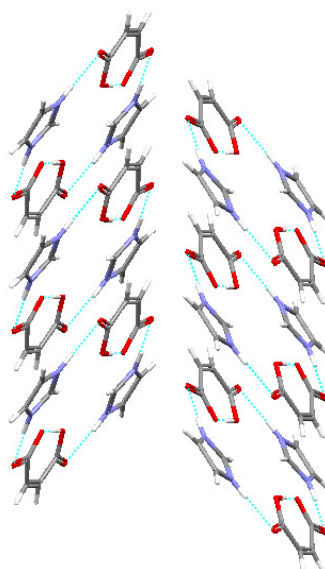


**Figure 7.2.8.3** Arrangement of quadruplets, viewed down the *a*-axis.

### 7.2.9 Fumaric Acid and Imidazole (MEQPED)

This structure was characterised by MacDonald *et al.*<sup>2</sup> and was produced by slow evaporation of an equimolar solution of the two components in methanol. The resulting binary compound was found to crystallise in a 1:1 ratio in the triclinic space group *P*-1, with *Z* = 2, to form a salt. The structure consists of monoanions hydrogen bonded head-to-tail in the *syn-syn* arrangement to create infinite 1-D chains. Adjacent chains are then bridged by hydrogen bonding across the cation molecules to create an infinite 2-D sheet (Figure 7.2.9.1).

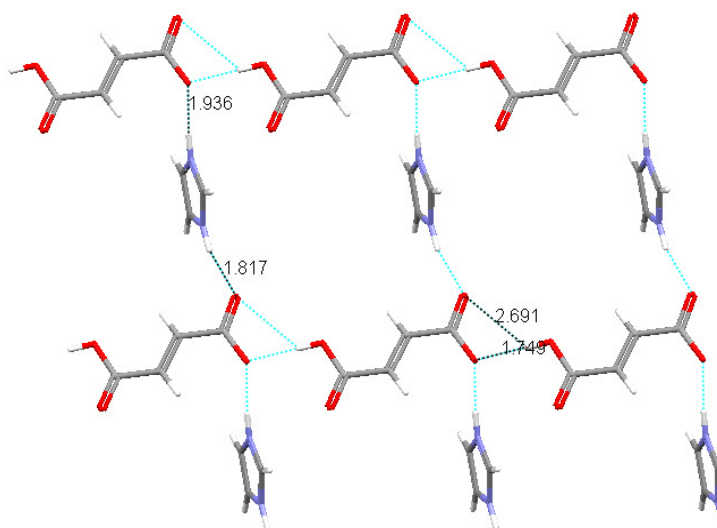


**Figure 7.2.9.1** Hydrogen bonded sheet of FmA-Im.

Adjacent sheets are related through inversion symmetry to give a centric crystal structure and therefore the adjacent sheets form pairs. The cations are stacked on top of each other with part of the ring of each cation overlapping in the column (Figure 7.2.9.2) which, judging from the fingerprint plot for the cation (Appendix, Table A11.1), is likely to be a CH- $\pi$  interaction. CH- $\pi$

interactions also occur between the cation CH and the anion double bond which show as a wing on the fingerprint plots of the ions. There are also anion-anion and cation-anion C-H...O hydrogen bonds which link adjacent sheets (2.704 and, 2.394 and 2.597 Å respectively) and also further stabilise the sheets (2.646 Å).

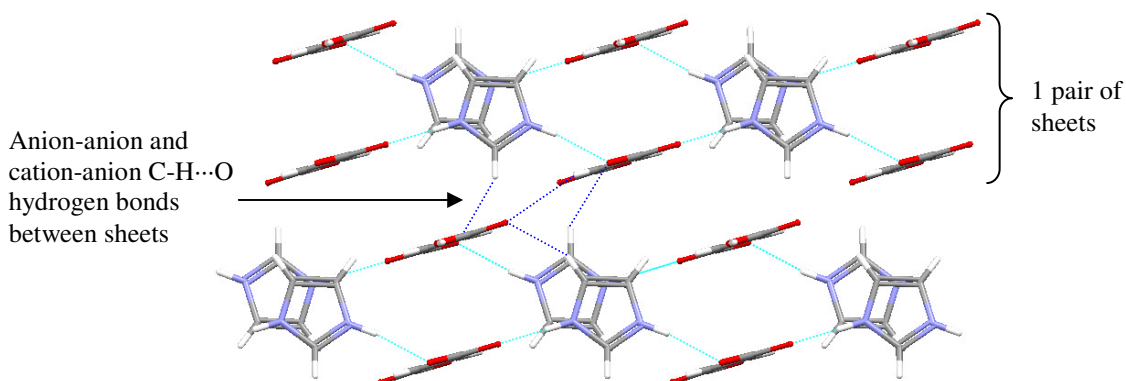


**Figure 7.2.9.2** Sheets viewed side-on, C-H...O hydrogen bonds shown in dark blue, viewed down *a*-axis.

#### 7.2.10 Discussion of Imidazole Structures

GlA-Im is the only combination in the series that a crystal structure was not obtained for, despite a solid product having formed. The resulting very small crystals were of poor quality and unsuitable even for analysis by synchrotron radiation, hence they were analysed by PXRD. This gave such a weak pattern that, although there are some vague similarities with the starting materials, the nature of the product cannot be conclusively determined. DSC analysis showed a melting point of 119.12° which is higher than either of the starting materials suggesting a new binary compound or polymorph may have formed. PmA-Im was the only combination to produce an oil from both crystallisation methods.

All the structures have a 1:1 stoichiometry except SbA-Im as it has an extra acid chain weaving through it, and MnA which ideally should be recollected. All of the diacids also form monoanions which is in keeping with the  $pK_a$  differences (all are greater than two units for the first ionisation).

Four of the above crystal structures were obtained during a study by MacDonald *et al.*<sup>9</sup> in the design of supramolecular layers via the self-assembly of Im and carboxylic acids. In this study it was noted that the OxA and AdA structures formed the same sheet structure (**Sheet 1**) with the anion chains aligned in an anti-parallel arrangement where the carboxyl groups in adjacent chains point in opposite directions as they are related by screw symmetry. The FmA-Im structure formed a sheet structure very similar to this, however, the anion chains are aligned in a parallel arrangement (**Sheet 2**) with the carboxyl groups pointing in the same direction. Hence, the ion pairs in this sheet are related by translational symmetry. These sheet structures are schematically represented in Figure 7.2.10.1.

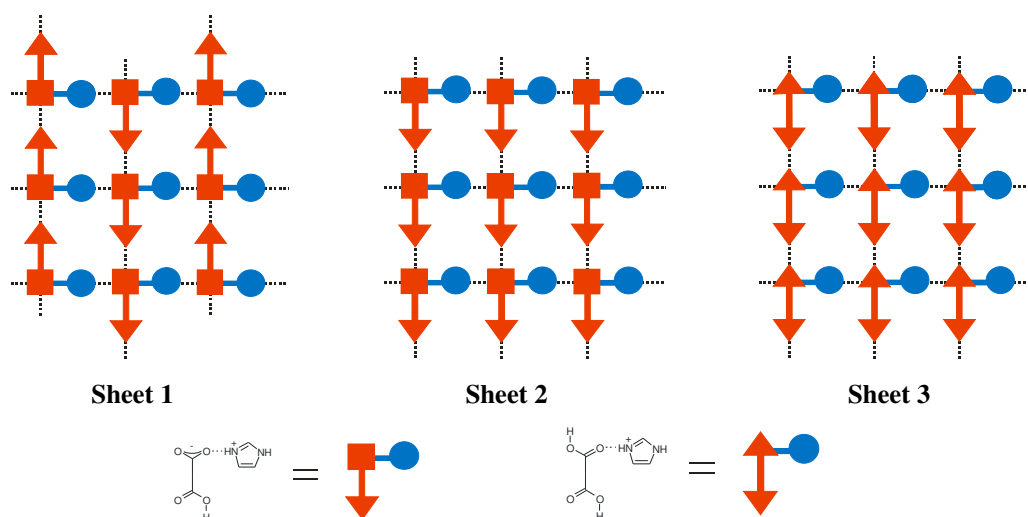


**Figure 7.2.10.1** Schematic representations of the sheet structures of the diacid-Im products.

The ScA-Im structure forms **Sheet 2** however the anions are hydrogen bonded together in the *anti-anti* configuration. This leaves the *syn* position on both the carboxylate and carboxyl groups available for hydrogen bonding to the cation instead of the *anti* position as seen in the other sheet structures. The difference between the carboxylate C-O and C=O bond distances for the ScA-Im structure (0.068 Å) is larger than that for the other sheet structures (range 0.002-0.049 Å) due to the very short hydrogen bond between the carboxyl and carboxylate groups. SbA-Im also forms **Sheet 1** however, due to the longer chain of the diacid, another acid chain can weave through the voids left in the sheet. MnA-Im forms a different structure from the other simple diacids, with the anions hydrogen bonded into dimers, not chains. This structure really needs to be recollected to properly understand what is going on, not only in terms of the nature of the disordered atoms but also to determine the (de)protonation of the components.

The TAs both form 3-D networks and the basis of these networks is similar. DLTA forms a sheet structure that is similar to **Sheet 3** (a combination of Sheets 1 and 2) with the hydrogens shared between the two carboxylate groups in the anion chain. In spite of the double well, strong hydrogen bond suggested by the data, the distance between the oxygen atoms is not particularly small (2.492 and 2.539 Å). Hydrogen bonds between the hydroxyl groups of the anions in adjacent sheets then link the sheets to form a 3-D network. In LTA-Im the head-to-tail anion chains are linked via the cations in a manner that follows the **Sheet 2** arrangement, however, the anion chains are further hydrogen bonded together, thus also creating a 3-D network.

Although the construction of the sheets is similar and the series can be classified into groups, the orientation of the cations changes within the sheet types. OxA-Im forms an undulating sheet with the cations only slightly protruding above and below the plane of the anions, however, in the AdA-Im structure the protrusion of the cations is quite pronounced even though it forms the same type of sheet. This may be to try to compensate for the voids in the structure that are created by the longer

carbon chain of the AdA. The presence of voids in the structure is also highlighted by the diffuse points and bumpy edge at the top right hand side of the fingerprint plots for the ions (Appendix, Table A11.1). The subsequent stacking of sheets is also different for each structure and appears to depend on the orientation of the cations to enable the maximum number of weak interactions such as C-H...O hydrogen bonds and, in some cases,  $\pi$ -interactions.

The density of the crystal structures decreases from OxA-Im to AdA-Im ( $1.61\text{--}1.3\text{ g cm}^{-3}$ ); SbA-Im has slightly higher density than AdA-Im ( $1.34\text{ g cm}^{-3}$ ) due to the interwoven acid chain filling the voids in the sheet (Figure 7.2.10.2). As usual the TAs have high densities with the FmA and MeA structures not far behind ( $1.56, 1.57, 1.426$  and  $1.46\text{ g cm}^{-3}$  respectively). The melting points generally follow this trend, however, SbA-Im has a lower melting point than AdA-Im even though it has a higher density.

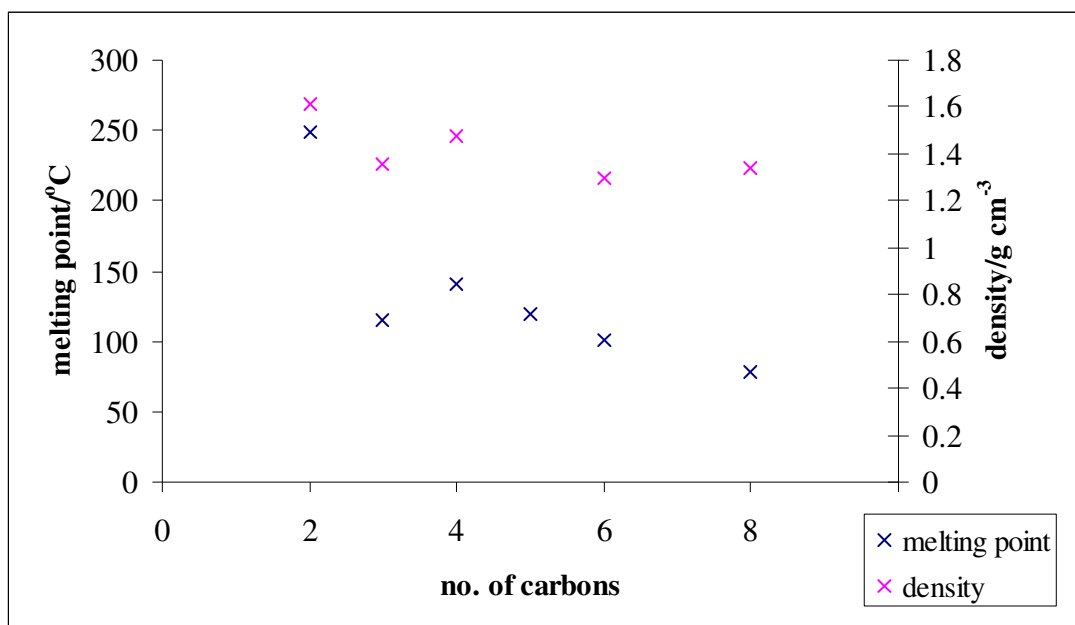


**Figure 7.2.10.2** Graph to show the variation in melting point and density with carbon chain length of the Im products.

### 7.3 1-METHYLIMIDAZOLE

#### 7.3.1 Oxalic Acid and 1-Methylimidazole

Crystallisation of these two components resulted in a binary compound that crystallised in the monoclinic space group  $P2_1/c$ , with  $Z = 4$ , with a 1:1 acid:base ratio. It was found that one of the carboxyl groups of the acid molecule has become methylated by the solvent, however at the other end of the molecule the acidic proton has been transferred to the base thus forming a salt (Figure 7.3.1.1).



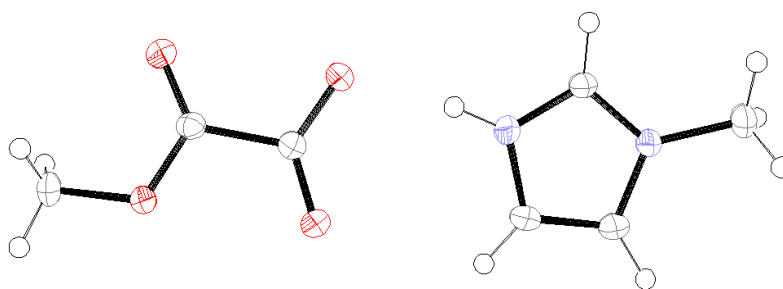


**Figure 7.3.1.1** Ortep diagram for the asymmetric unit of OxA and 1MI.

The methylation of one of the carboxyl groups prevents hydrogen bonding from this end of the anion resulting in a hydrogen bonded pair (1.80(1) Å). The pairs are arranged into ‘sheets’ with weak C-H...O hydrogen bonds linking the adjacent pairs (2.664, 2.296, 2.534, 2.475, 2.570 and 2.305 Å) (Figure 7.3.1.2). The sheets are not planar and instead appear to be undulating when viewed side-on. There are further weak C-H...O hydrogen bonds between methyl groups and anions of adjacent ‘sheets’ which are stacked so as the molecules do not eclipse each other.

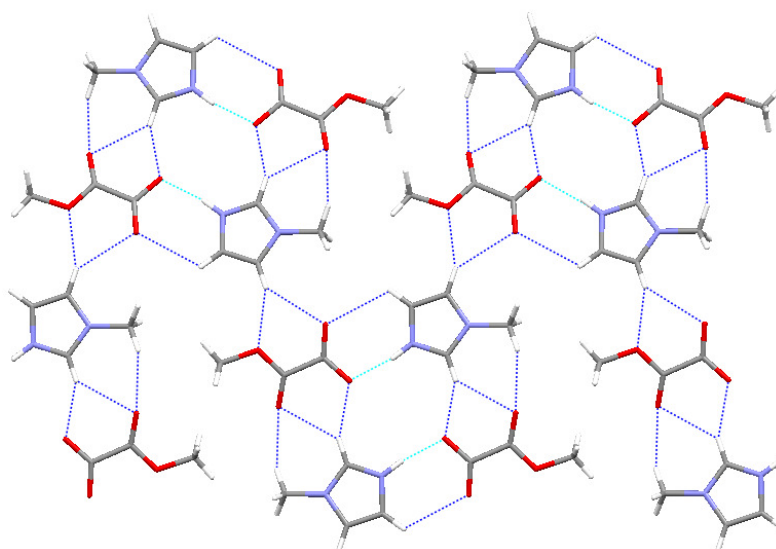


**Figure 7.3.1.2** N-H...O (light blue) and C-H...O (dark blue) hydrogen bonds between anions and cations.

### 7.3.2 Succinic Acid and 1-Methylimidazole

These compounds crystallised together in a 1:1 acid:base ratio in the monoclinic space group  $P2_1/c$  with  $Z = 4$ . The acid molecules lie across 2-fold rotation axis so as only half of each is shown in the asymmetric unit (Figure 7.3.2.1). Due to the poor quality of the crystals, the R-factor for the structure is quite high (12.68%) and some of the ellipsoids are not as expected. It was found that the cation is disordered over two positions in the unit cell that are approximately related by 2-fold rotation symmetry. Due to the poor data and the approximate symmetry relationship between the cations, the disorder was modelled as 50:50, however, the actual frequency of each position may be slightly different. Due to the  $\beta$ -angle being nearly  $90^\circ$  and the disorder of the cation it was also of concern that the structure was in the correct space group. It was not possible, however, to solve the



structure in a higher space group, furthermore it was decided that  $P2/c$  is the most appropriate space group to display the disorder. It was also found using ROTAX<sup>10</sup> that the crystal consists of a merohedral twin with the matrix (1 0 0, 0 1 0, 0 0 -1).

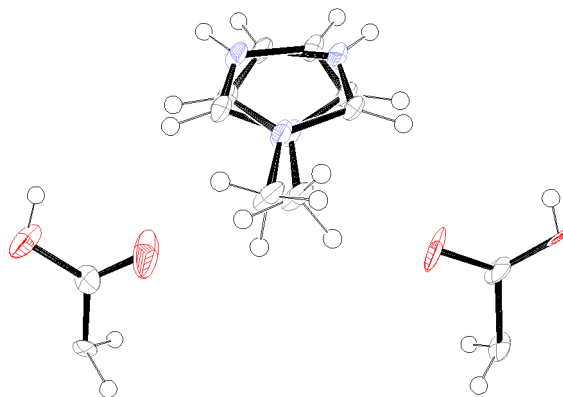


**Figure 7.3.2.1** Ortep diagram for the asymmetric unit of ScA and 1MI.

The acidic hydrogens have been found on each of the acid fragments; due to the acid molecules being on special positions these hydrogens are actually shared between adjacent acid molecules and hence each hydrogen has half occupancy. Although the other transferable hydrogen could not be located, chemically it cannot be attached to the acid molecules as these are involved in hydrogen bonding with themselves and the available sites for the hydrogen have been taken up by the half occupancy hydrogen. It was therefore determined that the hydrogen must have transferred to the base, as there was nowhere else for it to be and hence it was concluded a salt had formed.

As alluded to earlier, the structure consists of hydrogen bonded chains of monoanions in the *syn-syn* conformation with one hydrogen shared between each pair of carboxylate groups (1.72(2) and 1.72(2) Å). Cations are then subtended from these chains by N-H...O (1.93(2) and 1.92(2) Å) and C-H...O (2.050 and 2.047 Å) hydrogen bonds to form sheets (Figure 7.3.2.2). The C-H...O distances are particularly short and can only be attributed to the disorder in the structure and the poor data. In the following diagrams only one of the cation positions will be shown for clarity.

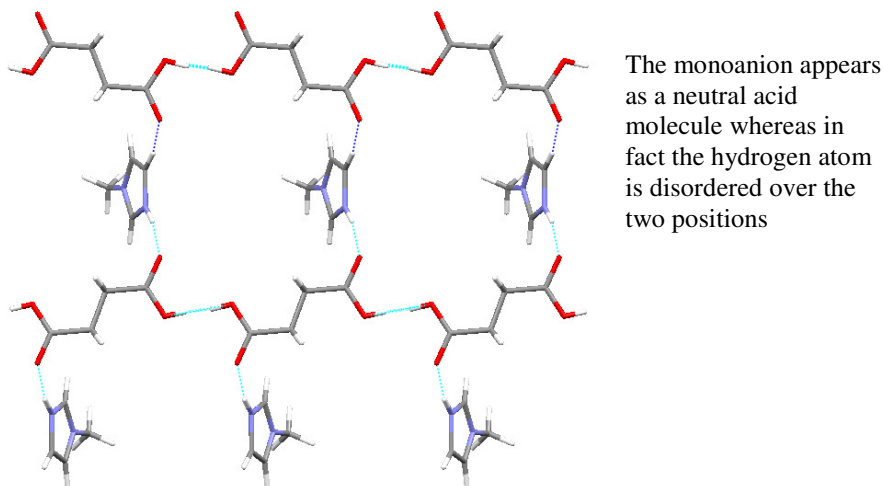


**Figure 7.3.2.2** Sheets of anions and cations, held together by hydrogen bonds: N-H...O (light blue), C-H...O (dark blue).

The cations are positioned below the plane of the anion chains and are nearly perpendicular to the plane of the anion chains. To maximise packing, each adjacent sheet is flipped 180° so as the cations of one sheet poke down and those of the sheet below poke upwards thereby filling the voids of each of the sheets (Figure 7.3.2.3)

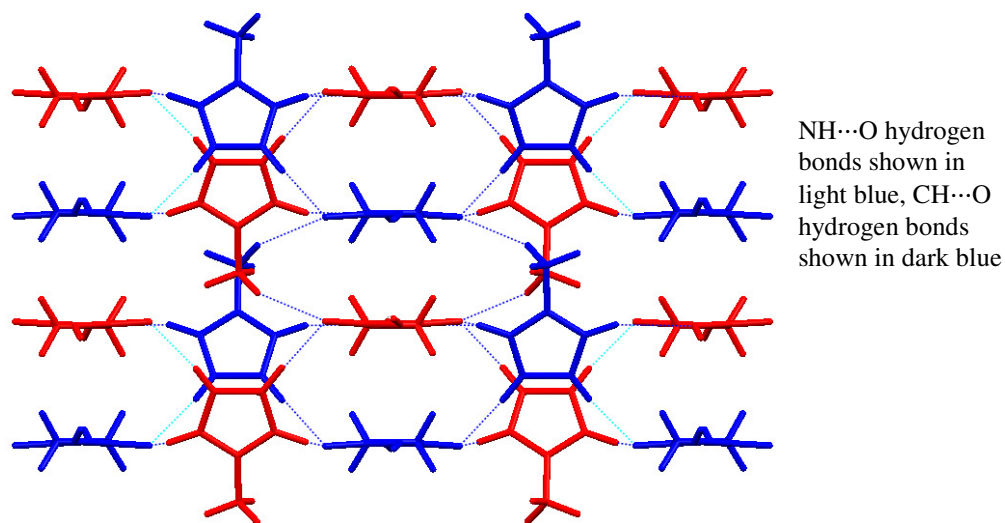


**Figure 7.3.2.3** Arrangement of adjacent sheets; the red sheet cations poke downwards filling the voids of the blue sheet below, and vice versa.

### 7.3.3 Glutaric Acid and 1-Methylimidazole

This structure also has a high R-factor (13.81%) and, again, not all of the transferable hydrogens could be found. It was initially solved in the triclinic space group *PI* however, it was found that there was inversion symmetry present and hence it was converted to *P-1* (with *Z* = 2) which reduced the R-factor. Due to the poor data some of the larger electron density peaks appeared in positions that were not chemically viable therefore the hydrogen positions were deduced from the arrangement of the molecules in the structure and the relevant bond distances.

According to the C-O and C=O bond distances O1A has a hydrogen attached as it has the longest of the two bond distances and the C1 carboxyl group has the largest difference between the two distances. This would hydrogen bond with O31A which concurs with this O atom having the longest C-O bond of this carboxylate group. If this group was protonated the hydrogen would be attached to the shorter C-O distance which is not likely. Therefore the hydrogen must be attached to the base molecule thus forming a cation. The difference between the C-O and C=O bond distances of the remaining two carboxyl(ate) groups are 0.037(8) and 0.024(8) Å for C5 and C35 respectively. One hydrogen was attached to O5B as this atom has the longest C-O distance as well as the largest C-O, C=O difference of the two groups. This atom would therefore hydrogen bond with O35A which has the longest C-O bond distance for the C35 carboxyl(ate) group. Again this suggests that the proton of this carboxyl group has been transferred to the base molecule thus

creating a system containing two monocations, one acid molecule and one dianion – a mixed system. Further work would need to be performed on this structure to confirm this. The O...O distances for this structure are 2.515(7) and 2.480(6) Å which is sufficiently short for low barrier hydrogen bonds or single well hydrogen bonds where the hydrogen is shared between the two groups. The strength of such a hydrogen bond will also influence the C-O and C=O bond distances, lessening the difference for a carboxyl group and increasing the difference for a carboxylate group. This explains the unexpected smaller difference in the C-O, C=O bond distances seen here.

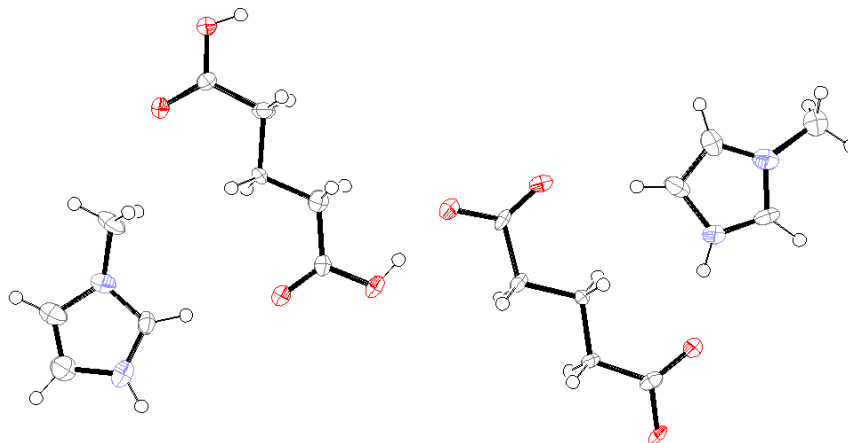


**Figure 7.3.3.1** Ortep diagram for asymmetric unit of GIA and 1MI.

The structure consists of alternate acid molecules and dianions hydrogen bonded head-to-tail in the *anti-anti* conformation (1.67(1) and 1.68(1) Å). The cations are subtended from the chains via N-H...O hydrogen bonds (1.77(1) and 1.84(1) Å) and are positioned in approximately the same plane as the acid-anion chains in order to maximise C-H...O hydrogen bonds between the cations and anions (range 2.236-2.626 Å) thus creating a sheet. Half of the cations are slightly tilted so as to accommodate the bulky methyl group into the sheet whilst retaining the C-H...O hydrogen bonds.

The cations pointing to the top of the page are slightly tilted to accommodate for the methyl group

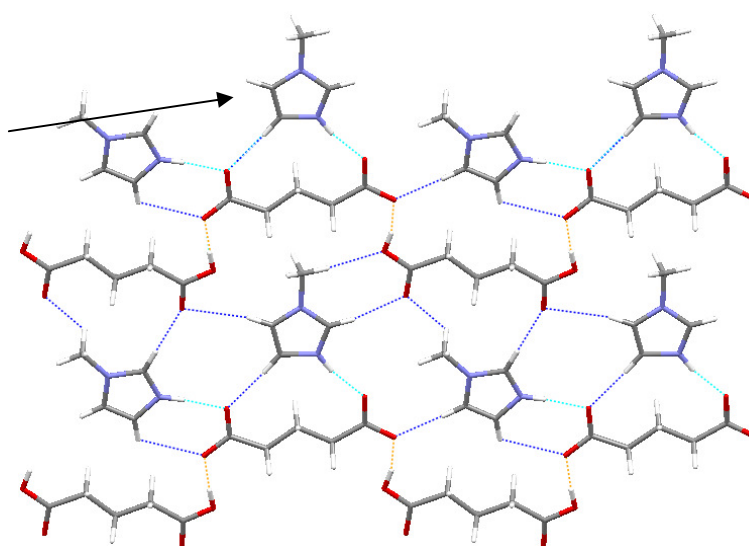


**Figure 7.3.3.2** Sheet held together by hydrogen bonds; N-H...O light blue, C-H...O dark blue, O-H...O orange.

The sheets are stacked so as the methyl groups from the tilted cations fill the small voids created in the adjacent sheet. There are further weak C-H...O hydrogen bonds from cation methyl groups and anion methylene groups to the anions to link the adjacent sheets. The sheets are stacked on top of each other so as the cations are above and below the acid-anion chains.

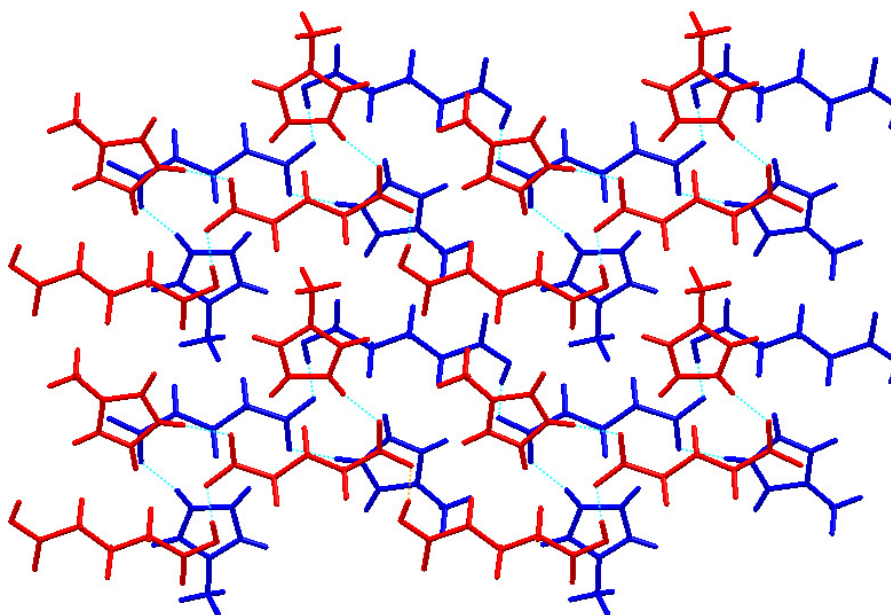


**Figure 7.3.3.3** Arrangement of sheets; bottom sheet coloured blue, top sheet coloured red.

#### 7.3.4 *D*-Tartaric Acid and 1-Methylimidazole (ZAMXIU)

The crystal structure was characterised by Fuller *et al.*<sup>7</sup> who crystallised it by dissolving the base in a warm 1:1 water:methanol mixture and then adding an equimolar amount of the acid. The solvent mixture was then removed by rotary evaporation before the solid was dried. The authors note that the ‘resulting white salt was gummy and proved difficult to re-crystallise;’ further work-up in acetonitrile eventually produced crystals suitable for SXR D.

The components were found to crystallise in a 1:1 acid:base ratio to form a salt in the monoclinic space group  $P2_1$ , with  $Z = 2$ . The monoanions form chains via the typical tartrate head-to-tail hydrogen bonding in the *syn-syn* conformation; adjacent chains are then linked by O-H...O hydrogen bonds between hydroxyl groups, and carboxyl and hydroxyl groups to form a sheet:

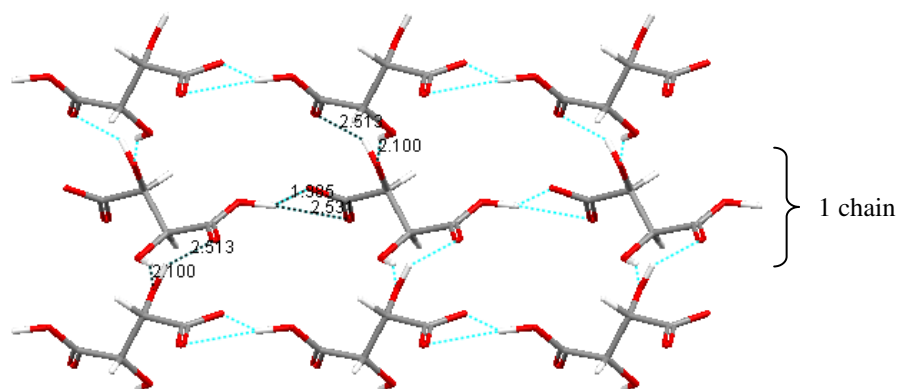


**Figure 7.3.4.1** Hydrogen bonded anion lattice.

The cations are subtended from the sheet by hydrogen bonds to the hydroxyl group of the anion ( $1.998 \text{ \AA}$ ) – this is unexpected as the carboxylate group will be a stronger acceptor. Instead the carboxyl and carboxylate groups form weak  $\text{C-H}\cdots\text{O}$  hydrogen bonds with adjacent cations within a sheet ( $2.231 \text{ \AA}$ ) and in the adjacent sheet ( $2.352$  and  $2.556 \text{ \AA}$ ).

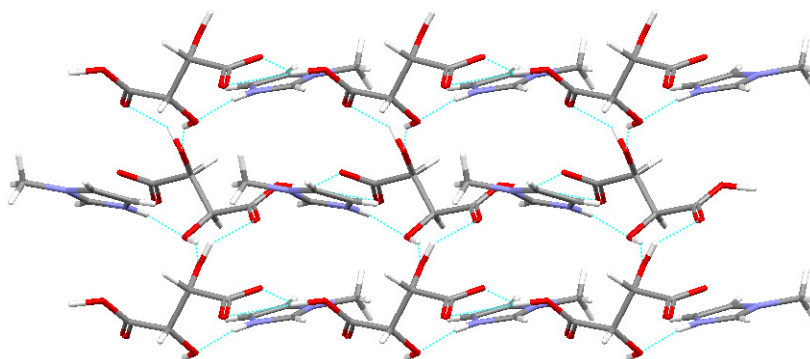


**Figure 7.3.4.2** Anion lattice with cations subtended from one of the hydroxyl groups.

When the structure is viewed down the  $a$ -axis it can be seen that the anion back bone of the sheet is in a zigzag formation with the cation alternately above and below it (Figure 7.3.4.3).

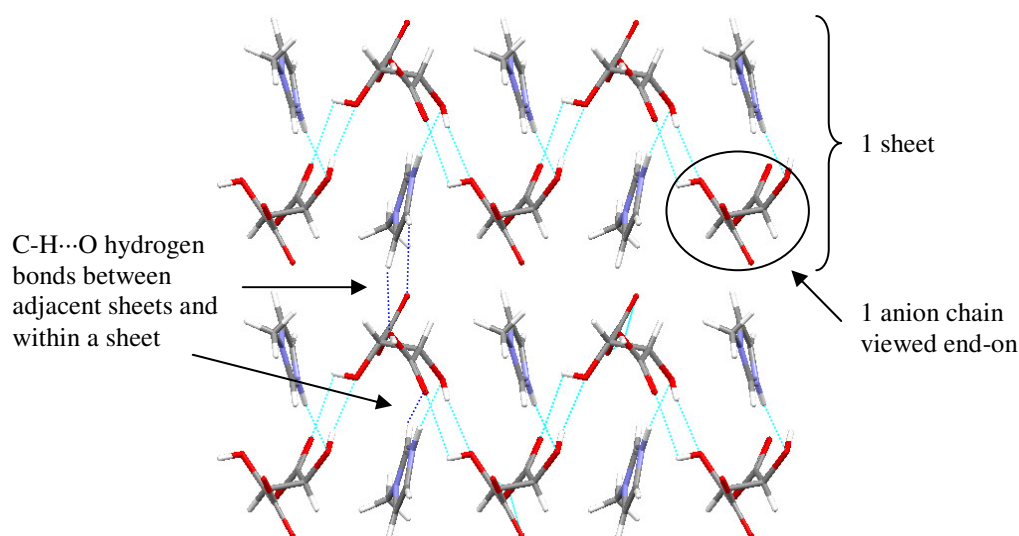


**Figure 7.3.4.3** Zigzag formation of the anion backbone of the sheet.

### 7.3.5 *DL-Tartaric Acid and 1-Methylimidazole*

These components crystallised in a 1:1 ratio to form a salt in the monoclinic space group  $P2_1/n$ , with  $Z = 4$ . The contents of the asymmetric unit are shown in Figure 7.3.5.1.

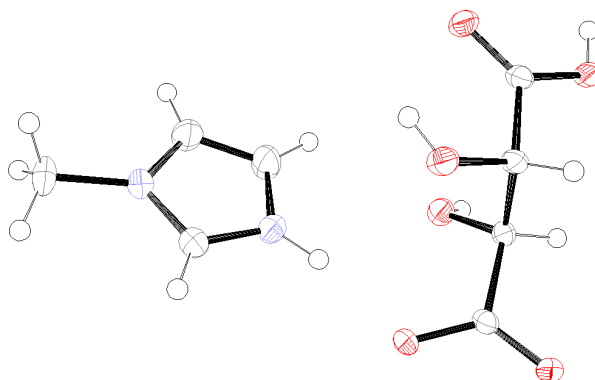


**Figure 7.3.5.1** Ortep diagram for the asymmetric unit of DLTA and 1MI.

The monoanions are hydrogen bonded head-to-tail to form a chain, which is further linked by hydrogen bonding involving the hydroxyl and carboxyl groups to form a sheet (Figure 7.3.5.2). Hydrogen bonding between hydroxyl and carboxylate groups extends the lattice down the  $b$ -axis thus creating a 3-D network.

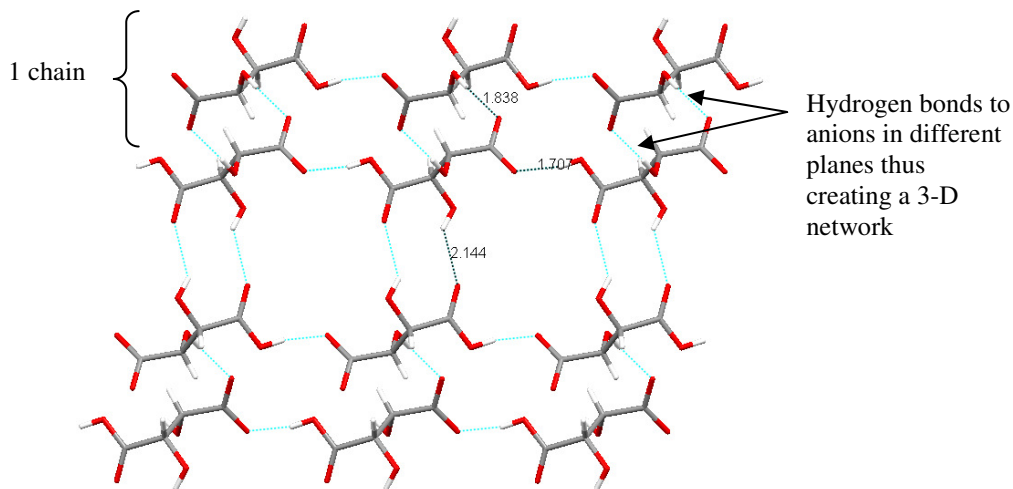


**Figure 7.3.5.2** Lattice arrangement of anion molecules, viewed down the  $b$ -axis (hydrogen bond distance error  $\pm 0.002$  Å).

The cations are then subtended from the lattice by hydrogen bonding from the carboxylate and hydroxyl groups (1.87(1) and 2.54(1) Å respectively). The cations are stacked in pairs with dipole-dipole interactions between them. This is supported by the lack of  $\pi$ -interactions on the fingerprint plot (Appendix, Table 11.2).

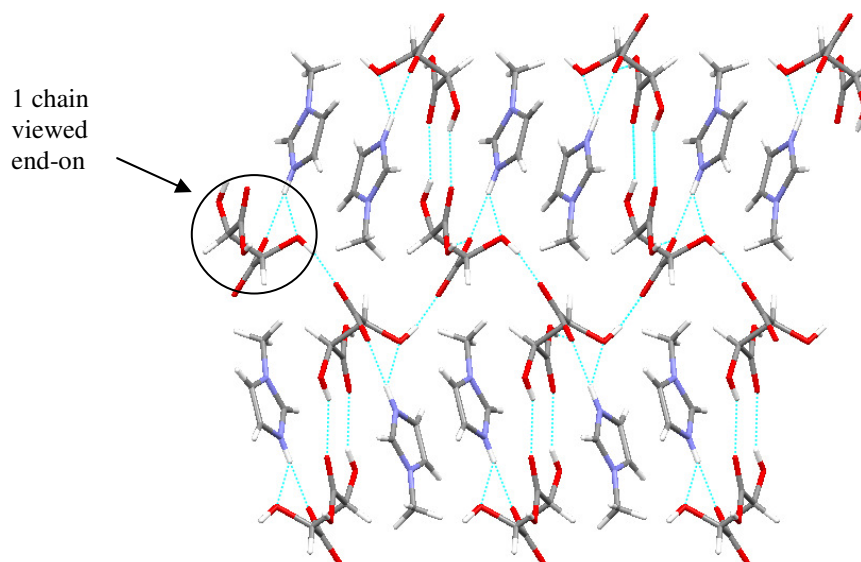


**Figure 7.3.5.3** Anion network with cations subtended from this, viewed down the *a*-axis.

### 7.3.6 Maleic Acid and 1-Methylimidazole

These two components reacted via a 1,4-Michael addition reaction to form a zwitterion (Figure 7.3.6.1). It should be noted that N23 has a positive charge and the C4 carboxylate group is negatively charged.

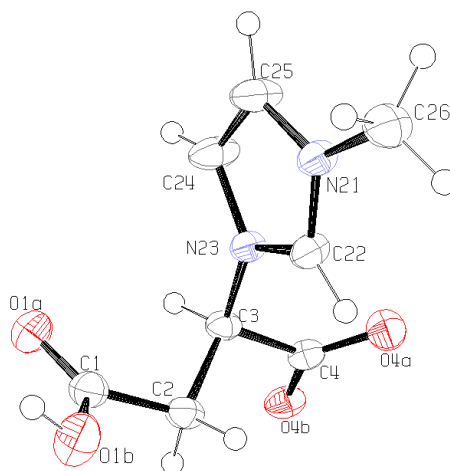


**Figure 7.3.6.1** Reaction of MeA and 1MI to form this zwitterion.

### 7.3.7 Discussion of 1-Methylimidazole Structures

Although acid-base combinations involving 1MI gave mainly solid compounds (only MnA and PmA gave oils), these were of poor crystalline quality with micro-crystals being produced for MeA, FmA and AdA. SbA-1MI produced a powder that when analysed by PXRD was found to be SUBRAC04. As the starting materials crystallised out separately in this combination, it suggests



that the crystal structures of the starting materials are more energetically favourable than that of a binary compound.

The only diacids that produced binary compounds were OxA, ScA, GlA, DTA and DLTA. The availability of only one of the nitrogens on the base for hydrogen bonding limits the number of strong N-H...O hydrogen bonds 1MI can form. This is reflected by the lower melting point temperatures found for each of the binary compounds compared to the acid-base combinations containing Im. Maximisation of C-H...O contacts through the positioning of the cations around the anions enables the compounds to form extended 2-D and 3-D structures that are not possible through purely N-H...O hydrogen bonding.

All of the structures have a 1:1 stoichiometry and the diacids are generally mono-deprotonated (in keeping with the  $pK_a$  differences) except GlA-1MI. Due to the poor data in this structure, the exact positions of the hydrogens have been based on the bond lengths and the data would need to be re-collected from better quality crystals, or using neutron diffraction to accurately locate the hydrogens.

In the OxA structure the acid is methylated preventing head-to-tail anion-anion hydrogen bonding from occurring. The small size of the acid molecule means that the functional groups of the components are in close proximity and hence available for a number of weak C-H...O intermolecular interactions which stabilise the sheet structure.

The ScA structure is an adaptation of **Sheet 3** with the anion chains bridged via C-H...O as well as N-H...O interactions across the cation, and the methyl groups of the cation pointing in opposite directions as depicted in **Sheet 4** (Figure 7.3.7.1).

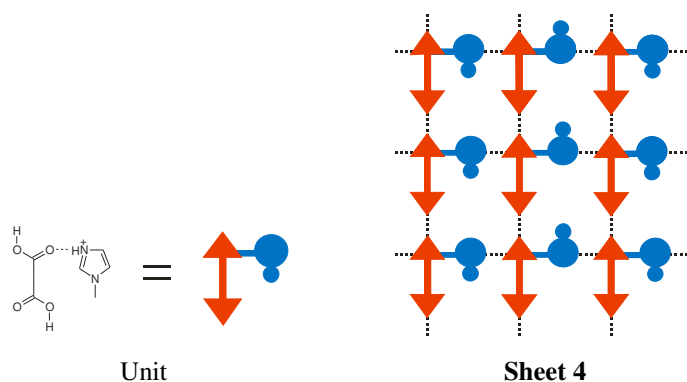


**Figure 7.3.7.1** Schematic representations of the Sheet structures in the 1MI binary compounds.

GlA-1MI also forms an adaptation of **Sheet 4** with the acid-anion chains hydrogen bonded in the *anti-anti* conformation instead of *syn-syn*. Similarly to the ScA-1MI structure, C-H...O hydrogen bonds are integral in the formation of the sheet structure. The sheets involving 1MI are also slightly different to the Im sheets as they have to accommodate the methyl group of the cation. In



the ScA structure the cation is tilted with its methyl group pointing out of the plane of the anion chains similar to that in the FmA-Im structure. The further C-H...O hydrogen bonds therefore link adjacent sheets together rather than stabilising the sheet itself. In the GlA-1MI structure the cations are positioned more in line with the plane of the sheet thereby increasing the C-H...O interactions within the sheet.

DTA-1MI forms a nearly identical sheet structure to LTA-Im with an adaptation of the **Sheet 2** arrangement, with the methyl groups pointing in the opposite direction to the carboxyl groups. Apart from the slightly different orientation of the cation in order to accommodate the methyl group of 1MI, the main difference between structures is the importance of C-H...O hydrogen bonds in the 1MI structure to link the adjacent sheets. The melting point and densities of the LTA-Im structure are significantly higher than those of the DTA-1MI structure (179°C, 1.56 g cm<sup>-3</sup> and 99.5°C, 1.471 g cm<sup>-3</sup> respectively) highlighting the impact of the methyl group on the intermolecular interactions and packing even when a similar structure is formed. DLTA-1MI consists of a different structure to those seen so far with the monoanions forming a 3-D network which the cations then fit into rather than being integral to the linking of the adjacent sheets.

The melting points and densities for the 1MI binary compounds do not correlate as well as the Im structures (Appendix, Table A8); the highest melting structure is OxA-1MI (179°C) which has the second lowest density in the series (1.44 g cm<sup>-3</sup>). The highest density structures are the TAs (1.471 and 1.56 g cm<sup>-3</sup>), however ScA-1MI also has a particularly high density (1.48 g cm<sup>-3</sup>) and, unusually, the melting point for the DTA and ScA structures are in the middle of the range. This suggests that in spite of the higher density of the structures, the intermolecular interactions are weaker and hence the melting point is decreased.

## 7.4 2-METHYLIMIDAZOLE

### 7.4.1 Oxalic Acid and 2-Methylimidazole

These compounds crystallised in a 1:2 acid:base ratio in the orthorhombic space group *Pbca*, with *Z* = 8. The R-factor is quite high (10.86%), however there were no problems during solving and refining the structure and the transferable hydrogens were found easily and their positions confirmed. The asymmetric unit was found to contain two cations and one dianion and hence the components formed a salt (Figure 7.4.1.1).

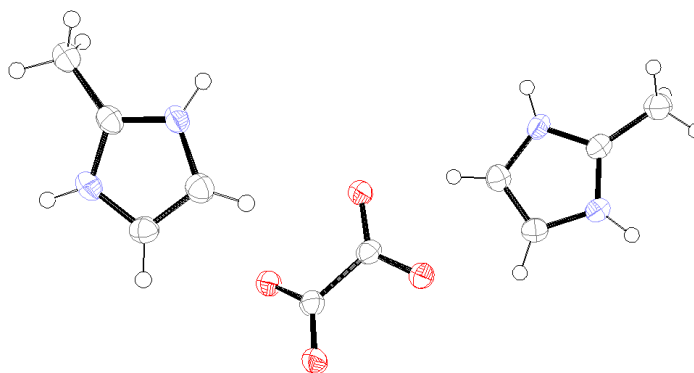


**Figure 7.4.1.1** Ortep diagram for the asymmetric unit of OxA and 2MI.

Each dianion is hydrogen bonded to the four surrounding cations in the same plane to form a sheet (Figure 7.4.1.2). Both of the nitrogens of the cation are bifurcated hydrogen bond donors; N21 and N33 are hydrogen bonded to one carboxylate group each, whereas N23 and N31 are hydrogen bonded to both carboxylate groups. The cations are positioned with their methyl groups pointing in clockwise and anti-clockwise arrangements around each of the anions to accommodate the bulky methyl group.

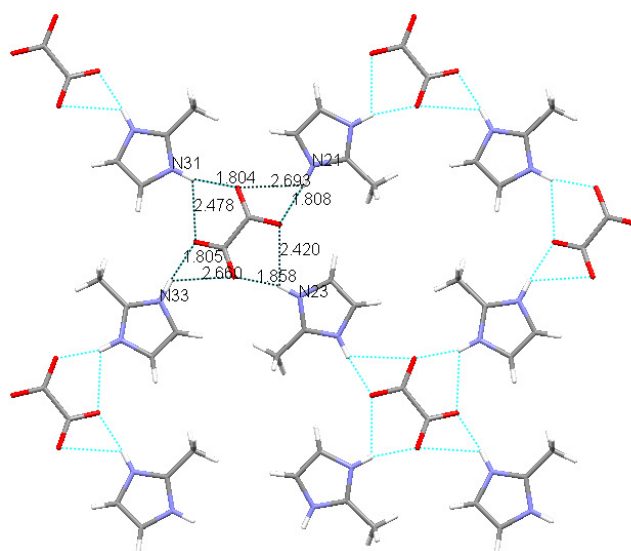


**Figure 7.4.1.2** Hydrogen bonding of the dianions and cations (error  $\pm 0.004$  Å), viewed down the *b*-axis.

When viewed down the *a*-axis it can be seen that the sheets are slightly undulating. There are weak C-H $\cdots$ O hydrogen bonds between the cation methyl groups and the anions in a pair of sheets of sheets, but none between adjacent pairs of sheets. Other weak C-H $\cdots$ O hydrogen bonds from the aromatic CHs of the cation further stabilise the sheet structure (2.580 and 2.570 Å).

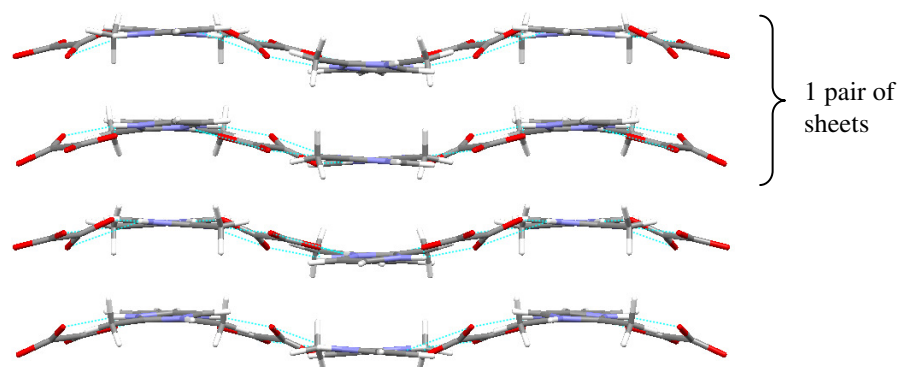


**Figure 7.4.1.3** Stacking of sheets into pairs.

When the structure is viewed down the *b*-axis, it can be seen that each of the four sheets shown above are arranged so as the molecules do not eclipse each other. The cations are positioned over each other in a parallel offset manner, allowing dipole-dipole interactions between the rings.

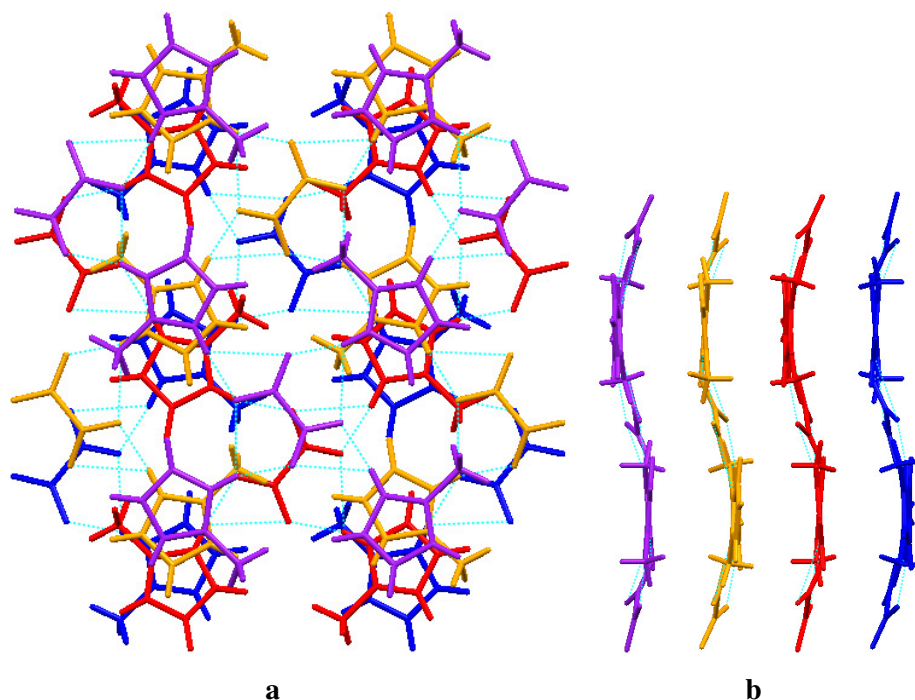


**Figure 7.4.1.4** a) Arrangement of stacked sheets, viewed down the *b*-axis; b) sheets viewed side-on, down the *a*-axis.

#### 7.4.2 Malonic Acid and 2-Methylimidazole

Initially, from the well-plate crystallisations this combination formed an oil, however, on crystallisation using Method 3 crystals were produced that were found to contain the components in a 1:1 ratio. The components crystallised in the orthorhombic space group  $Pna2_1$ , with  $Z = 4$ , to form a salt.

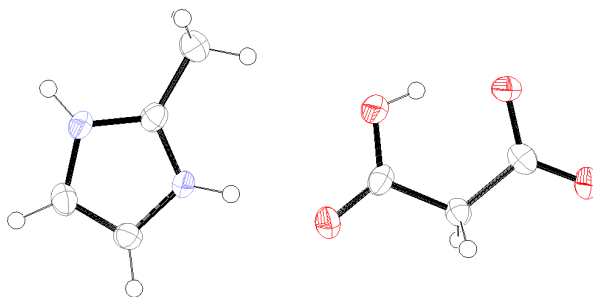


**Figure 7.4.2.1** Ortep diagram for the asymmetric unit of MnA and 2MI.

The structure consists of a hydrogen bonded chain of alternate monoanions and cations (Figure 7.4.2.2). The monoanion has retained one of its acidic hydrogens which is involved in a strong intramolecular hydrogen bond.

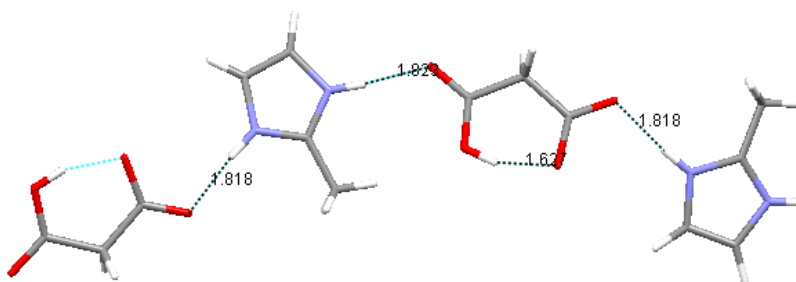


**Figure 7.4.2.2** Hydrogen bonded chain of anions and cations, hydrogen bond distances marked (error  $\pm 0.005$  Å).

The chains are arranged on top of each other to form stacks; the chains are aligned at an angle of  $58^\circ$  to the direction of the stack. The adjacent stacks of chains are also orientated at  $64^\circ$  to each other (Figure 7.4.2.3). This enables weak C-H $\cdots$ O hydrogen bonds between the cation and anions of adjacent stacks (cation aromatic CH to anion = 2.515 and 2.649 Å; cation methyl to anion = 2.696 Å); other weak C-H $\cdots$ O hydrogen bonds from the cation methyl group (2.491 Å) further stabilise the chain structure.

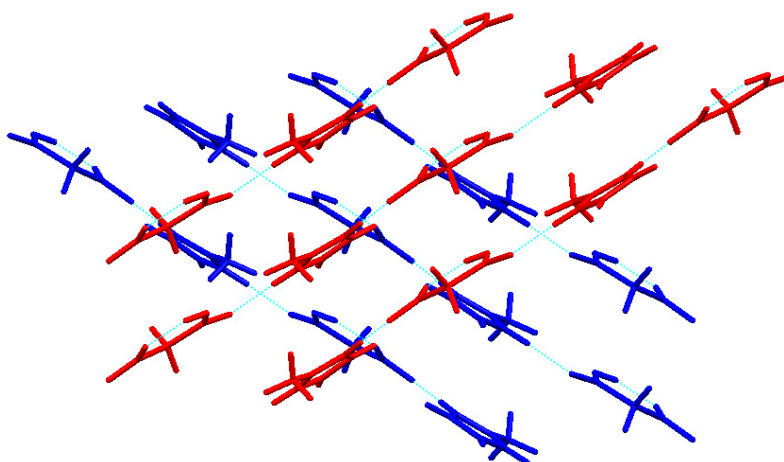


**Figure 7.4.2.3** Orientation of chains in adjacent stacks – one stack is coloured red and the other is coloured blue, viewed down the  $a$ -axis.

### 7.4.3 Succinic Acid and 2-Methylimidazole

These two compounds crystallised in a 1:1 ratio in the monoclinic space group  $P2_1/m$ , with  $Z = 4$ , to form a salt.

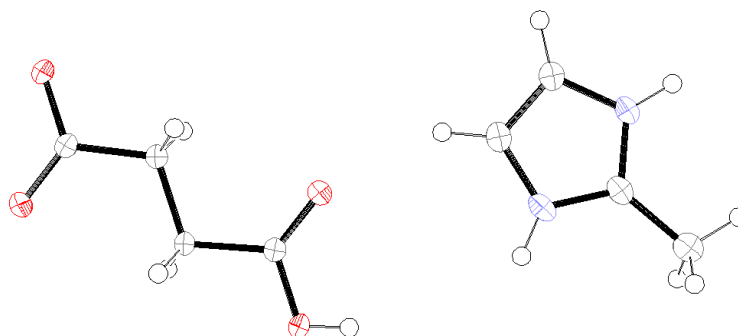


**Figure 7.4.3.1** Ortep diagram for the asymmetric unit of ScA and 2MI.

The structure consists of monoanions hydrogen bonded head-to-tail in the *syn-syn* conformation to form chains. These chains are then bridged by hydrogen bonding across the cations to form a sheet. This is possible due to the availability of both of the hydrogen bond donors on the cation. The distances of the N-H...O and O-H...O hydrogen bonds are noted in Figure 7.4.3.2; there are also weaker C-H...O hydrogen bonds present from the aromatic CHs and methyl groups (2.562 and 2.276, and 2.625 Å respectively). The sheets run parallel to the *ac*-plane.

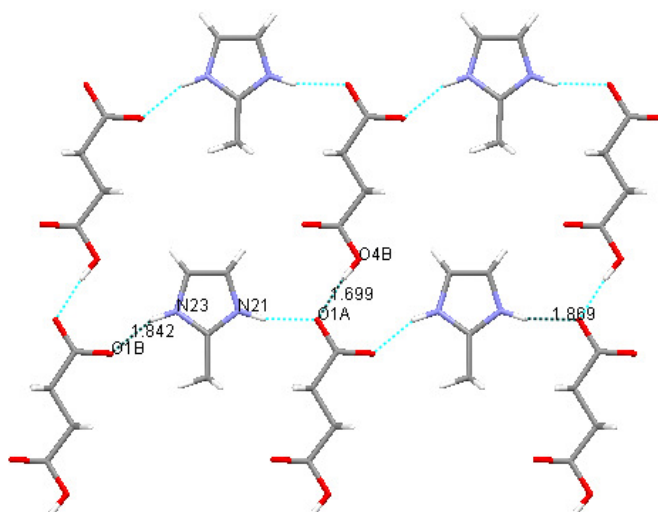


**Figure 7.4.3.2** Sheet structure with the hydrogen bond distances marked (error  $\pm 0.002$  Å), viewed down the *b*-axis.

The sheets are stacked in a staggered fashion to accommodate the bulky methyl group on the cation (Figure 7.4.3.3). Weak C-H...O hydrogen bonding between the cation methyl groups and the anions in adjacent sheets, links the sheets (2.664 Å).

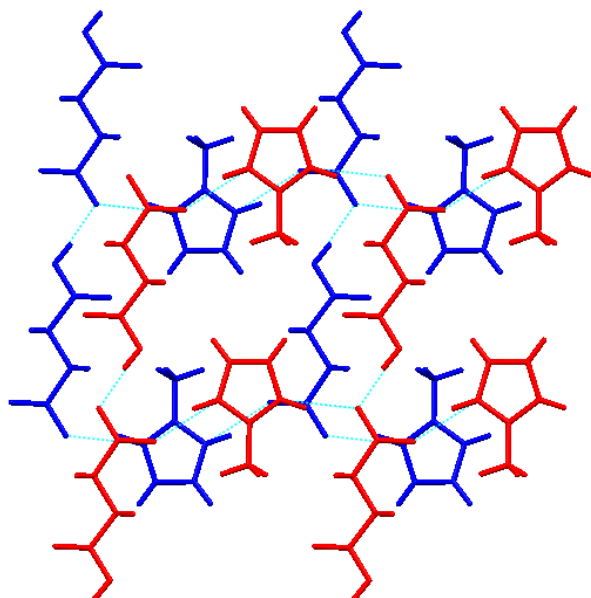


**Figure 7.4.3.3** Stacking of the sheets – one layer is coloured blue and the adjacent layer is coloured red.

#### 7.4.4 Glutaric Acid and 2-Methylimidazole

These compounds crystallised in a 1:1 ratio to form a salt in the triclinic space group *P*-1, with *Z*=2 to form a salt. The R-factor for this structure is quite high (9.41%), however, all of the hydrogens were found easily and their positions confirmed. The acidic hydrogens on the acid molecule are disordered and therefore have been modelled as half occupancy on each carboxylate groups, thus forming a monoanion.

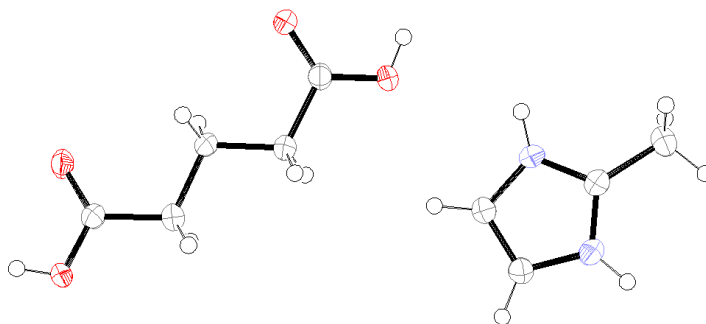


**Figure 7.4.4.1** Ortep diagram for the asymmetric unit of GIA and 2MI.

The structure consists of monoanions hydrogen bonded together in the *syn-syn* conformation to form a chain. Although the hydrogen is modelled as half occupancy on each of the carboxyl groups, with the short H...O and O...O distance (1.60(1) and 2.443(5) Å respectively) it is likely that the hydrogen is shared somewhere between the two oxygens. The H...O distance is slightly longer than the accepted distance range for a low-barrier hydrogen bond (1.2-1.5 Å), however, here the hydrogens have been fixed to idealised positions which do not take into account the typical lengthening of the D-H bond.

The chains are then linked together by hydrogen bonding across the cations to form sheets (Figure 7.4.4.2). The N-H...O hydrogen bonds are bifurcated, with the two acceptors from different anions. There are also weak C-H...O hydrogen bonds between the aromatic CHs of the cations and anions; however these are quite long and the small DHA angle also weakens them (C24 = 2.605 Å, 114.96° respectively; C25 = 2.757 Å, 107.84° respectively).

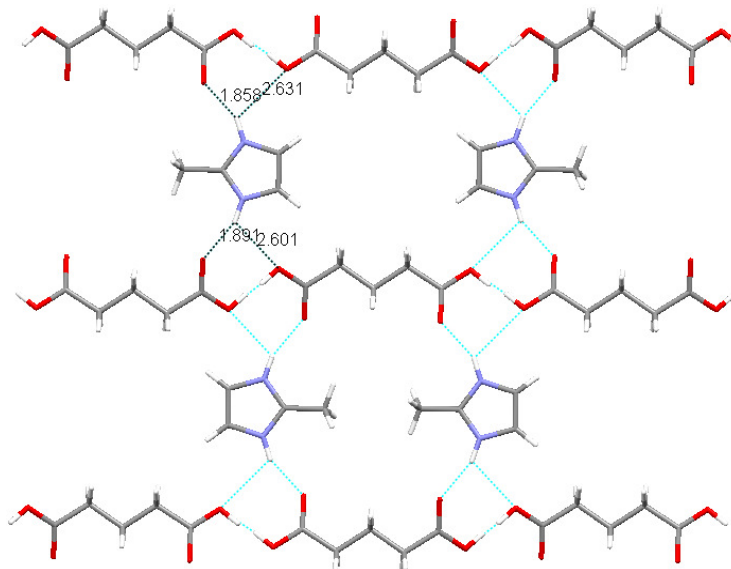


**Figure 7.4.4.2** Arrangement of molecules to form sheets (hydrogen bond distance error +/-0.004 Å).

The sheets are not planar and instead are slightly undulating with adjacent chains of each sheet being 180° out of phase with each other (Figure 7.4.4.3).

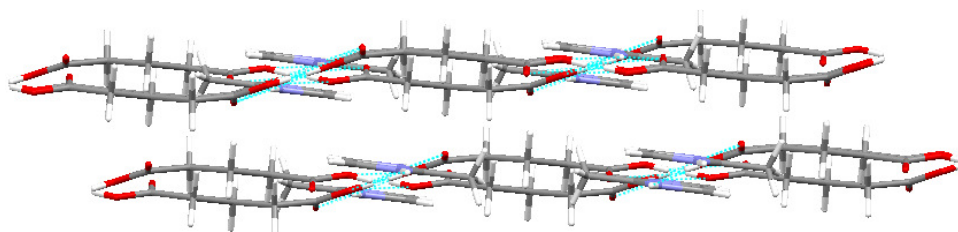


**Figure 7.4.4.3** Undulation of sheets, viewed side-on.

When the chains are viewed end-on it can be seen that the sheets are stacked in an offset manner so as the anions are above the cations and vice versa. This arrangement and the undulation of the chains means that the methylene groups of the anion chain are slightly raised to fill the void created by the cations. The anion methylene groups are also slightly lifted away from the methyl groups of the cations in the adjacent sheet.

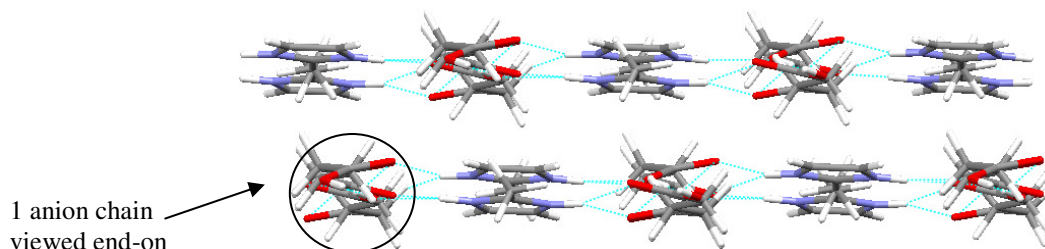


**Figure 7.4.4.4** Arrangement of sheets.

#### 7.4.5 Adipic Acid and 2-Methylimidazole

These compounds crystallised to form micro-crystals which were analysed by synchrotron radiation. The structure was found to contain the components in a 1:1 ratio in the triclinic space group *P*-1, with *Z* = 2. The asymmetric unit contains two halves of the diacid molecule which form an AdA molecule and a dianion, thus creating a mixed salt/co-crystal monohydrate system.

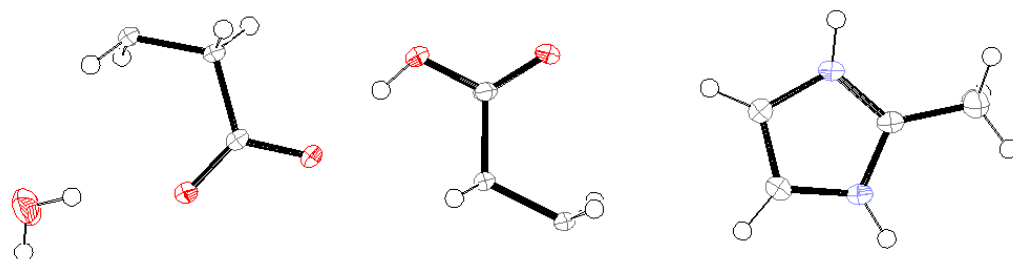


**Figure 7.4.5.1** Ortep diagram for the asymmetric unit of AdA and 2MI.

The structure consists of chains of anions hydrogen bonded head-to-tail in the *anti-anti* configuration. The chains are then bridged by hydrogen bonding across the cations and water molecules to form a sheet (Figure 7.4.5.2). The position of the cations also allows C-H...O hydrogen bonds between the anions and cations (2.694, 2.684, 2.607 and 2.718 Å). The anions and cations form a planar sheet with the water molecules positioned slightly above and below the plane.

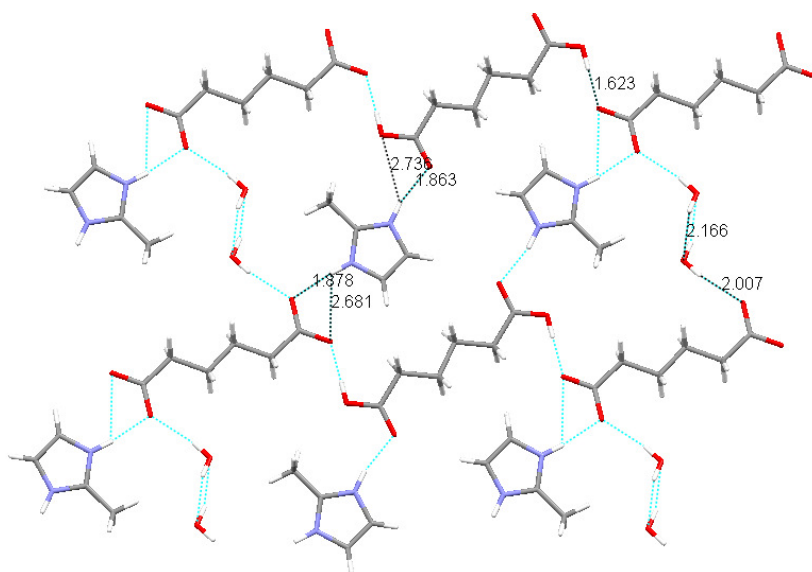


**Figure 7.4.5.2** Hydrogen bonded sheet of anions, cations and water molecules, distances marked (error +/- 0.003 Å).

The sheets are stacked on top of each other so as the molecules are not directly over each other; one of the oxygens of the carboxylate group is positioned over the centre of the cation ring.



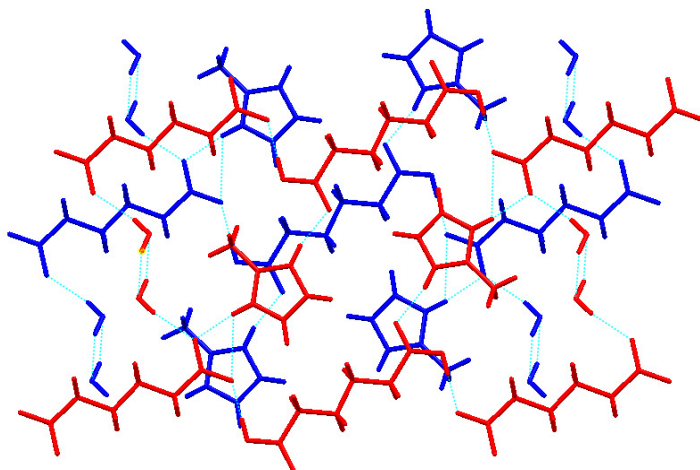


**Figure 7.4.5.3** Stacking of sheets, one coloured blue and adjacent coloured red.

#### 7.4.6 Suberic acid and 2-Methylimidazole

This structure crystallised in a 1:1 ratio in the triclinic space group *P*-1, with *Z* = 2, to form a salt. The carboxyl group of the monoanion is disordered -41.26% of the time in position 8 and 58.74% in position 9 (Figure 7.4.6.1).

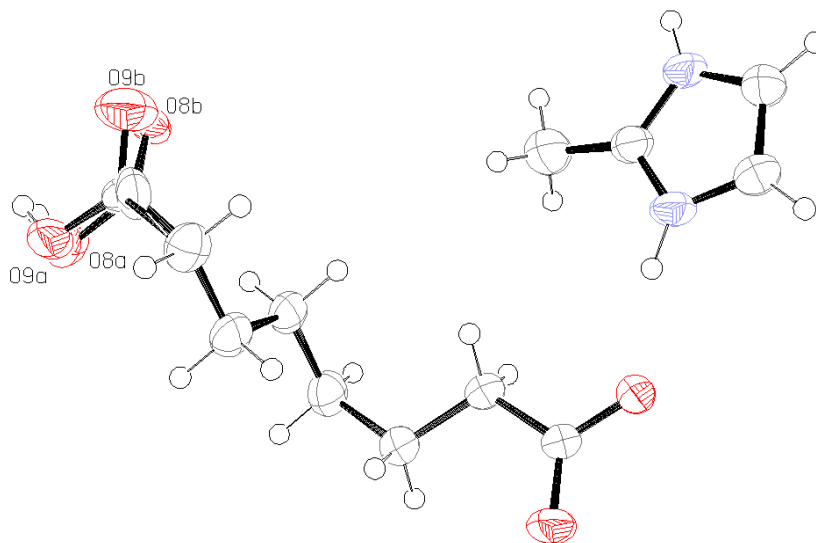


**Figure 7.4.6.1** Ortep diagram for the asymmetric unit of SbA and 2MI.

Again, the monoanions are hydrogen bonded together in the *syn-syn* conformation to form a chain; the chains are then linked to form a sheet via hydrogen bonding across the cations (Figure 7.4.6.2). The O-H...O hydrogen bond distances between the anions are 1.80(1) Å for the dominant carboxyl group position and 1.69(1) Å for the less prevalent position. There are also weak C-H...O hydrogen bonds, 2.628, 2.285 and 2.628 Å, however the former of these has quite a small *DHA* angle (119.89°, 143.34° and 135.63° respectively) and hence is unlikely to contribute significantly to stabilisation of the sheet.

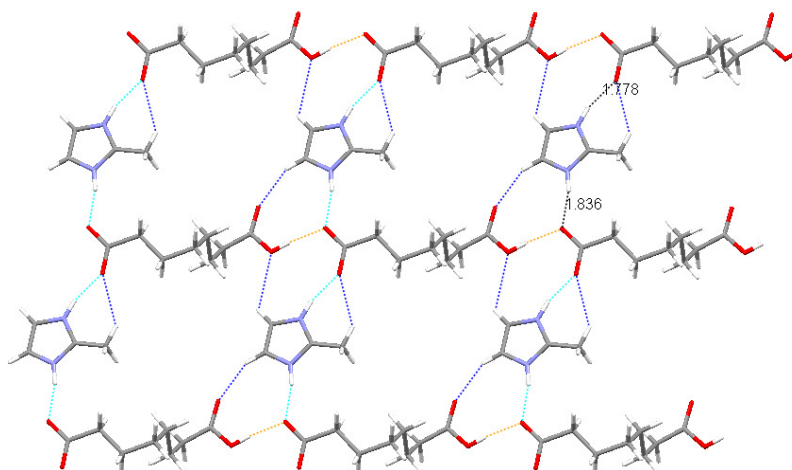


**Figure 7.4.6.2** The hydrogen bonded sheet, O-H...O hydrogen bonds shown in orange, N-H...O shown in light blue (distances marked, error  $\pm 0.003$  Å), C-H...O shown in dark blue.

The sheets form a staircase type 2-D network due to the anion adopting the *gauche* conformation across C4-C5 and C6-C7 (torsion angles  $-65.1(2)^\circ$  and  $8 = 56.0(13)^\circ$   $9 = 62.5(6)^\circ$  respectively) (Figure 7.4.6.3). The staircase type sheets are then stacked on top of each other, with the methyl groups of the cation pointing in opposite directions in adjacent sheets. The sheets are also offset so as the anion chains do not stack directly under each other but are instead under the cations.

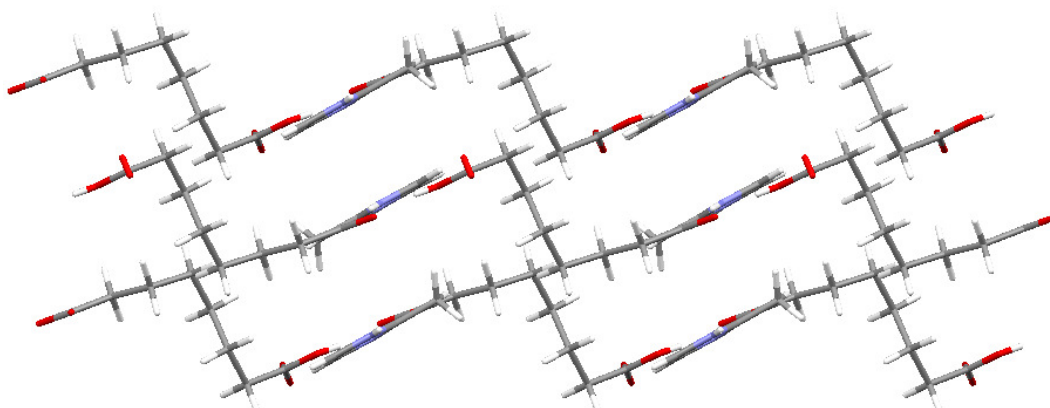


**Figure 7.4.6.3** Step formation of the sheets, viewed down the *b*-axis.

#### 7.4.7 *D*-Tartaric Acid and 2-Methylimidazole (ZELRIR)

Crystals of this structure were characterised by Fuller *et al.*<sup>7</sup> and were prepared by adding an equimolar amount of DLTA to a warm 1:1 water:methanol mixture of 2MI and leaving the solution to evaporate. The resulting binary compound crystallised in a 1:1 acid-base ratio in the monoclinic space group  $P2_1$ , with  $Z = 2$ , to form a salt. The structure consists of monoanions hydrogen bonded head-to-tail in the *syn-syn* conformation to create infinite 1-D chains. Adjacent chains are then bridged by N-H...O bonds between the cation and the anion to create a sheet (Figure 7.4.7.1). There are also weak C-H...O hydrogen bonds from the cation methyl group, however the *DHA* angles of

these are quite small and therefore they probably do not contribute significantly to the stabilisation of the sheet.

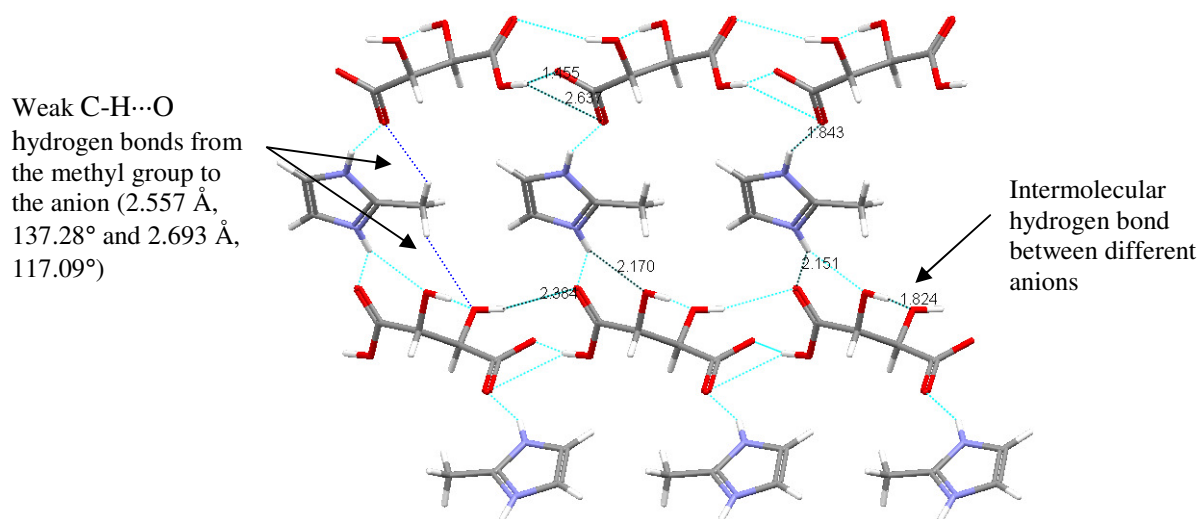


**Figure 7.4.7.1** Hydrogen bonded sheet structure.

The hydrogen bond between the two hydroxyl groups of the anion is an intermolecular hydrogen bond linking the anions in front of and behind the one shown in this sheet. This extends the sheet down the *a*-axis into a 3-D network (Figure 7.4.7.2).

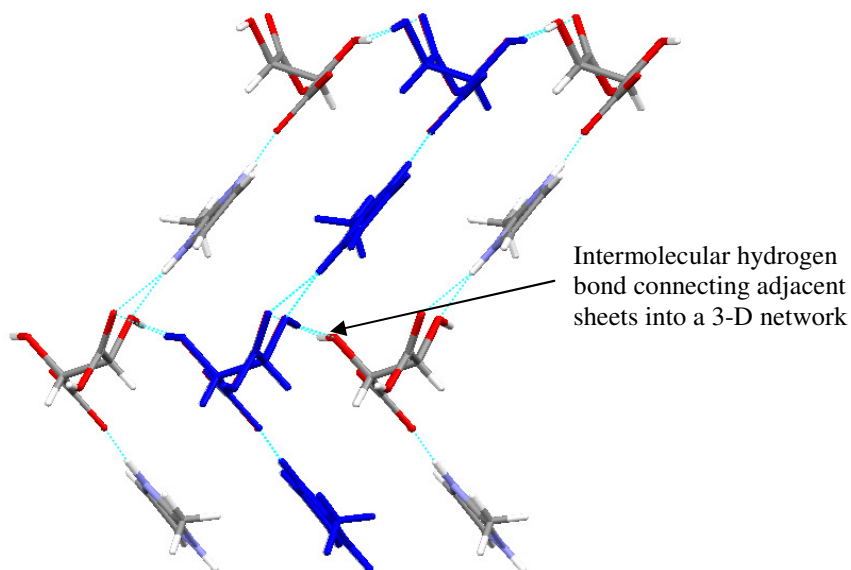


**Figure 7.4.7.2** Sheet viewed side-on to see the arrangement of the 3-D network; the middle sheet is coloured blue.

#### 7.4.8 *DL*-Tartaric Acid and 2-Methylimidazole

These components were found to crystallise in a 1:1 ratio in the triclinic space group *P*-*I*, with *Z* = 2, to form a salt. The contents of the asymmetric unit are shown in Figure 7.4.8.1.

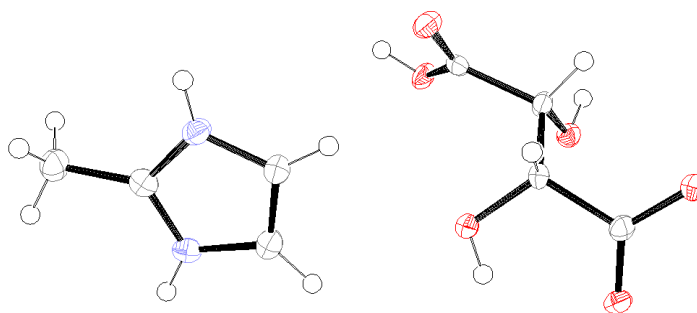


**Figure 7.4.8.1** Ortep diagram for the asymmetric unit of DLTA and 2MI.

The anions are hydrogen bonded head-to-tail in the *syn-syn* conformation to form 1-D chains; adjacent chains are linked by further hydrogen bonding between the carboxylate and hydroxyl groups of the anions to create a sheet (Figure 7.4.8.2).

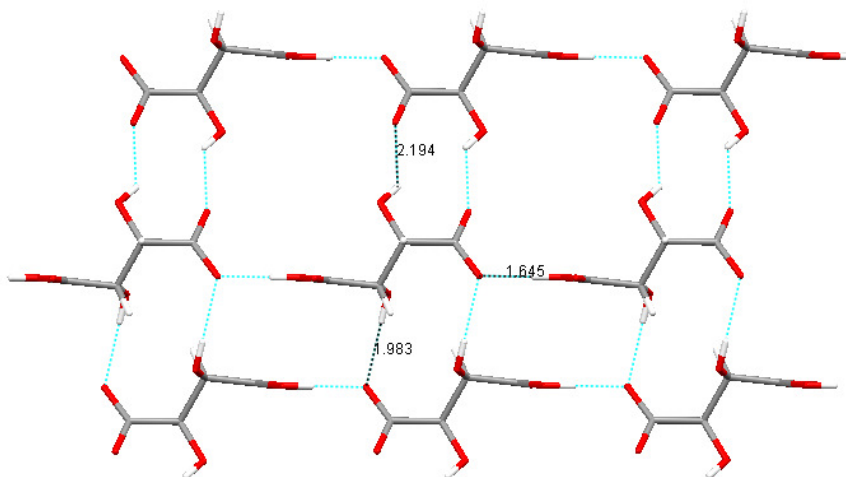


**Figure 7.4.8.2** 2-D lattice of hydrogen bonded anions (error  $\pm 0.003$  Å).

Cations are then subtended from this sheet by two bifurcated hydrogen bonds to the carboxyl, carboxylate and hydroxyl groups of the anion ( $N23 = 2.50(1)$  and  $1.98(1)$  Å, and  $N21 = 2.69(1)$  and  $1.93(1)$  Å). The cations act to bridge adjacent sheets to form a 3-D network (Figure 7.4.8.3).

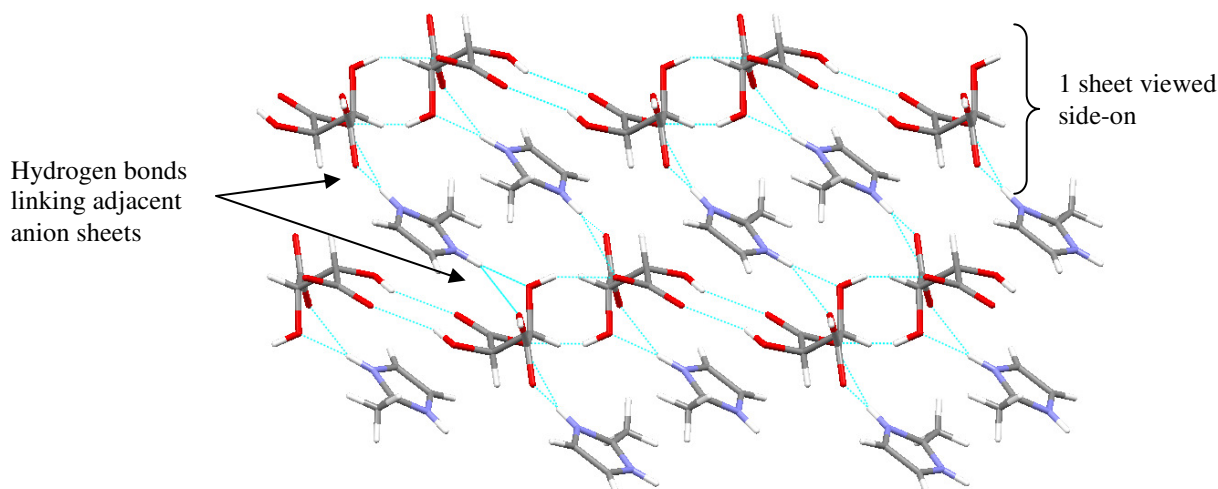


**Figure 7.4.8.3** 3-D network with sheet viewed side-on; the linking of the sheets by hydrogen bonding across the base molecules can be seen, viewed down the *a*-axis.

### 7.4.9 Fumaric Acid and 2-Methylimidazole

These two components crystallised in the monoclinic space group  $P2_1/m$ , with  $Z = 4$ . It was found that this salt is isostructural with that formed from the ScA-2MI combination. The asymmetric unit is shown in Figure 7.4.9.1.

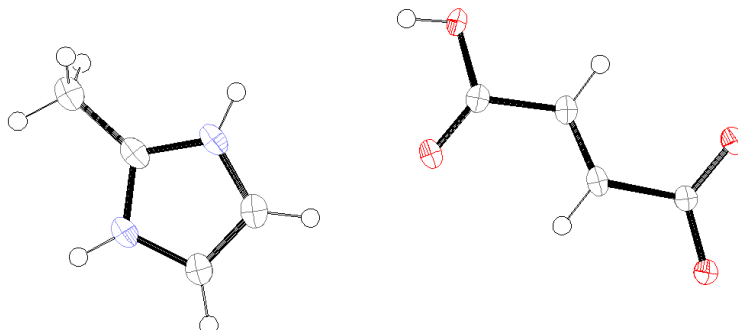


**Figure 7.4.9.1** Ortep diagram for the asymmetric unit of FmA and 2MI.

The hydrogen bond distances for the structure are shown in Figure 7.4.9.2, where the same sheet structure as ScA-2MI (Figure 7.4.3.2) can be seen.

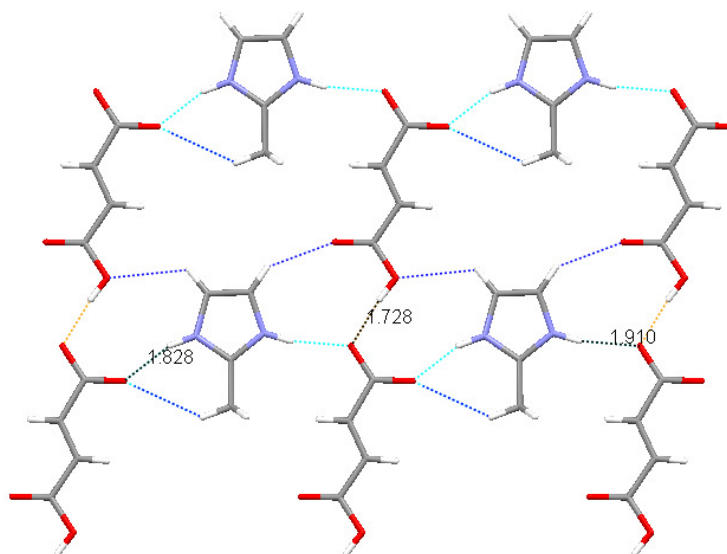


**Figure 7.4.9.2** Sheet structure, O-H...O hydrogen bonds shown in orange, N-H...O in light blue, C-H...O in dark blue (hydrogen bond distance error  $\pm 0.004$  Å).

Again the C-H...O bond angles are quite small for such weak hydrogen bonds ( $122.56^\circ$ ,  $134.98^\circ$  and  $145.12^\circ$ ) and hence their contribution to the sheet stabilisation is probably minimal. The sheets overlay in a nearly identical manner to ScA-2MI but with the molecules positioned slightly differently to that seen in Figure 7.4.3.3, resulting in a longer C...O distance ( $2.781\text{Å}$ ) between the cation methyl group and the anion, thus weakening the interaction.

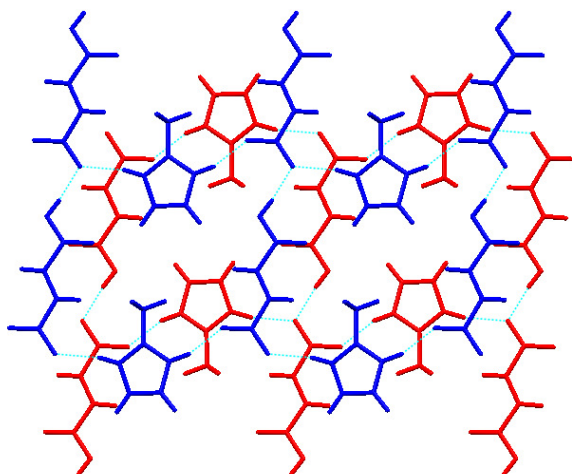


**Figure 7.4.9.3** Stacking of sheets; one sheet is coloured red, the adjacent is coloured blue.

#### 7.4.10 Discussion of 2-Methylimidazole Structures

Again, the acid-base combinations mainly resulted in crystalline products with only PmA remaining an oil. The MeA-2MI micro-crystals produced a very weak powder pattern that does not appear to correlate with either of the starting materials. The product was also analysed thermally and was found to have a melting point of 243°C – this is significantly higher than the melting point of either of the starting materials making it likely that a new product has formed, which possibly is binary.

All the structures have a 1:1 stoichiometry except OxA-2MI; most of the structures contain monoanions except OxA-2MI and AdA-2MI. As 2MI is the most basic of the aromatic amines, both the first and second ionisation of the diacid by the base generally has a  $pK_a$  difference of greater than two units (except MeA second ionisation), indicating that both mono- and di-deprotonation should result in stable salts.

The availability of both of the nitrogens on the cation for hydrogen bonding together with the weaker C-H...O hydrogen bonds leads to strong networks being created which is expressed in the high melting points of the structures (Appendix, Table A8). For the simple diacids, the melting point decreases overall as the number of carbons in the diacid chain increases (Figure 7.4.10.1). The melting points do not correlate as well with the densities as they do in the Im binary compounds; the high density of the MnA-2MI structure is not reflected by its melting point compared to the other structures. This may be because the other structures form sheets whereas MnA-2MI forms chains with a strong intramolecular hydrogen bond in the MnA, thus reducing its hydrogen bonding potential with the cation. AdA-2MI also has a lower melting point than expected which may be due to the voids in the structure that have been filled by water molecules. The TA structures have the highest melting points of approximately 200°C.

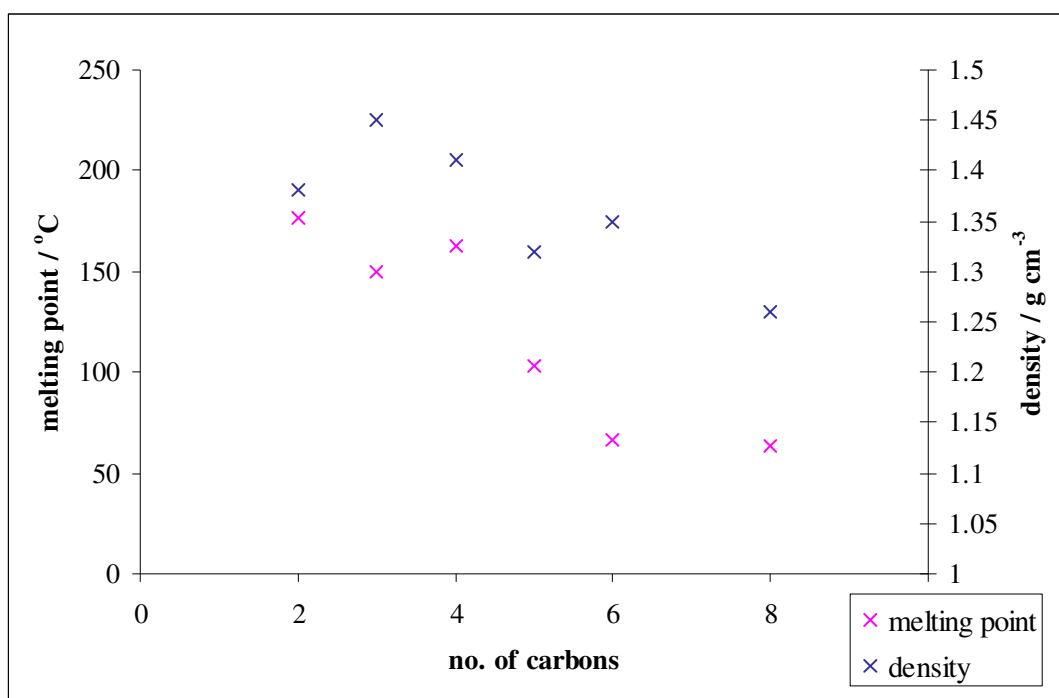


**Figure 7.4.10.1** Graph to show the variation in melting point and density with carbon chain length of the 2MI binary compounds.

ScA- and FmA-2MI are isostructural and follow a nearly identical molecular arrangement to **Sheet 2**. In addition to this arrangement, the methyl groups on the cation point in the same direction as the anion carboxyl groups; this is schematically represented in **Sheet 5**, Figure 7.4.10.2.

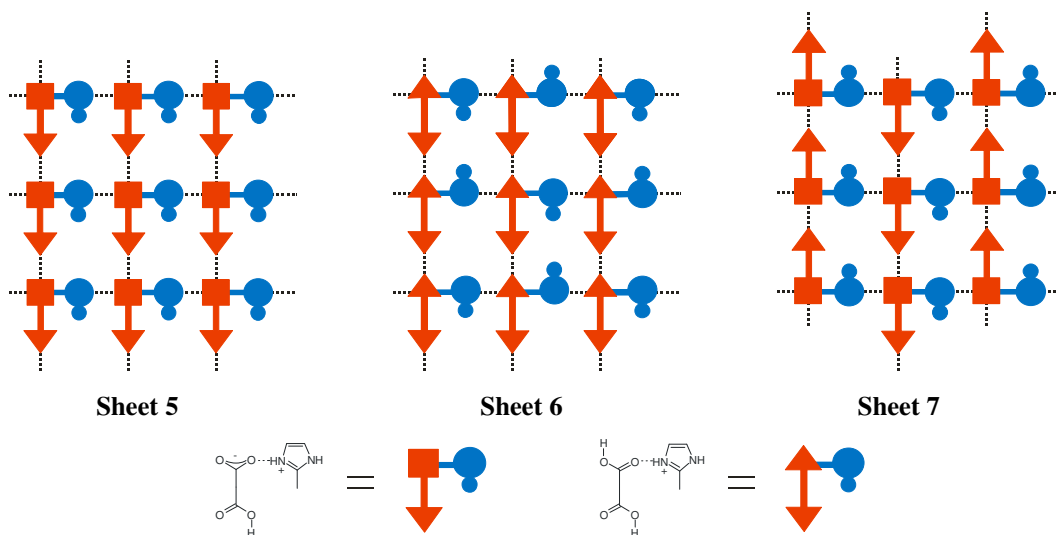


**Figure 7.4.10.2** Schematic representation of the sheet structures found in some of the 2MI binary compounds.

The GlA-2MI structure forms a very similar sheet structure to **Sheet 3** with the acidic proton shared between the two carboxylate groups in the anion chain. The cations are also orientated differently, with their methyl groups pointing towards each other in a pair of cations as is represented in **Sheet 6** (Figure 7.4.10.1). AdA-2MI also forms a similar sheet structure to GlA except that the anion-acid chain is hydrogen bonded in the *anti-anti* configuration whereas all the other anion-anion chains in



the 2MI sheet structures are in the *syn-syn* arrangement. SbA follows the **Sheet 5** arrangement, however, due to the 'S'-shape of the SbA the sheets are stepped rather than planar.

The OxA structure is different from the others in the 2MI series as it crystallises in a 1:2 acid:base ratio. This double deprotonation of the acid prevents a head-to-tail hydrogen bonded anion chain from forming; an arrangement which is also unlikely due to the smaller size of the anion compared to the cation. The MnA-2MI structure also differs from the sheet structures, due to the strong intramolecular hydrogen bond in the anion preventing head-to-tail hydrogen bonding of the anions.

DTA-2MI and DLTA-2MI form similar structures to the other TAs with anti-parallel anion chains linked by hydrogen bonds from the hydroxyl groups to form sheets. The sheets are then linked by hydrogen bonding across the cations to form a 3-D network. The manner in which the anion sheets in DTA-2MI are linked by the cations is similar to **Sheet 2**, with the methyl groups of the cations pointing in opposite directions as is depicted in **Sheet 7** (Figure 7.4.10.1). In DLTA-2MI the methyl groups of the cations point towards each other in pairs, as seen in **Sheet 6** (Figure 7.4.10.1).

In all of the non-hydroxy diacid structures, the cation is positioned in line with the approximately flat sheet. This orientation will maximise the C-H...O hydrogen bonds from both the aromatic CH and the methyl groups.

## 7.5 4-METHYLIMIDAZOLE

### 7.5.1 Oxalic Acid and 4-Methylimidazole

The components were found to crystallise in a 1:2 acid:base ratio with water in the monoclinic space group  $C2/c$ , with  $Z = 4$ , to form a salt hemihydrate. The asymmetric unit contains one cation, half a dianion and half a water molecule (Figure 7.5.1.1); the dianion lies across an inversion centre and hence is centrosymmetric and the water molecule lies across a 2-fold rotation axis.

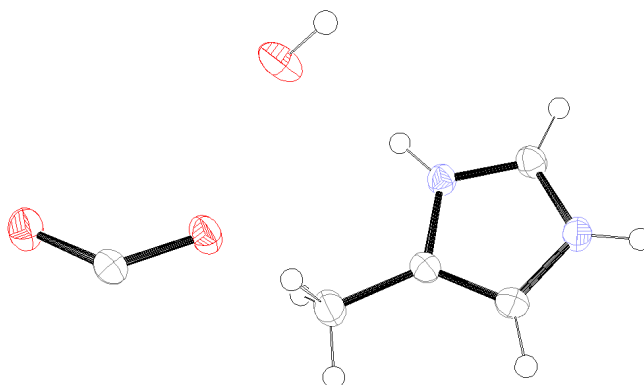


**Figure 7.5.1.1** Ortep diagram for the asymmetric unit of OxA and 4MI.



The dianions and cations are hydrogen bonded together to form a sheet; the hydrogen bond distances involved are shown in Figure 7.5.1.2. Each anion is surrounded by four cations, two with their methyl groups pointing to the top of the page and two pointing to the bottom of the page. Each cation has one monofurcated hydrogen bond donor and one bifurcated hydrogen bond donor. The availability of the two hydrogen bond donors creates a hydrogen bonded sheet.

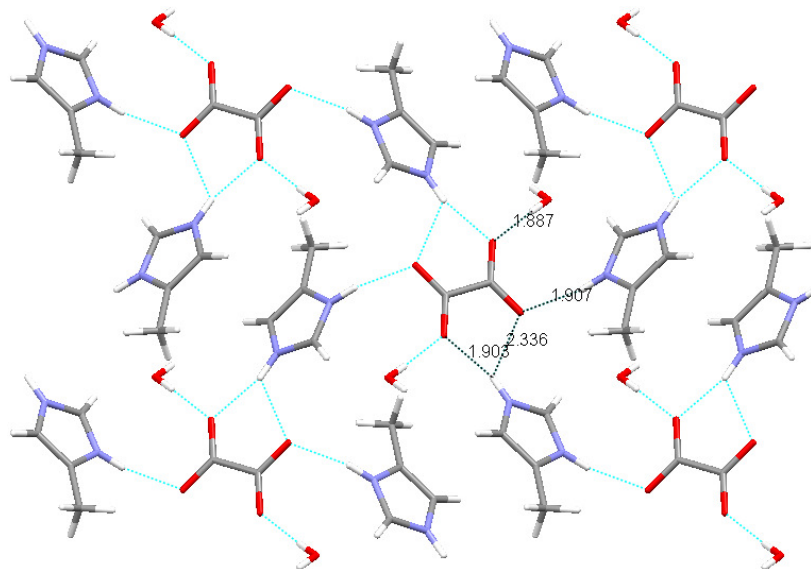


**Figure 7.5.1.2** Hydrogen bonded arrangement where one anion is hydrogen bonded to the surrounding four cations and two water molecules (hydrogen bond distance error  $\pm 0.002$  Å).

Adjacent sheets are then linked by hydrogen bonding across the water molecules (Figure 7.5.1.3). The sheets are arranged in an offset manner to accommodate the bulky methyl groups on the cations.

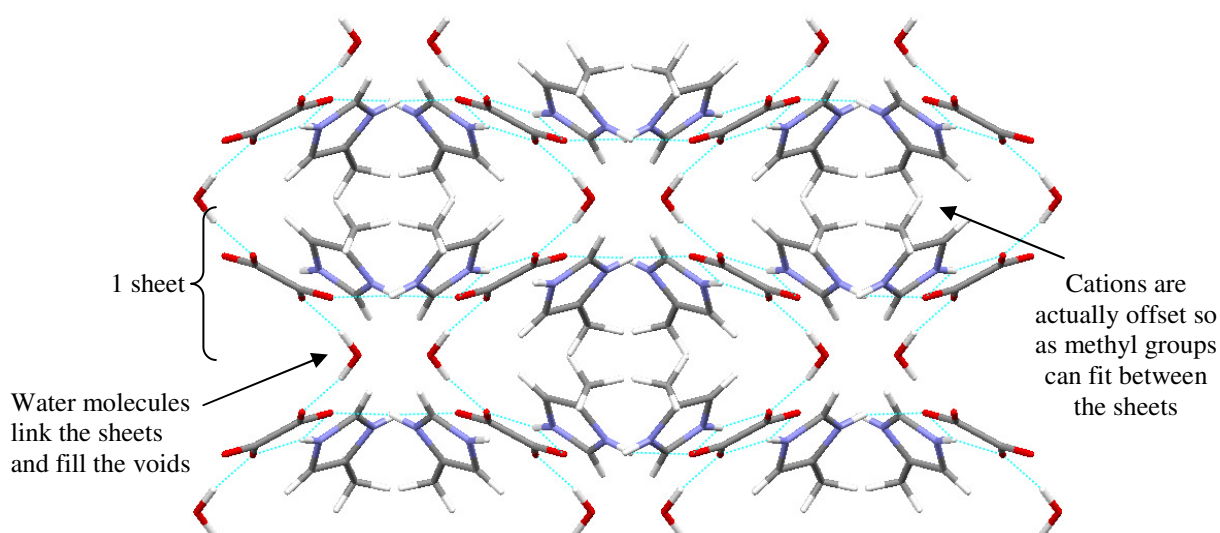


**Figure 7.5.1.3** Arrangement of sheets linked by hydrogen bonding across water molecules.

### 7.5.2 Succinic Acid and 4-Methylimidazole

These two compounds crystallised in a 1:1 acid:base ratio to form a mixed salt/co-crystal system in the monoclinic space group  $P2_1/c$ , with  $Z=4$ . Half a neutral ScA molecule and half a cation appear in the asymmetric unit as they lie across inversion centres.

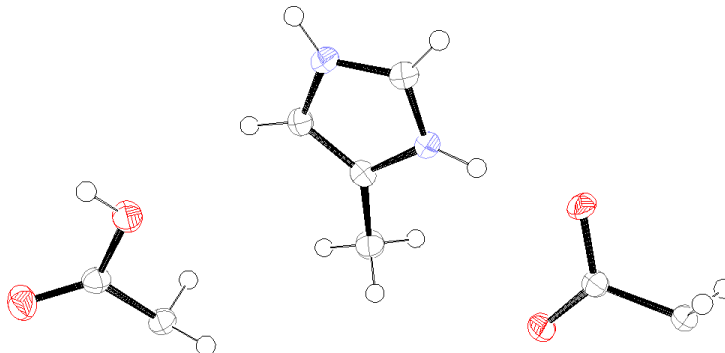


**Figure 7.5.2.1** Ortep diagram for the asymmetric unit of ScA and 4MI.

The acid and dianion molecules are hydrogen bonded head-to-tail in the *syn-anti* conformation to form a chain. Cations are linked to the anions by  $N-H\cdots O$  hydrogen bonds, but are only linked to the acid molecules by  $C-H\cdots O$  hydrogen bonds (2.334 and 2.567 Å) (Figure 7.5.2.2). There are also  $C-H\cdots O$  hydrogen bonds from the methyl group of the cation to the dianion (2.526 Å).

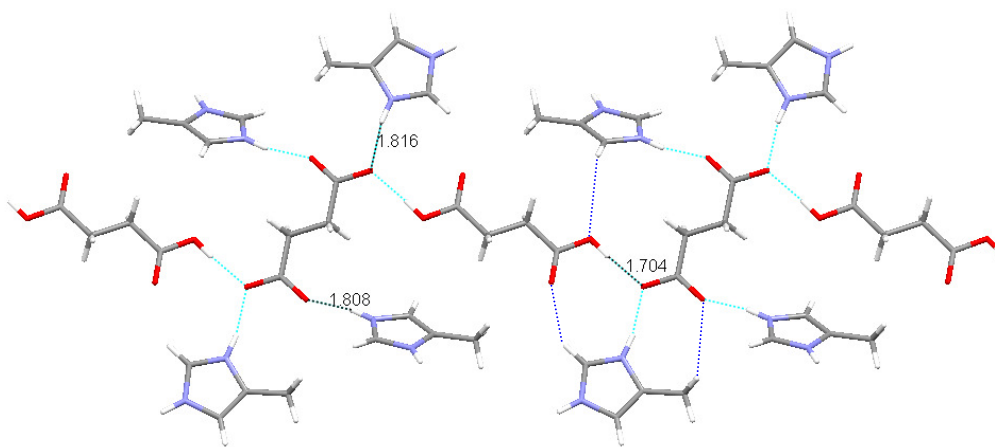


**Figure 7.5.2.2** Hydrogen bonded chain structure, hydrogen bond distances marked (error  $\pm 0.002$  Å),  $C-H\cdots O$  hydrogen bond examples shown in dark blue.

As 4MI has two nitrogens available as hydrogen bond donors, each chain is linked to four adjacent chains via hydrogen bonding across the cation to create a 3-D network (Figure 7.5.2.3). Adjacent chains are angled at  $43^\circ$  to each other due to the orientation of the shared cations.

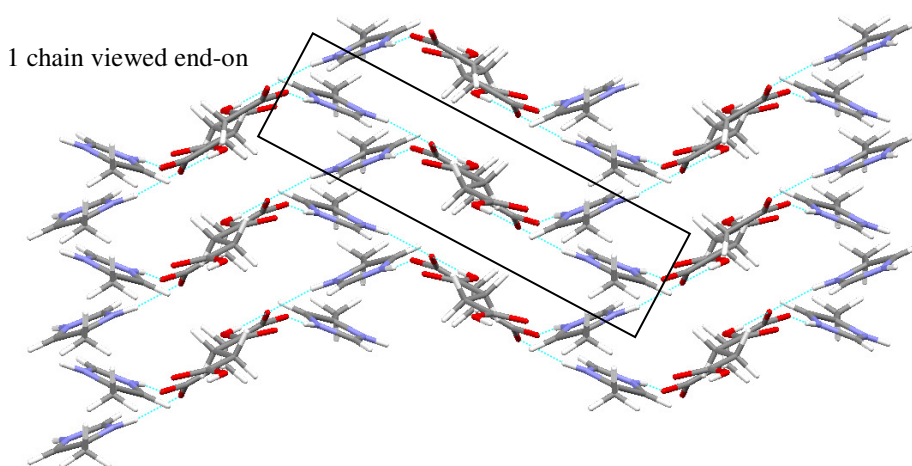


**Figure 7.5.2.3** 3-D network, one chain is highlighted; it can be seen that each of the cations are shared between two chains.

### 7.5.3 Glutaric Acid and 4-Methylimidazole

These two components crystallised in a 1:1 ratio in the monoclinic space group  $P2_1$ , with  $Z = 4$ , to form a salt. The asymmetric unit contains two monoanion-cation units (Figure 7.5.3.1).

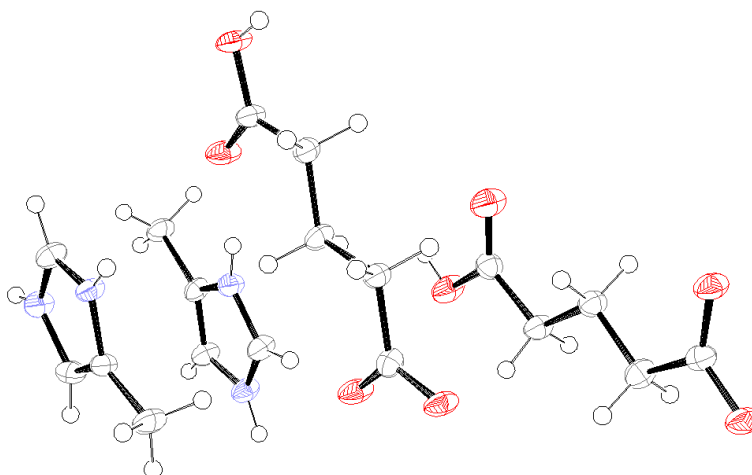


**Figure 7.5.3.1** Ortep diagram for the asymmetric unit of GIA and 4MI.

The two different monoanions in the asymmetric unit form two different hydrogen bonded chains; molecule 1 hydrogen bonds with itself in the *syn-anti* arrangement, and molecule 3 hydrogen bonds with itself in the *anti-anti* configuration. The cations are hydrogen bonded to both chains, linking them to form a flat sheet (Figure 7.5.3.2), there are also further C-H...O hydrogen bonds between the anions and cations (molecule 2 = 2.149 and 2.424 Å, molecule 4 = bifurcated, 2.316 and 2.642 Å).

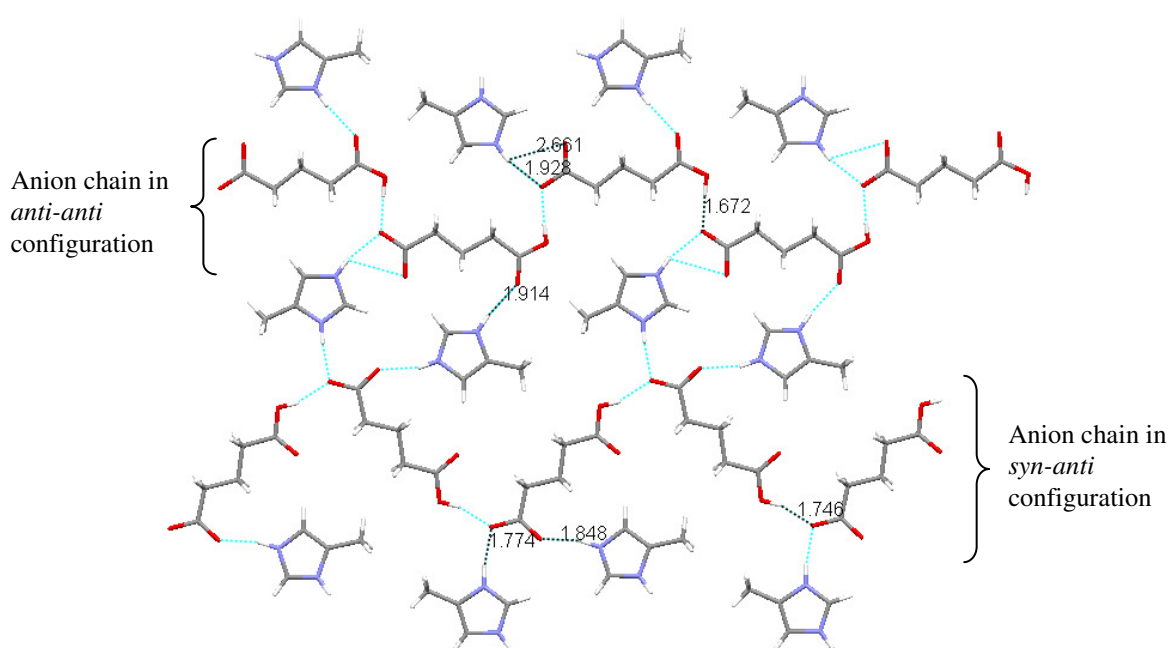


**Figure 7.5.3.2** Sheet arrangement containing both types of hydrogen bonded anion chain bridged by cations, hydrogen bond distances marked (error  $\pm 0.005$  Å).

The sheets stack on top of each other so that one type of anion chain is surrounded by the other type of anion chain (Figure 7.5.3.3). The cations form an offset stack where they are alternately orientated differently to accommodate the methyl group. The presence of  $\pi$ - $\pi$  interactions is further indicated by the fingerprint plots for the cations (Appendix, Table A11.4). There are C-H $\cdots$ O hydrogen bonds between the cation methyl groups and the anions of the adjacent sheets ( $2.617$  Å).

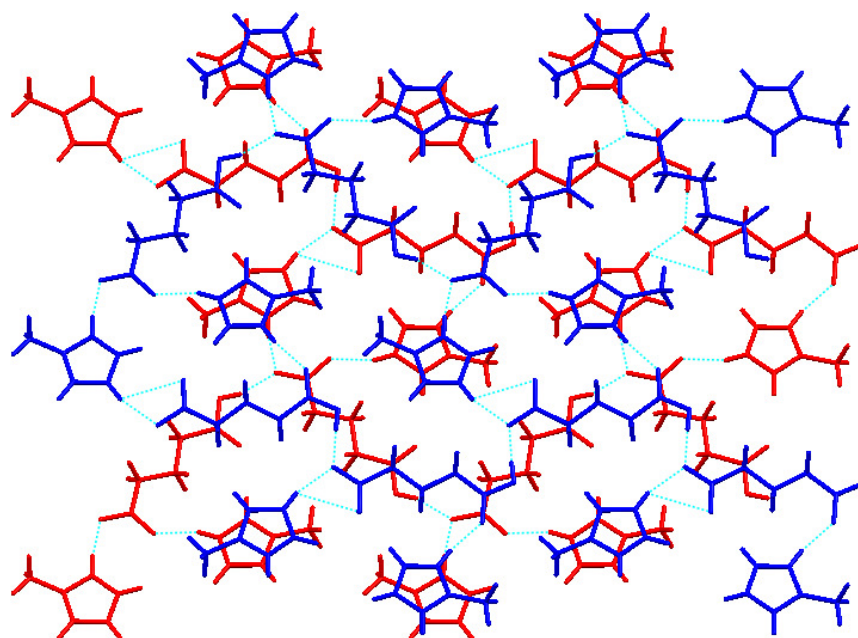


**Figure 7.5.3.3** Stacking of the sheets so as the different types of chains are next to each other – the central sheet is coloured red and the sheets above and below are coloured blue.

#### 7.5.4 Suberic Acid and 4-Methylimidazole

These compounds crystallised in a 1:1 ratio in the monoclinic space group  $P2_1/n$ , with  $Z = 4$  to form a salt (Figure 7.5.4.1). The R-factor is quite high (10.82%) however the positions of the transferable hydrogens were found easily and checked.

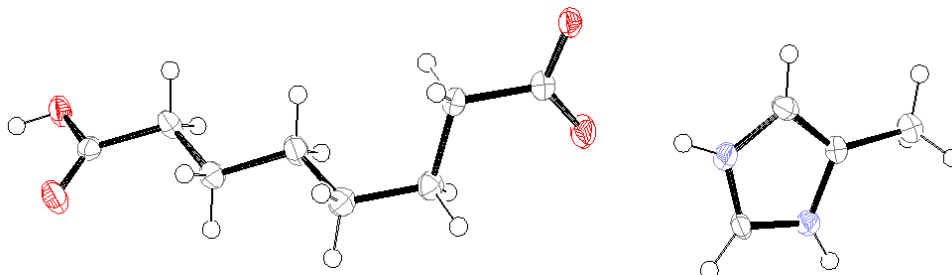


**Figure 7.5.4.1** Ortep diagram for the asymmetric unit of SbA and 4MI.

The structure consists of monoanions hydrogen bonded head-to-tail in the *syn-syn* configuration to form 1-D chains. Hydrogen bonding across the cations links the adjacent anion chains to form a sheet (Figure 7.5.4.2). The anion carbon backbone is mainly flat but adopts the *gauche* conformation across carbons 5 and 6 (torsion angle  $64.9(4)^\circ$ ). The planes of the carboxyl and carboxylate groups are also orientated at  $84.15^\circ$  to each other.

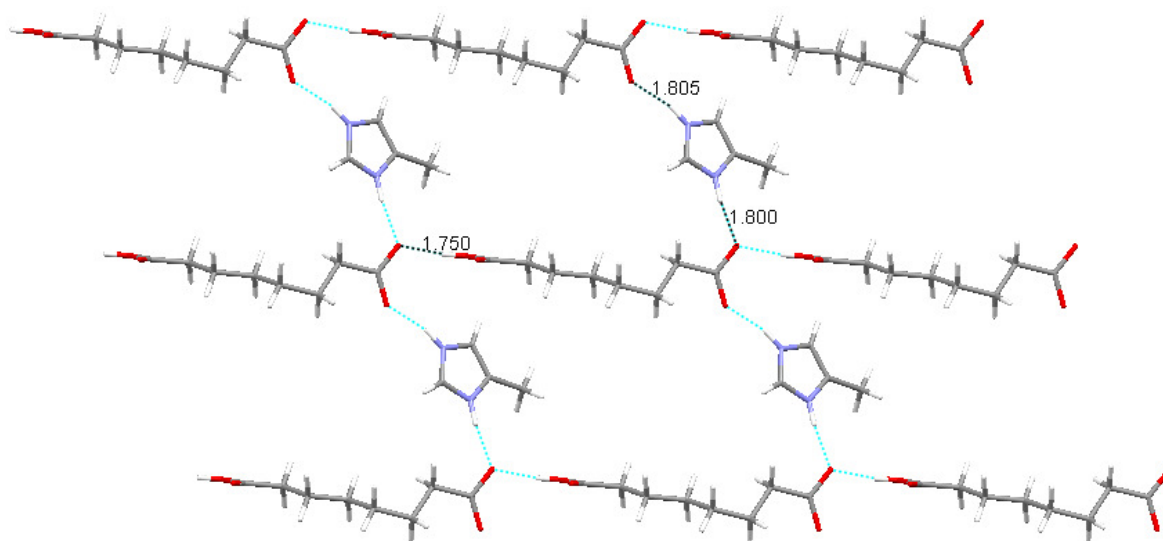


**Figure 7.5.4.2** Hydrogen bonded sheet viewed down the *b*-axis, hydrogen bond distances marked (error  $\pm 0.004$  Å).

The cations are out of the plane of the anion chains, with the methyl group pointing away from the sheet. This leads to the sheets being stacked in pairs with the methyl groups pointing to the outside of each sheet pair (Figure 7.5.4.3). The sheets are not offset along the *a*-axis so the methyl groups from each adjacent pair of sheets thereby fill the gaps in the lattice above and below. There are C-H $\cdots$ O hydrogen bonds from the cation to the anion which further stabilise the sheets (2.156, 2.716 and 2.641 Å).

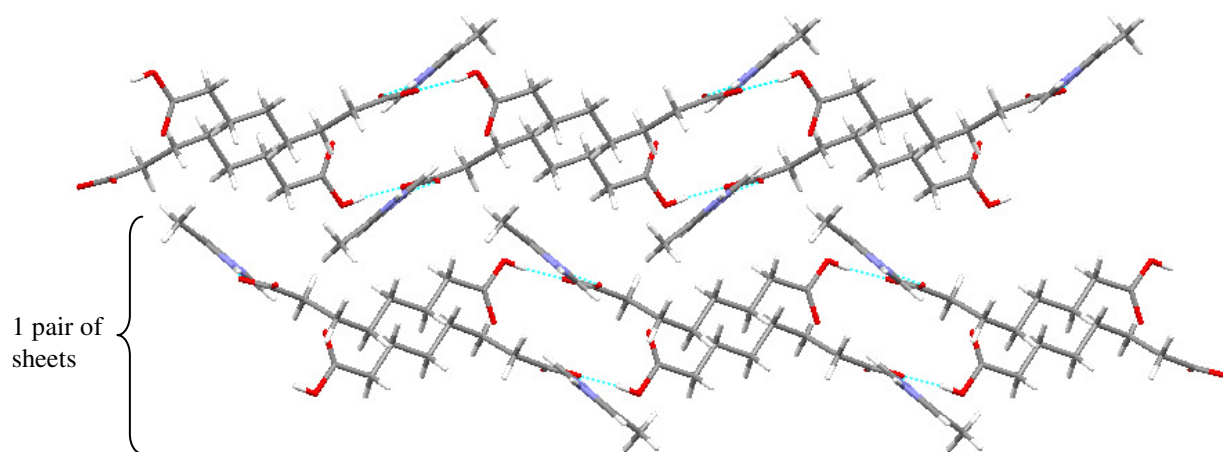


**Figure 7.5.4.3** Stacking of the sheets so as the methyl groups on the cations fill the voids in the adjacent pair of sheets.

#### 7.5.5 *L*-Tartaric acid and 4-Methylimidazole

This acid-base combination formed micro-crystals which were characterised using synchrotron data; they were found to have crystallised in a 1:1 ratio in the orthorhombic space group  $P2_12_12_1$ , with  $Z = 8$ , to form a salt.

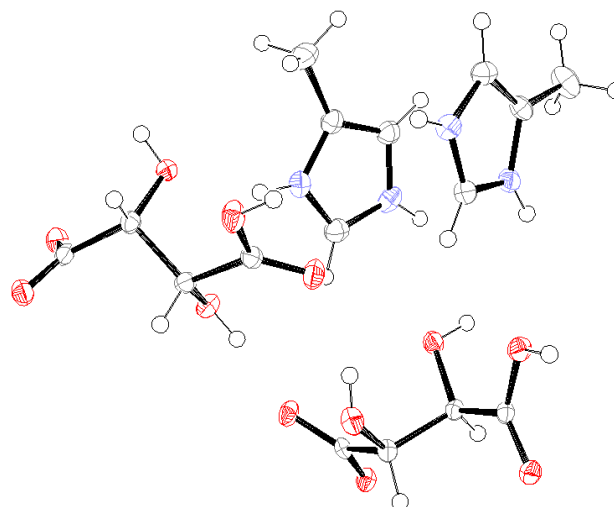


**Figure 7.5.5.1** Ortep diagram for the asymmetric unit of LTA and 4MI.

The monoanions are hydrogen bonded head-to-tail in the *syn-syn* conformation to form chains; the chains are linked by hydrogen bonds involving the anion hydroxyl groups. There are two different monoanion chains present, but their hydrogen bonding interactions are similar.



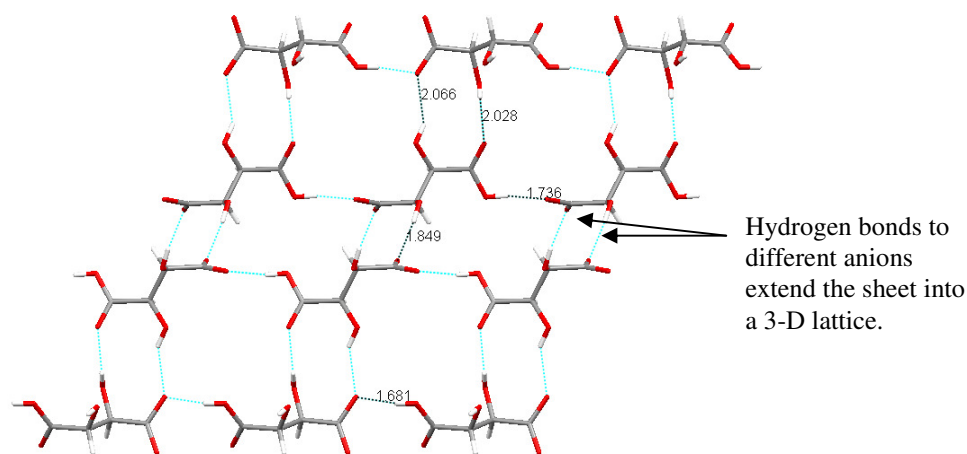


**Figure 7.5.5.2** Anion lattice, hydrogen bond distances marked (error  $\pm 0.003$  Å).

The cations are hydrogen bonded within the anion lattice; one of the anion chains has three cations subtended from it, whereas the other has only two (hydrogen bond distances for cation 2 = 1.97(1), 2.44(1), 1.95(1) and 2.68(1) Å; cation 4 = 1.91(1), 1.87(1) and 2.65(1) Å).

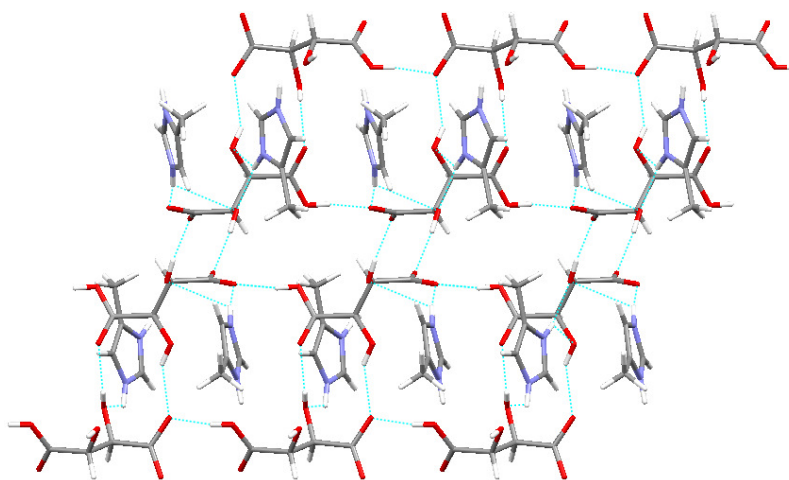


**Figure 7.5.5.3** Anion lattice with hydrogen bonded cations subtended.

The hydrogen bonding across the cations strengthens the anion lattice by further linking the anion chains. There are also weak C-H...O hydrogen bonds (cation 2 = 2.719, 2.470 and 2.648 Å; cation 4 = 2.376, 2.523, 2.391, 2.658 and 2.691 Å) that further stabilise the structure. The cations are stacked over each other, however, due to the large distance between the centroids (3.750 Å) and the orientation of the molecule,  $\pi$ -interactions between them are unlikely. When the 3-D lattice is viewed down the *b*-axis the two different types of anion chain can be seen:

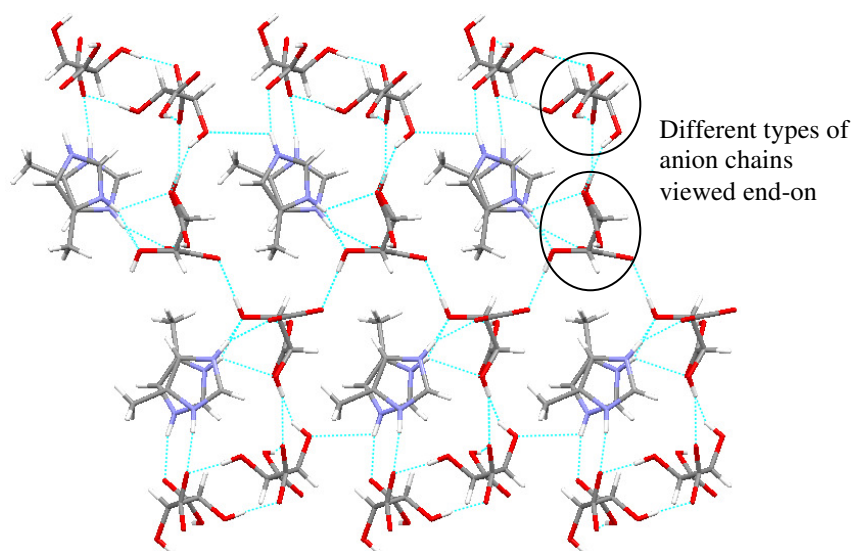


**Figure 7.5.5.4** Anion and cation hydrogen bonded lattice.

#### 7.5.6 *DL-Tartaric Acid and 4-Methylimidazole*

These compounds crystallised in a 1:1 ratio with water in the triclinic space group *P*-1, with *Z* = 2, to form a salt monohydrate.

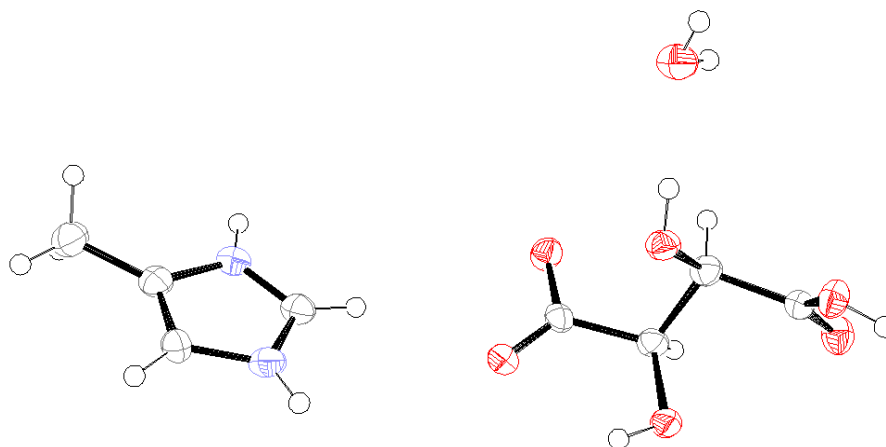


**Figure 7.5.6.1** Ortep diagram for the asymmetric unit of DLTA and 4MI.

The monoanions are hydrogen bonded head-to-tail in the *syn-syn* conformation to form chains; pairs of chains are linked together by hydrogen bonding between the carboxylate and hydroxyl groups to form a tape. The base molecules are positioned between the pair of chains and are hydrogen bonded to the hydroxyl groups of both, further strengthening the tape by N-H...O and C-H...O hydrogen bonds (distances for the former are marked in Figure 7.5.6.2, distances for the latter are 2.447, 2.517, 2.487, 2.658 and 2.622 Å).



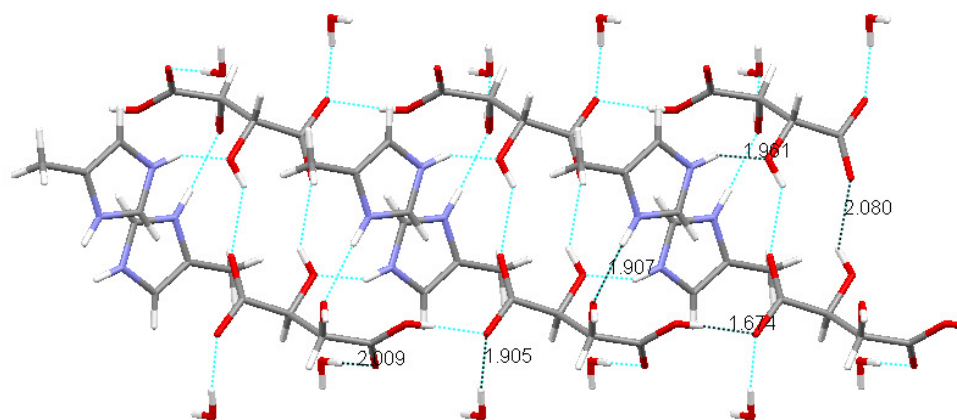


**Figure 7.5.6.2** Tape structure with subtended water molecules, N-H...O and O-H...O hydrogen bond distances marked (error  $\pm 0.004$  Å).

Water molecules are subtended from the tape and link adjacent tapes to form a 3-D network (Figure 7.5.6.3). Pairs of cations are stacked on top of each other in a parallel offset manner with the hydrogen of the protonated nitrogen over the centre of the cation ring (distance between centroid and H =  $3.265$  Å) which suggests the presence of  $\pi$ -interactions between the cations. This is not clear from the fingerprint plot (Appendix, Table A11.4).

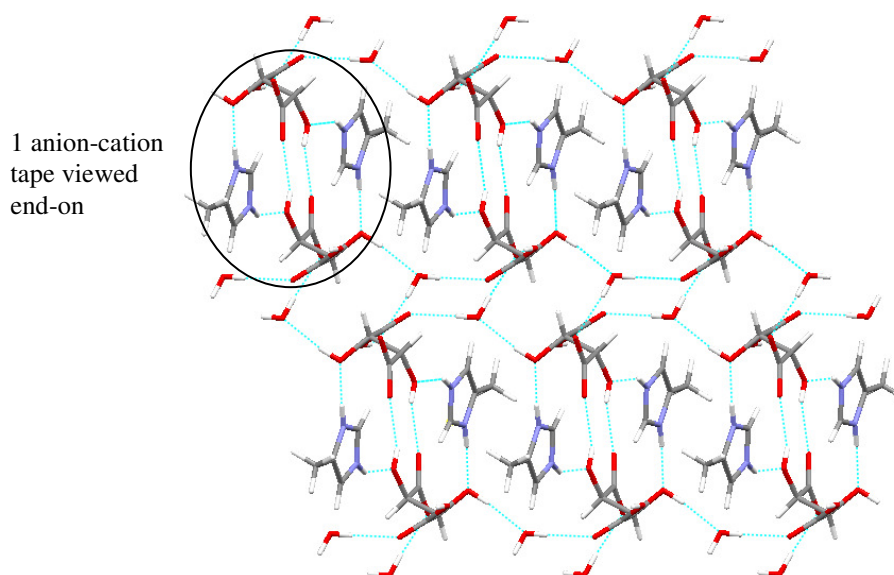


**Figure 7.5.6.3** 3-D network made up of anion-cation ladders linked by water molecules.

### 7.5.7 Maleic Acid and 4-Methylimidazole

These two compounds formed an oil from the well-plate crystallisations, however using Method 3 a solid product was formed that was found to contain the components in a 1:1 ratio in the monoclinic space group  $P2_1/c$ , with  $Z = 4$ , to form a salt (Figure 7.5.7.1). There is a strong intramolecular hydrogen bond ( $1.57(1)$  Å) between the carboxyl and carboxylate groups of the monoanion.

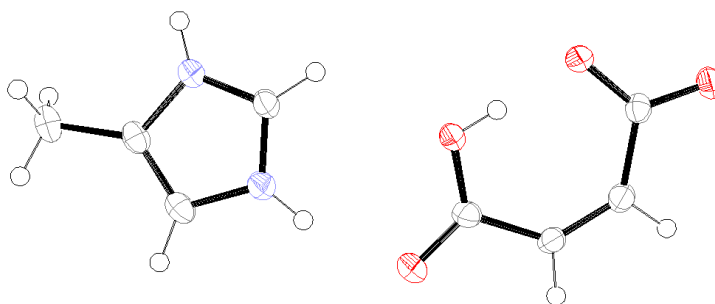


**Figure 7.5.7.1** Ortep diagram for the asymmetric unit of MeA and 4MI.

The components are hydrogen bonded together via N-H...O contacts to form a quadruplet (1.91(1), 1.94(1) and 2.58(1) Å). Further cation-anion and anion-anion weak aromatic C-H...O hydrogen bonds link adjacent quadruplets in to a 3-D array (2.373, 2.426, 2.484 and 2.633 Å, and 2.685 Å respectively). C-H...O hydrogen bonds from the methyl group further stabilise the array (2.633 and 2.709 Å).

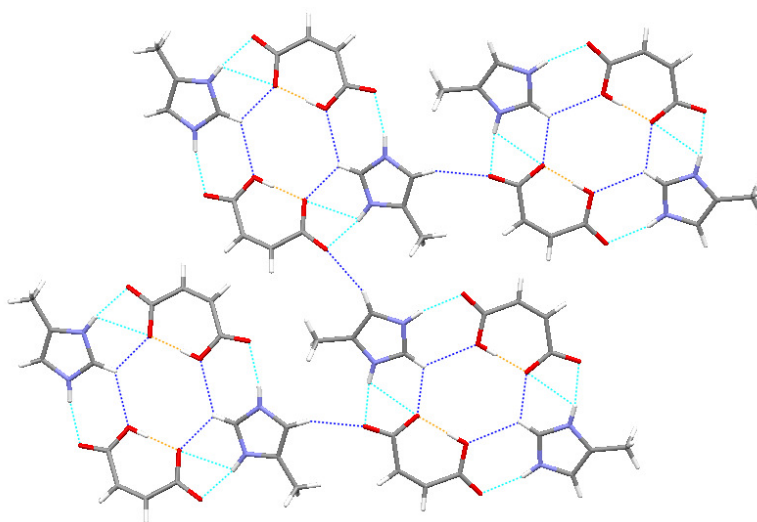


**Figure 7.5.7.2** Hydrogen bonded sheet; N-H...O light blue, C-H...O dark blue, O-H...O orange.

The units are stacked on top of each other in an offset manner so as the molecules of adjacent sheets do not eclipse each other.

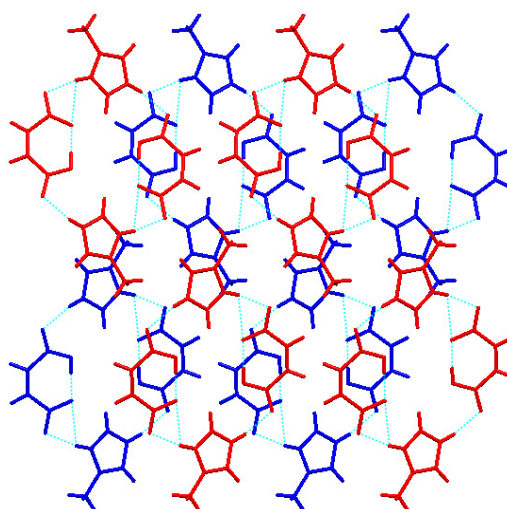


**Figure 7.5.7.3** Stacking of units - units form sheets, one is coloured red, the adjacent is coloured blue.

### 7.5.8 Discussion of 4-Methylimidazole Structures

MnA, AdA and PmA all produced oils via both crystallisation methods. PXRD analysis of the FmA-4MI combination gave a weak powder whose main peaks, though very weak, did not match that of FmA. HSM showed the compound to melt at 139-148°C which is significantly higher than the melting point of the base, and lower than that of the diacid, suggesting that a new binary compound may have formed.

Similarly to OxA-2MI, OxA-4MI crystallises in a 1:2 acid:base ratio with the OxA molecule having been di-deprotonated. The components again form sheets which, in this case, are linked by hydrogen bonding across water molecules to create a 3-D network. All the other structures have a 1:1 acid-base stoichiometry and contain monoanions except ScA-4MI which forms a mixed system. This is a little unexpected from the  $pK_a$  values as the second ionisation of the diacid has a  $pK_a$  difference of 1.88 units. MeA-4MI forms quadruplets, similar to those found in MeA-Im, with a strong intramolecular hydrogen bond in the monoanion.

Although the 4MI structures predominantly consist of 3-D networks rather than sheets, similarities with the other Im derivative structures can be drawn. ScA-4MI forms a 3-D structure that is made up of interconnecting stepped sheets. This basic sheet structure is similar to **Sheet 4** (Figure 7.3.7.1) with its cations pointing in opposite directions, however, the anion chains are hydrogen bonded in the *syn-anti* conformation. GlA-4MI forms sheets similar to **Sheet 6** (Figure 7.4.10.2), but which contain two types of parallel anion-anion chain; one is hydrogen bonded in the *anti-anti* configuration and the other is in the *syn-syn* arrangement. This is possible as  $Z'$  is greater than 1, with two monoanion-cation units in the asymmetric unit. SbA-4MI forms sheets similar to **Sheet 5** (Figure 7.4.10.2) but with the methyl group on the cation pointing in the opposite direction to the carboxyl group of the anion. The cation also protrudes out of the plane of the sheet therefore the methyl group of the cation of one sheet fills the void between the cations of the adjacent sheet. The torsion in the anion in the SbA-4MI structure may also increase the close packing and enable better accommodation of the methyl group into the structure than that of a flat alkyl chain in the *anti* conformation.

LTA-4MI is unusual within the TA-Im derivatives as it has  $Z' > 1$  with two monoanion-cation units in the asymmetric unit. Similarly to the GlA-4MI structure, this creates two types of anion chain which create a 3-D lattice. The cations then fit within this lattice, stabilising the 3-D network rather than linking adjacent anion sheets. DLTA-4MI also forms a different structure to those seen before, with pairs of anti-parallel anion chains from which the cations are subtended. The manner in which the cations are subtended is also uncommon to the TAs; the cations are hydrogen bonded to the anions via the hydroxyl groups rather than via the carboxyl or carboxylate groups. Water molecules

then connect the pairs of anion chains, a feature that is also not seen in any of the other TA-Im derivatives binary compounds.

The larger proportion of 3-D structures in the 4MI series may be due to the position of the methyl group on the base preventing close packing when in a flat orientation in line with the anions. Instead the cation is often lifted out of the plane of the anion chain/sheet to accommodate the bulky group. This also lifts the second hydrogen bond donor and hence hydrogen bonds are formed with anions in a different plane. This also results in fewer weak C-H...O hydrogen bonds from the methyl and aromatic CH groups of the cation.

The melting point and density of these structures decreases as the diacid chain length increases (Appendix, Table A8). MnA-4MI, for which no crystal structure was obtained, has the lowest melting point in the series. Its instability is reflected by its unwillingness to crystallise. The formation of hydrates in the OxA and DLTA structures does not lower the melting point, instead these two compounds have the highest melting point reflecting the added stability the incorporation of the solvent provides in these cases. The density of these structures is similar to the other structures in the series, suggesting it is the hydrogen bonding that is improved by the incorporation of the water rather than the close packing. The correlation of density with melting point is also the poorest for these two compounds.

## 7.6 1,2-DIMETHYLIMIDAZOLE

### 7.6.1 Succinic Acid and 1,2-Dimethylimidazole

These two compounds crystallised in a 1:1 acid:base ratio in the orthorhombic space group *Pccn*, with *Z* = 8, to form a salt. The monoanion adopts the *gauche* conformation (torsion angle  $-69.2(3)^\circ$ ) (Figure 7.6.1.1).

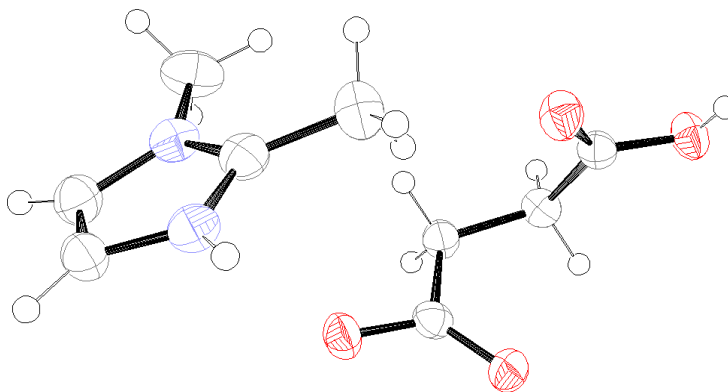
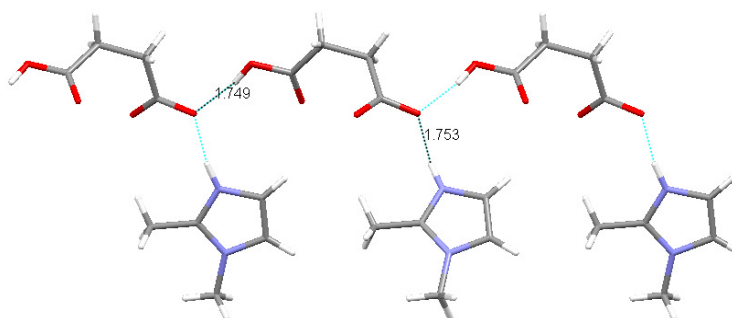


Figure 7.6.1.1 Ortep diagram for the asymmetric unit of ScA and DMI.

The monoanions are hydrogen bonded head-to-tail in the *syn-anti* conformation to form a chain from which the cations are subtended (Figure 7.6.1.2). The methyl group on atom N23 of the cation prevents further hydrogen bonding. The cations are positioned alternately in front of and behind the plane of the anion backbone.



**Figure 7.6.1.2** Chain structure with the anion backbone and subtended cations (hydrogen bond distance error  $\pm 0.003$  Å).

Adjacent chains are arranged into pairs so as the cations are interdigitating and the carbon chains of the anions are adjacent to each other (Figure 7.6.1.3). There are C-H...O hydrogen bonds from the aromatic CH and methyl groups of the cation to the anion (2.220 and 2.556 Å, and 2.442, 2.514, 2.645 and 2.623 Å) which strengthen the cation-anion chain and also link adjacent chains. The pairs of chains are positioned directly above each other to form a stack; adjacent stacks of pairs are arranged in a staggered fashion so as anions are beside cations.

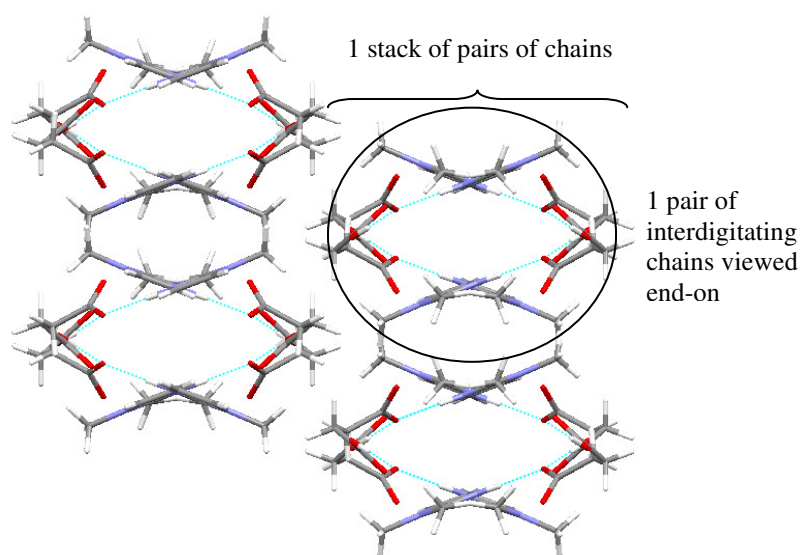


**Figure 7.6.1.3** Arrangement of the chains into pairs which are linked by C-H...O hydrogen bonds.

### 7.6.2 Glutaric Acid and 1,2-Dimethylimidazole

These compounds crystallised in a 1:1 ratio in the orthorhombic space group  $Pna2_1$ , with  $Z = 4$ , to form a salt.

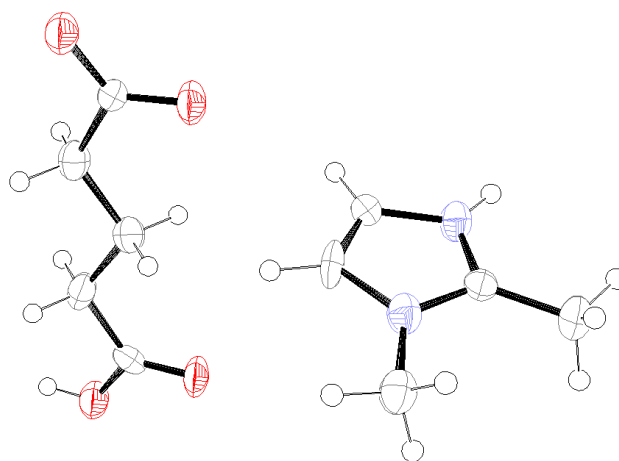


**Figure 7.6.2.1** Ortep diagram for the asymmetric unit of GlA and DMI.

This combination consists of planar chains of monoanions hydrogen bonded head-to-tail in the *anti-anti* configuration, with cations subtended from this chain (Figure 7.6.2.2).

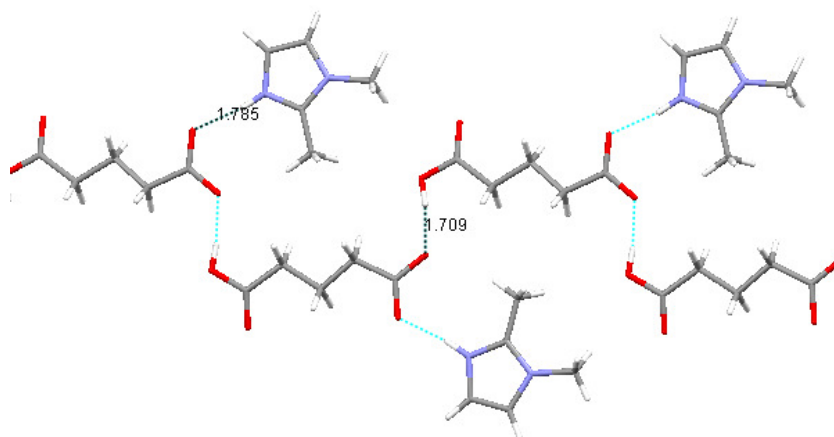


**Figure 7.6.2.2** The hydrogen bonded chain of anions and cations (error  $\pm 0.006$  Å).

The chains are then arranged into stacks – the molecules are positioned directly over each other but at an angle of approximately  $45^\circ$  to the direction of the stack. Adjacent stacks are at  $84^\circ$  to each other resulting in the arrangement shown in Figure 7.6.2.3. The positioning of the molecules enables C-H $\cdots$ O hydrogen bonds between the aromatic CH groups and anions in the adjacent stack (2.468 and 2.555 Å), as well as C-H $\cdots$ O hydrogen bonds involving the methyl groups of the cations (2.607, 2.705, 2.506, 2.555 and 2.404 Å) thus creating a 3-D network. The parallel and offset orientation of the molecules and the position of the methyl group over the centre of the cation ring suggests the possibility of C-H $\cdots\pi$  interactions. In spite of the non-classical orientation of the hydrogen with it not pointing towards the centre of the ring, the presence of C-H $\cdots\pi$  interactions is supported by the wing on the fingerprint plot (Appendix, Table A11.5). The complementary wing on the plot is hidden under other H $\cdots$ H interactions.

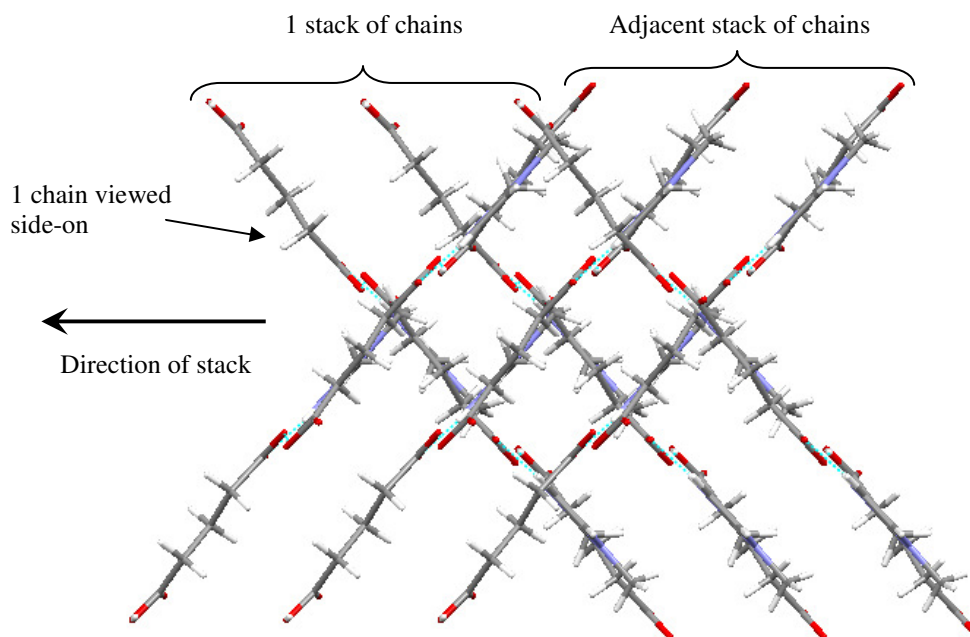


**Figure 7.6.2.3** Arrangement of the chains into stacks and the orientation of adjacent stacks, viewed down the *b*-axis.

### 7.6.3 *L*-Tartaric Acid and 1,2-Dimethylimidazole

These two compounds crystallised in the monoclinic space groups  $P2_1$ , with  $Z = 2$ , to form a salt. The contents of the asymmetric unit are shown in Figure 7.6.3.1.

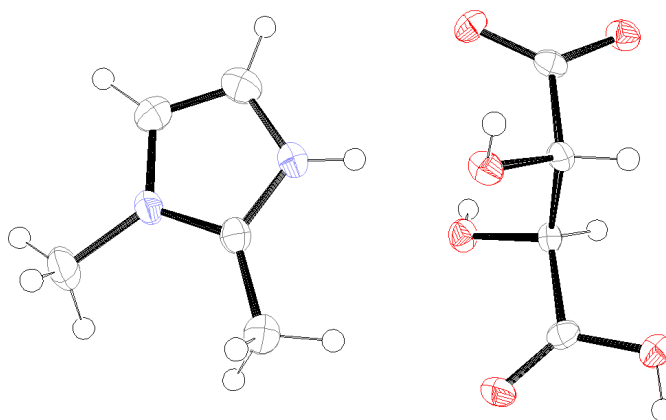


**Figure 7.6.3.1** Ortep diagram for the asymmetric unit of LTA and DMI.

The monoanions are hydrogen bonded head-to-tail in the *syn-syn* conformation and also between the carboxylate and hydroxyl groups to create a sheet. The hydrogen bond distances of which are shown in Figure 7.6.3.2.



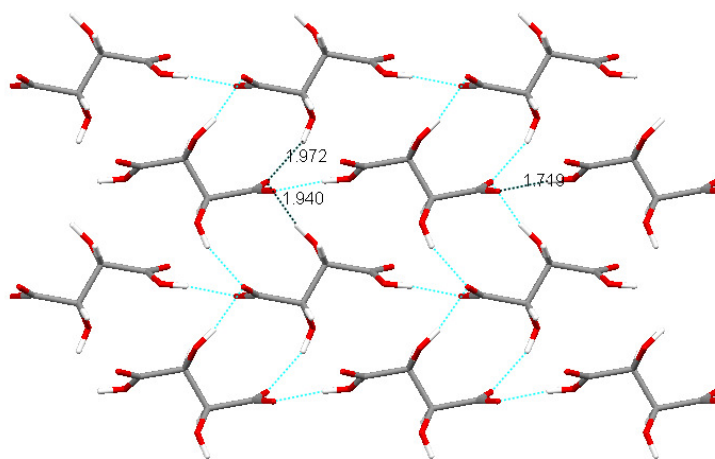


**Figure 7.6.3.2** Hydrogen bonded lattice of anions (error  $\pm 0.003$  Å), viewed down the  $c$ -axis.

Cations are subtended above and below the anion lattice in a trifurcated N-H $\cdots$ O hydrogen bond involving both of the anion hydroxyl groups and the carboxylate group (2.37(4), 2.19(3) and 2.58(3) Å respectively). Adjacent sheets then fit together with the cations interdigitating (Figure 7.6.3.3); both of the methyl groups of the cations are involved in C-H $\cdots$ O hydrogen bonding with the anions of the adjacent sheet (2.433, 2.676, 2.563 and 2.634 Å). One of the aromatic carbons is involved in C-H $\cdots$ O hydrogen bonding with the anions of the same sheet (2.191 Å). The cations are stacked in an offset manner however they are not parallel and their orientation with respect to each other is not conducive of  $\pi$ -interactions. The anions of the adjacent sheets are stacked directly over each other.

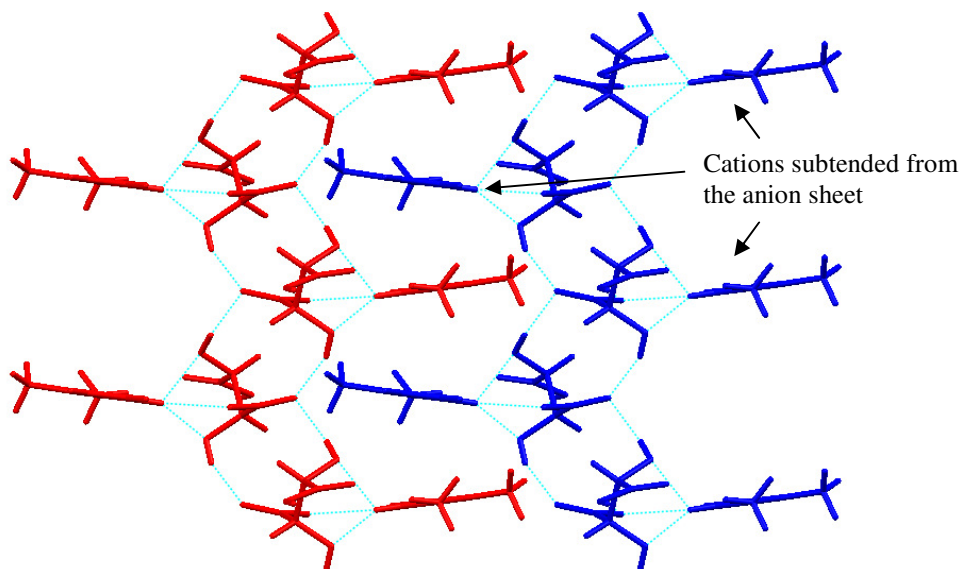


**Figure 7.6.3.3** Two adjacent sheets (coloured red and blue) viewed side-on with cations subtended either side of the anion core, viewed down the  $a$ -axis.



#### 7.6.4 *DL- Tartaric Acid and 1,2-Dimethylimidazole*

The compounds crystallised in a 1:1 ratio in the triclinic space group *P*-1, with *Z* = 2, to form a salt. During the latter stages of refinement SHELX<sup>11</sup> suggested alternative positions for the hydrogen atoms of the hydroxyl group on carbon 2. These were included in the refinement by modelling the hydrogen atoms as disordered with half occupancy in each position; this reduced the R-factor to 9.63%. When the structure was viewed it was found that there is hydrogen bonding between the hydroxyl groups on carbon 2 of adjacent monoanions. Although the two suggested positions have been included here, with the high R-factor and the very small mass of half a hydrogen, their positions cannot be conclusively determined.

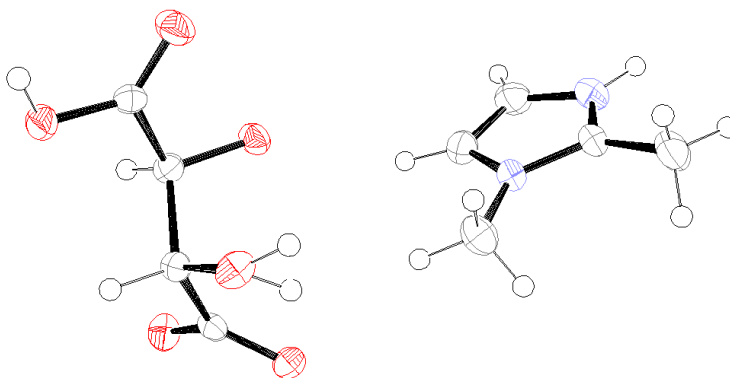


**Figure 7.6.4.1** Ortep diagram for the asymmetric unit of DLTA and DMI.

The monoanions are hydrogen bonded together head-to-tail (1.682 Å) to form a chain. Further hydrogen bonding between the hydroxyl groups results in a sheet.

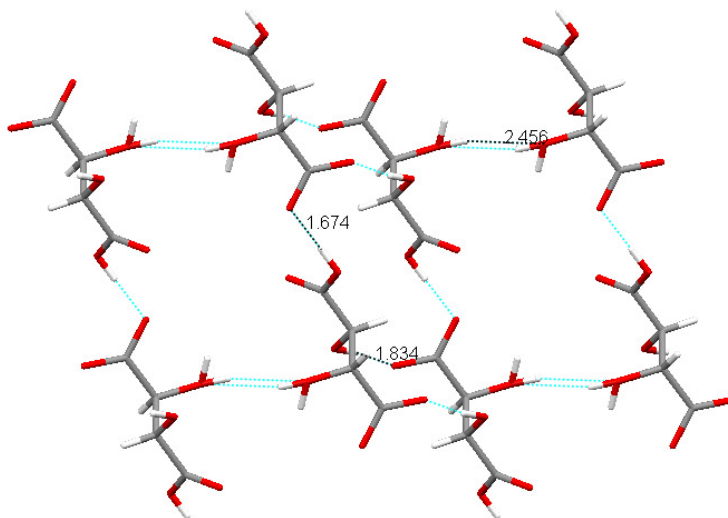


**Figure 7.6.4.2** Anion lattice, hydrogen bond distances marked (error +/-0.006 Å).

The cations are then subtended either side of the anion-sheet via a bifurcated hydrogen bond to the carboxyl and hydroxyl groups (2.00(5) and 2.29(5) Å respectively):

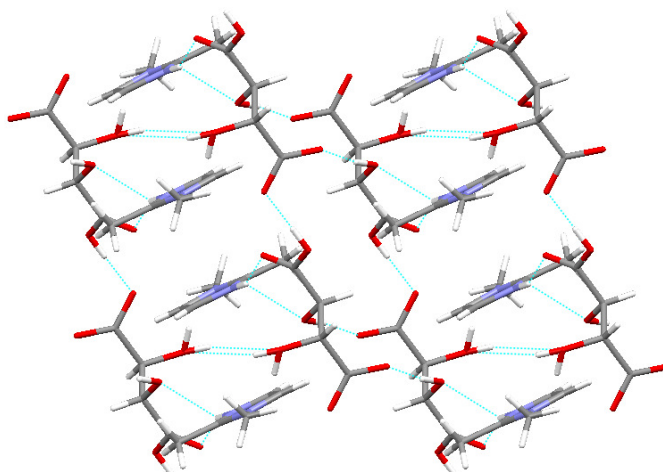


**Figure 7.6.4.3** Sheet structure with cations subtended.

The sheets are arranged so as the cations from adjacent sheets are interdigitating; the methyl groups are pointing in different directions so as the molecules can be more closely packed. The parallel cations are positioned on top of each other to form a stack, however they are not offset and the large distance between the centroids of the rings (3.856 Å) together with evidence from the fingerprint plot (Appendix, Table A11.5) suggests dipole-dipole interactions rather than  $\pi$ -interactions are present. A 3-D network is created as adjacent sheets are linked by C-H...O hydrogen bonds from the ring and methyl carbons of the cations (2.271 and 2.424 Å, and 2.599, 2.645, 2.507, 2.456 and 2.480 Å respectively).

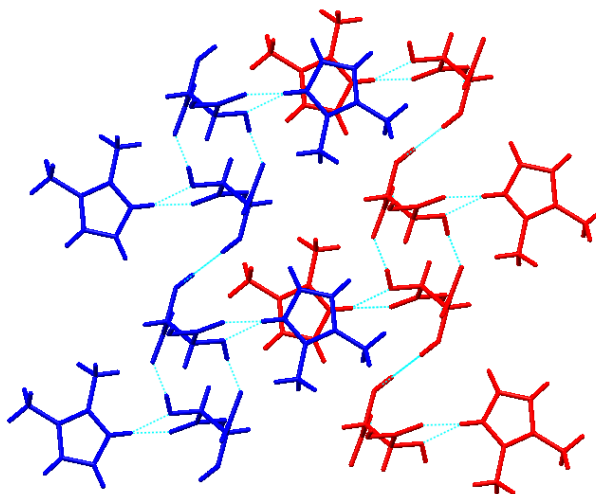


**Figure 7.6.4.4** Arrangement of sheets viewed end-on (down the  $a$ -axis); each sheet is coloured differently, the interdigitating cations of adjacent tapes stack on top of each other.

#### 7.6.5 Fumaric Acid and 1,2-Dimethylimidazole

These compounds crystallised in a 1:1 ratio in the monoclinic space group  $P2_1/n$ , with  $Z = 4$ , to form a salt. The contents of the asymmetric unit are shown in Figure 7.6.5.1. In spite of the high R-factor (10.20%) all the transferable hydrogens were located easily.

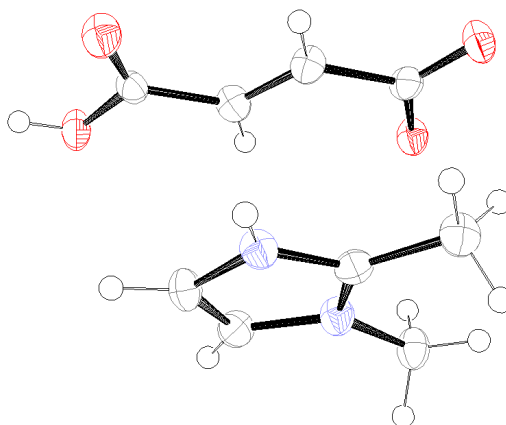


**Figure 7.6.5.1** Ortep diagram for the asymmetric unit of FmA and DMI.

The monoanions are hydrogen bonded head-to-tail in the *syn-anti* arrangement (1.72(1) Å) to form a zigzag chain. The cations are subtended in the same plane from the anion chains (1.78(1), 2.52(1) Å); the chains are then arranged into a sheet where the cations of adjacent chains are interdigitating, with C-H...O hydrogen bonds from the cation ring (2.610 Å) and methyl group (2.577, 2.661 Å) to the anion carboxyl group. One of the cation aromatic CH groups is not involved in any hydrogen bonding.

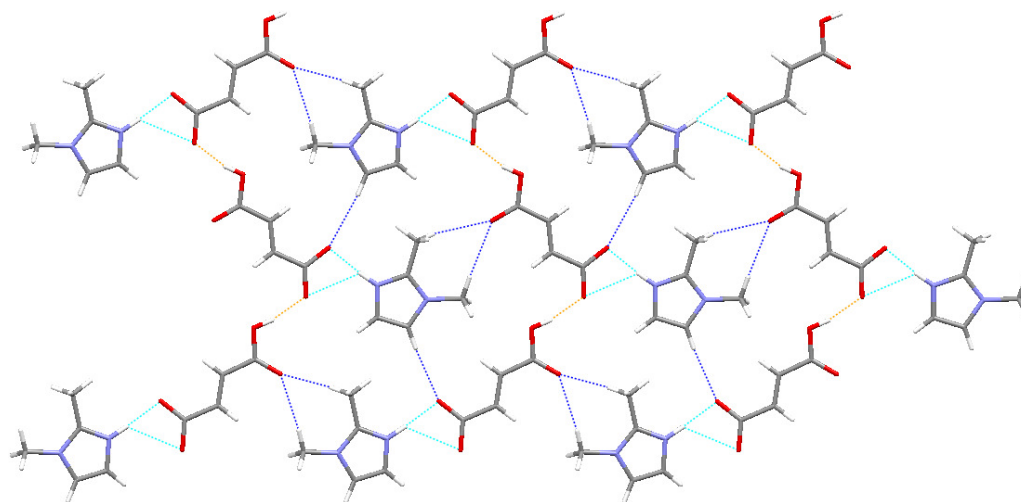


**Figure 7.6.5.2** Sheet structure of hydrogen bonded anions and cations, O-H...O orange, N-H...O light blue, C-H...O dark blue.

The sheets are then stacked so as the anions are above and below the cations and vice versa (Figure 7.6.5.3). The positioning of the anion double bond over the centre of the cation ring allows  $\pi$ - $\pi$  interactions between the ions. This is further supported by the features on the fingerprint plots of both the anion and the cation (Appendix, Table A11.5). There are also weak C-H...O hydrogen bonds between the methyl groups of the cations and the anions in adjacent sheets (2.644 Å).

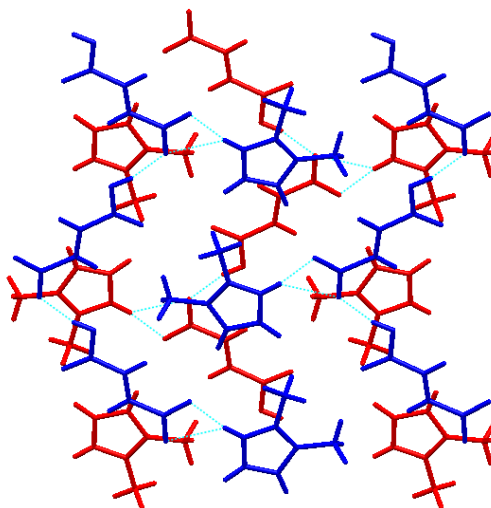


**Figure 7.6.5.3** Stacking of ‘sheets’, one is coloured red, the adjacent are coloured blue.

#### 7.6.6 Discussion of 1,2-Dimethylimidazole Structures

DMI forms the fewest binary compounds in the Im series, forming oils with OxA, MnA, AdA, PmA, SbA and MeA. This is due to there being two bulky methyl groups to accommodate into the structure, one of which is positioned on a nitrogen thus also preventing hydrogen bonding from this donor. The structures therefore predominantly consist of chain arrangements which are further stabilised by C-H...O hydrogen bonds from the methyl and aromatic CH groups of the base. The ScA-DMI structure is unusual in that the monoanion adopts the *gauche* conformation; in all the other ScA-Im derivative binary compounds the diacid has adopted the *anti* conformation.

The only structure to form a sheet similar to those seen elsewhere in the aromatic amines series is FmA-DMI. This structure is an adaptation of **Sheet 5** (Figure 7.4.10.2) with the anion chains hydrogen bonded together in the *syn-anti* configuration. The manner in which the cations are hydrogen bonded to the anion backbone is also slightly different with C-H...O hydrogen bonds instead of N-H...O linking one side of the cation. This hydrogen bonding configuration accommodates the second methyl group of the base into the structure.

LTA and DLTA form sheets instead of the 3-D structures seen elsewhere in the series. This is due not only to the increased size of the cation with two methyl groups so as it cannot fit into cavities created in an anion lattice, but also because of the unavailability of one of the hydrogen bond donors. In spite of this, the melting points are higher for the TA-DMI structures than those for the 1MI and 4MI structures, which is unexpected. The central feature along the diagonal of the DLTA fingerprint plot in DLTA-DMI is an artefact from the interaction of the disordered hydrogens on one of the hydroxyl groups and would not actually occur in the structure (Appendix, Table A11.5).

All of the DMI binary compounds contain a 1:1 acid:base stoichiometry and hence all of the diacids are mono-deprotonated. Another feature of the DMI binary compounds is their high melting points. The lowest melting DMI binary compound melts at 101.39° (GIA-DMI) which is higher than the lowest melting point for a characterised binary compound for each of the other bases in the Im derivatives series.

## 7.7 DISCUSSION OF IMIDAZOLE DERIVATIVES

The relationships between the different sheet types and their prevalence throughout the aromatic amines are shown on the next page in Figure 7.7. Twenty-one out of the above thirty-five structures follow at least the basic element of the sheet structures. Only three of the TA structures do not consist of one of the sheet structures; two form a 3-D anion lattice which the cation fits into though its hydrogen bonding is not integral to the lattice structure itself, and the remaining TA forms tapes due to the presence of water in the structure. The MnA and MeA structures also do not form sheets due to their strong intramolecular hydrogen bond preventing the formation of anion chains. OxA only forms one sheet structure with Im, perhaps the size of the cation for the methylated Ims prevents the formation of a sheet structure with this small anion.

The patterns in various other properties throughout the series are detailed in the rest of this section.

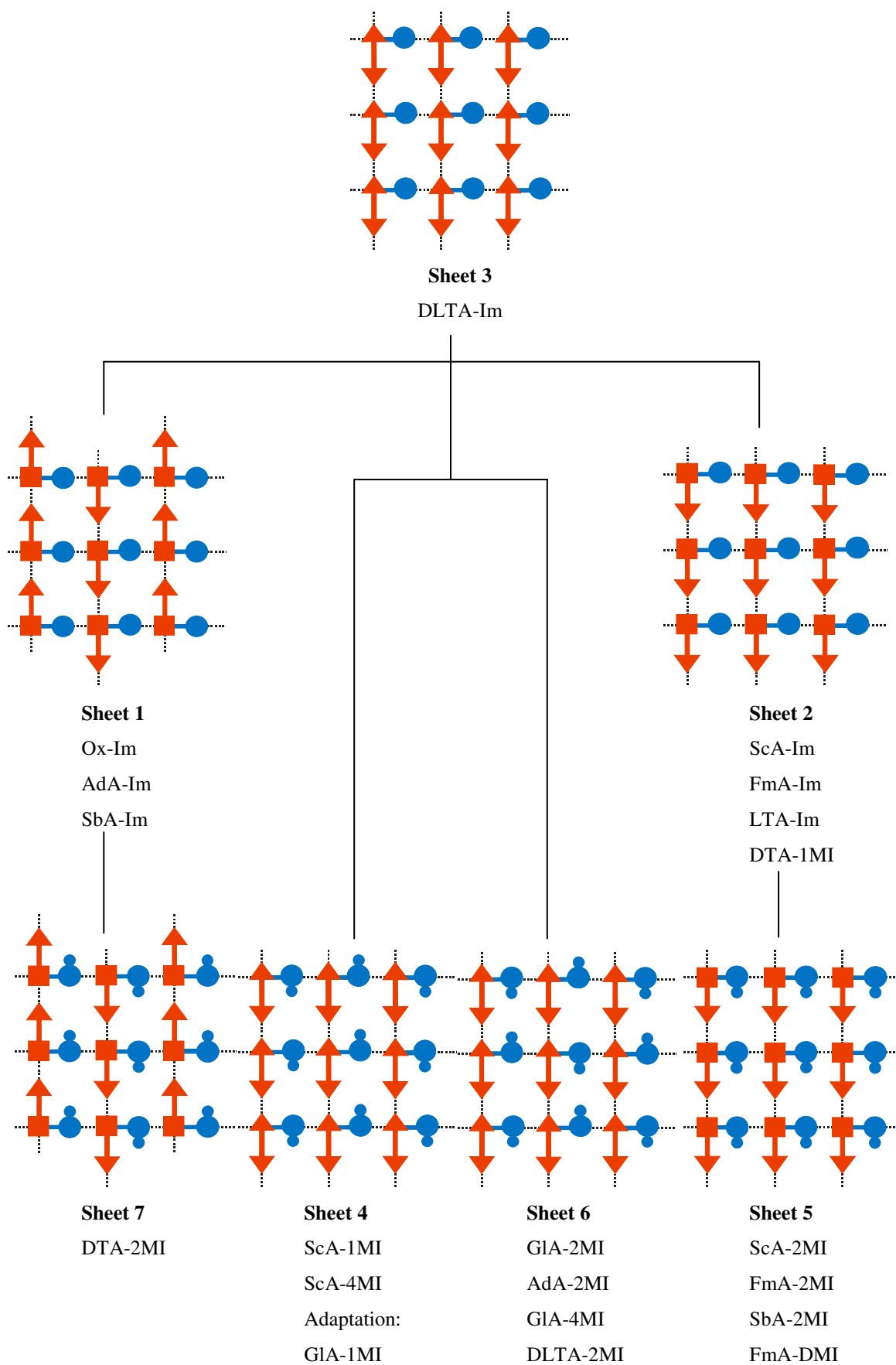


**Figure 7.7** Tree diagram showing the relationships between the schematic sheet structures in the Im derivative binary compounds.

### 7.7.1 Density and Melting Points

Figure 7.7.1 shows the melting points for each of the Im derivative binary structures. The TA and OxA combinations are the highest melting structures across the aromatic amines. ScA and FmA follow this trend closely showing that binary structures where the diacid contains four carbons are the most stable (obviously MeA is an exception). The high melting points of the OxA structures are unexpected but can be attributed to the cation and anion being of a complimentary size and hence close packing and close proximity of the hydrogen bonding groups contributes to the melting point. The SbA compounds have the lowest melting point which is as expected.

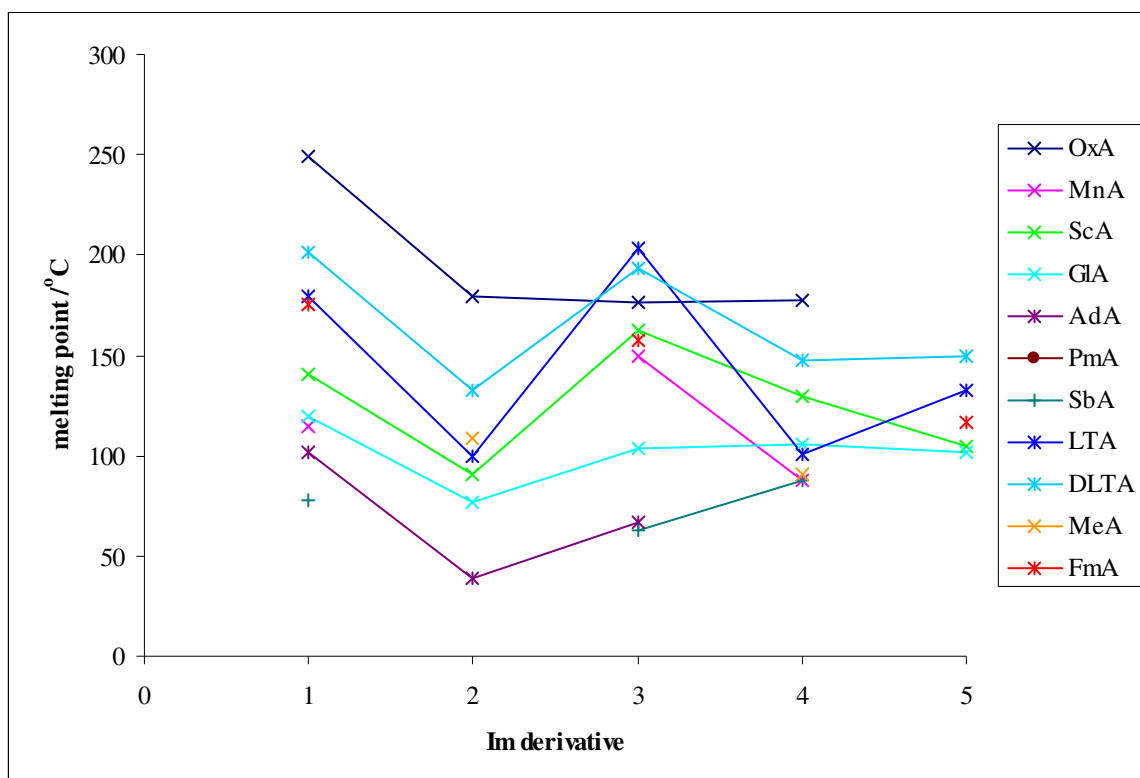


**Figure 7.7.1** Graph to show the variation in melting point with the Im derivative, 1 = Im, 2 = 1MI, 3=2MI, 4=4MI, 5=DMI. The points are not actually related and the fact that they are joined is purely for clarity when viewing the trends for each diacid.

### 7.7.2 Deprotonation and Stoichiometry Trends

From this series, it appears that short odd and long odd diacids, MnA and PmA, have difficulty crystallising as binary compounds, the optimum number of carbons being 4-5 and preferably an even diacid. The most common diacids to crystallise with the Im derivatives are ScA and the TAs. The Im derivative binary compounds mainly consist of a 1:1 acid:base stoichiometry; the only exceptions to this are OxA-4MI which has a 1:2 acid:base ratio and SbA-Im which has a neutral SbA chain weaving through the 1:1 sheet structure. There are only three hydrates which are dispersed throughout the series.

### 7.7.3 Bond distances

The C-O bond lengths vary significantly with the number and type of hydrogen bond donors linked to the oxygen atom. For the deprotonated carboxylate groups in this series, the difference between the C-O bond lengths is generally less than 0.06 Å; this concurs with the differences found by MacDonald *et al.* to be between 0.003 and 0.075 Å.<sup>9</sup> The larger differences in the C-O distances are due to strong hydrogen bonding lengthening the covalent C-O bond. Protonated carboxyl groups in this series generally have a difference between the C-O and C=O bond lengths of greater than 0.06 Å. GlA-1MI is an anomaly where the difference between the bond lengths is 0.031(8) Å for one of the carboxyl groups and 0.122(8) Å for the other. The only difference between these two groups is the number and strength of C-H...O hydrogen bonds to the C=O group; there are three CH hydrogen bonds to the carbonyl oxygen of the former carboxyl group, but only two to the latter. As C-H...O hydrogen bonds are relatively weak, the small difference in bond lengths for the carboxyl groups is unexpected. The other anomaly is for a disordered carboxyl group (SbA-2MI).

### 7.7.4 Hydrogen bonding

The most common configuration for the hydrogen bonded acid/anion chain is *syn-syn*, which has a range of O...O distances from 2.443-2.682 Å. *Anti-anti* and *syn-anti* are also present with the *anti-anti* interactions generally shorter than the overall average O...O distance (2.530 Å) and the *syn-anti* interactions longer than the average. All the TAs are hydrogen bonded together in *syn-syn* conformation.

There are four instances of possible single well or low barrier double well hydrogen bonds within the series all of which occur for O-H...O hydrogen bonds. In fact, the only structures where the acidic hydrogen cannot be located to just one carboxyl group occur within the aromatic amines series (DLTA-Im, ScA-1MI and GlA-2MI). This highlights the strength of the anion-anion chains in the Im derivatives structures. The only other instance of disorder of the acidic hydrogens within the anion chains in the aromatic amines is in the GlA-1MI structure. The O...O distances of these structures are all less than 2.500 Å except for the ScA-1MI structure where the distances are 2.522(15) and 2.543(13) Å. All of these are potentially low barrier hydrogen bonds; further data using neutron diffraction would need to be collected to determine accurately the position of the hydrogen within the interaction and confirm this.

The strong N-H...O hydrogen bonds between the cations and anions are generally around 1.85 Å however the range is up to 2.693 Å. The presence of two hydrogen bonds, one much shorter than the other is due to the asymmetry of the cation-anion hydrogen bonds and is a common occurrence throughout this series. The second longer hydrogen bond is sometimes thought of merely as a result



of the position of the cation due to the stronger hydrogen bond. The strongest N-H...O hydrogen bond in this series is 1.750(2) Å in the SbA-Im structure, however there are a number of structures with hydrogen bond distances only slightly longer than this value. The distribution of hydrogen bond lengths for N-H...O and C-H...O interactions are shown in Appendix, Figure A13.

C-H...O hydrogen bonds are prevalent throughout the series and are the weakest of the hydrogen bonds, with an average hydrogen bond distance of 2.52 Å. The shortest C-H...O hydrogen bonds are mainly from C22, the single carbon between the two nitrogens of the base (e.g. ScA-Im, GlA-4MI and SbA-4MI). This is because the ability of this carbon to act as a hydrogen bond donor is enhanced by its position between the two nitrogens which act inductively to decrease the electron density at adjacent CH protons. The next shortest C-H...O contacts are from DMI cations. For this to be due to the electron donating methyl groups, it would be expected that the Im structures would have the longest contact distances as the cation does not have any methyl groups. However, this is not the case; in fact, the Im C-H...O hydrogen bonds have an average distance of 2.491 Å which is slightly shorter than that of the methylated Ims (2.522 Å). Instead, the short contacts of some of the DMI structures must be due to close packing. The longest C-H...O hydrogen bond is given as 2.719 Å, however, on viewing the structure it can be seen that there are further contacts that are slightly longer than this. It must be assumed that due to the long distance of an already weak interaction, the contact does not contribute significantly to the overall stability of the structure.

#### 7.7.5 Other Intermolecular Interactions

In a number of the structures the ring of the cation is positioned over a negative carbonyl group from the diacid. Although here this close contact has been attributed to close packing and dipole-dipole interactions, the possibility of it being a  $\pi$ -interaction should not be excluded. The evidence for carbonyl- $\pi$  interactions is scarce in the literature; there are some examples present on the CSD including protein crystals and some other organic crystals<sup>12</sup>. In a study by Gautrot *et al.*<sup>13</sup> it was noted that for electron deficient aromatic rings, carbonyl- $\pi$  interactions are energetically favourable with a face approach of the carbonyl. In his study a model of the carbonyl- $\pi$  interactions was extrapolated from the anion- $\pi$  interaction studies, taking into account the differences between the systems, the carbonyl- $\pi$  interaction ‘can be predicted to be energetically favourable in the case of electron deficient aromatic rings.’ Further investigation using OPiX<sup>14</sup> to calculate the polarisation of the molecules in the structures described here would need to be performed to identify if this is a significant interaction.

### 7.7.6 Fingerprint Plots (Appendix, Tables A11)

In a minority of the fingerprint plots, some aspects of the plots are a product of the modelling of the structure. The fingerprint plots of monoanions with half occupancy hydrogens at each end of the molecule have a central spike that points towards the origin of the plot. This represents a very short head-on hydrogen-hydrogen intermolecular contact which causes this artefact (see DLTA-IM, ScA-1MI, GlA-2MI and DLTA-DMI, Appendix Tables A11.1, A11.2, A11.3 and A11.5 respectively).

The OxA plots for each of the OxA salts look similar being quite thin (except OxA-1MI) and only involved in hydrogen bonding as an acceptor; OxA-Im is slightly different due to it being a monoanion rather than a dianion and hence being a hydrogen bond donor as well as an acceptor. The dianion plots all look very similar and generally have a more spherical body than the OxA plots. The sparseness of points just above the diagonal of the plot is due to the lack of alkyl groups in the OxA, and hence it cannot donate CH interactions.

MeA produces an unusual plot for a monoanion in both of its structures, with only one long ‘arm’ in the plot and hence appearing more as a dianion. This is due to the strong intramolecular hydrogen bond in the anion which limits its hydrogen bond donating capacity. 2MI in FmA-2MI is also odd as it has a sharp feature along the diagonal that is green-yellow reflecting the large number of points at these  $d_i, d_e$  values. By studying the locations of the atoms relative to the Hirshfeld surface of the molecule, it would appear that the feature is due to strong C-H...O hydrogen bonds from the methyl group of the cation to the oxygens of the anion. This is very unusual as the C-H...O hydrogen bonds usually show up on the ‘arms’ of the fingerprint plot, rather than along the central diagonal. In fact, the thickening of the sharp features near  $(d_i, d_e) = (1.5, 1.2)$  is due to C-H...O hydrogen bonds (e.g. 4MI in ScA-4MI).

As expected, some of the plots that follow the same sheet structure look similar; the fingerprint plots for Im in AdA-Im and SbA-Im look similar and both structures follow **Sheet 1**. The SbA-Im plot is less diffuse at the top due to there being fewer voids in the structure. There are also head-on H...H contacts due to the neutral acid chain weaving through the sheet. The SbA fingerprint plot from the SbA-2MI and SbA-4MI structures also look very similar as both of the structures follow **Sheet 5**. The TAs in LTA-Im and DTA-1MI also look similar. A number of the fingerprint plots, however, do not look similar even though the ions are forming similar structures. For example, although LTA-Im and DLTA-1MI follow **Sheet 2**, the plots do not look as similar as expected. This may be due to the presence of the methyl group in the DLTA-1MI structure. The ScA plots for ScA-1MI and ScA-4MI also do not bear as much similarity as may be expected from their following the same sheet structure. This highlights the fact that although the basic layout of the

structure may be the same, the orientation of the molecules within this structure can drastically alter the intermolecular interactions.

## References

1. C. K. Johnson, ORTEP, C. K. Johnson, Report ORNL-3794, Oak Ridge National Laboratory, Tennessee, USA, 1965.
2. J. C. MacDonald, P. C. Dorrestein, M. M. Pilley, *Cryst. Growth Des.*, 2001, **1**, 29-38.
3. K. Pogorzelec, J. Garbarczyk, *Mol. Phys. Rep.*, 2002, **35**, 132.
4. D. R. Trivedi, A. Ballabh, P. Dastidar, *CrystEngComm.*, 2003, **5**, 358-367.
5. Mercury 1.5 - A Crystal Structure Visualisation Program, The Cambridge Crystallographic Data Centre, 2006.
6. C. B. Aakeröy, P. B. Hitchcock, *J. Mater. Chem.*, 1993, **3**, 1129-1135.
7. J. Fuller, R. T. Carlin, L. J. Simpson, T. E. Furtak, *Chem. Mater.*, 1995, **7**, 909-919.
8. M. N. G. James, M. Matsushima, *Acta Crystallogr., Sect. B*, 1976, **B32**, 1708-1713.
9. J. C. MacDonald, P. C. Dorrestein, M. M. Pilley, *Cryst. Growth Des.*, 2001, **1**, 29-38.
10. R. I. Cooper, R. O. Gould, S. Parsons, D. J. Watkin, *J. Appl. Cryst.*, 2002, **35**, 168-174.
11. SHELXS [includes SHELX97 and SHELXL97], Programs for Crystal Structure Analysis (Release 97-2), G. M. Sheldrick, Institut für Anorganische Chemie der Universität, 1998.
12. A. Gambaro, P. Ganis, F. Manoli, A. Polimeno, S. Santi, A. Venzo, *J. Organometallic Chem.*, 1999, **583**, 126-130.
13. J. E. Gautrot, P. Hodge, D. Cupertino, M. Helliwell, *New J. Chem.*, 2006, **30**, 1801-1807.
14. A. Gavezzotti, OPiX: A Computer Program Package for the Calculation of Intermolecular Interactions and Crystal Energies, University of Milano, 2006.

## CHAPTER 8

### Discussion With Respect to the Diacids

#### 8.1 INTRODUCTION

In order to identify trends for each diacid group, various parameters have been measured and compared, the results of which are described here. Two integral parameters to this work are the C-O and C=O bond distances for the carboxyl and carboxylate groups of the diacids as these are used to confirm the location of the transferable hydrogens. The values for these bond distances are given in the Appendix, Tables A15 and A16. In the cases where the position of the hydrogen from the C-O and C=O bond distances has not agreed with the peaks in the electron density map, this has been noted and the hydrogens have been placed according to the difference between the C-O and C=O bond lengths of the atoms involved. There are two instances of this disagreement (FmA-AEI and GlA-1MI), both of which occur when the hydrogen is part of a hydrogen bond which forms an anion/acid molecule chain. The significance of this will be discussed further in Section 8.3.1. Unsurprisingly, the difference between the C-O, C=O bond distances for the anions that have been methylated are particularly large due to the accommodation of the methyl group.

#### 8.2 TRENDS IN DEPROTONATION AND STOICHIOMETRY

The ratio between the mono- and di-deprotonated species for each of the diacids is approximately 50:50 except for MnA and MeA which are all mono-deprotonated, and the TAs which are mostly mono-deprotonated. The shorter chain diacid species (not including MnA, MeA and TAs) are not entirely in concurrence with the frequency found on the CSD (noted in Section 2.6.1) where monoanions were more common than dianions. This is most likely due to the smaller sample size in this work. The frequency of the MnA, MeA and TA species are in agreement with that found on the CSD. As the difference between the first and second ionisation  $pK_a$  values decreases as the diacid chain length increases, it may be expected that a similar number of monoanions and dianions will form for the longer chain diacids. Although this is seen in the CSD structures, it is not reflected in this study. It has also been suggested by Serajuddin and Pudipeddi, that when the two  $pK_a$  values

of the acidic groups are close, it might be difficult to isolate monosalts and instead a disalt or mixture of salts might be formed.<sup>1</sup> SbA has a difference of 0.88 units between the  $pK_a$  values of its acidic groups, the smallest of the series, however in the results described here it most commonly forms monosalts.

It is interesting that the TAs both predominantly form monoanions in spite of generally having  $pK_a$  differences of greater than 2.5 units for both the first and second ionisation, indicating that dianions are also feasible. The  $pK_a$  values are similar to those of FmA which forms an approximately equal number of mono and dianions. This suggests that something else, such as the hydrogen bonding potential, is directing the deprotonation. It has been noted by Barnes *et al.*<sup>2,3</sup> that when polycarboxylic acids react with amines, it is the ability to form stable hydrogen bond networks that decides which of the possible products will crystallise. This will be discussed further in the next section.

A number of mixed systems have been found to have formed; these are unexpected as it is noted by Maurin *et al.* that for the formation of a stable salt, ionisation must be ‘effectively complete such that a single ionisation state is formed.’<sup>4</sup> An incompletely ionised system is less stable as it lacks uniform molecular composition. This is not expressed by the results here as the melting points of the mixed systems are not the lowest within the groups. It is surprising that there is a number of ionisation states present in the binary compounds – it would be expected that the diacids are ionised evenly when the amines are protonated. The presence of a dianion and a neutral molecule in a binary compound may be due to the first and second ionisation of the diacid being of a similar value, as the mixed systems only occur for diacids with a difference between their  $pK_a$  values of 1.4 units or less. Some of the mixed systems have been obtained from weak data produced by poor crystals. It could be considered that the poor crystal quality may be partly to do with the mixture of ionised components. Whether this is true or not, the mixed systems require further analysis using neutron diffraction or NMR to accurately locate the position of the acidic hydrogens in the acid-anion chains.

Methylation of a diacid by the solvent prevents the formation of a dianion and can also, in the case of MnA and MeA, render the monoanion incapable of intramolecular hydrogen bonding. Methylation of the diacid only occurs for MeA and OxA (once and twice respectively). This may be due to the acidity of these diacids as they have the lowest  $pK_a$  values of the series (Appendix, Table A2). It should also be noted that only MeA reacts with the base compounds to form a new compound, which occurs in two instances. This is due to the presence of the exposed double bond in MeA.

In spite of the 1:1 acid-base stoichiometry of the crystallisation solutions, there are a number of structures which contain the components in different stoichiometries. In spite of the chemical

simplicity of the compounds involved, the stoichiometries are unpredictable and can only be generally rationalised in terms of the deprotonation patterns and hydrogen bonding synthons of the components. Although trends in stoichiometry are seen in some of the even diacids, these are dependent on the base the binary compound contains.

There are a number of structures where  $Z'$  is greater than 1 (OxA-TMBA, ScA-TMBA, MeA-TMBA, SbA-AEI, FmA-AEI, GIA-TEMED, GIA-4MI, LTA-4MI and MeA-Idn). This is a phenomenon that is currently under investigation as the reasons for its occurrence are unclear.<sup>5-7</sup> As the structures are not particular to a diacid, it can only be assumed that it is some property of the base, or the combination of the base with the diacid that results in more than one acid-base unit in the asymmetric unit. Babu and Nangia suggest that strong hydrogen bonds (in particular O-H...O hydrogen bonds) are a dominant force in the formation of high  $Z'$  polymorphs.<sup>8</sup> Results from this study agree with their findings as most of the O...O distances in the  $Z' > 1$  structures found here, are less than the average (2.53Å).

There are a number of hydrate binary compounds present in the dataset, these most commonly form for the short chain simple diacids and DLTA. The inclusion of water into the TA structures may partly be a consequence of its presence as the crystallisation solvent. As a small molecule that has good hydrogen bonding potential, it can fit into small cavities and provide additional structure stability via hydrogen bonds linking the acid-base supramolecular structures.

### 8.3 HYDROGEN BONDING

For a typical hydrogen bond an increase in H...A is likely to involve a large deviation of  $\theta$  from 180°. This can be seen in Appendix Figure A14; it can also be seen that the O-H...O are on average closer to 180° than N-H...O hydrogen bonds.

#### 8.3.1 Anion/Acid Hydrogen Bonding

Over half of the 78 structures discussed here contain anion-anion or acid-anion chains, which are mainly hydrogen bonded head-to-tail except for five which involve TAs and are instead hydrogen bonded via the hydroxyl group. All of the TAs form hydrogen bonded acid/anion chains which concurs with the results from CSD searches. It was also found that structures that do not contain acid/anion chains do exist though they are rare. For TA co-crystals, the proportion of structures that have hydroxyl-carboxyl(ate) or hydroxyl-hydroxyl hydrogen bonded chains is higher than that for the monoanions. The head-to-tail acid/anion chains are predominantly in the *syn-syn* conformation, and the hydroxyl-carboxyl(ate) hydrogen bonds are mainly to the *anti* position of the carboxyl(ate).

The TA binary compounds can retain the head-to-tail hydrogen bonding of their parent compounds more commonly than the other diacids due to the hydroxyl groups. These provide additional hydrogen bonding sites, with which sufficient hydrogen bonds with other molecules in the binary compound can still be formed. It should be noted, however, that the base molecules rarely hydrogen bond to the acid via the hydroxyl groups and instead mainly hydrogen bond via the carboxyl(ate) group. Indeed, the hydroxyl groups are often involved in linking the anion chains into a 2-D lattice from which the cations are subtended. In this way, the hydroxyl groups appear to stabilise the anion network rather than the acid-base network. The greater hydrogen bonding ability of the TAs also usually results in higher melting temperatures for their binary compounds.

Conversely, MnA, MeA and PmA do not form any acid/anion chains; this is also supported by the results from CSD searches. For MnA and MeA the lack of acid/anion chains is probably due to the intramolecular hydrogen bonding they often experience. Although only two structures containing PmA have been discussed here, there is a further eight binary compounds present on the CSD which also do not contain acid/anion chains. This does not necessarily mean, however, that PmA is particularly adverse to forming acid/anion chains but perhaps PmA will only form binary compounds with bases with which it can form strong hydrogen bonds. The nature and arrangement of the hydrogen bonding group therefore inhibits the formation of the chains.

OxA is only involved in anion-anion chains in two of the structures (Im and DAE), both of which form strong hydrogen bonds in the *syn-syn* conformation (O...O distance 2.588 and 2.572 Å respectively). This is not reflective of the frequency of acid/anion chains on the CSD where most OxA monoanions and mixed systems are involved in acid/anion chains. Of the acid/anion chains, most are in the *syn-syn* conformation, however *anti-anti* and *syn-anti* conformations do exist. Notably none of the OxA co-crystals on the CSD contain acid/anion chains.

CSD searches for binary compounds containing ScA, GlA, FmA and the TAs also agreed with the results from this work that monoanions and mixed systems mainly form acid/anion chains whereas the neutral species do not. No acid/anion chains were found during CSD searches for MeA and SbA which reflects the results found here for MeA, however, all of the SbA binary structures synthesised in this project contain acid-anion chains.

Of the structures containing head-to-tail acid/anion chains, three of these contain monoanions for which the position of the hydrogen was found to be shared over each carboxylate group. In another four the locations of the hydrogens within the chain were not found easily from the electron density map. To some extent this was due to poor data from poor crystals, but it has been noted by Steiner that the behaviour of an O-H...O<sup>-</sup> interaction is similar to a strong hydrogen bond between molecular species.<sup>9</sup> A significant indicator of the strength of a hydrogen bond from SXRD data is the distance between the donor and acceptor atoms; the O...O distances in the acid/anion chains



range between 2.442-2.682 Å, i.e. at least 0.12 Å less than the upper limit for a strong hydrogen bond. The structures which have disordered hydrogens in their acid/anion chains, or hydrogens that were difficult to position mainly have O...O distances less than the average (2.526 Å), suggesting the hydrogens are shared between the donor and acceptor groups. A further indicator of a strong hydrogen bond is the lengthening of the C-O bond for a carboxylate group when the C-O, C=O bond distances would normally be expected to be similar. Although this is seen for some of the acid/anion hydrogen bonds the effect is obscured by other anion-cation hydrogen bonds the carboxylate group is also involved in. GlA is the most common diacid for these structures, but all are for mid-length (3-5C) diacids (includes hydroxy and alkene diacids); they most commonly occur with Im derivatives.

The greater proportion of the acid/anion chains are hydrogen bonded together in the *syn-syn* conformation, these hydrogen bonds span the range of O...O distances therefore creating both the strongest and weakest hydrogen bonds. The *anti-anti* conformation hydrogen bonds are twice as numerous and slightly shorter than the *syn-anti* conformation hydrogen bonds (O...O distance range 2.461-2.543 Å and 2.488-2.578 Å respectively). There are no *anti-syn* hydrogen bonds present.

### 8.3.2 Acid-Base Hydrogen Bonding

Usually the *syn* position is less sterically hindered and hence is often exploited by strong molecular interactions.<sup>10</sup> Therefore when a strong acid/anion chain forms, which usually occupies the *syn* position, the base instead hydrogen bonds to the *anti* position of the carboxylate. For structures which do not contain acid/anion chains, particularly dianions, the base usually hydrogen bonds to the acid via both the *syn* and *anti* position.

It was found that the OxA dianion commonly hydrogen bonds to the cation via bifurcated hydrogen bonds; two possible synthons are shown in Figure 8.3.2.1; **a** can be considered as an approximately *anti* conformation and **b** as approximately *syn*. The third synthon was found with the neutral OxA molecule.

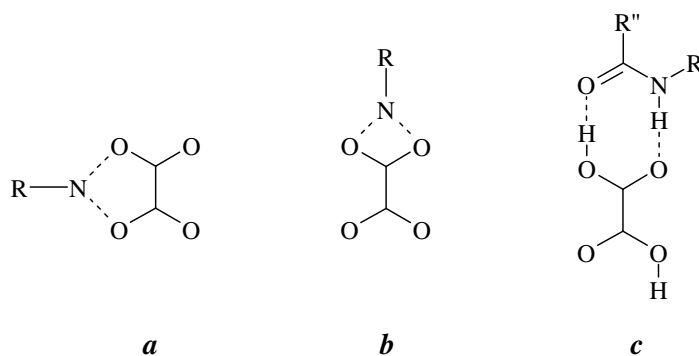


**Figure 8.3.2.1** Hydrogen bonding arrangements for an OxA dianion and neutral molecule. Diagrams for **a** and **b** are purely skeletal – hydrogens and charges are not included, nor are double bonds.

Out of the ten structures discussed here, eight consist of an OxA anion involved in one or more bifurcated hydrogen bond of type **a** from the cation; two of these also contained type **b** bifurcated hydrogen bonding however there were no instances when type **b** was seen alone. Two of the structures do not contain any bifurcated hydrogen bonding: the nitrogen of Idn is involved in an amide group which forms a hydrogen bonded unit with each of the carboxylate groups separately, as in **c**, and the OxA-IMI structure contains weak bifurcated C-H...O type **a** hydrogen bonds rather than N-H...O hydrogen bonds. These results are concurrent with analyses of the oxalate structures present on the CSD; out of 147 structures containing the monoanion, dianion and neutral OxA, only three contained type **b** bifurcated hydrogen bonding of the oxalate anion. Predominantly the structures contain type **a** bifurcated hydrogen bonded with one bifurcated hydrogen bond being more common for the monoanions, and two bifurcated hydrogen bonds being more common for the dianions. For co-crystals containing neutral OxA molecules, monofurcated hydrogen bonds are more common. When the base molecule or cation has two hydrogen bond donor groups, similar to that seen in type **c**, monofurcated hydrogen bonds are preferred, though bifurcated bonds do still occur. Out of the CSD structures, three contain both types **a** and **b** bifurcated hydrogen bonding.

### 8.3.3 Intramolecular hydrogen bonding

In three of the MnA structures the monoanion has strong intramolecular hydrogen bonding, of the remaining two structures one has anion-anion hydrogen bonding (Im) to form a dimer and the other has acid-base hydrogen bonded chains (Idn). This concurs with a CSD search of the MnA monoanion, where the monoanion was found to exist both with intramolecular hydrogen bonding and where the carboxylate groups are solely involved in intermolecular hydrogen bonding, with the former being more prevalent. The occurrence of a strong intramolecular hydrogen bond is restricted to the binary compounds; a CSD search for co-crystals containing the neutral MnA species found no examples of intramolecular hydrogen bonding either. The internal hydrogen bonding in the MnA monoanion leads to a stable approximately planar five-membered ring.

The pure solid form of MeA and the monoanion are both stabilised by a strong intramolecular hydrogen bond; this leads to the very wide separation of  $pK_a$  values for MeA compared to FmA. The intramolecular hydrogen bond also leads a stable approximately planar six-membered ring. There are five instances of strong intramolecular hydrogen bonding in the MeA salt and co-crystal structures; in the remaining one case, the acid has been methylated by the solvent rendering it incapable of intramolecular hydrogen bonding as a monoanion. This concurs with the results of CSD searches for binary compounds containing the MeA monoanion, and neutral species.

## 8.4 ANION/ACID CONFORMATION AND BOND DISTANCES

### 8.4.1 Carbon-Carbon Bond Lengths

OxA and its anions have a characteristically long C-C bond; average C-C bond lengths are usually 1.54 Å, however, the C-C bond lengths are mainly greater than this (Appendix, Table A17). There are a few anomalies from this trend which may be due to the poor quality of the crystals resulting in weak synchrotron data. The C-C bond lengths of the other diacids are as expected.

### 8.4.2 Carbon Backbone Conformation

Most of the diacids, except MeA, take on an *anti* conformation, though *gauche* conformations also exist. The torsion angle range and average for each of the diacids are given in Appendix, Table A18. Despite the greater flexibility of longer chain diacids, they still adopt a predominantly *anti* conformation. GlA has the highest proportion of *gauche* conformations while AdA always adopts the *anti* conformation. The diacid molecules which exhibit the greatest degree of torsion are GlA in GlA-TEMED and SbA in SbA-2MI. Both of these structures have quite low melting points for their groups. AdA and PmA may not exhibit much torsion in the studied binary compounds as the increased torsion may result in structures that have such low melting points that they are oils at 4°C and above. Perhaps, solid structures form most often when the *anti* conformation is adopted. This is not supported by the structures on the CSD however, where PmA takes slightly more bent conformations than planar. Further CSD searches show that while ScA and, to a lesser extent, SbA are predominantly planar, GlA has approximately equal numbers of planar and bent structures. This fluctuation between the conformation of the diacids again appears to reflect whether the chain has an even or odd number of carbons.

Planar structures are inherently more stable than bent structures though the *gauche* conformation can increase stability in certain structures (e.g. 1,2-difluoroethane) – this is known as the ‘*gauche* effect.’ A reduced orbital overlap can be compensated for by adopting the *gauche* conformation. The *gauche* effect is unlikely to contribute here as there are no highly electronegative elements to alter the electron density. Instead, the conformation of the molecule is likely to be due to the development of directional hydrogen bonding interactions. These will also contribute to the stability of the structure, thus reducing the effect of any energetically favourable conformations.

### 8.4.3 Angle Between Carboxyl(ate) Planes

The angles between the COO(H) planes in each of the diacids have been measured and are tabulated in Appendix, Table A19. When these values are averaged across each of the simple diacids the following graph can be drawn:

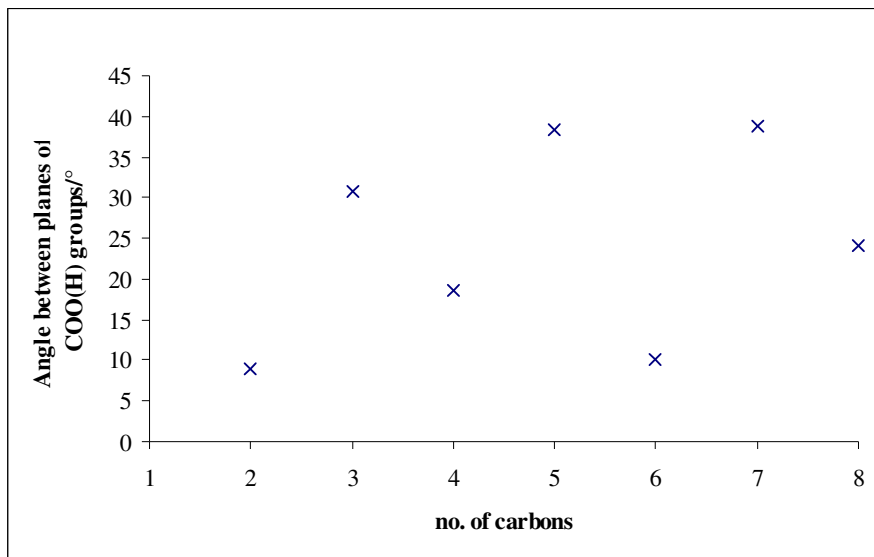


**Figure 8.4.3.1** Variation of the angle between planes of COO(H) groups with the number of carbons in the diacid chain.

It can be seen that generally as the number of carbons in the diacid chain increases, the average angle between the COO(H) planes also increases. This is most likely due to the increased torsion as the chain length increases. Although the deviation of each torsion angle from planarity may be small, when these are accumulated over a long molecule, the angle between the COO(H) groups will increase. It is interesting that the angle between the planes alternates for the odd and even diacids, with the even diacids having smaller deviations from planarity. This is a property that is also expressed in the pure diacids.

Although all the OxA structures discussed here are approximately planar, twisted conformations where the COO(H) groups are not in the same plane also exist on the CSD though they are not as numerous. Deviation of the COO(H) planes from planarity in acid/anion chains results in further stepped or twisted chains. ScA and MeA are usually planar although the twisting of the COO(H) groups does occur on the CSD also. FmA is usually exactly planar, however some large angles between the COO(H) groups in the FmA-AEI structure increase the average value. This structure was obtained from weak data from poor crystals – the poor data may be due to this combination not being very stable as the acid has to take on this orientation which is not preferred and hence poor crystals form. A similar situation may be found for the MeA-TMBA structure.

The TAs both have similar angles between their COO(H) planes: 54.2° for D/LTA and 51.0° for DLTA. The smallest angle between the planes for the TAs is 25.99° for DLTA-IMI which is unusual as the rest of the structures do not have an angle less than 40°. In a paper by Akkurt *et al.*<sup>11</sup> various dihedral angles between planes for other TA nitrogen-containing binary compounds are noted which range between 62° and 32° for ammonium tartrate and aminoethylammonium tartrate respectively; the values found here lie within this range.

## 8.5 CRYSTALLOGRAPHIC PATTERNS

A study by Brock and Dunitz<sup>12</sup> has shown that when both components in a system are achiral, the adducts generally crystallise in centrosymmetric space groups; similar considerations have been found to occur if one component of a binary compound is a racemic mixture.<sup>13, 14</sup> This is because the occurrence of inversion centres, especially unoccupied inversion centres, seems to be particularly favourable in molecular crystals. Indeed the most common space group for this dataset is *P*-1, with *P*2<sub>1</sub>/*c* following closely behind. Nearly a quarter of the structures contain a component that lies across a special position and therefore is centrosymmetric. Of the diacids, FmA and ScA are most commonly centrosymmetric, however none of the TAs or MeA are centrosymmetric. Vishweshwar notes that diacids generally ‘occupy the inversion centre special position in a near planar *anti* orientation of C=O groups in the crystal.’<sup>15</sup> This is supported by the results in this study. In PmA-Idn both of the components lie on two-fold rotation axes, and here the COOH groups are in the *syn* arrangement instead.

The range of accessible space groups is constrained if one of the components is a single enantiomer of a chiral compound and hence the D/LTA binary compounds mainly crystallise in *P*2<sub>1</sub>. In a study of chiral versus racemic building blocks by Farrell and co-workers,<sup>16</sup> they note that the overall supramolecular structures of the enantiomer and racemic products are ‘remarkably similar despite the different space groups exhibited.’ Comparison of the TA structures is best seen in the aromatic amine group where most of the crystals consist of anion chains that are linked via the cations. Similarities in the basic structure are also seen in the Idn binary compounds, however these involve hydroxyl-carboxyl anion chains rather than head-to-tail anion chains. It should also be noted that DLTA spontaneously resolved in the presence of one base (DAE) only.

## References

1. A. T. M. Serajuddin, M. Pudipeddi, Salt-Selection Strategies, in *Handbook of Pharmaceutical Salts; Properties, Selection and Use*; P. H. Stahl, C. G. Wermuth (Eds.), Verlag Helvetica Chimica Acta/Wiley-VCH: Zurich, 2002, 135-160.
2. J. C. Barnes, T. J. R. Weakley, *Acta Crystallogr., Sect. C*, 1997, **53**, 9700018.
3. J. C. Barnes, R. W. Longhurst, T. J. R. Weakley, *Acta Crystallogr., Sect. C*, 1998, **C54**, 1347-1351.
4. M. B. Maurin, D. J. W. Grant, P. H. Stahl, The Physicochemical Background: Fundamentals of Ionic Equilibria, in *Handbook of Pharmaceutical Salts; Properties, Selection and Use*; P. H. Stahl, C. G. Wermuth (Eds.), Verlag Helvetica Chimica Acta/Wiley-VCH: Zurich, 2002, 9-17.
5. G. R. Desiraju, *CrystEngComm*, 2007, **9**, 91-92.
6. J. W. Steed, *CrystEngComm*, 2003, **5**, 169-179.
7. K. M. Anderson, J. W. Steed, *CrystEngComm*, 2007, **9**, 328-330.
8. N. J. Babu, A. Nangia, *CrystEngComm*, 2007, **9**, 980-983.
9. T. Steiner, *Chem. Commun.*, 1999, 2299-2300.
10. S. G. Fleishman, S. S. Kuduva, J. A. McMahon, B. Moulton, R. D. B. Walsh, N. Rodríguez-Hornedo, M. J. Zaworotko, *Cryst. Growth Des.*, 2003, **3**, 909-919.
11. M. Akkurt, I. Celik, S. Ozbey, E. Kendi, *Z. Krist.-New Cryst. Struct.*, 2000, **215**, 71-72.
12. C. P. Brock, J. D. Dunitz, *Chem. Mater.*, 1994, **6**, 1118-1127.
13. C. J. Burchell, G. Ferguson, A. J. Lough, C. Glidewell, *Acta Crystallogr., Sect. B*, 2000, **B56**, 1054-1062.
14. C. J. Burchell, G. Ferguson, A. J. Lough, C. Glidewell, *Acta Crystallogr., Sect. C*, 2001, **C57**, 311-314.
15. P. Vishweshwar, A. Nangia, V. M. Lynch, *Cryst. Growth Des.*, 2003, **3**, 783-790.
16. D. M. M. Farrell, G. Ferguson, A. J. Lough, C. Glidewell, *Acta Crystallogr., Sect. B*, 2002, **B58**, 272-288.

## CHAPTER 9

### Conclusions and Further Work

#### 9.1 CONCLUSION

During this study, the novel structures of 42 salts, 11 co-crystals and 6 mixed salt/co-crystal systems have been prepared and characterised, providing the opportunity to compare and contrast the impact of various factors on the crystal structures and properties of a total of 61 salts, 11 co-crystals, and 8 mixed salt/co-crystal systems. Although some broad conclusions across the whole range of compounds can be drawn, most of the conclusions are specific to a compound or series of compounds. Other conclusions can also be made regarding the methods used in this study and their application to salt and co-crystal screening.

Although binary compounds were formed for most of the acid-base combinations, a number of oils were also formed, often for the odd diacid combinations and in particular MnA. It has been speculated that this may be due to a combination of factors including the orientation of the functional groups and the solubility of the diacid in the chosen solvent. Further research into the pH-solubility relationships across the diacid series would shed more light on this trait.

From the results, the even diacids, in particular ScA and OxA, and GlA are most likely to form binary compounds, irrespective of the base. It was also found that monosalts are generally more common, even for dibases.

Across the range of binary compounds formed, the interplay between  $pK_a$ , deprotonation, stoichiometry and hydrogen bonding has been investigated, with particular reference to the ‘rule of three.’ For the first ionisation/protonation of the compounds the ‘rule of three’ was found to be too conservative and instead a ‘rule of two’ was used as a better guide. A ‘rule of two’ is generally a useful tool as the difference between the  $pK_a$  values (calculated in water) predicts the protonation of the binary compound. However, this was not found to be the case with the amides; the amides used have very basic  $pK_a$  values therefore giving large  $pK_a$  differences, however all of the amides formed co-crystals. The Mo salt structures that also include a secondary amine show that this effect must be due to the carbonyl group. This indicates the limitations when only using  $pK_a$  to predict salt versus co-crystal formation.

A further limitation to the ‘rule of two’ is noted when the second ionisation values of the compounds are considered. The dibases used in this study (DAE and TEMED) always formed diprotonated cations, in spite of the small  $pK_a$  differences (often less than two units). This is also the case in structures where there is more than one base molecule present in the asymmetric unit. The different ionisations of the acid and base molecules optimise the hydrogen bonding contacts in the structures. Indeed, the preferred hydrogen bonding motifs and packing requirements appear to direct the deprotonation and, to some extent, the stoichiometry of the components in the structure. However, the variation in stoichiometry in some of the structures is difficult to rationalise.

Some of the bases form structures that are particular to the base, e.g. TMBA often forms approximately the same hydrogen bond motif thus resulting in similar supramolecular structures. The Im derivatives also generally form anion(-acid) chains which the cations bridge to form sheets. Knowledge of the type of supramolecular structure each base forms can help in predicting the type of structure that may form when other similar compounds are used. This can also be useful in predicting the protonation and stoichiometry of the components. However, again, there are limitations, as even very similar compounds such as DAE and AEI can form quite different structures; DAE and AEI generally take different molecular conformations in spite of the only difference between them being an oxygen in place of a nitrogen.

A knowledge of the alternation in properties across a series of starting materials has proved a useful asset as a number of structures have shown alternation in the phase of the product formed (in particular AEI and Mo), and alternation in the supramolecular structure and melting point of the binary compound formed (Idn). Indeed the Mo even-diacid salts all have a similar hydrogen bonding synthon.

Other properties regarding the diacids have also been expressed and should be considered when selecting binary compound formers:

- ScA and FmA can form binary compounds that are isostructural (TEMED and Mo) or have similar supramolecular structures (Pyr).
- MnA and MeA nearly always have a strong intramolecular hydrogen bond thus preventing the formation of anion chains (this is in accordance with Etter’s rules).
- Due to the small size of the OxA dianion, it can achieve a different hydrogen bond arrangement where a bifurcated hydrogen bond donor hydrogen bonds to both carboxylate groups. This arrangement is not possible in the other diacids.
- From the results it would appear that DLTA is more likely to form binary compounds than DTA or LTA. Further investigation into this trend would need to be performed to determine if this is a general feature for racemic compounds versus a single enantiomer.



Another property of the diacid starting materials is the acid/anion hydrogen bonded chains which form in over half of the binary compounds, in particular with the Im derivatives. These chains are usually in the stronger *syn-syn* conformation.

The Im derivatives are an interesting group as most of the structures follow a similar sheet arrangement. As the number and position of the methyl groups are the only differences in the base molecular structures, this group is useful to observe how the orientation of the cation and the intermolecular interactions adapt to accommodate the group. Indeed, the weak C-H...O hydrogen bonds are particularly important throughout this group. In the Im structures, an approximate alternation in melting points is observed. The only odd diacid to form a binary compound in the series forms a different structure to the even diacids, however, this structure appears incomplete and should be re-collected.

The results have also shown that molecules of similar shapes and sizes are not necessarily required to form salts or co-crystals. Instead, the arrangement and number of hydrogen bonding groups is much more significant in salt/co-crystal formation. In the Im derivatives, 1MI and DMI form the fewest binary compounds due to one of the nitrogens being methylated. This is also expressed in the nitrogen-containing heterocycles where Pyr forms less binary compounds than Idn, and DMIdn does not form any.

The knowledge gained from the hydrogen bond networks provides insights in understanding and predicting the proton transfer and hydrogen bonding networks of multi-component APIs involving structurally similar molecular species to the A-B complexes seen here. In the acid/anion chains, potential strong hydrogen bonds have been identified which require further investigation using neutron diffraction to accurately locate the position of the hydrogen and confirm the nature of the interaction. Possible carbonyl- $\pi$  interactions have also been suggested, however, their significance as an interaction also requires further investigation. Fingerprint plots have been useful not only in identifying some of the  $\pi$ -interactions, but also to compare the structures. This is not always the case, however, as sometimes structures that appear similar do not express this in their fingerprint plots.

The well-plate crystallisation method used in this study has been shown to be a convenient and quick method for producing a limited number of binary compounds on a micro-scale. It also often results in the formation of oils and crystalline products of insufficient quality to be accurately identified. Indeed, the well-plate crystallisations often resulted in oils for the odd diacids, particularly MnA. The MnA binary compounds on the CSD have been synthesised using different solvents suggesting that under different conditions, MnA and other the odd diacids may form more binary compounds. More studies should be performed in a range of solvents to investigate this.

Another problem with the well-plate crystallisations was the amount of product formed. In the pharmaceutical industry the amount of API available is often limited and therefore micro-scale screens have to be performed. As found in this study, the small amount of product limits the analyses that can be performed and the extent to which these can be taken. For example, the PXRD analysis performed in this study was a quick scan that produced a weak pattern due to the small amount of product available. The DSC scans could also not be repeated to further investigate interesting areas of the scan as there was insufficient product. Instead the DSC was used as a screening tool itself where the samples were run at high scan-rates. In hindsight it would have been better to run these at lower speeds to get more accurate melting points and so as the thermal events did not start to overlap. When a number of events appeared on the scan, the cause of these events could not be investigated using a combination of DSC and TGA. Instead a single crystal of the correct unit cell was melted using HSM. Also, due to the crystallisation method used and the small scale, the evaporation occurred quite quickly often resulting in poor quality, small crystals which were difficult to obtain a crystal structure from and, consequently, had a high R-factor. Well-plate crystallisation is a viable high-throughput method, however, any solid products should then be re-crystallised on a larger scale to obtain better crystals for structure analysis, or more product for analysis by PXRD. This would also enable a more thorough thermal analysis before the salt/co-crystal selection stage where the thermal profile is crucial. Well-plate crystallisations should also be performed in a number of different solvents which cover the different solubilities of the range of compounds.

This thesis has shown that the formation of structures by binary systems would appear to be even more complex than the formation of crystal structures by single component systems. On this basis there is clearly scope for continuation in the quest for more data. The interaction relationships that have been highlighted in the work also promote the value of making systematic studies.

## 9.2 FURTHER WORK

First of all, it would be of interest to try to ‘fill in the gaps’ in the dataset so far acquired. This includes MnA-Im where there are two conflicting structures present on the CSD, AdA-DAE for which there are no co-ordinates available on the CSD and MnA-TMBA which produced an incommensurate structure. By completing the series it would not only provide a fuller picture of the trends and patterns but knowledge of the crystallisation methods and solvent which formed these compounds may provide reasons as to why the binary compounds did not form in the first place. Neutron diffraction and NMR should also be used to define the positions of the transferable hydrogens, particularly in possible strong hydrogen bonds.

To further investigate the factors affecting salt formation, the effects of solvent and temperature on the product should also be studied. It would also be of great interest to further assess the physical properties of the binary compounds and how these relate those of the starting materials. As it is important to have a complete understanding of the properties of pharmaceutical materials it would be ideal to thermally characterise the materials using DSC and thermogravimetric analysis (TGA) to gather information regarding melting, purity, polymorphism, waters of hydration and decomposition.

Nangia has drawn attention to the use of the  $pK_{HB}$  scale in the formation of binary compounds.<sup>1</sup> The first  $pK_{HB}$  values were obtained by Taft *et al.*<sup>2-4</sup> and the scale was then extended by Laurence and Berthelot<sup>5</sup> who demonstrated that its use allows the prediction of the preferred hydrogen bonding site in drugs. They also note that there is ‘little or no relationship between the  $pK_{HB}$  scale of proton sharing and the  $pK_a$  scale of proton transfer.’ This scale should be further investigated and applied to the dataset to see if it reveals further insights into the formation of salts and co-crystals. It may be of particular use with amides where the  $pK_a$  scale does not appear to be appropriate.

Although this study has provided a number of conclusions, it has also emphasised that trends and patterns are often specific to a family of compounds. It would therefore be of interest to extend this study to different acids and bases. The use of a series of compounds has highlighted nuances in the structures and properties that may well have otherwise been missed and therefore it is suggested that similar series and groups are constructed.

**References**

1. A. Nangia, Designing Hydrogen Bonded Supramolecular Structures and Co-Crystals, in *Pharmaceutical Co-Crystals* Conference; Amsterdam, 2006.
2. R. W. Taft, D. Gurka, L. Joris, P. von R. Schleyer, *J. Am. Chem. Soc.*, 1969, **91**, 4801-4808.
3. D. Gurka, R. W. Taft, *J. Am. Chem. Soc.*, 1969, **91**, 4794-4801.
4. L. Joris, J. Mitsky, R. W. Taft, *J. Am. Chem. Soc.*, 1972, **94**, 3438-3442.
5. C. Laurence, M. Berthelot, *Perspect. Drug Discov.*, 2000, **18**, 39-60.

## APPENDIX

In the appendix, various Tables are given showing  $pK_a$  differences, an overview of the results, the product melting points and the cell parameters of the binary compounds synthesised and those found on the CSD. Further structure information is given in the CD attached to the cover. A short introduction to Hirshfield surfaces and fingerprint plots is summarised and followed by the fingerprint plots for each of the binary compounds discussed, including those from the CSD.

A number of structural parameters have also been tabulated and graphs plotted.

Some pure form structures were produced during the attempted binary crystallisations. Their unit cell parameters are detailed in Table A21 and the cif files are available on the CD.

### CSD Search results:

	Monosalts	Disalts	Co-crystals	Mixed systems
OxA	45	79	36	20
MnA	21	7	9	2
ScA	11	16	42	8
GlA	5	11	17	0
AdA	12	7	17	2
PmA	2	1	5	0
SbA	1	1	6	0
TAs	152	43	22	6
MeA	2	145	13	3
FmA	25	42	39	18

**Table A1** Number of monosalts, disalts, co-crystals and mixed systems present on the CSD (search only includes organics).

			Pyr		Idn		TMBA		DAE		AEI		Mo		TEMED		2MI		DMI		DMIdn		4MI		1MI		Im	
	pK <sub>a</sub>	1	16.62		18.39		10.75		9.89		9.16		8.97		8.86		7.88		7.76		7.75		7.49		7.01		6.95	
	1	2	-		14.58		-		6.77		-		-		5.58		-		-		-		-		-		-	
OxA	1.23	4.19	15.39	12.43	17.16	14.20	9.52	6.56	8.66	5.70	7.93	4.97	7.74	4.78	7.63	4.67	6.65	3.69	6.53	3.57	6.52	3.56	6.26	3.30	5.78	2.82	5.72	2.76
					13.35	10.39			5.54	2.58					4.35	1.39												
MeA	1.83	6.07	14.79	10.55	16.56	12.32	8.92	4.68	8.06	3.82	7.33	3.09	7.14	2.90	7.03	2.79	6.05	1.81	5.93	1.69	5.92	1.68	5.66	1.42	5.18	0.94	5.12	0.88
					12.75	8.51			4.94	0.70					3.75	-0.49												
MnA	2.83	5.69	13.79	10.93	15.56	12.70	7.92	5.06	7.06	4.20	6.33	3.47	6.14	3.28	6.03	3.17	5.05	2.19	4.93	2.07	4.92	2.06	4.66	1.80	4.18	1.32	4.12	1.26
					11.75	8.89			3.94	1.08					2.75	-0.11												
TA	2.98	4.34	13.64	12.28	15.41	14.05	7.77	6.41	6.91	5.55	6.18	4.82	5.99	4.63	5.88	4.52	4.90	3.54	4.78	3.42	4.77	3.41	4.51	3.15	4.03	2.67	3.97	2.61
					11.60	10.24			3.79	2.43					2.60	1.24												
FmA	3.03	4.44	13.59	12.18	15.36	13.95	7.72	6.31	6.86	5.45	6.13	4.72	5.94	4.53	5.83	4.42	4.85	3.44	4.73	3.32	4.72	3.31	4.46	3.05	3.98	2.57	3.92	2.51
					11.55	10.14			3.74	2.33					2.55	1.14												
ScA	4.20	5.61	12.42	11.01	14.19	12.78	6.55	5.14	5.69	4.28	4.96	3.55	4.77	3.36	4.66	3.25	3.68	2.27	3.56	2.15	3.55	2.14	3.29	1.88	2.81	1.40	2.75	1.34
					10.38	8.97			2.57	1.16					1.38	-0.03												
GIA	4.31	5.41	12.31	11.21	14.08	12.98	6.44	5.34	5.58	4.48	4.85	3.75	4.66	3.56	4.55	3.45	3.57	2.47	3.45	2.35	3.44	2.34	3.18	2.08	2.70	1.60	2.64	1.54
					10.27	9.17			2.46	1.36					1.27	0.17												
AdA	4.43	5.41	12.19	11.21	13.96	12.98	6.32	5.34	5.46	4.48	4.73	3.75	4.54	3.56	4.43	3.45	3.45	2.47	3.33	2.35	3.32	2.34	3.06	2.08	2.58	1.60	2.52	1.54
					10.15	9.17			2.34	1.36					1.15	0.17												
PmA	4.48	5.42	12.14	11.20	13.91	12.97	6.27	5.33	5.41	4.47	4.68	3.74	4.49	3.55	4.38	3.44	3.40	2.46	3.28	2.34	3.27	2.33	3.01	2.07	2.53	1.59	2.47	1.53
					10.10	9.16			2.29	1.35					1.10	0.16												
SbA	4.52	5.40	12.10	11.22	13.87	12.99	6.23	5.35	5.37	4.49	4.64	3.76	4.45	3.57	4.34	3.46	3.36	2.48	3.24	2.36	3.23	2.35	2.97	2.09	2.49	1.61	2.43	1.55
					10.06	9.18			2.25	1.37					1.06	0.18												

Table A2 pK<sub>a</sub> differences in water

			Pyr		Idn		TMBA		DAE		AEI		Mo		TEMED		2MI		DMI		DMIdn		4MI		1MI		Im	
	pK <sub>a</sub>	1	16.30		17.97		11.76		10.88		10.12		9.11		9.01		8.09		7.97		7.97		7.72		7.27		7.21	
	1	2			14.39		-		7.66		-		-		5.93		-		-		-		-		-		-	
OxA	6.19	9.21	10.11	7.09	11.77	8.75	5.57	2.55	4.68	1.66	3.93	0.91	2.92	-0.10	2.81	-0.21	1.89	-1.13	1.78	-1.24	1.77	-1.25	1.53	-1.49	1.07	-1.94	1.02	-2.00
					8.19	5.17			1.47	-1.55					-0.27	-3.29												
MeA	6.81	11.13	9.50	5.17	11.16	6.84	4.96	0.63	4.07	-0.25	3.32	-1.01	2.31	-2.02	2.20	-2.12	1.28	-3.04	1.17	-3.16	1.16	-3.17	0.91	-3.41	0.46	-3.86	0.41	-3.92
					7.58	3.25			0.86	-3.47					-0.88	-5.21												
MnA	7.83	10.74	8.48	5.56	10.14	7.22	3.94	1.02	3.05	0.13	2.30	-0.62	1.29	-1.63	1.18	-1.74	0.26	-2.66	0.15	-2.77	0.14	-2.78	-0.11	-3.02	-0.56	-3.47	-0.61	-3.53
					6.56	3.64			-0.16	-3.08					-1.90	-4.82												
FmA	8.03	9.47	8.27	6.83	9.94	8.50	3.73	2.29	2.85	1.41	2.09	0.66	1.08	-0.36	0.98	-0.46	0.06	-1.38	-0.06	-1.49	-0.07	-1.50	-0.31	-1.75	-0.76	-2.20	-0.82	-2.26
					6.35	4.92			-0.37	-1.81					-2.11	-3.54												
ScA	9.22	10.66	7.08	5.64	8.74	7.30	2.54	1.10	1.65	0.21	0.90	-0.54	-0.11	-1.55	-0.22	-1.65	-1.14	-2.58	-1.25	-2.69	-1.26	-2.70	-1.50	-2.94	-1.95	-3.39	-2.01	-3.45
					5.16	3.72			-1.56	-3.00					-3.30	-4.74												
GIA	9.34	10.46	6.97	5.84	8.63	7.51	2.43	1.30	1.54	0.42	0.79	-0.33	-0.22	-1.35	-0.33	-1.45	-1.25	-2.37	-1.36	-2.48	-1.37	-2.49	-1.62	-2.74	-2.07	-3.19	-2.12	-3.25
					5.05	3.93			-1.67	-2.80					-3.41	-4.53												
AdA	9.46	10.46	6.84	5.84	8.51	7.51	2.30	1.30	1.42	0.42	0.67	-0.33	-0.35	-1.35	-0.45	-1.45	-1.37	-2.37	-1.48	-2.48	-1.49	-2.49	-1.74	-2.74	-2.19	-3.19	-2.25	-3.25
					4.93	3.93			-1.80	-2.80					-3.53	-4.53												
PmA	9.51	10.47	6.79	5.83	8.46	7.50	2.25	1.29	1.37	0.41	0.62	-0.34	-0.40	-1.36	-0.50	-1.46	-1.42	-2.38	-1.54	-2.49	-1.54	-2.50	-1.79	-2.75	-2.24	-3.20	-2.30	-3.26
					4.88	3.92			-1.85	-2.81					-3.58	-4.54												
SbA	9.55	10.45	6.75	5.85	8.42	7.52	2.21	1.31	1.33	0.43	0.57	-0.32	-0.44	-1.34	-0.54	-1.44	-1.46	-2.36	-1.58	-2.47	-1.59	-2.48	-1.83	-2.73	-2.28	-3.18	-2.34	-3.24
					4.83	3.94			-1.89	-2.78					-3.63	-4.52												

Table A3 pK<sub>a</sub> differences in methanol

		Aliphatic amines				N-containing heterocycles				Aromatic amines				
		TMBA	DAE	AEI	TEMED	Pyr	Idn	DMIdn	Mo	Im	1MI	2MI	4MI	DMI
Simple diacids	OxA	rxn ssf1327	PEPMOM	QAMRIF	06skc0058		06skc0068	OXALAC	06skc0036	MEQPAZ	rxn 06skc0034	06skc0026	06skc0053	
	MnA	WU 07skc0030	WOBXIU		QAFVID		06skc0046			UMURAV		WU 07skc0027	WU	
	ScA	WU 07skc0032	PINNIJ	07skc0016	ISUTEV	06skc0040	ssf1338	SUCACB	06skc0035	MEQPON	06skc0052	06skc0029	06skc0051	06skc0028
	GIa	ssg0302	06skc0073		06skc0065		07skc0005	GLURAC02			06skc0047	06skc0049	06skc0042	06skc0048
	AdA	07skc0019	ZZZGYW				07skc0011	ADIPAC	06skc0037	MEQQEE		ssf1337		
	PmA	07skc0018				WU PIMELA04	07skc0003	PIMELA04						
	SbA			06skc0043				SUBRAC04		06skc0002	SUBRAC04	06skc0005	06skc0013	
Hydroxy diacids	LTA	TARTAC05	DTA= EDATAR10	XAGDAK			ssg0307			HAZHEV	DTA= ZAMXIU	DTA= ZELRIR	ssg0304	07skc0031
	DLTA	07skc0009	ENHTAR from exp		04mbh0608	TARTDL01	ssg0306		04skc0004	04skc0001	06skc0082	04skc0002	04skc0007	06skc0027
Alkene diacids	MeA	rxn ssf1328	ROHKUU		07skc0020		WU 07skc0026		07skc0004	IMZMAL	ssg0301		WU 07skc0024	
	FmA	07skc0007	07skc0017	06skc0067	QAFVEZ	06skc0081		FUMAAC	06skc0061	MEQPED		07skc0013		07skc0022

Table A4 Results

Key:

salt	Mixed system	Co-crystal	Salt hydrate	Components reacted
Starting material	Starting material solvate	Micro-crystalline product	amorphous	oil

rxn = reaction with solvent

WU = obtained using crystallisation Method 3



File name	A-B	Contents of asymmetric unit	R-factor	Space Group	Z	Study Temp./K	$a/\text{\AA}$	$b/\text{\AA}$	$c/\text{\AA}$	$\alpha/^\circ$	$\beta/^\circ$	$\gamma/^\circ$	Cell Volume/ $\text{\AA}^3$
04mbh0608	DLTA-TEMED	$\text{A}^{2-}:\text{B}^{2+}:\text{3H}_2\text{O}$	4.36	P-1	2	120	6.1179(14)	8.6720(24)	15.1817(75)	90.918(33)	91.411(27)	99.792(23)	793.31(33)
04skc0001	DLTA-Im	$\text{A}^-:\text{B}^+$	9.34	C2/c	8	120	25.0655(50)	4.9767(10)	19.1418(38)	90	129.418(30)	90	1844.67(589)
04skc0002	DLTA-2MI	$\text{A}^-:\text{B}^+$	6.35	P-1	2	120	7.5625(18)	8.3396(28)	9.1932(58)	66.466(31)	71.905(24)	73.034(20)	495.83(76)
04skc0004	DLTA-Mo	$\text{A}^-:\text{B}^+:\text{H}_2\text{O}$	3.58	P-1	2	120	7.6152(7)	8.2002(11)	10.1113(12)	98.680(10)	106.417(8)	105.156(8)	567.11(30)
04skc0007	DLTA-4MI	$\text{A}^-:\text{B}^+:\text{H}_2\text{O}$	6.70	P-1	2	120	7.3760(15)	7.6241(25)	10.2107(28)	88.858(25)	71.015(15)	82.337(20)	537.95(34)
06skc0002	SbA-Im	$\text{A}:\text{2A}^-:\text{2B}^+$	5.23	P-1	2	120	8.7148(3)	11.4826(3)	16.9691(5)	81.721(2)	81.814(2)	77.987(2)	1632.45(9)
06skc0005	SbA-2MI	$\text{A}^-:\text{B}^+$	5.80	P-1	2	120-293	7.3683(4)	9.0497(3)	10.7486(5)	76.546(3)	80.396(2)	76.933(3)	674.05(6)
06skc0013	SbA-4MI	$\text{A}^-:\text{B}^+$	10.82	$\text{P2}_1/\text{n}$	4	120	8.8691(7)	13.2988(17)	12.1250(14)	90	109.500(7)	90	1348.09(36)
06skc0026	OxA-2MI	$\text{A}^{2-}:\text{2B}^+$	10.86	Pbca	8	120	13.3293(19)	13.1137(16)	14.0233(21)	90	90	90	2451.22(6)
06skc0027	DLTA-DMI	$\text{A}^-:\text{B}^+$	9.63	P-1	2	120	7.5275(3)	9.4025(4)	9.9908(4)	64.266(2)	68.172(2)	74.175(2)	586.06(7)
06skc0028	ScA-DMI	$\text{A}^-:\text{B}^+$	6.85	Pccn	8	120	20.5769(12)	7.3521(4)	14.0383(8)	90	90	90	2123.76(2)
06skc0029	ScA-2MI	$\text{A}^-:\text{B}^+$	4.80	$\text{P2}_1/\text{m}$	4	120	8.1472(7)	6.4965(5)	9.0107(5)	90	97.401(4)	90	472.95(3)
06skc0034	OxA-1MI	$\text{A}^-:\text{B}^+$	6.09	$\text{P2}_1/\text{c}$	4	120	6.4624(4)	18.8186(10)	7.1493(5)	90	98.878(4)	90	859.03(6)
06skc0035	ScA-Mo	$\frac{1}{2}\text{A}^{2-}:\text{B}^+$	4.43	$\text{P2}_1/\text{c}$	2	120	10.9078(5)	7.6984(2)	8.6167(3)	90	105.403(2)	90	697.58(4)
06skc0036	OxA-Mo	$\frac{1}{2}\text{A}^{2-}:\text{B}^+$	2.80	$\text{P2}_1/\text{c}$	2	120	9.6872(5)	6.5461(3)	10.8209(5)	90	102.698(3)	90	669.41(5)
06skc0037	AdA-Mo	$\frac{1}{2}\text{A}^{2-}:\text{B}^+$	14.03	P-1	1	120	5.8219(3)	7.4643(6)	9.8058(7)	79.046(3)	77.621(4)	81.676(4)	406.22(4)
06skc0040	ScA-Pyr	$\frac{1}{2}\text{A}:\text{B}$	7.22	P-1	1	120	5.7490(25)	6.5410(28)	9.9030(45)	80.396(21)	78.704(20)	71.706(25)	344.50(32)
06skc0042	GlA-4MI	$\text{2A}^-:\text{2B}^+$	5.59	$\text{P2}_1$	4	120	7.5360(4)	14.2180(8)	9.7160(6)	90	96.571(3)	90	1034.20(11)
06skc0043	SbA-AEI	$\text{A}:\text{2A}^-:\text{A}^{2-}:\text{4B}^+$	11.52	P-1	8	120	11.1497(7)	13.0874(9)	18.9733(11)	88.072(4)	79.300(4)	65.645(3)	2475.51(44)
06skc0046	MnA-Idn	$\frac{1}{2}\text{A}:\text{1}\frac{1}{2}\text{B}$	11.15	C2/c	4	120	16.6403(10)	14.4382(5)	7.6872(5)	90	117.299(2)	90	1641.20(19)
06skc0047	GlA-1MI	$\text{A}:\text{A}^{2-}:\text{2B}^+$	13.81	P-1	2	120	8.1285(6)	9.1297(7)	13.7387(11)	89.781(4)	89.170(4)	79.782(5)	1003.28(9)
06skc0048	GlA-DMI	$\text{A}^-:\text{B}^+$	7.93	$\text{Pna2}_1$	4	120	10.4056(16)	22.8884(40)	4.6392(9)	90	90	90	1104.91(3)
06skc0049	GlA-2MI	$\text{A}^-:\text{B}^+$	9.41	P-1	2	120	5.3800(3)	8.1542(6)	12.6592(10)	78.350(4)	82.962(4)	84.496(4)	538.37(5)
06skc0051	ScA-4MI	$\frac{1}{2}\text{A}:\frac{1}{2}\text{A}^{2-}:\text{B}^+$	4.90	$\text{P2}_1/\text{c}$	4	120	3.9015(2)	17.3293(10)	13.8628(7)	90	96.299(3)	90	931.61(3)
06skc0052	ScA-1MI	$\text{A}^-:\text{B}^+$	12.68	$\text{P2}/\text{c}$	4	120	18.1170(10)	6.6790(4)	7.4250(3)	90	90.008(0)	90	898.45(1)
06skc0053	OxA-4MI	$\frac{1}{2}\text{A}^{2-}:\text{B}^+:\text{H}_2\text{O}$	4.85	C2/c	4	120	9.1937(6)	13.5734(6)	10.5047(5)	90	99.252(4)	90	1293.83(9)
06skc0058	OxA-TEMED	$\frac{1}{2}\text{A}^{2-}:\frac{1}{2}\text{B}^{2+}:\text{H}_2\text{O}$	3.23	$\text{P2}_1/\text{c}$	2	120	7.5550(3)	10.9180(4)	8.1170(2)	90	111.565(2)	90	622.67(15)
06skc0061	FmA-Mo	$\frac{1}{2}\text{A}^{2-}:\text{B}^+$	4.07	$\text{P2}_1/\text{c}$	4	120	10.7285(4)	7.7897(3)	8.8064(3)	90	106.793(2)	90	704.58(4)
06skc0065	GlA-TEMED	$\text{3A}^-:\text{1}\frac{1}{2}\text{B}^{2+}$	14.72	$\text{P2}_1/\text{n}$	6	120	17.3078(22)	9.0088(14)	18.9320(26)	90	105.305(7)	90	2847.23(57)
06skc0067	FmA-AEI	$\text{2A}:\text{2A}^{2-}:\text{4B}^+$	14.72	P-1	8	120	8.1621(6)	9.3259(5)	21.3026(12)	86.922(4)	88.863(3)	87.350(4)	1617.22(5)

File name	A-B	Contents of asymmetric unit	R-factor	Space Group	Z	Study Temp./K	<i>a</i> /Å	<i>b</i> /Å	<i>c</i> /Å	<i>Alpha</i> /°	<i>Beta</i> /°	<i>Gamma</i> /°	Cell Volume/Å <sup>3</sup>
06skc0068	OxA-Idn	A:2B	15.97	P2 <sub>1</sub> /c	4	120	8.322(4)	11.203(5)	11.915(5)	90	97.79 (3)	90	1100.61(12)
06skc0073	GlA-DAE	A <sup>2-</sup> :B <sup>2+</sup>	6.03	P2 <sub>1</sub> /n	4	120	8.6426(5)	6.0715(5)	18.9467(14)	90	102.765(5)	90	969.63(11)
06skc0081	FmA-Pyr	½A:B	5.31	P2 <sub>1</sub> /n	2	120	11.6287(3)	5.1904(2)	11.9417(3)	90	108.971(2)	90	681.62(5)
06skc0082	DLTA-1MI	A <sup>-</sup> :B <sup>+</sup>	5.72	P2 <sub>1</sub> /n	4	120	7.5192(3)	7.0534(3)	18.9307(8)	90	100.552(2)	90	987.03(4)
07skc0003	PmA-Idn	½A: ½B	5.91	Cmcm	8	120	6.8156(6)	12.7537(12)	14.1899(11)	90	90	90	1233.44(2)
07skc0004	MeA-Mo	reaction	14.56	P2 <sub>1</sub> /c	4	120	5.7683(9)	13.7020(27)	14.4419(26)	90	97.458(11)	90	1131.79(17)
07skc0005	GlA-Idn	A:B	4.16	Cc	4	120	5.3007(4)	19.3739(2)	10.0780(9)	90	94.012(6)	90	1032.43(16)
07skc0007	FmA-TMBA	½A <sup>2-</sup> :B <sup>+</sup>	19.26	P2 <sub>1</sub> /c	2	120	11.5690(95)	6.3070(54)	16.6760(127)	90	101.543(45)	90	1192.10(113)
07skc0009	DLTA-TMBA	A <sup>2-</sup> :2B <sup>+</sup> :2H <sub>2</sub> O	12.02	P-1	2	120	8.3059(4)	10.8568(8)	15.6687(11)	71.627(3)	77.606(4)	81.799(4)	1305.36(17)
07skc0011	AdA-Idn	A:2B	9.34	P2 <sub>1</sub> /c	4	120	7.7814(3)	22.3584(11)	9.1957(5)	90	103.329(3)	90	1556.77(11)
07skc0013	FmA-2MI	A <sup>-</sup> :B <sup>+</sup>	6.88	P2 <sub>1</sub> /m	2	120	8.0829(5)	6.2852(4)	9.0979(6)	90	97.551(4)	90	458.19(3)
07skc0016	ScA-AEI	½A: ½A <sup>2-</sup> :B <sup>+</sup>	6.12	P-1	2	120	5.7652(4)	8.2911(5)	9.0772(4)	87.558(4)	73.569(4)	81.599(3)	411.70(5)
07skc0017	FmA-DAE	½A <sup>2-</sup> :½B <sup>2+</sup>	3.61	P-1	1	120	5.0677(3)	5.5917(4)	7.2473(4)	91.984(3)	103.960(4)	99.504(3)	195.97(2)
07skc0018	PmA-TMBA	A <sup>-</sup> :B <sup>+</sup>	6.92	Pna2 <sub>1</sub>	4	120	11.5504(7)	22.2264(10)	6.6309(4)	90	90	90	1702.31(2)
07skc0019	AdA-TMBA	½A: ½A <sup>2-</sup> :B <sup>+</sup>	7.91	P2 <sub>1</sub> /c	4	120	11.8885(5)	6.2179(3)	21.9459(9)	90	104.852(2)	90	1568.08(9)
07skc0020	MeA-TEMED	A <sup>-</sup> :½B <sup>2+</sup>	10.29	P2 <sub>1</sub> /c	2	120	5.7536(6)	14.8551(24)	10.1829(15)	90	100.799(9)	90	854.92(15)
07skc0022	FmA-DMI	A <sup>-</sup> :B <sup>+</sup>	10.20	P2 <sub>1</sub> /n	4	120	7.6480(7)	11.6730(9)	11.2040(1)	90	93.547(4)	90	998.32(10)
07skc0024	MeA-4MI	A <sup>-</sup> :B <sup>+</sup>	5.19	P2 <sub>1</sub> /c	4	120	5.5883(2)	22.5838(12)	7.3581(4)	90	98.578(3)	90	918.24(4)
07skc0026	MeA-Idn	4A:2B	11.81	P2 <sub>1</sub> /c	8	120	31.3779(13)	12.3307(6)	7.1600(3)	90	92.68(2)	90	2766.57(4)
07skc0027	MnA-2MI	A <sup>-</sup> :B <sup>+</sup>	8.02	Pna2 <sub>1</sub>	4	120	11.4966(19)	18.7024(27)	3.9535(5)	90	90	90	850.06(2)
07skc0030	MnA-TMBA	incommensurate				120	8.1650(4)	15.5860(9)	20.4290(11)	90	90	90	
07skc0031	LTA-DMI	A <sup>-</sup> :B <sup>+</sup>	5.18	P2 <sub>1</sub>	2	120	7.6534(8)	6.9693(7)	10.5603(10)	90	104.616(5)	90	545.05(7)
07skc0032	ScA-TMBA	2A <sup>-</sup> :2B <sup>+</sup> : H <sub>2</sub> O	10.85	P2 <sub>1</sub> /c	8	120	13.5580(5)	9.1910(3)	25.2770(9)	90	105.232(2)	90	3039.15(17)
ssf1327	OxA-TMBA	4A <sup>-</sup> :4B <sup>+</sup>	9.88	P-1	8	120	11.1890(70)	11.2080(60)	21.9060(130)	84.512(7)	85.814(7)	89.942(7)	2727.21(36)
ssf1328	MeA-TMBA	2A <sup>-</sup> :2B <sup>+</sup>	4.98	P2 <sub>1</sub> /c	8	120	6.6154(15)	30.4775(68)	15.2817(34)	90	90.924(2)	90	3080.71(12)
ssf1337	AdA-2MI	½A: ½A <sup>2-</sup> :B <sup>+</sup> : H <sub>2</sub> O	5.16	P-1	2	120	4.8629(3)	7.9978(5)	16.5263(11)	96.951(1)	94.475(1)	107.384(1)	604.44(3)
ssf1338	ScA-Idn	A:2B	5.08	P-1	2	120	5.5097(15)	9.5290(20)	13.0300(30)	104.839(3)	91.938(3)	95.093(3)	657.54(7)
ssg0301	MeA-1MI	reaction	6.27	P2 <sub>1</sub> 2 <sub>1</sub> 2 <sub>1</sub>	4	120	7.7110(2)	8.2850(4)	13.8440(5)	90	90	90	884.43(6)
ssg0302	GlA-TMBA	½A:A <sup>2-</sup> :2B <sup>+</sup>	4.46	C2	2	120	23.0890(70)	6.4030(20)	18.4960(60)	90	94.025(3)	90	2727.68(15)
ssg0304	LTA-4MI	2A <sup>-</sup> :2B <sup>+</sup>	3.16	P2 <sub>1</sub> 2 <sub>1</sub> 2 <sub>1</sub>	8	120	7.5842(14)	8.2124(16)	32.3630(60)	90	90	90	2015.71(7)

File name	A-B	Contents of asymmetric unit	R-factor	Space Group	Z	Study Temp./K	<i>a</i> /Å	<i>b</i> /Å	<i>c</i> /Å	<i>Alpha</i> /°	<i>Beta</i> /°	<i>Gamma</i> /°	Cell Volume/Å <sup>3</sup>
ssg0306	DLTA-Idn	A:B	4.40	P2 <sub>1</sub> /c	4	120	5.1062(11)	18.1980(40)	10.4320(20)	90	97.060(2)	90	962.02(4)
ssg0307	LTA-Idn	A:B	3.01	P2 <sub>1</sub> 2 <sub>1</sub> 2 <sub>1</sub>	4	120	5.3880(13)	9.9210(30)	18.2650(50)	90	90	90	976.3(5)
EDATAR10	DTA-DAE	A <sup>2-</sup> :B <sup>2+</sup>	3.8	P2 <sub>1</sub>	2	283-303	8.990(5)	8.817(5)	5.973(4)	90	105.58(10)	90	456.053
ENHTAR	DTA-DAE	A <sup>-</sup> :½B <sup>2+</sup>	4.0	P4 <sub>1</sub> 2 <sub>1</sub> 2	4	283-303	7.531(4)	7.531(4)	30.065(8)	90	90	90	1705.165
HAZHEV	LTA-Im	A <sup>-</sup> :B <sup>+</sup>	4.1	P2 <sub>1</sub>	2	173	7.569(1)	6.953(1)	8.993(2)	90	101.55(1)	90	463.693
IMZMAL10	MeA-Im	A <sup>-</sup> :B <sup>+</sup>	3.9	P2 <sub>1</sub> /c	4	283-303	10.869(1)	5.523(1)	14.614(3)	90	102.85(2)	90	855.300
ISUTEV	ScA-TEMED	½A:½A <sup>2-</sup> :½B <sup>2+</sup>	4.19	P-1	1	298	5.637(<1)	8.710(<1)	8.843(<1)	96.22(<1)	93.41(<1)	97.60(<1)	426.626
MEQPAZ	OxA-Im	A <sup>-</sup> :B <sup>+</sup>	4.43	P2 <sub>1</sub> /n	4	298	5.688(4)	17.513(4)	6.810(2)	90	105.55(4)	90	653.540
MEQPED	FmA-Im	A <sup>-</sup> :B <sup>+</sup>	4.2	P-1	2	297	7.478(2)	7.747(2)	8.416(2)	69.69(2)	81.42(2)	66.18(2)	418.272
MEQPON	ScA-Im	A <sup>-</sup> :B <sup>+</sup>	4.35	P-1	2	297	6.583(2)	7.421(3)	9.648(2)	67.89(3)	73.91(2)	81.40(3)	419.021
MEQQEE	AdA-Im	A <sup>-</sup> :B <sup>+</sup>	5.03	Pna2 <sub>1</sub>	8	297	17.021(4)	10.679(3)	12.076(5)	90	90	90	2195.021
PEPMOM	OxA-DAE	A <sup>-</sup> :½B <sup>2+</sup> :½H <sub>2</sub> O	4.47	C2/c	4	283-303	17.971(1)	5.669(<1)	13.952(1)	90	126.87(<1)	90	1137.211
PINNIJ	ScA-DAE	A <sup>-</sup> :½B <sup>2+</sup>	4.3	P2 <sub>1</sub> /c	2	283-303	5.358(1)	12.947(3)	9.608(2)	90	95.26(2)	90	663.701
QAFVEZ	FmA-TEMED	½A:½A <sup>2-</sup> :½B <sup>2+</sup>	3.23	P-1	1	298	5.533(1)	8.603(<1)	8.903(<1)	93.48(<1)	95.02(1)	98.08(1)	416.859
QAFVID	MnA-TEMED	A <sup>-</sup> :½B <sup>2+</sup>	8.64	P-1	1	283-303	5.514(1)	8.989(1)	9.110(1)	113.62(<1)	90.79(<1)	97.67(<1)	408.940
QAMRIF	OxA-AEI	A <sup>2-</sup> :2B <sup>+</sup>	4.1	C2/c	4	283-303	17.473(5)	5.916(2)	10.346(3)	90	118.69(2)	90	938.170
ROHKUU	MeA-DAE	A <sup>-</sup> :½B <sup>2+</sup>	3.55	P-1	1	283-303	5.726(1)	6.552(1)	8.800(<1)	92.65(1)	95.89(1)	105.47(1)	315.574
UMURAV	MnA-Im	A <sup>-</sup> :B <sup>+</sup> :3?H <sub>2</sub> O	4.07	P-1	1	293	7.257(<1)	8.302(1)	9.341(1)	62.82(1)	75.55(<1)	88.07(<1)	482.681
VARHOM	MnA-Im	2A <sup>-</sup> :2?B <sup>+</sup>	10.53	P-1	2	293	7.231(2)	8.296(4)	9.235(4)	115.97(3)	102.84(3)	91.74(3)	480.419
WOBXIU	MnA-DAE	A <sup>-</sup> :½B <sup>2+</sup> :½H <sub>2</sub> O	4.4	P2/n	2	283-303	8.028(1)	8.701(1)	9.543(2)	90	105.90(1)	90	641.078
XAGDAK	LTA-AEI	A <sup>-</sup> :B <sup>+</sup> :H <sub>2</sub> O	4.95	P2 <sub>1</sub>	2	283-303	7.603(<1)	7.503(<1)	8.798(<1)	90	92.96(<1)	90	501.230
ZAMXIU	DTA-1MI	A <sup>-</sup> :B <sup>+</sup>	4.35	P2 <sub>1</sub>	2	283-303	7.609(2)	7.587(2)	9.414(2)	90	105.24(3)	90	524.353
ZELRIR	DTA-2MI	A <sup>-</sup> :B <sup>+</sup>	5.73	P2 <sub>1</sub>	2	283-303	4.739(1)	16.281(3)	6.746(1)	90	100.90(<1)	90	511.110
ZZZGYW	AdA-DAE	No co-ordinates		P2 <sub>1</sub> /a	2	283-303	9.410	10.820	5.550	90	101.73	90	553.279

**Table A5** Cell parameters for the binary compounds discussed in this work.

## Aliphatic Amines

	TMBA			DAE			AEI			TEMED		
	Melting point /°C	Density / g cm <sup>-3</sup>	Packing index /%	Melting point /°C	Density / g cm <sup>-3</sup>	Packing index /%	Melting point /°C	Density / g cm <sup>-3</sup>	Packing index /%	Melting point /°C	Density / g cm <sup>-3</sup>	Packing index /%
OxA	154.19	1.14	66.2	PEPMOM	1.508		QAMRIF	1.502		212-219	1.29	71.4
MnA	121.26, 163.52			WOBXIU	1.483					QAFVID	1.317	
ScA	57.76	1.12	64.8	PINNIJ	1.483		89.23	1.45	73.8	ISUTEV	1.372	
GLA	83.7-89.3	1.11	66.6	156.56	1.32	69.6				79.02	1.33	72.7
AdA	122.45	1.17	69.0	ZZZGYW	1.24		39.33					
PmA	100.5	1.34	69.1	108.83								
SbA	66.7-80.5, 130			130.99			60.42	1.26	69.3			
LTA				EDATAR	1.526		XAGDAK	1.519				
DLTA	159.4-167.7	1.13	66.4	ENHTAR	1.529					226.34	1.34	71.8
MeA	96.43	1.12	65.2	ROHKUU	1.538		T <sub>g</sub> =117-125			104.62	1.35	71.2
FmA	130.37	1.04	63.4	228.63	1.49	76.4	142.65	1.46	72.7	QAFVEZ	1.388	

Table A6 Melting point, density and packing index of the aliphatic amine binary compounds.

## Nitrogen-containing Heterocycles

	Pyr			Idn			Mo		
	Melting point /°C	Density / g cm <sup>-3</sup>	Packing index /%	Melting point /°C	Density / g cm <sup>-3</sup>	Packing index /%	Melting point /°C	Density / g cm <sup>-3</sup>	Packing index /%
OxA				128.2-131.9	1.58	74.8	137.64	1.31	67.7
MnA				72.14	1.47	72.4			
ScA	69.98	1.39	72.3	124.58	1.47	72.6	143.91	1.39	74.1
GLA				98.81	1.40	70.6			
AdA	15.67			83.78	1.36	69.6	135.57	1.31	72.6
PmA				92.25	1.34	69.1			
SbA	108.8			45.33			93.1-96.6, 130.6		
LTA				92.3-98.2	1.61	74.5			
DLTA				112.1-119.7	1.63	75.2	86.5-97.3	1.49	71.6
MeA				43.0	1.53	71.7	188.13		
FmA	71.1	1.39	71.6	84-93,108-116			138.1-143.8	1.37	72.1

Table A7 Melting point, density and packing index of the N-containing heterocycle binary compounds.

## Aromatic Amines

	Im			1MI			2MI			4MI				DMI	
	Melting point /°C	Density / g cm <sup>-3</sup>	Packing index /%	Melting point /°C	Density / g cm <sup>-3</sup>	Packing index /%	Melting point /°C	Density / g cm <sup>-3</sup>	Packing index /%	Melting point /°C	Density / g cm <sup>-3</sup>	Packing index /%	Melting point /°C	Density / g cm <sup>-3</sup>	Packing index /%
OxA	249-251	1.61		172-186	1.44	72.8	175.2-178.6	1.38	69.5	177	1.39	70.6			
MnA	115	1.356					149.4-150.1	1.45	71.7	87.96					
ScA	141-144	1.48		90.83	1.48	75.2	162.68	1.41	71.2	129.58	1.43	72.0	104.16	1.34	69.7
GlA	119.12			76.35	1.42	73.7	103.53	1.32	68.2	105.42	1.38	71.0	101.39	1.37	72.8
AdA	101.5-103	1.3		38.74			66.76	1.35	71.5						
PmA															
SbA	77.8-83.4	1.34	72.1				63.2	1.26	68.4	88.12	1.26	68.5			
LTA	179-181	1.56		98-101	1.471		203-204	1.509		101.08	1.53	72.6	127.6-138.3	1.50	73.7
DLTA	201.77	1.57	72.0	129-136	1.56	74.7	193.29	1.56	73.8	145.9-150.0	1.54	73.9	147.7-151.0	1.40	68.9
MeA	IMZMAL	1.426		108.15			243			88.6-92.1	1.43	71.2			
FmA	175-180	1.46		123.41			154.7-159.3	1.44	71.3	139-148			112.2-121.2	1.41	72.4

**Table A8** Melting point, density and packing index of the aliphatic amine binary compounds.

### Hirshfeld Surfaces

This method for exploring molecular crystals involves a novel partitioning of crystal space into Hirshfeld surfaces which encode information about all intermolecular interactions simultaneously. Crystal space is partitioned based on Hirshfeld's stockholder partitioning scheme;<sup>1</sup> from this a weighting function  $w(\mathbf{r})$  can be defined (Eqn 1.) where  $\rho_i(\mathbf{r})$  is a spherical atomic electron distribution located at the  $i$  th nucleus

$$w(\mathbf{r}) = \frac{\sum_{i \in \text{molecule}} \rho_i(\mathbf{r})}{\sum_{i \in \text{crystal}} \rho_i(\mathbf{r})} \quad \text{Eqn. 1}$$

The weight function represents the ratio between the sum of spherical atom electron densities for a molecule (the *promolecule*) and the sum of the entire crystal (the *procrystal*), and therefore the Hirshfeld surface envelops that region of space surrounding a particular molecule in a crystal where the electron distribution of the promolecule exceeds that due to any other molecule.<sup>2</sup> The Hirshfeld surface for a particular molecule is defined by  $w(\mathbf{r}) = 0.5$ , and the volume occupied by the molecule in the crystal is that region where  $w(\mathbf{r}) \geq 0.5$ .<sup>3</sup>

The contact distances from each point on the surface are given by two parameters:

$d_i$  distance from the surface to the nearest atom interior to the surface

$d_e$  distance from the surface to the nearest atom outside exterior to the surface

These parameters can be plotted on a surface using colour coding. Five different functions can be mapped onto the surface; two of these,  $d_e$  and *shape index*, are particularly helpful for distinguishing different polymorphs.

- On a  $d_e$  surface flat red regions indicate hydrogen-bond acceptor regions; flat green regions indicate hydrogen-bond donor regions. Regions above the plane of the molecule are variously green or blue showing 'average' and more distant contacts respectively.

- A  $d_i$  surface is similar except that close contacts from hydrogen bond donor regions are shown in red and hydrogen bond acceptor regions are shown in green. The presence of blue features can give indications as to the stacking of molecules. Hirshfeld surfaces are smooth and leave small voids where no single molecule dominates the procrystal electron density, therefore not all parts of the surfaces are touching and for points in these regions  $d_e$  is generally greater than  $d_i$ .

- *Shape index* is a dimensionless measure of 'which' shape; it can be used to identify complementary hollows (red) and bumps (blue) where two molecular Hirshfeld surfaces touch one another. The patterns of touching red and blue triangles are characteristic to particular stacking arrangements of aromatic rings.

<sup>1</sup> F. L. Hirshfeld, *Theor. Chim. Acta*, 1977, **44**, 129-138.

<sup>2</sup> M. A. Spackman, J. J. McKinnon, 2002, 378-392.

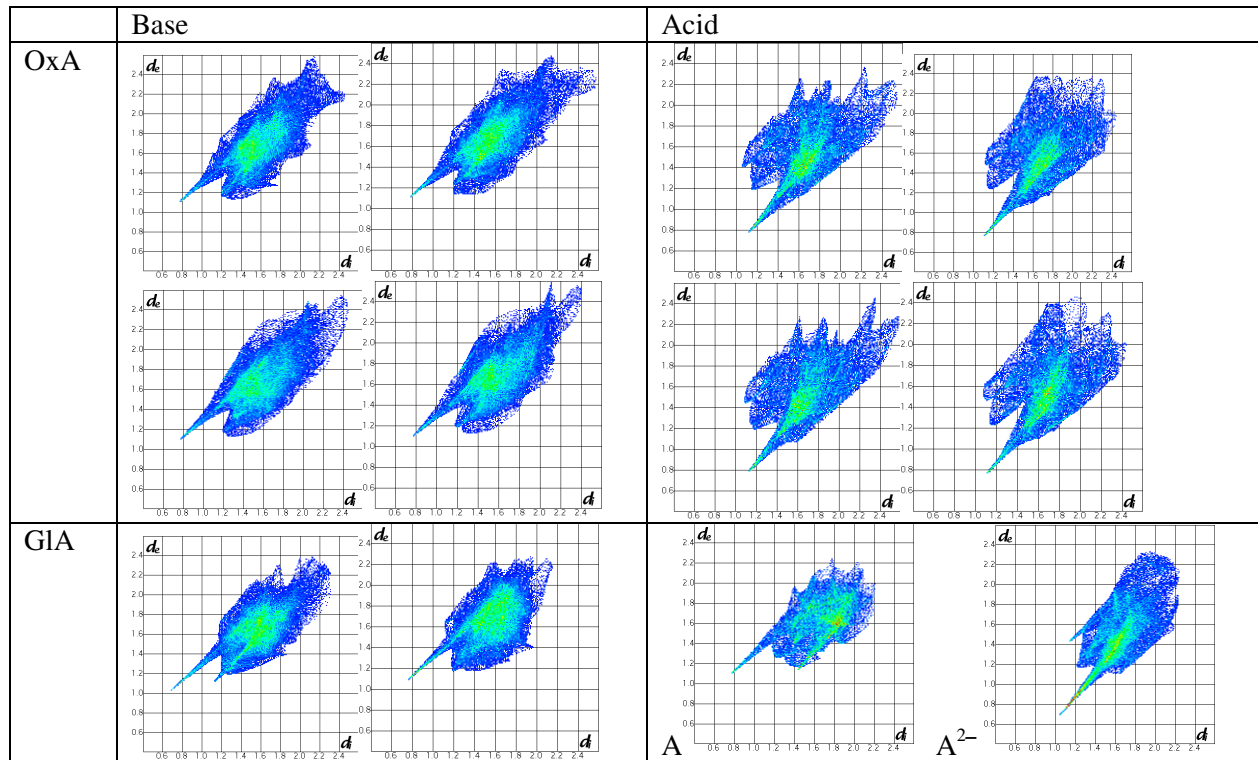
<sup>3</sup> J. J. McKinnon, A. S. Mitchell, M. A. Spackman, 1998, **4**, (11), 2136-2141.

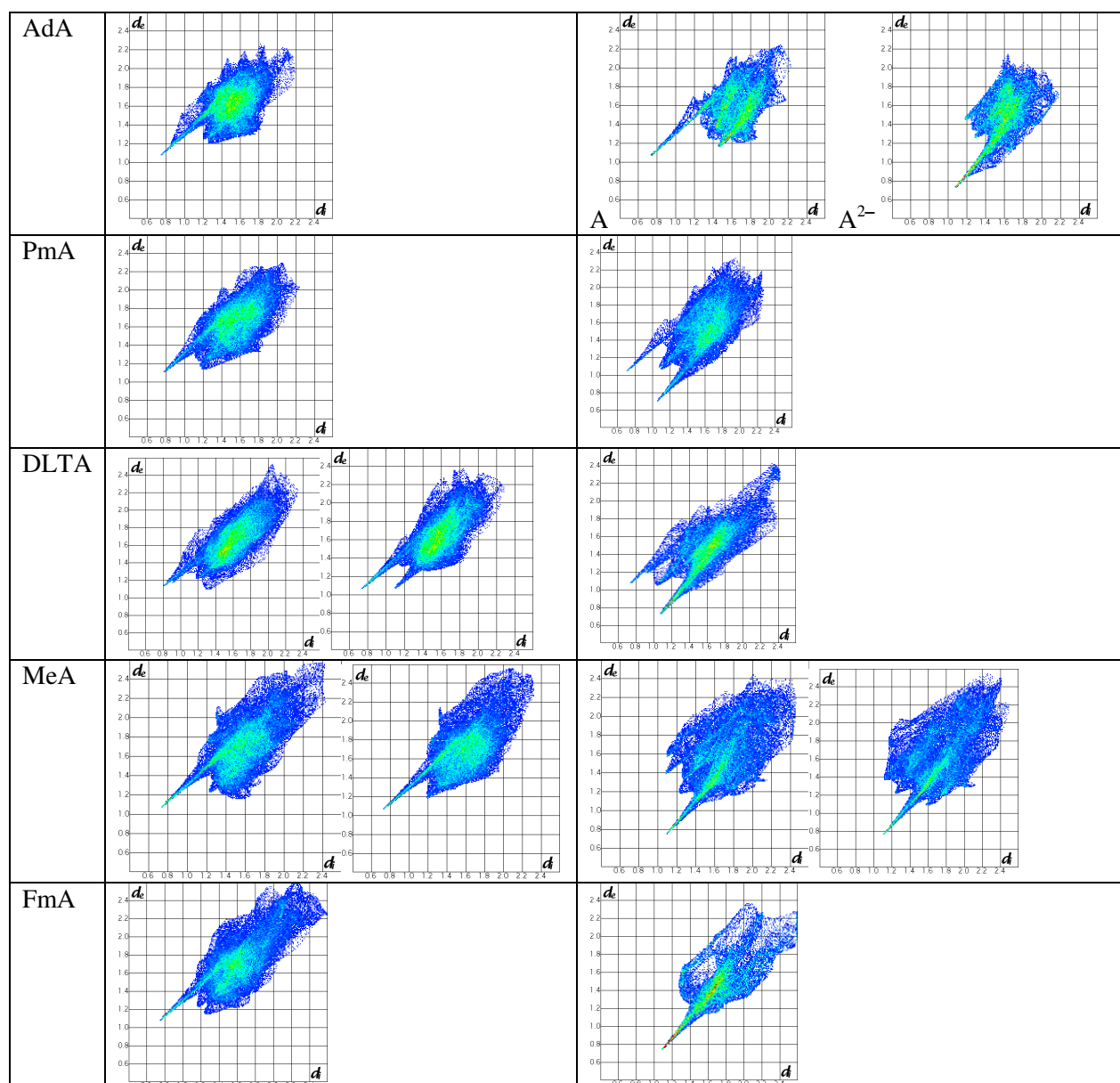
### Fingerprint Plots

The information from  $d_e$  and  $d_i$  surfaces can be viewed simultaneously by plotting a 2D ‘fingerprint’ plot. Fingerprint plots involve distributing the  $d_e$  and  $d_i$  data for each surface point into bins of discrete intervals for both of the parameters. Each point on the graph then represents a bin of width 0.01Å in these two distances and the colour of each point is a function of the fraction of surface points in that bin. Blue indicates relatively few points, green a moderate fraction and red is many points. Different sections of the fingerprint plot are contributed to by different interactions and hence the plot takes on various shapes and colour distributions when different intermolecular interactions are dominant. For example, strong hydrogen bonding gives two spikes pointing towards the bottom left corner; for a hydrogen bond acceptor  $d_i > d_e$ , and if a hydrogen bond acceptor is present this is shown by the spike with  $d_e > d_i$ . In this way a fingerprint plot gives a visual quantitative representation of the type and geometry of intermolecular interaction experienced by a molecule. Different space groups and crystal structures are represented in the fingerprint plots – similar compounds (i.e. within the same family) that have similar crystal structures will have very similar fingerprint plots.

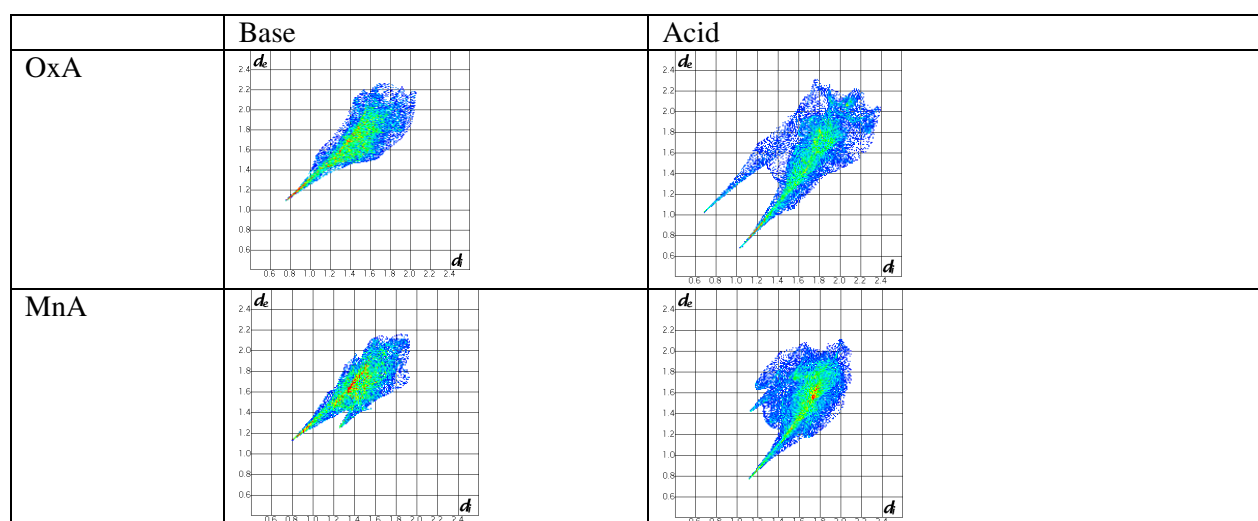
#### A9 Aromatic Amines:

##### A9.1 TMBA

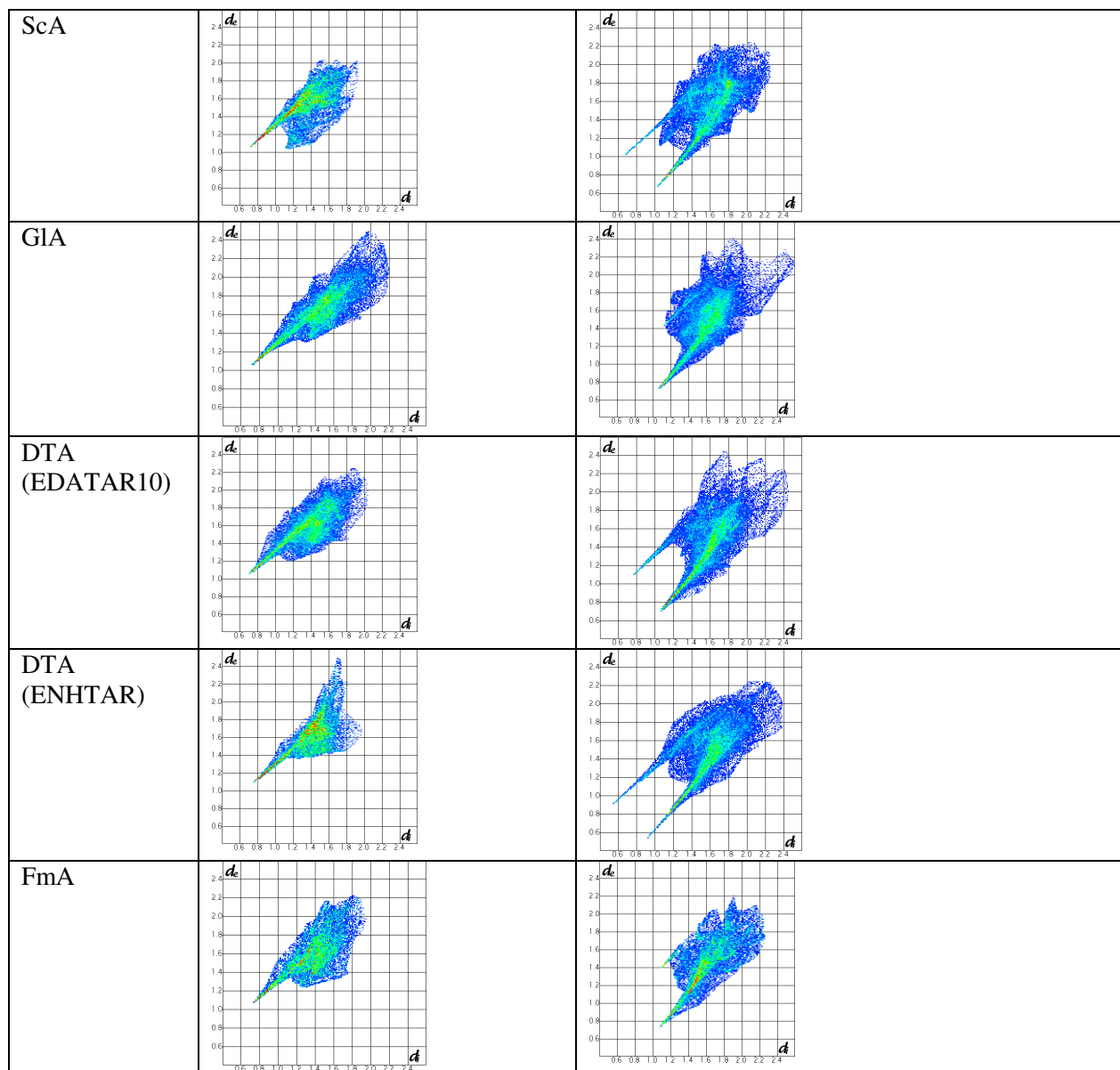




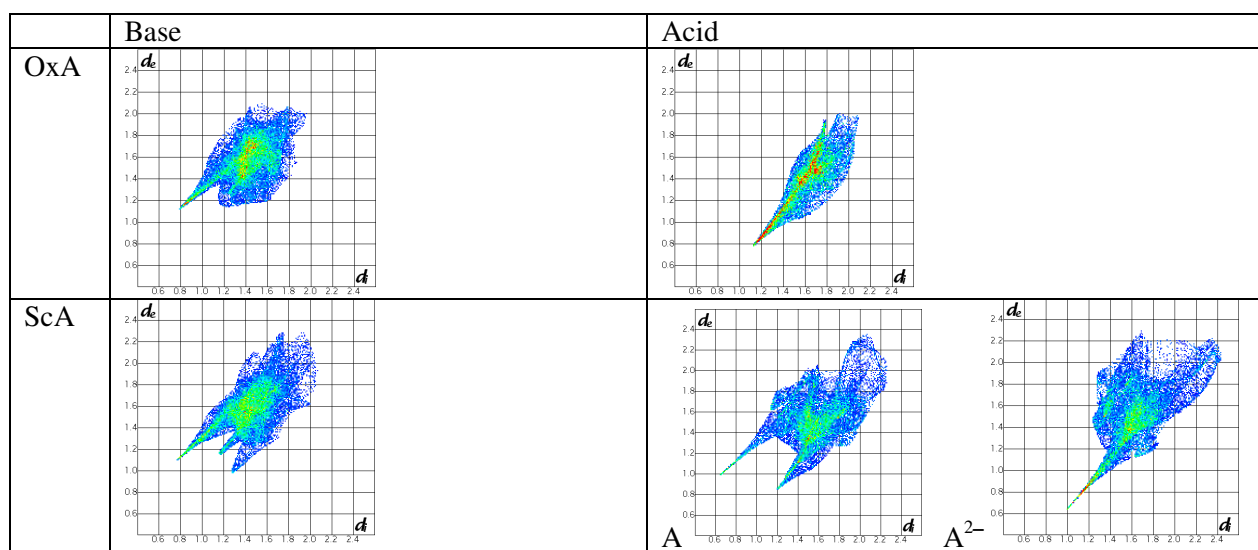
## A9.2 DAE

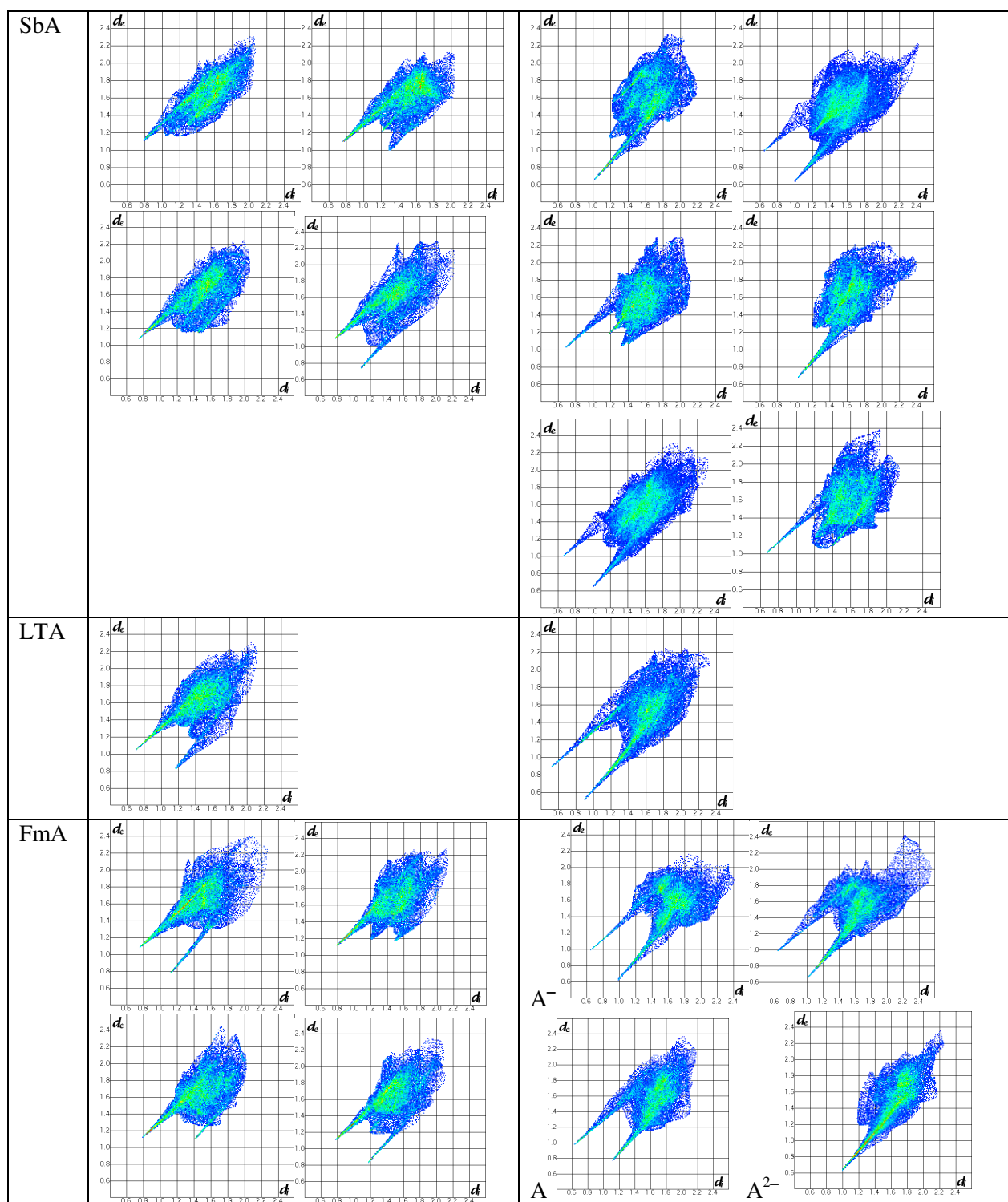




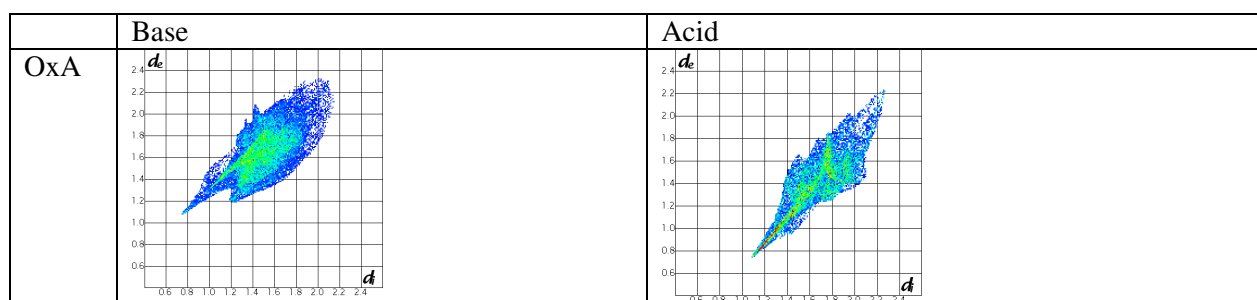


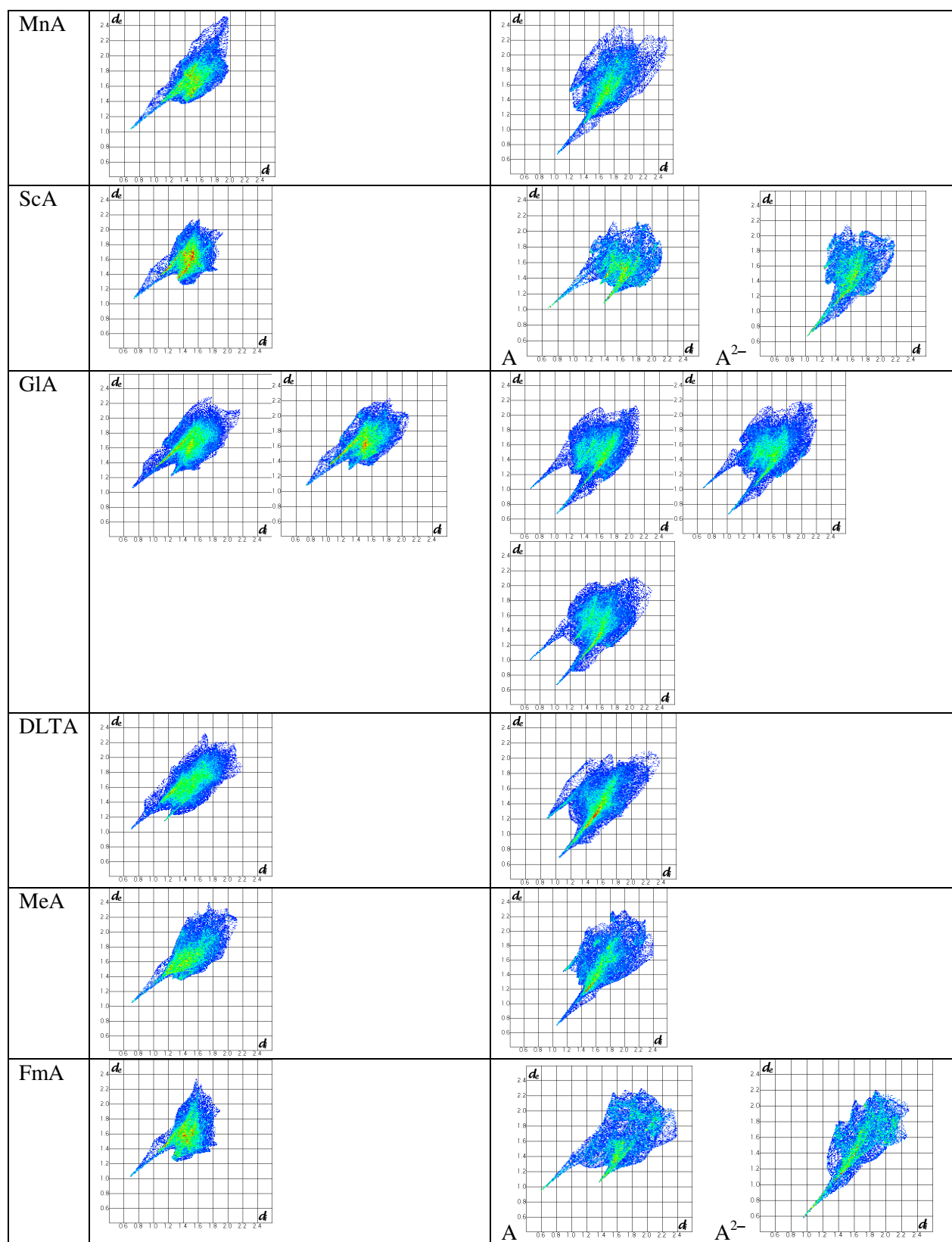
## A9.3 AEI

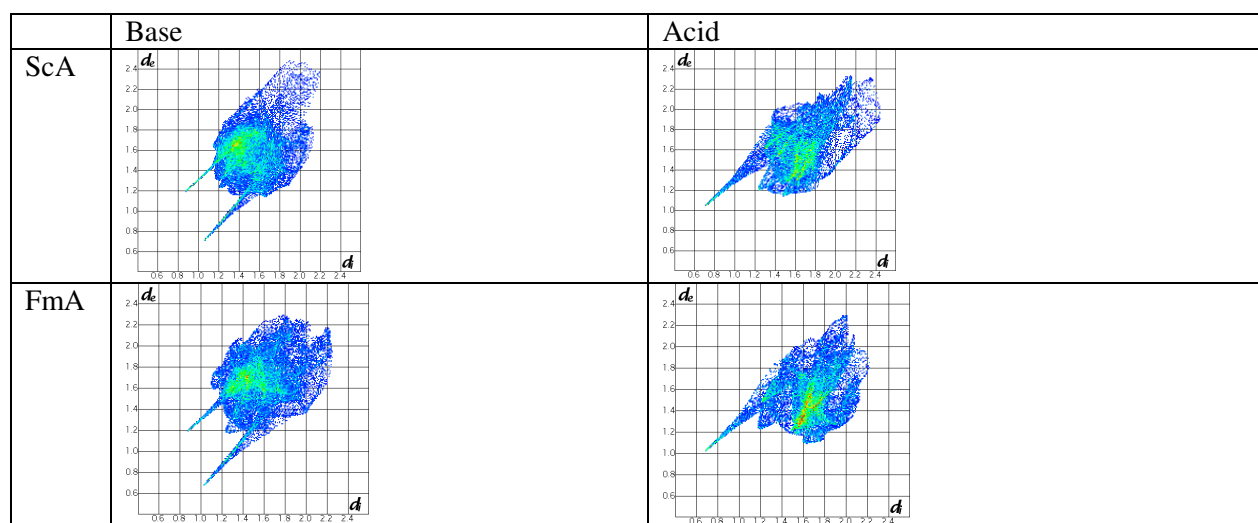
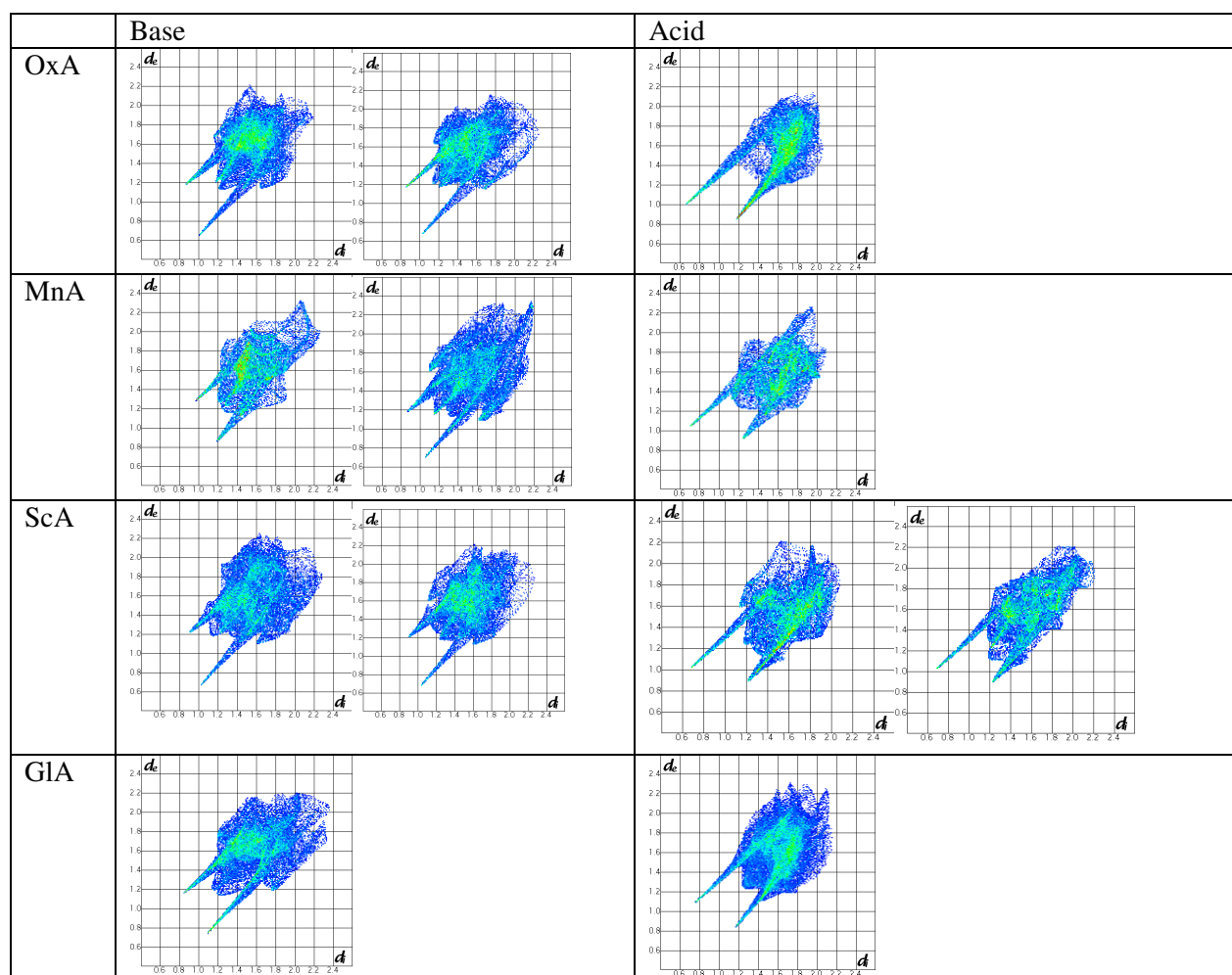


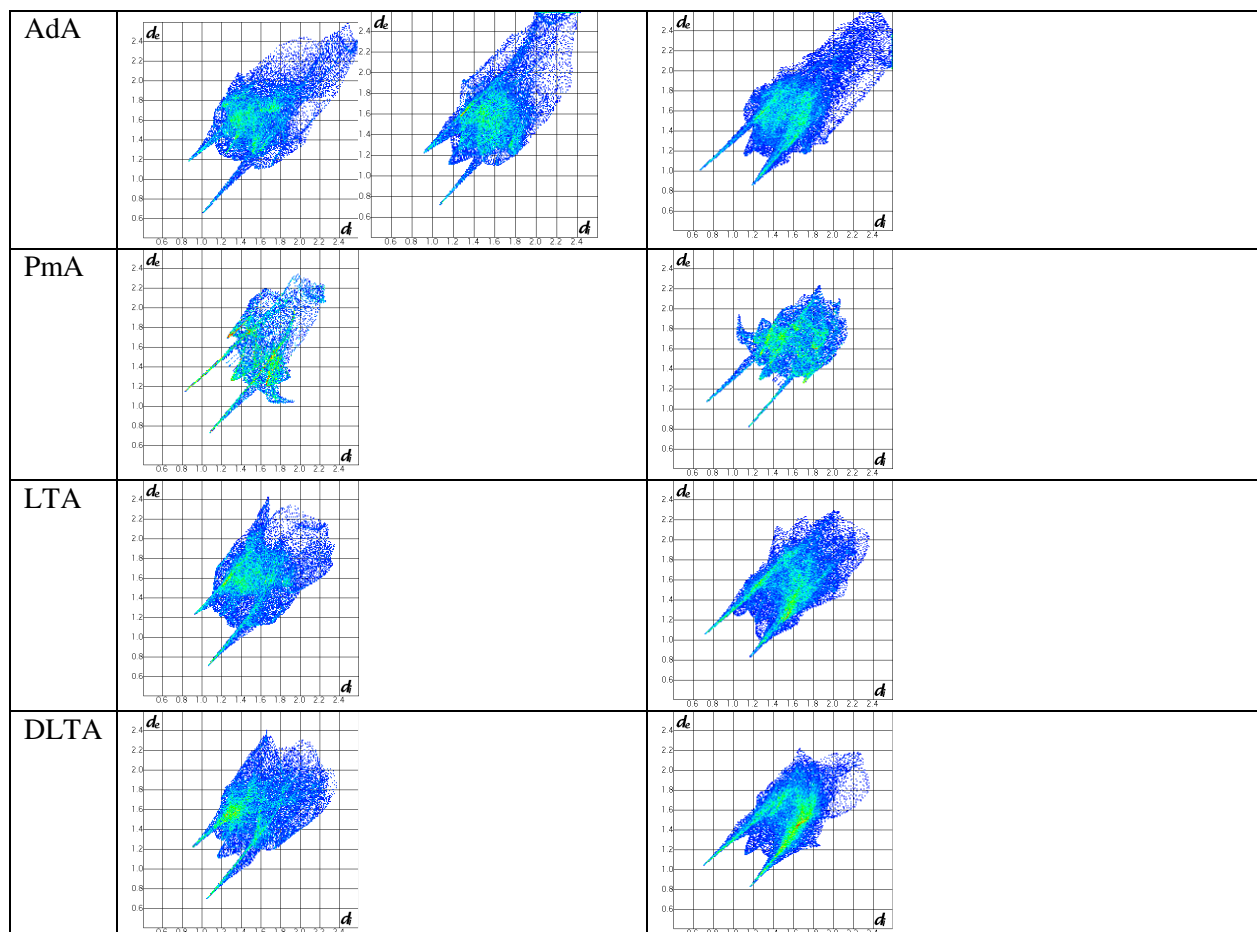


## A9.4 TEMED

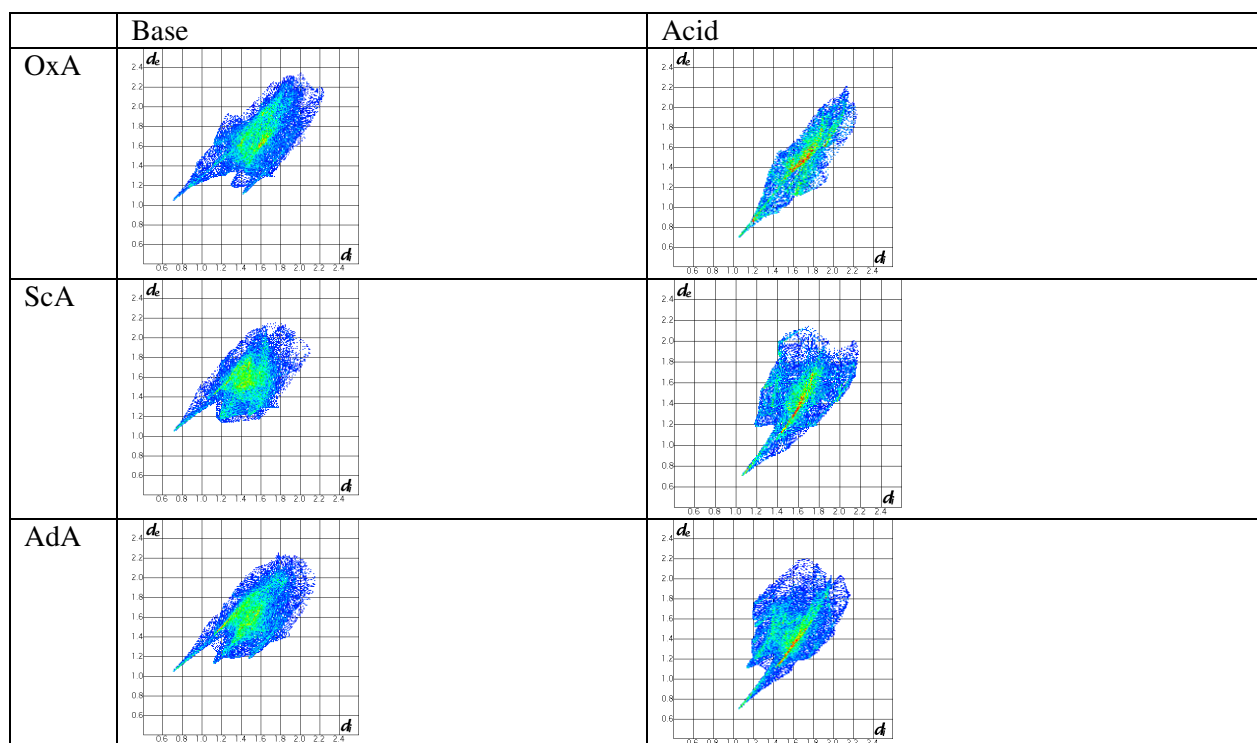


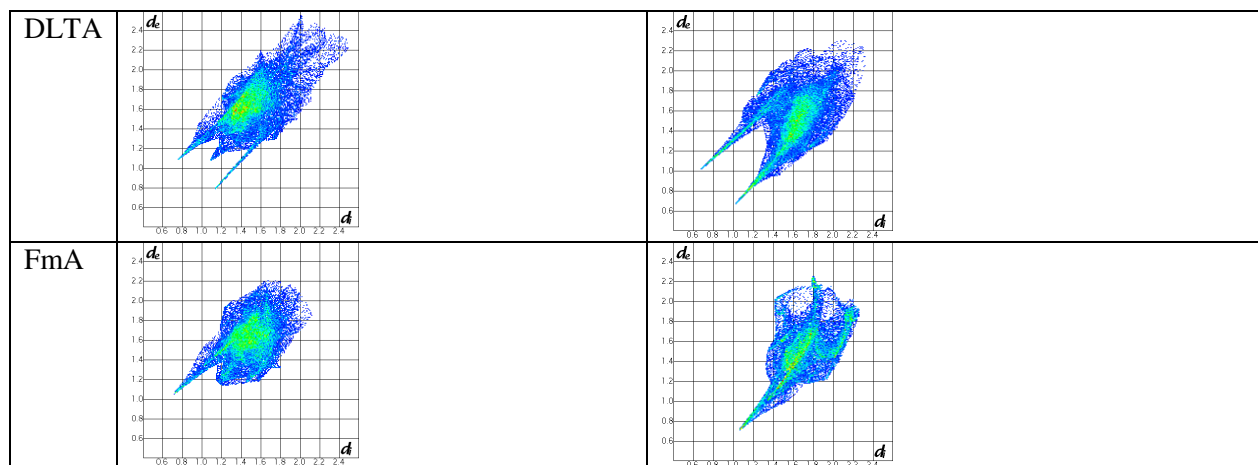


**A10 Nitrogen-containing Heterocycles:****A10.1 Pyr****A10.2 Idn**

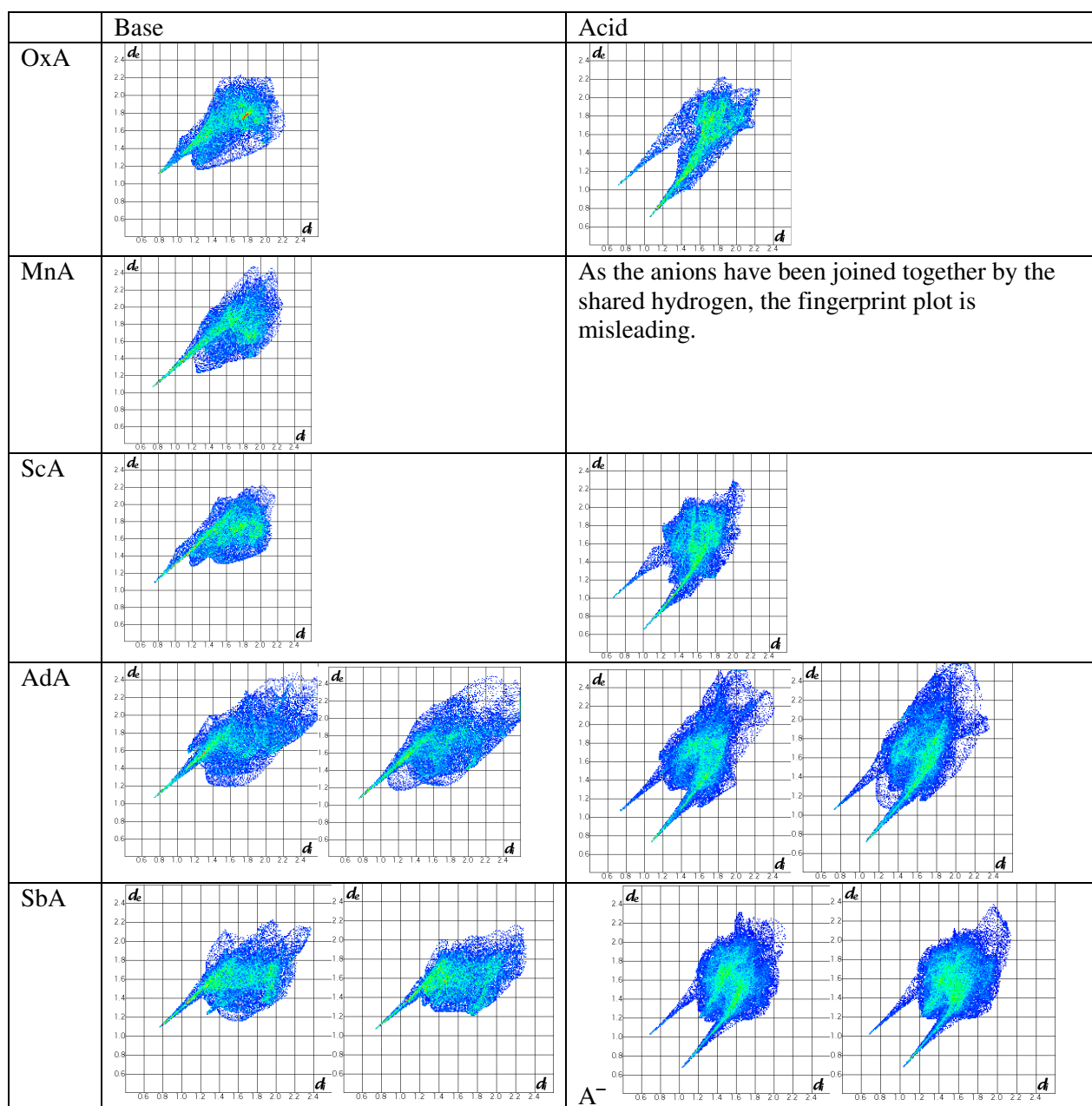


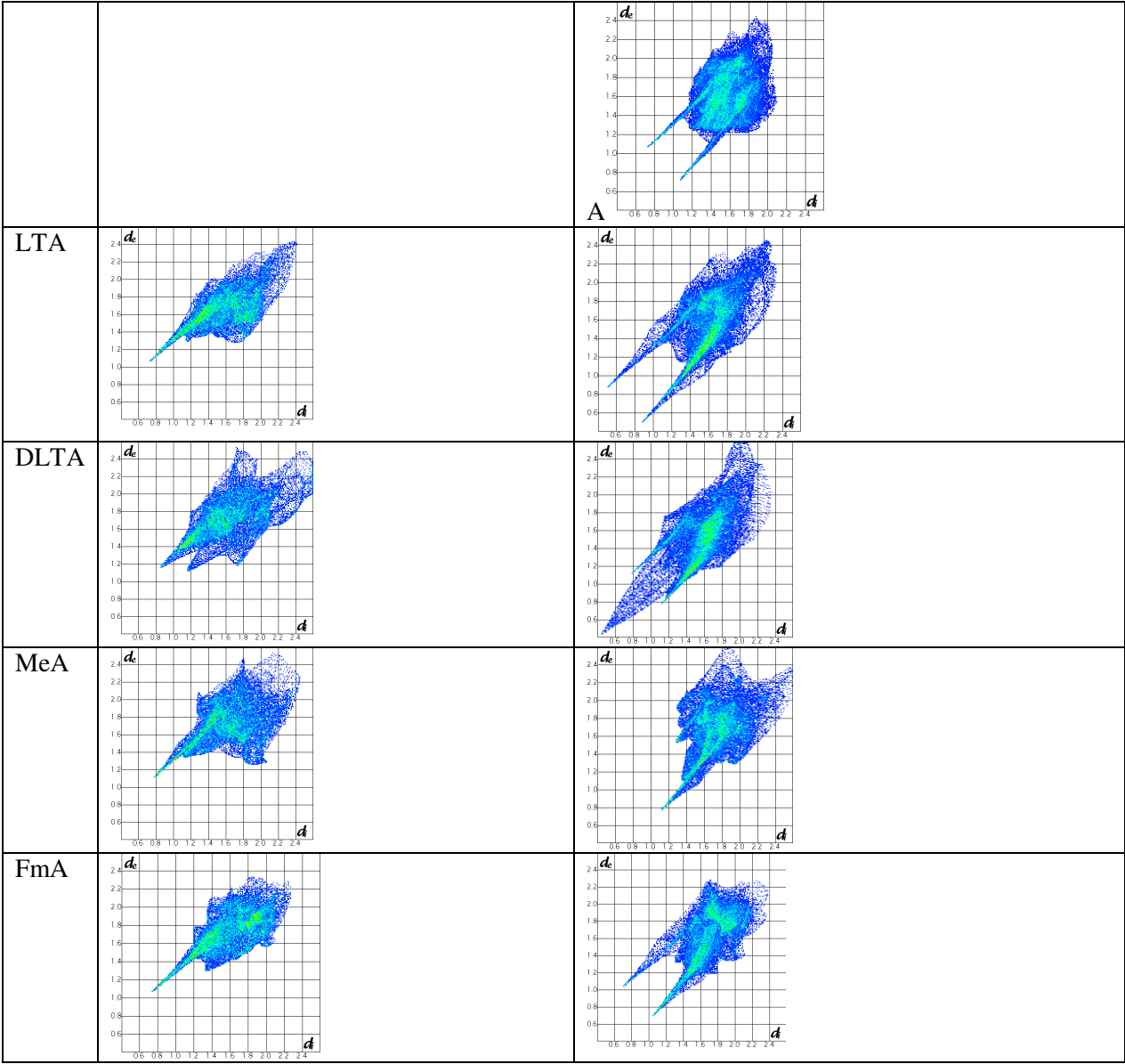
### A10.3 Mo



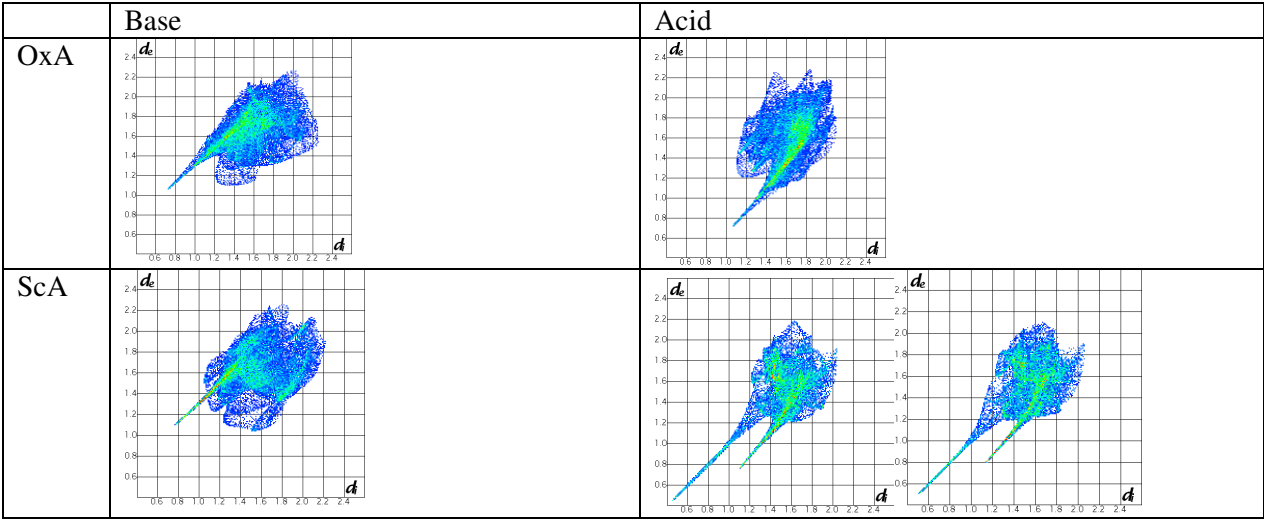


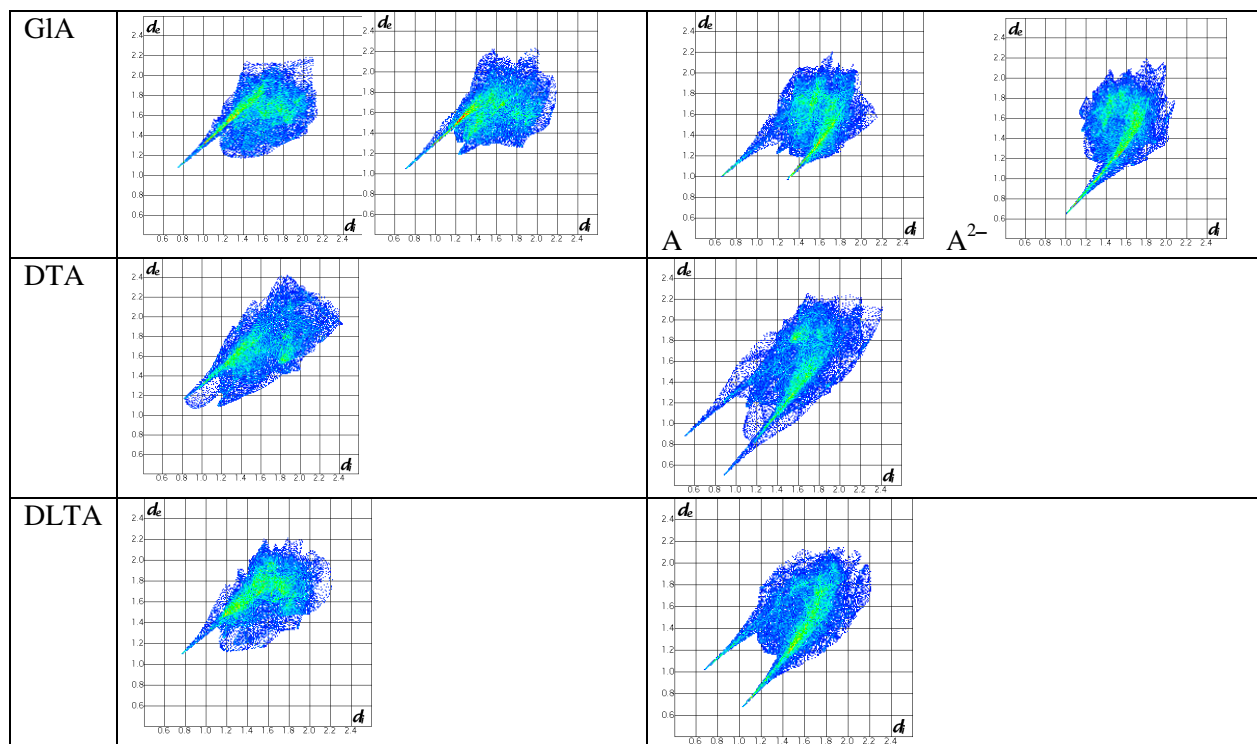
**A11 Aromatic Amines:**  
**A11.1 Im**



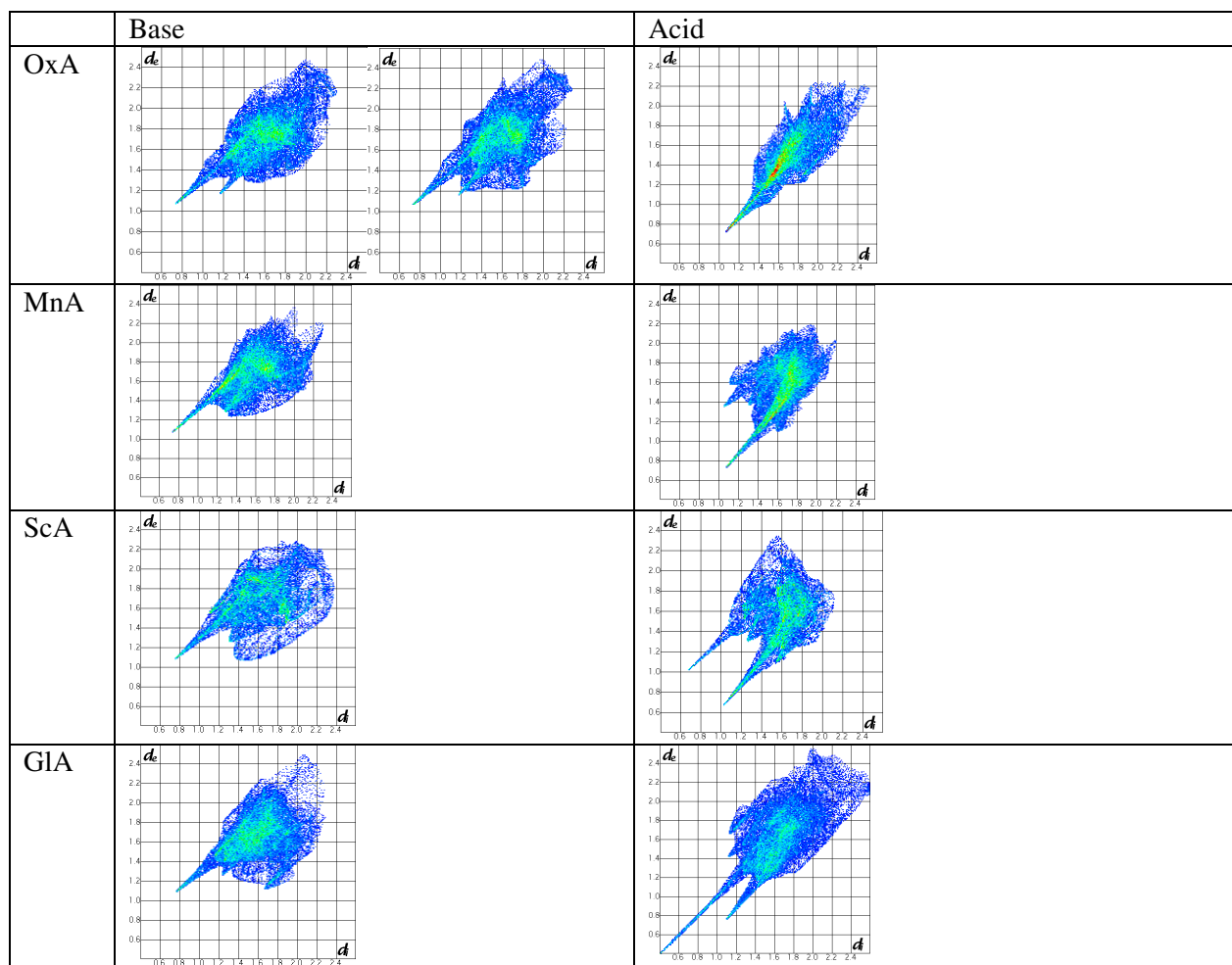


A11.2 IMI

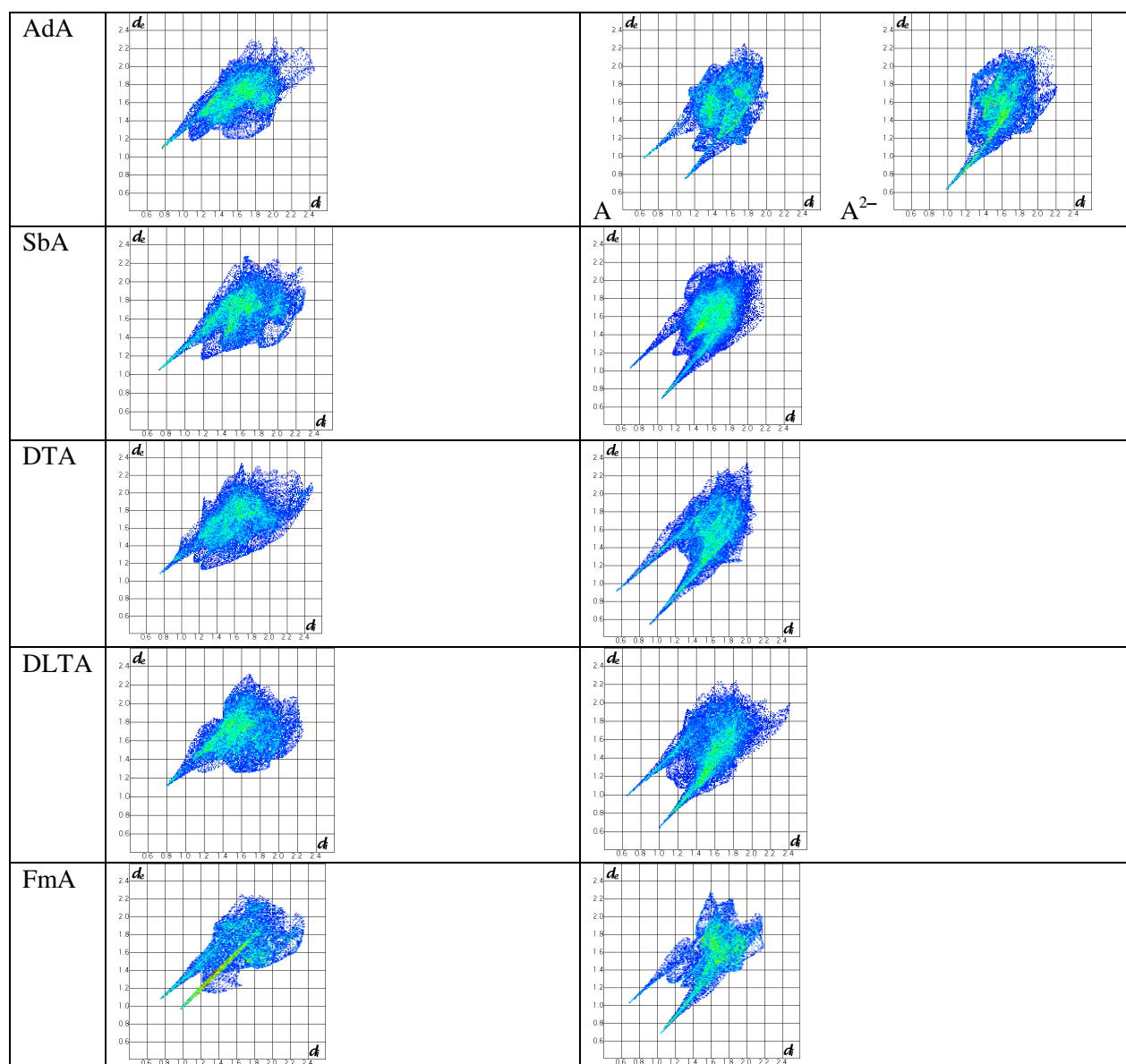




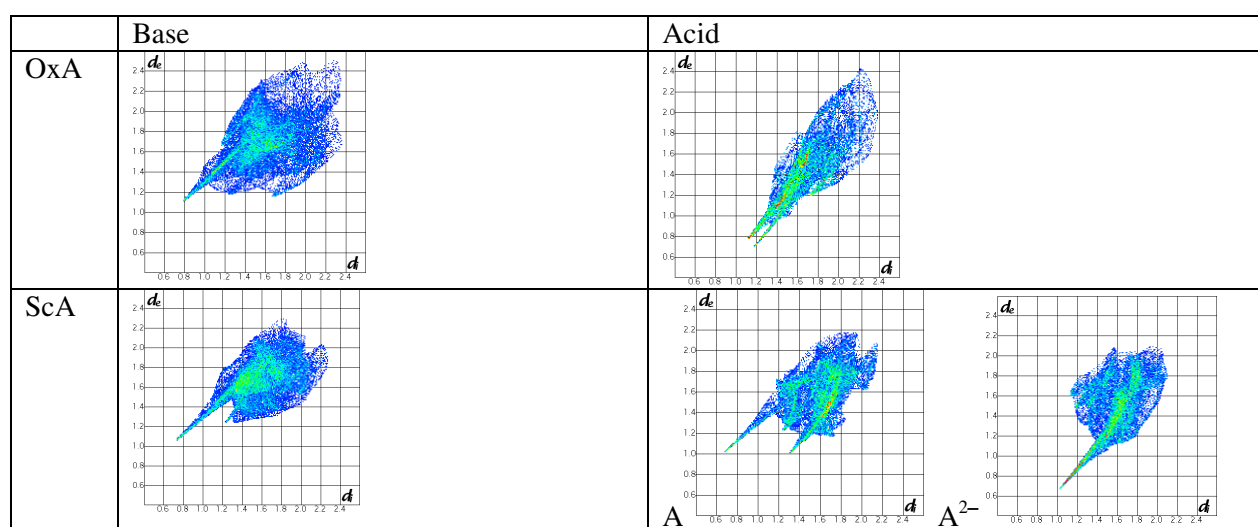
### A11.3 2MI

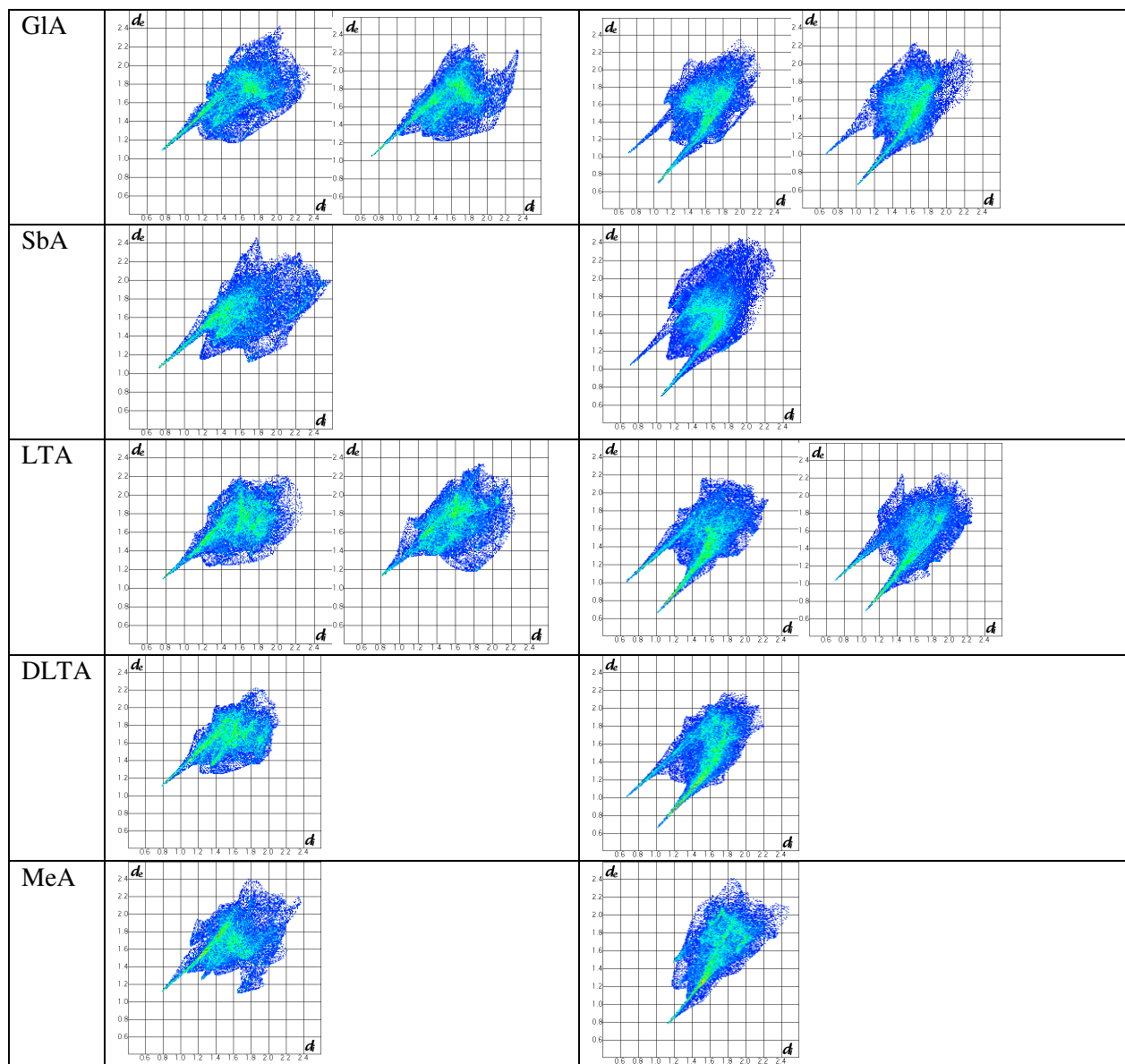




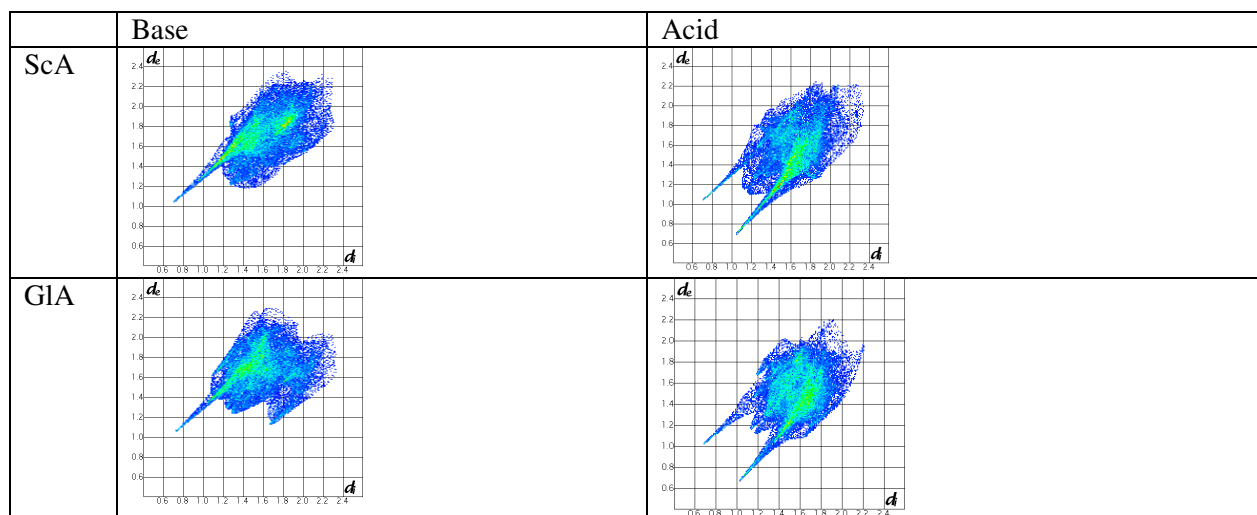


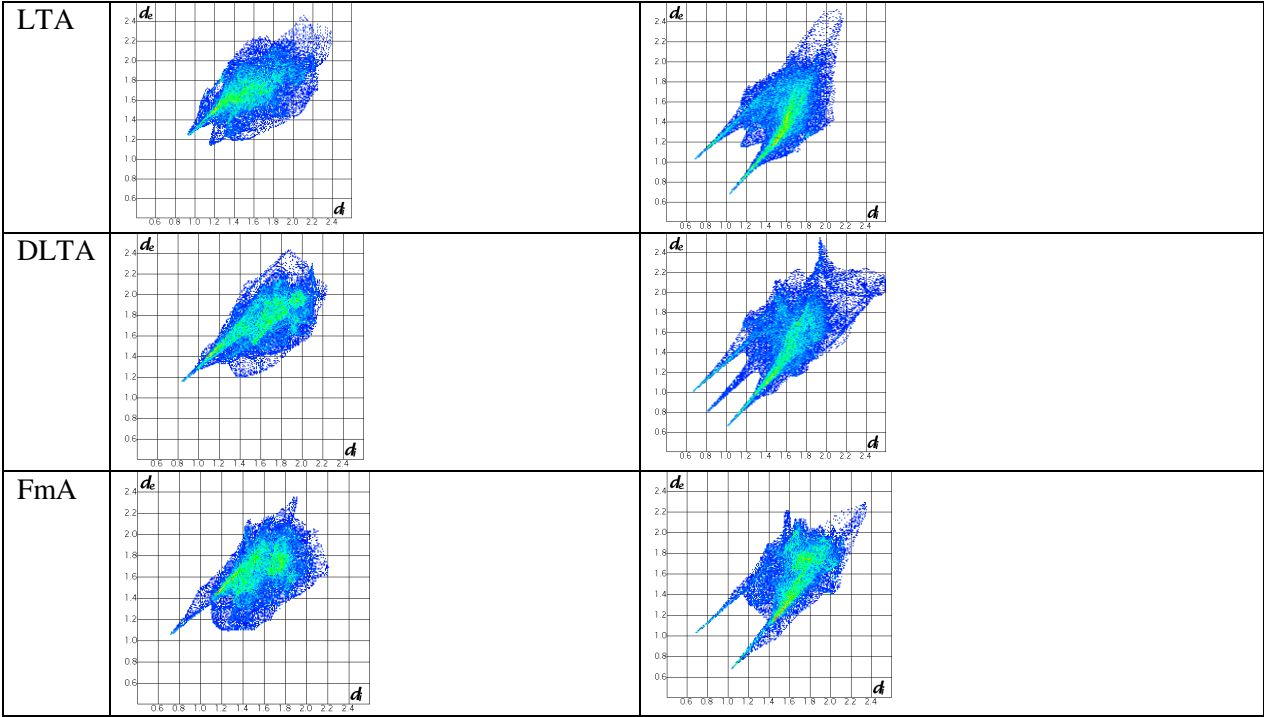
#### A11.4 4MI





### A11.5 DMI





	DAE		AEI	
	Torsion angle /°	C-C bond distance /Å	Torsion angle /°	C-C bond distance /Å
OxA	180.00	1.503	65.86	1.501
MnA	180.00	1.507	-	-
ScA	180.00	1.514	63.36	1.507
GlA	74.10	1.500	-	-
AdA	no co-ordinates	no co-ordinates	-	-
PmA	-	-	-	-
SbA	-	-	-73.38 -63.90 -69.17 53.86	1.510 1.453 1.405 1.497
DTA/LTA	EDATAR10 =172.02 ENHTAR = -71.34	1.512 1.503	-61.36	1.504
DLTA	-	-	-	-
MeA	180.00	1.511	-	-
FmA	180.00	1.518	56.26 -65.38 -71.54 -68.85	1.510 1.506 1.525 1.473
average	Anti = 178.67 Gauche = 72.72	1.509	64.81 (all gauche)	1.490

**Table A12** Torsion angles and C-C bond distances for DAE and AEI cations in their respective binary structures.

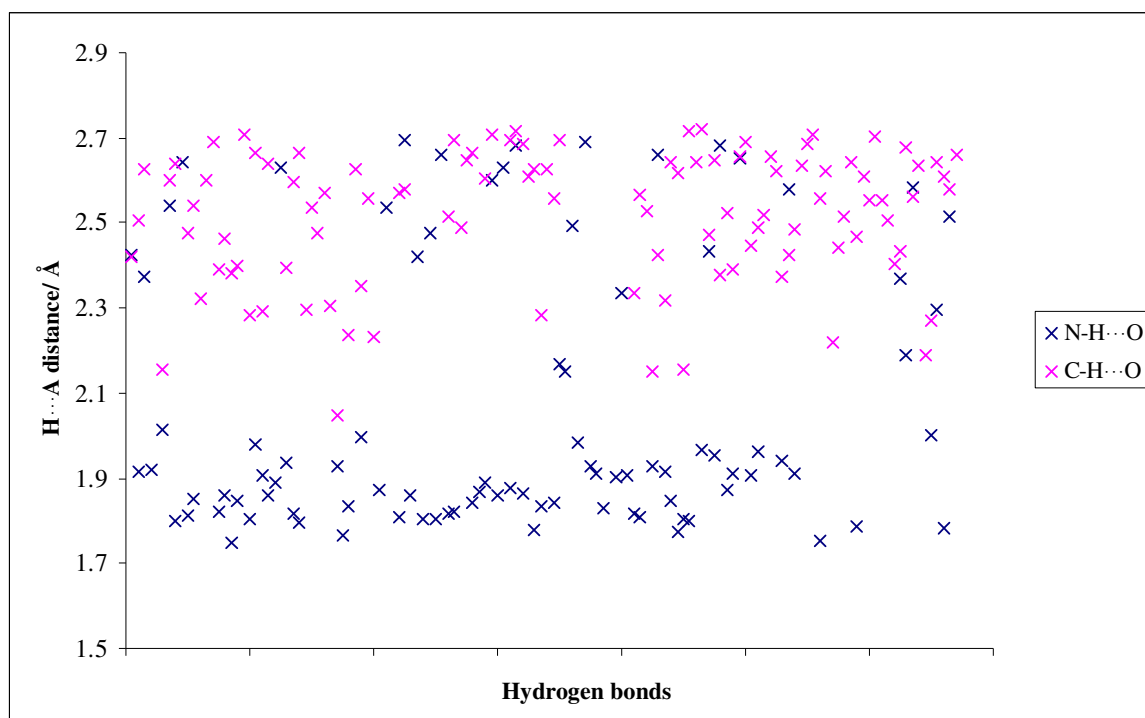


**Figure A13** Graph to show the hydrogen bond distances for N-H...O and C-H...O interactions between acid and base molecules of Im-derivative binary compounds.

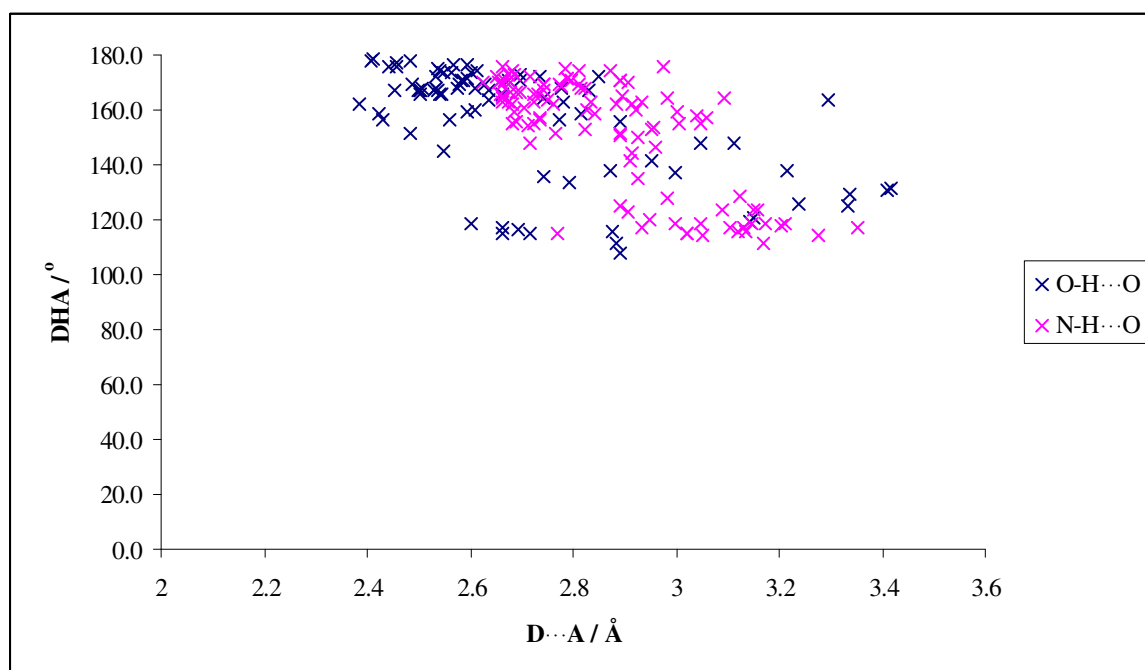


**Figure A14** Graph to show the distribution of the geometries of O-H...O and N-H...O hydrogen bonds across all of the binary compounds.

**C-O, C=O bond distance and O...O distance**

The following tables compare the C-O, C=O bond distances in accordance with the hydrogen bond motif that they are part of; in Table A15 the carboxyl/carboxylate groups form head-to-tail acid/anion chains, and in Table A16 the carboxyl/carboxylate groups are involved in hydrogen bonding with base or water molecules. An 'H' in the third column indicates that the carboxylate group is protonated; 1/2H indicates disordered hydrogens. The smallest difference in C-O, C=O distances is shown in blue, the largest in red. The maximum and minimum O...O distances are coloured in the same manner.

Base	Acid		C=O	error	C-O	error	difference	O...O distance	type of H bonding
TMBA	ScA	H	1.218	5	1.313	5	0.095	2.488	syn-anti
			1.239	4	1.279	5	0.040	2.502	syn-anti
			1.256	4	1.262	5	0.006		
		H	1.228	5	1.307	5	0.079		
	PmA	H	1.208	5	1.322	5	0.114	2.595	syn-anti
			1.238	4	1.284	4	0.05		
DAE	OxA		1.236		1.246		0.010	2.572	syn-syn
		H	1.199		1.304		0.105		
	ScA		1.249		1.262		0.013	2.580	syn-syn
		H	1.200		1.313		0.113		
	DLTA	H	1.211		1.320		0.109	2.527	syn-syn
			1.242		1.249		0.007		
AEI	ScA		1.233	2	1.293	2	0.060	2.464	anti-anti
		H	1.220	3	1.312	3	0.092		
	SbA	H	1.241	6	1.306	6	0.065	2.562	syn-syn
			1.229	6	1.283	6	0.054	2.483	anti-anti
		H	1.191	6	1.325	6	0.134	2.515	syn-syn
			1.234	6	1.281	6	0.047		
			1.234	6	1.272	6	0.038		
		H	1.207	6	1.319	6	0.112		
			1.247	5	1.271	5	0.024		
		H	1.222	5	1.306	5	0.084		
	FmA		1.241	6	1.29	6	0.049	2.461	syn-syn
		H	1.239	6	1.304	5	0.065	2.442	syn-syn
		H	1.224	6	1.289	6	0.065	2.519	syn-syn
		H	1.219	6	1.309	6	0.090	2.466	syn-syn
			1.275	6	1.275	6	0.000		
		H	1.233	6	1.297	5	0.064		
			1.243	5	1.284	6	0.041		
			1.243	5	1.280	6	0.037		
	LTA	H	1.231		1.274		0.043	2.452	syn-syn
			1.223		1.278		0.055		
TEMED	ScA		1.244		1.260		0.016	2.514	anti-anti
		H	1.206		1.319		0.113		
	GIA		1.253	9	1.291	9	0.038	2.497	anti-anti
		H	1.217	9	1.379	11	0.162	2.529	"
			1.249	9	1.254	10	0.005	2.543	"
		H	1.213	9	1.300	9	0.087		
			1.192	8	1.292	9	0.100		
		H	1.186	8	1.326	9	0.140		
	FmA		1.244		1.252		0.008	2.516	anti-anti

		H	1.209		1.312		0.103		
Mo	DLTA	H	1.208	2	1.314	2	0.106	2.538	syn-syn
			1.245	2	1.259	2	0.014		
Im	OxA		1.229		1.254		0.025	2.588	syn-syn
		H	1.198		1.303		0.105		
	MnA	1/2H	1.209		1.282		0.073	2.454	syn-syn
	ScA		1.220		1.288		0.068	2.478	anti-anti
		H	1.219		1.307		0.088		
	AdA		1.250		1.252		0.002	2.561	syn-syn
		H	1.198		1.304		0.106	2.593	syn-syn
			1.222		1.271		0.049		
		H	1.198		1.312		0.114		
	SbA	H	1.212	2	1.329	2	0.117	2.564	syn-syn
			1.249	2	1.277	2	0.028	2.551	syn-syn
			1.245	2	1.278	2	0.033	2.647	syn-syn
		H	1.216	2	1.326	2	0.110	2.682	syn-syn
		H	1.221	2	1.320	2	0.099		
		H	1.221	2	1.318	2	0.097		
	LTA	H	1.206		1.303		0.097	2.503	syn-syn
			1.236		1.264		0.028		
	DLTA	1/2H	1.219	6	1.286	6	0.067	2.492	syn-syn
		1/2H	1.225	6	1.290	6	0.065	2.539	syn-syn
	FmA	H	1.212		1.309		0.097	2.568	syn-syn
			1.238		1.269		0.031		
1MI	ScA	1/2H	1.194	11	1.308	11	0.114	2.522	syn-syn
		1/2H	1.241	12	1.261	11	0.021	2.543	syn-syn
	GIA	H	1.205	8	1.327	8	0.122	2.514	anti-anti
		H	1.258	8	1.289	8	0.031	2.480	anti-anti
			1.232	8	1.273	8	0.041		
			1.252	8	1.281	8	0.029		
	DTA		1.215		1.279		0.064	2.482	syn-syn
		H	1.215		1.289		0.074		
	DLTA		1.244	3	1.271	2	0.027	2.534	syn-syn
		H	1.214	3	1.303	2	0.089		
2MI	ScA		1.240	3	1.283	3	0.043	2.535	syn-syn
		H	1.208	3	1.326	3	0.118		
	GIA	1/2H	1.224	4	1.291	4	0.067	2.456	syn-syn
		1/2H	1.228	4	1.289	4	0.061	2.443	syn-syn
	AdA		1.2491	16	1.2797	16	0.0306	2.461	anti-anti
		H	1.2337	16	1.2994	15	0.0657		
	SbA	H	1.22	15	1.27	3	0.05	2.635	syn-syn
		H	1.21	2	1.36	4	0.15	2.524	syn-syn
			1.235	2	1.278	2	0.043		
	DTA	H	1.224		1.308		0.084	2.486	syn-syn
			1.248		1.265		0.017		
	DLTA	H	1.232	3	1.290	3	0.058	2.484	syn-syn
			1.228	3	1.292	3	0.064		
	FmA	H	1.212	4	1.318	4	0.106	2.564	syn-syn
			1.248	4	1.269	4	0.021		
4MI	ScA	H	1.210	2	1.318	2	0.108	2.541	syn-anti
			1.241	2	1.280	2	0.039		
	GIA		1.243	5	1.278	5	0.035	2.511	anti-anti
		H	1.208	5	1.315	5	0.107	2.555	syn-anti
			1.233	5	1.293	5	0.060		
		H	1.218	5	1.323	5	0.105		

	SbA	H	1.202	4	1.328	4	0.126	2.582	syn-syn
			1.239	4	1.276	4	0.037		
	LTA	H	1.211		1.306		0.095	2.569	syn-syn
			1.242		1.266		0.024	2.510	syn-syn
			1.253		1.264		0.011		
		H	1.222		1.302		0.080		
	DLTA		1.239	4	1.288	4	0.049	2.500	syn-syn
H		1.228	4	1.309	4	0.081			
DMI	ScA	H	1.214	3	1.321	3	0.107	2.578	syn-anti
			1.234	3	1.284	3	0.050		
	GIA		1.246	6	1.267	6	0.021	2.536	anti-anti
		H	1.204	7	1.317	7	0.113		
	LTA	H	1.215	3	1.320	5	0.105	2.555	syn-syn
			1.264	4	1.266	3	0.002		
	DLTA		1.250	5	1.256	5	0.006	2.504	syn-syn
		H	1.214	5	1.310	5	0.096		
	FmA		1.262	5	1.268	5	0.006	2.544	syn-anti
H		1.220	5	1.330	5	0.110			

**Table A15** C-O, C=O bond distances and O...O distances in Å, where the carboxyl/carboxylate groups form head-to-tail acid/anion chains.

Base	Acid		C=O	error	C-O	error	difference
TMBA	OxA		1.243	10	1.271	10	0.028
		Me	1.226	10	1.341	10	0.115
			1.245	9	1.265	9	0.020
		Me	1.207	10	1.322	9	0.115
		Me	1.210	10	1.331	10	0.121
			1.232	9	1.247	9	0.015
		Me	1.169	10	1.317	9	0.148
			1.222	9	1.248	9	0.026
	GIA		1.242	2	1.277	2	0.035
			1.259	3	1.266	3	0.007
		H	1.217	3	1.310	3	0.093
	AdA		1.253	5	1.259	5	0.006
			1.239	6	1.267	6	0.028
	DLTA		1.247	3	1.272	3	0.025
		Me	1.213	4	1.351	4	0.138
			1.249	4	1.264	4	0.015
		Me	1.209	4	1.349	4	0.140
	FmA		1.238	11	1.276	12	0.038
DAE	MnA		1.234		1.269		0.035
		H	1.219		1.297		0.078
	GIA		1.252	3	1.258	3	0.006
			1.242	3	1.275	3	0.033
	DTA		1.242		1.261		0.019
			1.242		1.258		0.016
	MeA		1.236		1.273		0.037
			1.217		1.298		0.081
	FmA		1.2530	2	1.2703	2	0.0173
AEI	OxA		1.248		1.25		0.002
TEMED	OxA		1.239	2	1.261	2	0.022



	MnA	H	1.204		1.307		0.103
			1.246		1.254		0.008
	DLTA		1.245	3	1.259	3	0.014
			1.23	2	1.282	2	0.052
	MeA		1.25	5	1.276	5	0.026
		H	1.219	5	1.313	5	0.094
Pyr	ScA	H	1.199	5	1.336	5	0.137
	FmA	H	1.22	2	1.31	2	0.09
Idn	OxA	H	1.217	8	1.297	9	0.080
	MnA	H	1.204	7	1.325	7	0.121
	ScA	H	1.2249	18	1.3069	19	0.082
		H	1.2228	18	1.3090	19	0.0862
	GIA	H	1.216	4	1.330	4	0.114
		H	1.219	4	1.328	3	0.109
	AdA	H	1.218	4	1.305	4	0.087
		H	1.211	4	1.327	4	0.116
	PmA	H	1.213	3	1.329	3	0.116
	LTA	H	1.2091	18	1.3215	17	0.1124
		H	1.2100	18	1.3224	17	0.1124
	DLTA	H	1.222	2	1.307	3	0.085
		H	1.212	3	1.316	2	0.104
	MeA	H	1.268	7	1.275	7	0.007
		H	1.239	6	1.295	6	0.056
		H	1.221	7	1.315	7	0.094
		H	1.222	7	1.329	7	0.107
		H	1.227	7	1.311	6	0.084
		H	1.263	7	1.264	7	0.001
		H	1.222	7	1.316	7	0.094
		H	1.238	7	1.304	6	0.066
Mo	OxA		1.24	2	1.263	2	0.023
	ScA		1.259	2	1.261	2	0.002
	AdA		1.257	7	1.259	7	0.002
	FmA		1.257	2	1.263	2	0.006
Im	MnA		1.247		1.256		0.009
	MeA	H	1.231		1.285		0.054
			1.230		1.282		0.052
1MI	OxA		1.228	2	1.264	2	0.036
		Me	1.202	3	1.329	3	0.127
2MI	OxA		1.248	4	1.267	4	0.019
			1.252	4	1.255	4	0.003
	MnA	H	1.231	5	1.283	5	0.052
			1.231	5	1.296	6	0.065
4MI	OxA		1.248	2	1.254	2	0.006
	MeA		1.247	2	1.286	2	0.039
		H	1.235	2	1.290	2	0.055

**Table A16** C-O, C=O bond distances and O...O distances in Å, where the carboxyl/carboxylate groups are involved in hydrogen bonding with base or water molecules. 'Me' indicates the carboxylate group is methylated.

**C-C bond distances in OxA**

Base	Refcode	Carbon atoms	Distance / Å	error	Deprotonation
2imdzone	06skc0068	c1-c2	1.521	10	neutral
tetmeBuam	src1327	c1-c2	1.514	12	methylated mono
		c31-c32	1.532	11	methylated mono
		c51-c52	1.555	11	methylated mono
		c71-c72	1.56	11	methylated mono
DAE	PEPMOM	c13-c14	1.544	2	mono
AEI	QAMRIF	c3-c3'	1.559	5	di
morph	06skc0036	c1-c1'	1.551	3	di
TEMED	06skc0058	c1-c1'	1.557	4	di
2MI	06skc0026	c1-c2	1.568	5	di
4MI	06skc0053	c1-c1'	1.570	3	di
1MI	06skc0034	c1-c2	1.564	3	methylated mono
Im	MEQPAZ	c4-c5	1.554		mono

**Table A17** Table of C-C bond distances in OxA and the deprotonation of the OxA molecule.**Torsion of Diacid Chain**

	Torsion of <i>anti</i> conformation /°		Torsion of <i>gauche</i> conformation /°		Torsion of <i>cis</i> conformation /°	
	range	average	range	average	range	average
ScA	170.53-179.93	174.75	58.98-69.23	64.34		
GIa	159.39-179.13	174.88	55.53-74.76	69.23		
AdA	161.47-180.00	175.64				
PmA	168.93-180.00	176.82	69.41	69.41		
SbA	171.14-180.00	171.46	55.94-65.15	62.6		
L/DTA	170.63-179.61	176.17				
DLTA	170.53-179.93	174.75				
MeA					0.04-1.55	0.902
FmA	177.16-180.00	179.46				

**Table A18** Range of, and average torsion angles for each conformation for each diacid

	Pyr	Idn	TMBA	DAE	AEI	Mo	TEMED	2MI	DMI	4MI	1MI	Im	average
OxA		2.53	22.56 13.95 20.8 15.75	3.5	19.7	0	0	12.59		0	4.68	0.8	8.99
MnA		45.87		8			8.3	4.50				87.5	30.83
ScA	0	0 0	73.82 84.59	65	0 0	0	0 0	0.00	80.34	0 0	6.5	5	18.54
GlA		10.86	53.94 22.65	86.04			82.55 88.87 76.86	26.07 25.92 (disordered)	8.03	7.40	3.73 4.57		38.27
AdA		15.36	0 0	no co-ord.		0						22.1 23.2	10.11
PmA		0	77.71										38.86
SbA					14.12 33.96 21.95 3.15			16.49		84.15		16.08 12.12 14.68	24.078
MeA		0.63 2.91 2.95 0.18	74.83 78.64	12			15.26			2.14		1.1	19.06
FmA	0		0	0	44.37 12.82 49.8 8.66	0		0.00	3.12			1.5	10.94
L/DTA				EDATAR10 43.5 ENHTAR 60.5	51			66.7			58.1	45.3	54.18
DLTA		40.79	41.37			66.2	50.33	54.09	55.89	63.19	25.99	61.16	51.00

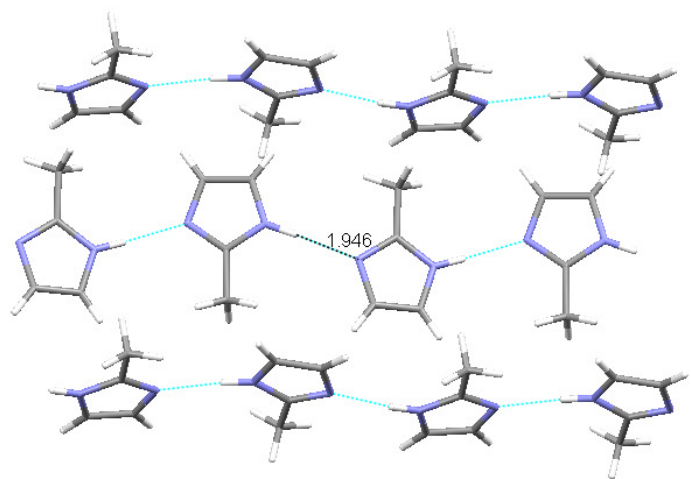
**Table A19** Angle (°) between planes of COO(H) groups in the binary compounds.

## Pure compounds

File name	Compound	R-factor	Space Group	Z	Study Temp./K	<i>a</i> /Å	<i>b</i> /Å	<i>c</i> /Å	<i>Alpha</i> /°	<i>Beta</i> /°	<i>Gamma</i> /°	Cell Volume/Å <sup>3</sup>
06skc0003	2MI	5.34	P2 <sub>1</sub> 2 <sub>1</sub> 2 <sub>1</sub>	4	120	6.008(<1)	8.152(1)	9.690(1)	90	90	90	474.67(1)
06skc0074	Idn	13.73	I4 <sub>1</sub> /a	8	120	7.632(<1)	7.632(<1)	13.171(1)	90	90	90	767.23(1)

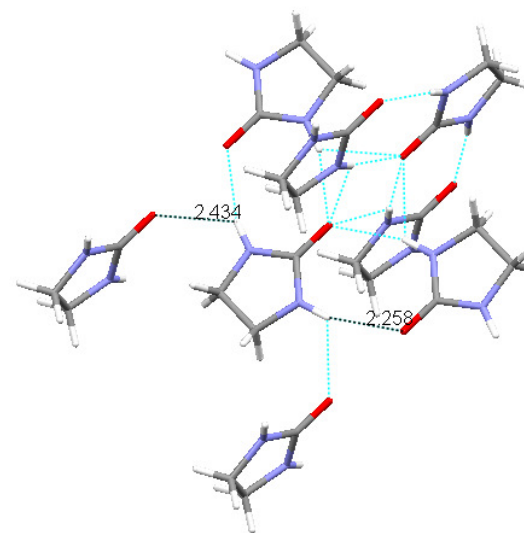
**Table A20** Cell parameters for pure 2MI and Idn. Idn has been determined in *I4<sub>1</sub>/a* as this is the only space group the structure solved in. Platon suggests *I4<sub>1</sub>/amd*, however, for these purposes the supramolecular structure and hydrogen bonding can be seen clearly in *I4<sub>1</sub>/a*.

## 2MI



1-D chains where methyl group alternately points in opposite directions; adjacent chains are approximately perpendicular to each other.

## Idn



3-D network where each Idn molecule is hydrogen bonded to the surrounding six.